Applications of transcription factor-based biosensors for strain development and evolutionary engineering

Inaugural dissertation

for the attainment of the title of doctor
in the Faculty of Mathematics and Natural Sciences
at the Heinrich Heine University Düsseldorf

presented by

Roberto Giuseppe Stella
from Amsterdam, The Netherlands

Jülich, July 2021

The thesis has been conducted at the Institute of Bio- and Geosciences, IBG-1: Biotechnology, Forschungszentrum Jülich, from January 2018 until June 2021 under the supervision of Prof. Dr. Julia Frunzke.

Published by permission of the
Faculty of Mathematics and Natural Sciences at
Heinrich Heine University Düsseldorf

Supervisor: Prof. Dr. Julia Frunzke
Institute of Bio- and Geosciences, IBG-1: Biotechnology,
Forschungszentrum Jülich, Jülich

Co-supervisor: Prof. Dr. Martina Pohl
Institute of Bio- and Geosciences, IBG-1: Biotechnology,
Forschungszentrum Jülich, Jülich

Date of the oral examination: 18/10/2021

“Failure is simply the opportunity to begin again, this time more intelligently”

Henry Ford

The studies presented in this dissertation have been published in the following articles:

Stella, R. G., Wiechert, J., Noack, S., & Frunzke, J. (2019). Evolutionary engineering of *Corynebacterium glutamicum*. *Biotechnology journal*, *14*(9), 1800444.

Tenhaef, N.*, Stella, R.*, Frunzke, J., & Noack, S. (2021). Automated Rational Strain Construction Based on High-Throughput Conjugation. *ACS Synthetic Biology*, *10*(3), 589–599.

Stella, R. G., Gertzen, C. G. W., Smits, S. H. J., Gätgens, C., Polen, T., Noack, S., & Frunzke, J. (2021). Biosensor-based growth-coupling and spatial separation as an evolution strategy to improve small molecule production of *Corynebacterium glutamicum*. *Metabolic Engineering*, 68, 162–173.

Stella, R.G., Baumann, P., Lorke, S., Münstermann, F., Wirtz, A., Wiechert, J., Marienhagen, J., Frunzke, J. (2021). Biosensor-based isolation of amino acid-producing *Vibrio natriegens* strains. *Metabolic Engineering Communications*, 13, e00187.

**These authors contributed equally to this work*

List of abbreviations

AHAS	Acetohydroxyacid synthase
ALE	Adaptive laboratory evolution
ATCC	American Type Culture Collection
BHI	Brain heart infusion medium
BHIN	BHI with additional NaCl
bp	base pair
CRISPR	Clustered regularly interspaced short palindromic repeats
eYFP	enhanced Yellow Fluorescent Protein
FACS	Fluorescence-activated cell sorting
FRET	Förster resonance energy transfer
HPLC	High performance liquid chromatography
LB	Lysogeny broth
MNNG	N-methyl-N'-nitro-N-nitrosoguanidine
OD	Optical density
PCR	Polymerase chain reaction
rbALE	repetitive batch Adaptive laboratory evolution
RBS	Ribosomal binding site
SNP	Single nucleotide polymorphism
TF-based biosensor	Transcription factor-based biosensors
UV	Ultraviolet
WT	Wild type
μ_{max}	Maximum specific growth rate

Further abbreviations not included in this section are according to international standards, as, for example, listed in the author guidelines of the Journal of Cell Biology (https://rupress.org/jcb/pages/standard-abbreviations).

Table of Contents

1. Abstract

The transition of our current economy to a sustainable bioeconomy requires efficient and high performing microbial strains for the production of chemical building blocks and fuels. However, the construction and improvement of microbial producer strains is time consuming and costly. In this thesis, several ways to improve this process using transcription factor(TF)-based biosensors have been investigated.

First, we used TF-based biosensors to obtain positive amino acid-producing *Vibrio natriegens* strains. *V. natriegens* is a Gram-negative, non-pathogenic slight-halophilic bacterium that has recently been demonstrated to be a promising new host for molecular biology and next generation bioprocesses. Its most remarkable property is a doubling time of under 10 minutes. In this work, the LysG biosensor from *Corynebacterium glutamicum* was adapted for expression in *V. natriegens*, to couple positive amino acid production to a fluorescent output. Afterwards, we performed a mutagenesis and screening approach, using fluorescence-activated cell sorting (FACS) to isolate highly fluorescent cells (potential producer cells). Using this approach, individual L-lysine, L-arginine and L-histidine producer cells could be obtained. Investigation of these isolates by whole genome sequencing revealed key mutations for positive amino acid production in *V. natriegens*.

Second, we used TF-based biosensors to investigate novel evolutionary engineering strategies. Evolutionary engineering is a proven and powerful method to improve the performance of microbial producer strains. However, it is typically not possible to directly apply it to increase production of industrially interesting molecules, due to the lack of an appropriate selection regime. To address this problem, we used TF-based biosensors to couple production to growth. More specifically, the growth rate of *C. glutamicum* was coupled to the intracellular concentration of L-valine, L-leucine, L-isoleucine and L-methionine. This was enabled by integrating a synthetic regulatory circuit, based on the TF-based biosensor Lrp, upstream of two growth-regulating genes, *pfkA* and *hisD*. Using these strains, selection for mutants with increased growth rates should theoretically lead to the selection of mutants with increased production. Modeling and experimental data showed that evolutionary strategies based on spatial separation were required to limit the selection of 'cheater' cells that escaped the evolutionary pressure. This was achieved by an agar-plate based selection strategy, which enabled the high-throughput isolation of amino acid producing clones that showed a stable production phenotype during repetitive cultivations. Whole genome sequencing of the obtained L-valine producing mutants highlighted the acetohydroxyacid synthase (AHAS) as a mutational hotspot. Modeling of the AHAS enzyme provided insight into the functional effect of the different mutations.

Finally, we used the construction of TF-based biosensor variants as an application example to demonstrate an automated cloning workflow for *C. glutamicum* rational strain construction. At present, cloning is most often a manual, time-consuming and repetitive process that would highly benefit from automation. Therefore, we designed an automated cloning workflow covering DNA part creation by PCR, DNA assembly by Gibson assembly and transformation into *Escherichia coli* by heat-shock transformation. The key step is an automated conjugation workflow, which enables fast, easy and high-throughput transfer of plasmids from *E. coli* to *C. glutamicum*. Using this approach, we could create and analyse 44 biosensor variants in 8 days, with a minimal amount of manual work required. Analysis of these variants led to the novel insight that Lrp possibly also has repressor functionality.

In conclusion, the work presented in this thesis provides novel insights into the use of TF-based biosensors to improve strain construction workflows, including the development of new producer strains, the improvement of evolutionary engineering strategies, and the transfer from manual to automated laboratory workflows.

2. Scientific context and key results of this thesis

2.1. Industrial biotechnology – taking different approaches towards the same goal

For at least 8,000 years, humans have utilized microorganisms as production tools (Demain et al., 2010; Nielsen and Keasling, 2016). While early applications used microorganisms to make human lives more pleasant, by producing fermented foods and beverages, we now look at microbes to solve important global challenges, such as climate change and renewable production of energy and chemicals. Biotechnology, the research field that covers the application of biology to make product and processes useful to humans, has rapidly developed since the last century, with many breakthroughs in both technological development and biological understanding. This has resulted in the application of microbes in many different processes, to make a wide range of different products including chemicals, biofuels and pharmaceuticals. However, it still takes a lot of time and money (typically 6-8 years and of $50 million) to develop a microbial strain into an industrial workhorse (*i.e.* into a strain that performs at a level that matches industrial requirements) (Nielsen and Keasling, 2016). Over the years, different approaches have been developed to improve the performance of microbial production strains in bioprocesses, which have become distinct disciplines in the field of biotechnology. The key to drastically reduce the time and effort to create new and better bioprocesses is likely in the integration of these disciplines. Therefore, an overall aim of this thesis was to investigate the integration of several strain improvement approaches, which are first introduced below.

The identification and isolation of microorganisms with the goal to find potential producer strains started at the beginning of the previous century, when the first non-food and beverage bioprocesses were developed. Examples are the mixed production of acetone, butanol and ethanol by *Clostridium acetobutylicum* (attributed as the first process in industrial biotechnology) (Weizmann, 1919), the production of citric acid by *Aspergillus niger* (Currie, 1917), and the production of glycerol by yeast (Demain et al., 2010; Nielsen and Keasling, 2016). The most famous bioprocess is probably the production of penicillin, first by *Penicillium notatum*, which sparked a revolution in the fight against infectious diseases (Demain et al., 2010). Using bacterial cultivation and isolation techniques, researchers were able to identify microbes that naturally produced detectable amounts of a certain molecule or set of molecules of interest, which could be exploited for industrial and/or medical use. While many microbial species have since been discovered and used for the production of (novel) molecules, we have barely scratched the surface of the microbial diversity waiting to be explored. For example, *Streptomyces* species alone are estimated to produce more than 150,000 different bioactive compounds (Watve et al., 2001). Furthermore, different microbes can feature characteristics that are desirable in an industrial setting, such as stress tolerance, the ability to grow on a wide range of substrates or at elevated temperatures. Therefore, the identification and development of novel microbial producer strains is important, and would benefit from methods to speed up this process.

While finding a natural producer is a good starting point for a production process, improvement of strain performance is often possible and required. The key performance indicators for a microbial bioprocess are the titer (final product concentration), rate (speed of production) and yield (amount of production obtained per amount of substrate used), sometimes shortened to TRY (Nielsen and Keasling, 2016). The required numbers for these parameters are dictated by the process economics and vary widely per product. Strain improvement looks specifically at engineering of the microbe to increase process performance. The oldest techniques for strain improvement utilized a process that is responsible for every biological development in nature: evolution. Evolution is arguably the most important concept in biology, as “nothing in biology makes sense except in the light of evolution” (Dobzhansky, 1973). However, next to its importance in understanding biology, it is also a ‘tool’ that can be applied to improve microbial strain performance under process relevant conditions. Due to the

short generation time of microbes (which can be almost 1 million times shorter than that of humans; *i.e.* comparing 10 minutes to 18 years), occurrence and selection of variants with improved properties is possible within a feasible timeline. Over time and with growth, bacteria obtain mutations at a certain rate, which can also be increased artificially, for example by adding a mutagen (a chemical which causes modifications of DNA) or by UV radiation. By testing the properties of evolved cells, mutants with better performance can be identified and isolated, and this process can then be repeated starting from the preferred strain. The potential of evolution for strain improvement is very well demonstrated with the increase of penicillin production by *Penicillium chrysogenum*. By performing iterative cycles of mutagenesis and screening, production was more than 10,000-fold increased (Nielsen and Keasling, 2016; Thykaer and Nielsen, 2003). Evolution has been successfully applied already in the early days of strain improvement because it allows for a 'black box' approach to microbes. It is not necessarily required to know about the inner workings of the cells, as long as you can screen or select for strains with enhanced properties. Finding such a 'selectable output' is the main challenge in evolutionary engineering. Especially challenging is the selection of cells with higher production of an inconspicuous, non-growth coupled molecule, which does not provide a survival advantage for the cell under any cultivation condition. Unfortunately, this type of molecule is often exactly what we want to produce. While the penicillin story demonstrates the power of evolution, it did take multiple years and a lot of effort (and money) to obtain better producer strains. Therefore, there is a large need for methods that can couple the production of molecules to an easily selectable output, to speed up the strain development process.

Strain improvement strategies were further expanded with the advancement of molecular cloning tools, which was driven by key developments such as the solving of the DNA structure (Crick and Watson, 1953), the discovery of restriction enzymes (Smith and Welcox, 1970) and the establishment of polymerase chain reaction (PCR) and DNA sequencing (Cameron et al., 2014). These developments helped to increase our understanding of biology, which in turn led to the discovery of novel biological systems that could be refined into biological tools. We need the products of biology to engineer biology. Biological systems that have been adapted for engineering use are ubiquitous and ever increasing. Early examples are the use of plasmids for gene (over)expression and to facilitate genomic modifications, enzymes such as thermo-stable DNA polymerases used in PCR, restriction enzymes and ligases for cloning (Sambrook et al., 2001), and more recently the use of CRISPR systems to speed up strain development (Jinek et al., 2012). In many cases, molecular cloning tools have been applied for 'targeted' or 'rational' modification of the DNA sequence, which is in contrast to the 'untargeted' approach of mutagenesis, screening and selection. One important advantage of rational strain engineering over evolutionary engineering is the possibility to design and express genes that enable the production of molecules that are not natively produced by the host microbe. An early example is the expression of genes in *E. coli* to make human insulin (Goeddel et al., 1979), a more recent example the production of the antimalarial drug artemisinin by *Saccharomyces cerevisiae* (Paddon et al., 2013). With an increased understanding of biology also came the realization that biology is incredibly complex, and targeted engineering approaches are still mostly *ad hoc* and take a long time to develop. Therefore, the available microbial toolbox should be improved further, and be applied to develop novel producer strains and design novel evolutionary engineering strategies.

Finally, for most of its history, the development of microbial strains has been a manual process. Most of the laboratory work is done by people, especially in academic laboratories. This is in large contrast to other engineering disciplines, such as the automotive industry, in which people have been largely replaced by robots. In biotechnology, laboratory automation has many benefits for strain development, including time and cost savings due to optimization and miniaturization, less manual errors and a general increase in quality and quantity (Appleton et al., 2017a; Hillson et al., 2019;

SYNTHACE, 2018). A recent, global movement to speed up the transition to laboratory automation in biotechnology has been the development of biofoundries (Hillson et al., 2019), which aim to transfer complete strain engineering workflows to robotic systems. Still, after a century of manual biotechnology, there have been many methods developed for manual use, which have to be transferred to lab robots. Thus, efforts are required to increase and develop the use of laboratory automation, which promises an overall improvement of the strain development process, by decreasing the required time and costs and improving the throughput.

Key topics of this thesis

To speed up the transition of our current economy to a sustainable bioeconomy, an integrated, multidisciplinary approach should be taken to biotechnology, using the available engineering toolbox, the power of evolution and the rapidity of lab automation to both improve production strains and to develop new ones. In this thesis, steps towards this goal are investigated. In particular, the aim is to:

i) Apply transcription factor-based biosensors to develop *Vibrio natriegens*, an emerging biotechnological host, towards a producer strain
ii) Apply transcription factor-based biosensors to create synthetic regulatory circuits coupling amino acid production to growth in *Corynebacterium glutamicum*, thereby creating novel ways to use evolutionary engineering for strain improvement;
iii) Integrate a molecular cloning workflow for targeted engineering of *C. glutamicum* on a robotic platform, to create and characterize multiple transcription factor-based biosensor variants.

The application of transcription factor(TF)-based biosensors forms an integral part of this thesis, and an overview of their development and application is introduced in the next section.

2.2. Biosensors

2.2.1. The need for sensors

Biological sensors are essential to all forms of life; just imagine how you would survive without the ability to see, hear, smell, feel and taste. Sensing is also essential in the microbial sphere, and microorganisms have evolved a wide array of systems to interact with their environment. Furthermore, sensing is not limited to interactions with the extracellular space; on the intracellular level an intricate system of sensory circuits is required by cells to maintain homeostasis. The term 'biosensor' can therefore cover a wide range of different biological systems that vary in complexity and purpose. This has resulted in their application as biological tools for different objectives, such as the use of whole cell biosensors to detect environmental pollution (Roggo and van der Meer, 2017), the design of medical biosensors (Kojima et al., 2020), and the development of intracellular sensors that can detect light, temperature, osmolarity, and specific molecules (Schallmey et al., 2014; Zhang and Keasling, 2011). Covering all biosensors and their applications is beyond the scope of this thesis. Therefore, the focus will be on the use of genetically encoded biosensors for microbial strain development, with an emphasis on TF-based biosensors.

For microbial strain development, sensors are also essential, as they are needed to measure strain performance and to determine if one strain is better than the other. Many non-biological methods are used for this purpose, such as optical density measurements as an indicator of growth and pH-probes for measuring acid production. To measure production of specific molecules, methods such as high pressure liquid chromatography (HPLC), gas chromatography (GC) and mass spectrometry (MS) are frequently used (Lin et al., 2017). However, a problem with these methods is the available throughput. Nowadays it is possible to generate a large amount of strain variants very quickly, using

the different strain engineering methods described previously. This places the bottleneck on the characterization of this strains, and methods to increase the throughput are required (Dietrich et al., 2010; Lin et al., 2017). Genetically encoded biosensors enable the high-throughput detection of molecules of interest, and different biosensor systems have been implemented to improve the strain optimization process. Frequently used genetically encoded biosensor systems can be divided into three main classes; sensors based on RNA-aptamers (riboswitches), sensors based on Förster resonance energy transfer (FRET) and sensors based on transcription factors (TF-based biosensors) (Figure 1A) (Lin et al., 2017; Zhang et al., 2015).

RNA-aptamer-based biosensors are based on the conformational change of the RNA secondary structure upon ligand binding (Figure 1A). For example, binding of a ligand can change the structure to enable translation of the RNA molecule, resulting in a detectable output (*e.g.* expression of a fluorescent protein) (Lin et al., 2017).

FRET-based sensors typically consist of two fluorescent proteins that are connected by a ligand binding domain (Lin et al., 2017; Steffen et al., 2016) (Figure 1A). The fluorescent proteins are chosen as such that the emission wavelength of one is the excitation wavelength of the other. Thus, when the two proteins are in close proximity, excitation of the first protein will lead to a cascade reaction where emitted light of the first protein excites the second fluorescent protein, which finally emits light at its specific emission wavelength. The key factor modifying the measured output is the proximity of the two proteins, which is altered by substrate binding at the ligand binding domain. Thus, depending on ligand binding, the measured ratio of the emission wavelengths from the first and second protein will change (Steffen et al., 2016).

TF-based biosensors are based on transcription factors, which are proteins that bind to DNA to modulate the expression of one or multiple genes (Lin et al., 2017; Mahr and Frunzke, 2016) (Figure 1A). Ligand binding can result in a conformational change in the transcription factor, which can lead to either an increase or decrease of expression. By changing the expressed gene (*e.g.* to one encoding a fluorescent protein), the concentration of a particular ligand of interest can be coupled to a measurable output. TF-based biosensors are one of the most common biosensor types used for strain improvement, and multiple different TF-based biosensors have been developed in the past years (Mahr and Frunzke, 2016).

2.2.2. Transcription factor-based biosensors

Bacterial transcription factors played a key role in our understanding of bacterial regulatory circuits, as the studies of Francois Jacob and Jacques Monod on the *lac* operon and the LacI transcription factor led them to postulate how bacteria use regulatory circuits to interact with their environments (Jacob and Monod, 1961). Transcription is carried out by the RNA polymerase, but the rate of transcription initiation, elongation and termination is controlled by transcription factors. Transcription factors can function as an activator or as a repressor of their respective target genes (Figure 1A). While regulation of transcription is complex and based on multiple different types of transcription factors (Browning and Busby, 2016), there are transcription factors that are very specific in both their ligand and DNA binding. These TFs represent key targets for TF-based biosensor development. In natural systems, the binding of a ligand to a transcription factor usually results in the increased or decreased expression of a gene or set of genes encoding proteins that modify the concentration of the ligand. Examples are the increased expression of genes encoding a catabolic pathway, to metabolize the ligand (Schleif, 2000), or the increased expression of genes encoding an exporter for the ligand, to prevent accumulation of toxic ligand concentrations (Lange et al., 2012). Due to the modularity of transcription factor-based gene expression (*i.e.* the separation of transcription factor, cognate promoter and target

gene), it is usually relatively easy to change the target gene into a reporter (*e.g.* a gene encoding a fluorescent protein), thereby creating a useable biosensor.

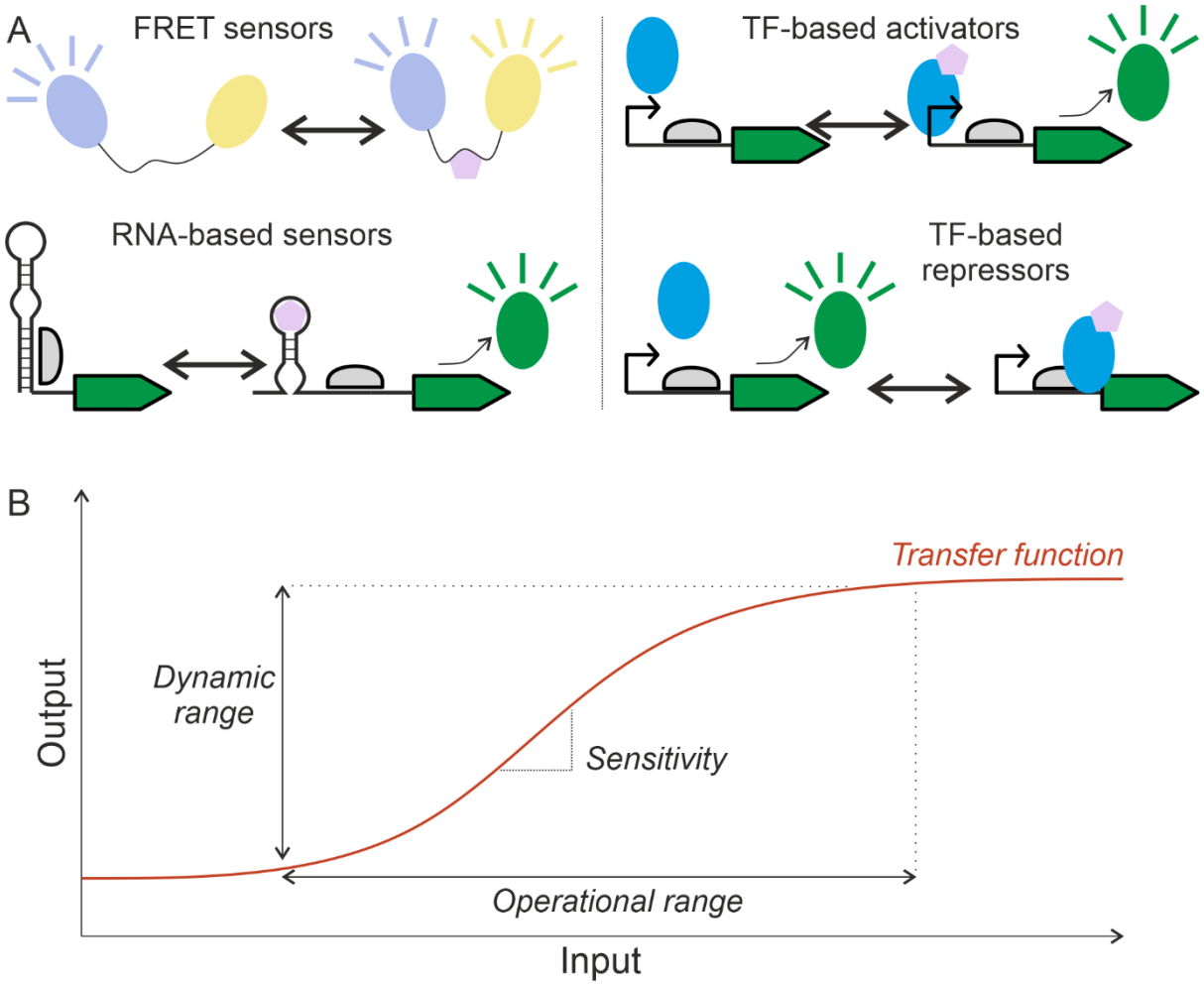

Figure 1: Schematic overview of main classes of biosensors used for microbial strain improvement and their most important characteristics. *A) Förster resonance energy transfer (FRET) biosensor, RNA-aptamer-based biosensor and transcription factors (TF)-based biosensors, showing output signal in absence (left of arrow) and presence (right of arrow) of ligand binding; fluorescent proteins are shown as oval shapes, colored cyan, yellow or green, transcription factors are shown as blue oval shapes, ligands are shown as pink pentagons, and ribosomal binding sites are shown as grey half-ovals. B) Typical biosensor input-output relationship, highlighting derived parameters.*

TF-based biosensors have been developed for the detection of a variety of different molecules, including amino acids (Binder et al., 2012; Chou and Keasling, 2013; Mustafi et al., 2012), co-factors such as NADPH (Siedler et al., 2014), organic acids (Dietrich et al., 2013), aromatics (Chou and Keasling, 2013; Raman et al., 2014), fatty acids (Zhang et al., 2012) and antibiotics (Lin et al., 2017; Mahr and Frunzke, 2016). They have been applied to analyze the concentration of intracellular metabolites during growth. This enables the monitoring of product formation in a culture in time and the detection of differences in intracellular metabolite concentration in homogenic cultures (Kiviet et al., 2014; Mustafi et al., 2012, 2014; Rogers and Church, 2016). Furthermore, they have been applied to screen and select for enzymes or cells with improved properties. For example, a biosensor that couples metabolite concentration to expression of a fluorescent reporter can be used in combination with fluorescence activate cell sorting (FACS). High-throughput sorting of the most fluorescent cells in a populations can subsequently lead to the isolation of strains or enzymes with improved properties (Binder et al., 2012; Mahr et al., 2015; Schendzielorz et al., 2014). This is further discussed in Section

2.3 and Chapter 3.3. Another way to select cells using biosensors is by coupling production to expression of genes conferring a fitness advantage under specific cultivation conditions, such as genes encoding antibiotic resistance (Dietrich et al., 2013; Leavitt et al., 2017; Raman et al., 2014; Snoek et al., 2018). Biosensors have also been applied to couple intracellular metabolite concentration to expression of genes encoding enzymes of metabolic pathways, which has been used to dynamically regulate pathway expression based on the concentration of a toxic intermediate (Dahl et al., 2013), or to maintain production in producer strains by coupling product concentration to expression of an antibiotic resistance marker (Xiao et al., 2016), or to expression of an essential gene (D'Ambrosio et al., 2020; Rugbjerg et al., 2018). Strategies to use biosensor-based regulatory circuits to couple production to growth, which allows for selection of improved producers based on their growth rate, is discussed in Section 2.4 and Chapter 3.2.

To describe the performance of a biosensor, several parameters are frequently used, which are operational range, dynamic range, sensitivity, specificity and the transfer function (Figure 1B) (Dietrich et al., 2010). The operational range describes the range of ligand concentrations in which the sensor is functional (*i.e.* a change in ligand concentration results in a change of sensor output). The dynamic range describes the difference between the highest and lowest sensor output. The sensitivity describes the relationship (the slope) between a change in ligand binding and the change in output (*i.e.* a very sensitive sensor shows a large difference in output upon a small difference in ligand binding, and vice versa). Specificity describes if the sensor binds only one specific molecule, or a set of (related) molecules. The transfer function describes the complete relation between ligand binding and sensor output within the operational range (*i.e.* this can be visualized as the 'curve' indicating the sensor signal in a graph in which ligand binding versus sensor output is plotted; Figure 1B). The parameters of a transcription factor have been shaped by evolution to be optimal for their physiological function in their native host. For biotechnological use, the sensor parameters can often be improved for the desired application. Several strategies for sensor modification have been shown, and are further discussed in Section 2.5, and Chapter 3.4.

TF-based biosensors can be used in their native host (*i.e.* the species that naturally expresses this transcription factor), or transferred to other hosts (Skjoedt et al., 2016; Sonntag et al., 2020). To realize the orthogonal transfer of a biosensor, modifications of the sensor-construct are often required, such as a different expression vector (plasmid backbone) and the use of a promoter upstream of the transcription factor that is functional in the heterologous host. Several TF-based biosensors have been modified for expression in non-native hosts, which is further discussed in Section 2.3, and Chapter 3.3.

2.2.3. The Lrp and LysG biosensors of *Corynebacterium glutamicum*

For the studies described in this thesis, two previously established biosensors were used that are based on the amino acid-responsive transcription factors Lrp and LysG of *C. glutamicum*. Lrp is a transcriptional activator of *brnFE*, encoding a two-component export system for L-methionine and branched chain amino acids (Lange et al., 2012). LysG is a transcriptional activator of *lysE*, which encodes a basic amino acid exporter (Bellman et al., 2001). In *C. glutamicum*, the transcription factors are critical parts of self-contained detoxification systems. Increase in intracellular amino acid concentration leads to more binding of those amino acids to Lrp or LysG. This in turn increases the expression of the Lrp or LysG target genes, which encode amino acid exporters. The exporter expression finally leads to a decrease of the intracellular amino acid concentration, which in turn leads to a decreased expression of the exporter system. Hereby, accumulation of high intracellular amino acid concentrations is prevented, while amino acids are not exported at low intracellular concentrations.

The Lrp-based biosensor was developed by placing *eyfp*, encoding the fluorescent reporter eYFP, downstream of the Lrp cognate promoter (*i.e.* the *brnFE* promoter) (Mustafi et al., 2012). The sensor was shown to be sensitive to L-valine, L-isoleucine, L-methionine and L-leucine (Mustafi et al., 2012). The Lrp biosensor has been applied for online monitoring of amino acid production, and to visualize differences in intracellular amino acid concentration between isogenic cells (Mustafi et al., 2014). Furthermore, the Lrp sensor was used in adaptive laboratory experiments. After expression of the Lrp sensor in the L-valine producing strain *C. glutamicum ΔaceE*, iterative FACS of the most fluorescent cells resulted in the isolation of a mutant with showed improved L-valine production and decreased production of the by-product L-alanine (Mahr et al., 2015).

The LysG-based biosensor was developed by placing *eyfp* downstream of the LysG cognate promoter (*i.e.* the *lysE* promoter) (Binder et al., 2012). The sensor was shown to be sensitive to L-histidine, L-arginine and L-lysine (Binder et al., 2012). The LysG biosensor has been used in mutagenesis and screening experiments, where a library of mutants was first created, and single cells with a high fluorescence were sorted and characterized (Binder et al., 2012). Mutants that produced increased amounts of L-lysine and L-arginine were obtained. Furthermore, the LysG sensor has also been used for the high-throughput screening of enzyme variants, for example for MurE and ArgB libraries (Binder et al., 2013; Schendzielorz et al., 2014).

Both the Lrp and LysG biosensor have been used in studies investigating microbial production of amino acids. Amino acid production is a billion dollar business, and almost all amino acids are industrially produced by microbes (Becker et al., 2018; Becker and Wittmann, 2012). High volume products are L-glutamate, which is used as a human food supplement in the form of monosodium glutamate (MSG), and L-lysine, which is used as a food supplement for animals, together with L-threonine, L-tryptophan and L-methionine (Eggeling and Bott, 2015). Thus, the improvement of microbial amino acid production process is commercially very interesting.

2.3. Using transcription factor-based biosensors to develop novel microbial hosts

According to recent estimates, earth might be home to one trillion (10^{12}) microbial species (Locey and Lennon, 2016). Up to now, we obtained only a relatively small fraction of that number of species in pure cultures, and only a minuscule proportion has been developed into production hosts. A few species can be regarded as major microbial workhorse in biotechnology, including *E. coli* (Theisen et al., 2017), *S. cerevisiae* (Diethard et al., 2017) and *C. glutamicum* (Becker and Wittmann, 2016). Due to decades of research, they are used in a variety of industrial processes, and almost all molecular tools which have been developed so far have been adapted to these model hosts. Still, there are many other species that might have characteristics that are industrially interesting. The development of such novel strains would benefit from the toolbox that is already available for established hosts. In this thesis, we investigated the transfer of the Lrp and LysG biosensors of the established industrial workhorse *C. glutamicum* to the potential novel industrial workhorse *V. natriegens*. The results are described in this section after a short introduction of both microorganisms.

2.3.1. *Corynebacterium glutamicum*

C. glutamicum is an established industrial workhorse that is used in multiple industrial processes (Becker et al., 2018). It was first isolated in 1957 for its ability to secrete L-glutamate, but has since been engineered to produce a wide range of different products, including other amino acids, proteins, organic acids, plastic precursors and aromatics (Becker et al., 2018; Eggeling and Bott, 2005; Kinoshita et al., 1957). Due to its research history spanning more than 60 years, enough knowledge on *C. glutamicum* is available to fill entire books (Eggeling and Bott, 2005), and only a limited overview can be given here. The original isolate was named *Micrococcus glutamicus*, and many other L-glutamate

producers have been isolated that were originally classified in different genera (*e.g. Brevibacterium*, *Microbaterium* and *Arthrobacter*). A later revision, however, reclassified all of them as *C. glutamicum* (Becker and Wittmann, 2016; Eggeling and Bott, 2005). The genus name *Corynebacterium* originates from the Coryneform (club-like) shape that these bacteria show in some phases of their growth, and *glutamicum* refers to the production of L-glutamate (Eggeling and Bott, 2005).

C. glutamicum is a nonmotile, Gram-positive, facultative anaerobic soil bacterium that is able to grow on different substrates, including a variety of carbohydrates, organic acids and alcohols (Becker and Wittmann, 2016; Eggeling and Bott, 2005). *C. glutamicum* is non-pathogenic and has the GRAS (generally regarded as safe) status. The genome of the WT strain *C. glutamicum* ATCC 13032 was published in 2003; it contains about 3000 genes located on one single chromosome (Kalinowski et al., 2003). A comprehensive overview of its metabolome is available, including information about regulation (Becker et al., 2018; Pfeifer-Sancar et al., 2013; Schröder and Tauch, 2010).

C. glutamicum has multiple properties that make it a good production host, including growth to high cell densities, a high biomass specific production rate and a relatively good resistance to stress. It is relatively resistant to shear stress, oxidative stress (due to high catalase expression), high osmotic pressure and moderate changes in pH and temperature (Becker and Wittmann, 2016; Eggeling and Bott, 2005; Lee et al., 2016). Shortly after its discovery and isolation, industrial production processes were established with *C. glutamicum*. Following establishment of initial bioprocesses for the production of L-glutamate, and quickly afterwards L-lysine, *C. glutamicum* strains were developed that produced all essential amino acids except for L-methionine (Becker and Wittmann, 2016). This was already achieved in 1978. With the development of the genomic engineering toolbox, *C. glutamicum* was further applied for the production of more amino acids, diamins, vitamis, terpenoids, organic acids, polymer precursors, alcohols and proteins (Becker et al., 2018). A large number of molecular tools are available, including expression plasmids, integration vectors for genomic modification, a set of inducible and constitutive promoters, and TF-based biosensors (Baritugo et al., 2018; Becker et al., 2018; Wendisch, 2014). However, genome engineering of *C. glutamicum* is still rather time-consuming, especially in comparison to microbes such as *E. coli* and *S. cerevisiae*. This is mainly due to *C. glutamicum*'s rigid cell wall lowering DNA uptake, and difficulties in establishing modern engineering tools based on CRISPR. While several CRISPR systems have been described for use with *C. glutamicum*, including CRISPR/Cpf1 (Jiang et al., 2017) and CRISPRi (Cleto et al., 2016), their application is not yet widespread. Therefore, *C. glutamicum* would benefit from methods to speed up genomic engineering, which are discussed in Section 2.5 and Chapter 3.4 of this thesis.

2.3.2. *Vibrio natriegens*

While the marine bacterium *V. natriegens* was isolated around the same time as *C. glutamicum*, it was not developed into an industrial strain. First described in 1958, as 'isolate M11' living in marsh mud in Sapelo Island (Georgia, USA), it was originally identified as a member of the *Pseudomonadales* (which is now classified as an order of Gammaproteobacteria), mainly based on the presence of a single, polar flagellum (Payne, 1958). The epithet *natriegens* was given because it requires sodium to grow ('*natrium*' meaning sodium, and '*egens*' to need) (Payne, 1960; Payne et al., 1961). After changing its classification a couple of times, it was finally categorized as a *Vibrio* (Austin et al., 1978; Baumann et al., 1971; Hoff et al., 2020; Payne et al., 1961; Webb and Payne, 1971). With some intervals, some studies on *V. natriegens* have been described. However, only since roughly five years has there been a surge in interest to develop it into a novel microbial workhorse. Still, the available knowledge is inferior to that available on *C. glutamicum*, which is exemplified by the timing of the first reviews on *V. natriegens*, which were published from 2020 (Hoff et al., 2020; Thoma and Blombach, 2021).

V. natriegens is a non-pathogenic, Gram-negative, slight halophile with a high nutrient versatility, able to grow on a wide variety of carbohydrates and organic acids (Baumann et al., 1971; Payne, 1958). It is a facultative anaerobe that does not produce gas under anaerobic conditions, is able to use nitrate as an electron acceptor and store polyhydroxybutyrate (PHB) as an internal storage compound (Baumann et al., 1971). The genome of *V. natriegens* was first sequenced in 2013 and consists of two chromosomes, which were predicted to contain approximately 4700 genes (Maida et al., 2013; Wang et al., 2013).

V. natriegens most characteristic property is its unrivaled growth rate, with a reported doubling time under 10 minutes (Eagon, 1962; Hoffart et al., 2017). This very fast doubling time requires high protein production, which was shown to be facilitated by high ribosome numbers (Aiyar et al., 2002). Efforts are currently underway to leverage the high doubling time to shorten standard molecular biology processes (Weinstock et al., 2016). *V. natriegens* was shown to be a potential production host for next generation biotechnology, due to having a very high biomass specific substrate consumption rate (q_s), which was at least two fold higher than that of *Escherichia coli*, *Pseudomonas putida*, *Corynebacterium glutamicum* and yeast, under both anaerobic and aerobic conditions (Hoffart et al., 2017). Also, an increase in anaerobic alanine production was shown by deletion of several genes (Hoffart et al., 2017). Furthermore, *V. natriegens* high capacity for translation makes it an attractive platform for cell free protein production (Des Soye et al., 2018; Failmezger et al., 2018; Wiegand et al., 2018). While initial progress on the development of *C. glutamicum* was relatively slow due to the lack of available tools at the time of its initial development, *V. natriegens* can benefit from current knowledge and tools that can be transferred from other microbes. Several studies have contributed to improving the available toolbox for engineering *V. natriegens*, describing protocols for transformation (Dalia et al., 2017; Weinstock et al., 2016), characterization of genetic parts and tools (*e.g.* promoters, plasmids) (Tschirhart et al., 2019), use of CRISPRi (Lee et al., 2019), first developments of a production platform strain (Pfeifer et al., 2019) among others (Hoff et al., 2020; Thoma and Blombach, 2021). This has led to the comparably quick development of *V. natriegens* strains for the production of L-alanine (Hoffart et al., 2017), poly-β-hydroxybutyrate (Dalia et al., 2017), 2,3-butanediol (Erian et al., 2020), melanin (Wang et al., 2020), violacein and β-carotene (Ellis et al., 2019).

Development of *V. natriegens* into different production strains could be accelerated with TF-based biosensors. Therefore, we aimed to establish TF-based biosensors in *V. natriegens*. In particular, we chose to express two biosensors from *C. glutamicum*, based on LysG and Lrp, which were previously introduced. The results of this work form part of this thesis (Chapter 3.3) and are summarized below.

2.3.3. Expression of TF-based biosensors in *V. natriegens* to increase amino acid production

Expression of the LysG-based and Lrp-based biosensors from *C. glutamicum* in *V. natriegens* required some modification of the sensor sequences (Figure 2A). First, the plasmid backbone was changed, since the original pJC1 vector is based on kanamycin resistance, which is not recommended for *V. natriegens* due to its natural resistance to this antibiotic (Hoff et al., 2020). Instead, the pBR322 backbone was used, which was originally developed for *E. coli* (Bolivar et al., 1977). Second, the native promoters upstream of *lysG* and *lrp* are not likely to be active in *V. natriegens*, since *V. natriegens* and *C. glutamicum* are not closely related (belonging to Proteobacteria and Actinobacteria, respectively). A library of promoters from the Anderson promoter library were used (Anderson, 2006), which where shown to be active with different strength in *V. natriegens* (Stukenberg et al., 2021; Tschirhart et al., 2019), creating a series of sensor variants (Figure 2A). Furthermore, a ribosomal binding site (RBS) active in *V. natriegens* and a linker sequence were added to the gene sequences, to facilitate translation in *V. natriegens*. All sensor variants were tested for their output in *V. natriegens* cultures supplemented with the effector amino acids (*i.e.* L-lysine, L-histidine and L-arginine for LysG, and L-

methionine, L-leucine, L-isoleucine and L-valine for Lrp). Only for the LysG sensor-variants induced with L-lysine, a clear difference between background and induced expression was observed and a dose-response relationship could be established (Figure 2B)

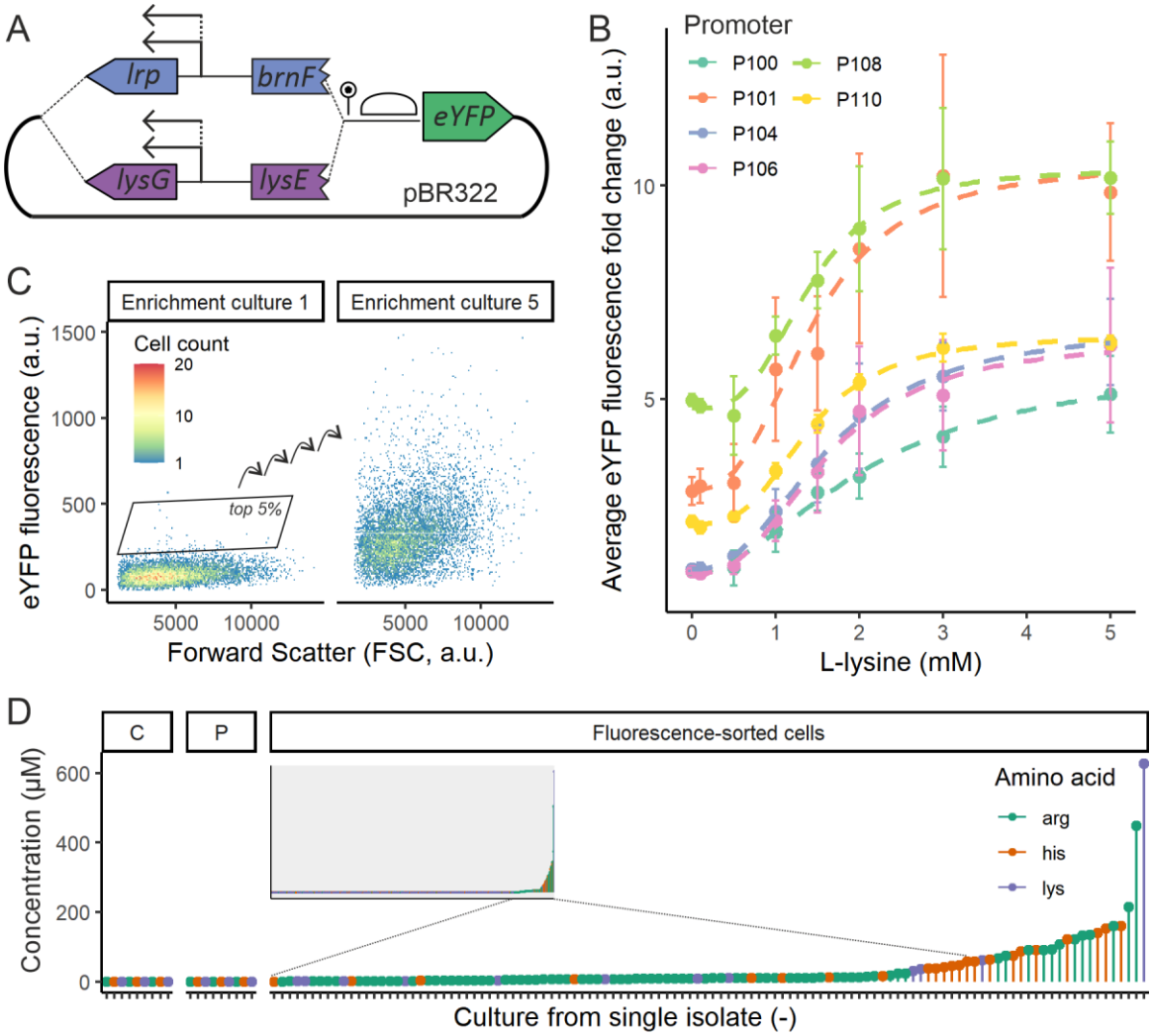

***Figure 2: Design and expression of two transcription factor-based biosensors in* V. natriegens** *(Adapted from Chapter 3.3) A) Schematic overview of LysG and Lrp biosensor design for expression in* V. natriegens*. Different sensor variants were created using promoters from the Anderson promoter library to express* lrp *or* lysG*. B) Dose-response signal of the LysG based biosensor variants and L-lysine. A Hill-curve was fitted to the measured values. For all fluorescence measurements, fluorescence per cell of 10.000 cells per culture were measured and averaged, and fold change over background was calculated. Average and standard deviation of three cultures are shown (n = 3). Promoters from the Anderson promoter library are shown as abbreviations (P100 = J23100, etc.). C) FACS scatterplots showing distribution of single cells treated with 3.0 g l^{-1} MNNG for the first and final enrichment culture (n=10000). D) Overview of amino acid production of single isolates. C denotes control strain (non-MNNG treated, main population sorted), P denotes parental strain. Small frame shows amino acid concentrations of all fluorescence-sorted cells, selection shows strains for which more than 10 µM extracellular amino acid was measured.*

The absence of LysG biosensor output in cultures induced with L-histidine and L-arginine can not be readily explained, as *V. natriegens* is able to take up and grow on these amino acids (Baumann et al., 1971; Ellis et al., 2019). However, it is possible that uptake is low in presence of glucose, as catabolite repression is a common regulation mechanism in bacteria, which should be further investigated for *V. natriegens*. The absence of Lrp biosensor output could also be due to amino acid uptake problems, but it is also possible that *lrp* was not correctly transcribed or translated in *V. natriegens*, or that it

could not induce expression of its cognate promoter. Since the upstream promoter was similar for *lrp* and *lysG* in the biosensors, and both genes have a similar GC content, it is unlikely that transcription of *lrp* was problematic. Since LysG was successfully expressed, it is also unlikely that translation was not possible for Lrp. Furthermore, some differences in fluorescence output were measured between the different sensor variants featuring promoters with different strengths, which suggest that Lrp was expressed but expression of its target genes was not induced by effector binding. Therefore, the most likely problem is in the promoter binding and the modification of transcription output in relation to effector binding, in *V. natriegens*. Multiple studies report the successful transfer of a transcription factor from one species to another (Lin et al., 2017; Mahr and Frunzke, 2016; Skjoedt et al., 2016; Sonntag et al., 2020), but no clear information is available on what determines if a transcription factor will function in the new host or not. When the transcriptional activator BenM from *Acinetobacter* sp. ADP1 was expressed in the yeast *S. cerevisiae*, specific placement of the BenM operator site in a modified yeast promoter was required to obtain a functioning sensor (Ambri et al., 2020). Construction of such hybrid promoters might improve sensor functioning in non-native host, but this is complicated for Lrp since it has no clear operator sequence (Lange et al., 2012). Future studies could look into the direction of creating more different Lrp biosensor variants for expression in *V. natriegens*, using methods further described in Section 2.5.

To demonstrate the application of TF-based biosensor for the development of (novel) host strains, we continued with the P106-LysG biosensor (Figure 2B) and subjected the sensor strain to a mutagenesis and screening protocol to isolate amino acid producing mutants. First, to generate genotypic diversity, a culture carrying the P106-LysG-biosensor was mutagenized with MNNG (N-methyl-N'-nitro-N-nitrosoguanidine) (Adelberg et al., 1965), to create a library of mutants. Second, repetitive FACS of 300,000 of the top 5% fluorescent cells was done (Figure 2C). Each MNNG treated culture showed an upward shift in fluorescence after three to four enrichment steps, and after the fourth enrichment step single cells were sorted on plates for the top 5% fluorescent cells. Cells that formed colonies were grown in microtiter plates and the concentration of extracellular positively charged amino acids was quantified by HPLC measurement (Figure 2D). From 245 measured strains, 37 produced more than 10 µM extracellular amino acids (15%). *V. natriegens* strain were obtained that produced L-lysine, L-arginine and L-histidine.

Whole genome sequencing was performed on the top L-lysine, L-histidine and L-arginine producers to identify causal mutations for the producer phenotype. For the top L-lysine, L-histidine and L-arginine producers, 23, 35 and 23 single nucleotide polymorphisms (SNPs) were identified, respectively. SNPs were found in genes encoding enzymes directly active in amino acid biosynthesis or degradation, and in other pathways related to amino acid metabolism. Examples are a mutation in *gapA* encoding 4-hydroxy-tetrahydrodipicolinate synthase active in L-lysine biosynthesis, a mutation in a gene encoding an agmatine deiminase active in L-arginine degradation, and a mutation in a gene encoding a serine ammonia-lyase, which is linked to L-histidine metabolism via co-factor regeneration (see also Chapter 3.3).

V. natriegens strains producing these amino acids have not been described before, and their isolation shows the strength of TF-based biosensors for the development of novel producer strains. While the FACS-based selection scheme was successful to select *V. natriegens* producer strains, it is relatively complicated to apply. In contrast, screens based on growth, either in liquid cultures or on plates, are more easy to use. To improve the screening and selection of strains, we investigated the differences between such selection schemes, in combination with novel evolutionary strategies based on TF-based biosensors. The results are described in the next section.

2.4. Using biosensors to improve evolutionary strategies

As previously discussed, adopting evolution for strain development is a proven and powerful way to improve the performance of strains. In this section, various aspects of evolution and different evolutionary strategies are investigated first, followed by a discussion of different methods to select for better producer strains. Finally, a novel evolutionary strategy for small molecule production, based on growth coupling in *C. glutamicum* using the Lrp biosensor, is presented.

2.4.1. The theory of laboratory evolution

"Biology is the study of complicated things that have the appearance of having been designed with a purpose" (Dawkins, 1986). It is important to realize this, when studying evolution, because the results of laboratory evolution are not the perfectly designable solution that is desired by the experimenter. Rather, microorganisms will take anything that work under the applied selective pressure, and run with it.

The process we observe as microbial evolution is the combination of two phenomena: first, the imperfect replication of a cell, leading to genomic variation (which is sometimes also due to other factors, such as homologous gene transfer or mobile elements), and second, the differences in fitness of these variants. Biological fitness is defined as a quantitative measure of the contribution of a specific organism or genotype to future generations owing to differential survival, reproduction or both, that is associated with its phenotype (Barrick and Lenski, 2013). Biological fitness is always relative, and depends on the environment of the cell, which includes factors such as nutrient availability, temperature, acidity, and most importantly, other competing microbes. Thus, to influence the outcome of laboratory evolution experiments, scientist can change either the amount or type of variants that are created (*i.e.* by mutagenesis experiments that target the complete DNA sequence or only specific areas), or alter the cellular environment to improve the relative fitness of a certain phenotype (Figure 3). Deciding how this can be done best requires a more detailed understanding of the processes underlying laboratory evolution.

Understanding laboratory evolution experiments requires two 'perspectives': population genetics, which covers the mathematical framework for describing rates of evolutionary change as a function of different processes, and molecular biology, which covers the relation between mutation and phenotype (Barrick and Lenski, 2013). Important fundamental processes of population genetics are mutation rate, genetic drift and selective pressure.

The mutation rate is the rate at which mutations occur in a genome, which is usually given as mutations per cell per division, or mutations per base pair per replication. Historically, there have been two contrasting views on how the mutation rate is influenced (*i.e.* what causes mutations). The first theory states that the mutation rate is dependent on the environment and organisms can actively induce specific mutations to adapt themselves to specific situations. This theory of evolution is known as Lamarckism (Lamarck, 1809). The second theory states that the mutation rate is independent of the environment and mutations happen at random, and due to selection by the environment a mutant with improved characteristics will thrive over his less well adapted competitors. This theory is know as (neo-)Darwinism, and is nowadays generally accepted to correctly describe evolution, in contrast to Lamarckism (Darwin, 1859). Thus, in laboratory evolution, we should assume mutations to be occurring at random and independent of the environment. There are some sidenotes to be made here, as novel insights show that sometimes the mutation rate of bacteria does actually dependent on the environment, as exemplified by prophages (bacterial viruses that are integrated into the genome) that are activated under stressful conditions (Nanda et al., 2015). Nevertheless, the effect of mutations is random, and their effect on biological fitness determines if they will remain in the population. To

design evolutionary engineering experiments, it is therefore appropriate to assume a certain, stable, mutation rate of random mutations.

For bacteria, the mutation rate is typically found to be in the range of 10^{-9} to 10^{-10} per base per replication (Barrick and Lenski, 2013; Drake, 1991; Lee et al., 2012). This is close to the overall error rate of DNA replication, which is the product of errors made by DNA polymerase and the error reducing effect of proofreading and mismatch repair systems (Lee et al., 2012; Maslowska et al., 2018; Schaaper, 1993). Typical mutations induced by DNA replication are point substitution mutations (the substitution of one base for another base). The observation that these occur more frequently than other mutations, such as insertions or deletions, further indicates that replication is the main introducer of variation during laboratory evolution. However, it should be mentioned that some types of mutations, such as integration of mobile genetic element, as well as large scale rearrangements of genomic DNA, are more difficult to identify with current (short read) sequencing technology and are therefore not always accurately reported (Barrick and Lenski, 2013). Furthermore, it is important to keep in mind that these results are from laboratory experiments, in which the replication rates of bacteria are orders of magnitude higher than is typical in nature. Therefore, the contribution of replication errors to the total mutation rate might be way lower in natural environments, while 'horizontal' gene transfer (*i.e.* transfer of genetic information between cells, for example by plasmid conjugation or viral infection) significantly contributes to the generation of diversity in nature (Barrick and Lenski, 2013). Nevertheless, for laboratory evolution experiments these results can be used to estimate a mutation rate, which provides the first important aspect to keep in mind when designing laboratory experiments (Figure 3).

While the occurrence of mutations can be approximated by a certain rate, an understanding of molecular biology is required to relate a mutation to its effect on fitness. Due to the complexity of microorganisms (and all other forms of life), we usually have to rely on causal observations to describe the effect of mutations (*i.e.* we characterize a mutant and compare its phenotype to the non-mutant). Mutations can be categorized as beneficial, neutral and deleterious (sometimes lethal). Again, it is important to realize that this is always in relationship to the environment. Mutations that are beneficial under laboratory conditions are not likely to be beneficial under natural environments, as microbes have been adapted to their natural environment by million years of evolution, which is very different from the laboratory environment. Furthermore, mutations can be described by their effect on cellular function. Small scale mutations, such as point substitution mutations and insertions or deletions of a few nucleotides, can either occur in non-coding or coding regions of DNA (*i.e.* synonymous, frameshift, nonsense and missense mutations). It is sometimes possible to predict the effect of a mutation in protein sequences, for example a nonsense mutation at the start of the sequence will likely prevent the expression of the original protein. Furthermore, for enzymes on which structural information is available, the effect of mutations can be inferred from their location. When they are in the active site, or at a site important for allosteric regulation, they probably affect conversion rates or regulation, respectively. Larger scale mutations, such as amplifications, deletions, or insertions, can lead to disruption of gene sequences, but also to multiple other regulatory effects that are hard to predict. The type of mutation that is required to get a strain with a certain, desired, phenotype is hard (often impossible) to predict. In general, quantitative improvements, such as increased growth rate, can often be obtained by one or more small scale mutations. In contrast, qualitative mutations, such as the consumption of a non-native substrate, often require more complex mutations. This is very well exemplified by the Lenski large long-term evolution experiments, in which 12 parallel cultures of *E. coli* have been grown in glucose-limited minimal salts medium for more than 25 years, with a daily transfer to new media (Lenski, 2017). While mutations to increase the growth rate occurred in all lines, only one obtained a mutation to take up citrate, another nutrient (Blount et

al., 2008). This required a tandem duplication of *citT*, encoding a citrate transporter which is normally only active in the absence of oxygen (Blount et al., 2012). The duplicated copy was under a different promoter, and expressed in the presence of oxygen. To specifically induce certain types of mutations, a plethora of methods have been designed (Simon et al., 2019), such as addition of a mutagen (Adelberg et al., 1965), but also more targeted methods such as MAGE (Wang et al., 2009) and CRISPR-AID (Ma et al., 2016). For example, CRISPR-AID is a fusion of dCas9 (catalytically dead Cas9) and a cytidine deaminase (AID), which allows for induced mutations at a specific site in the genome (Figure 3). To conclude, it can be very helpful to consider the type of mutation, or the gene that needs to be mutated, when designing a laboratory evolution experiment (Figure 3).

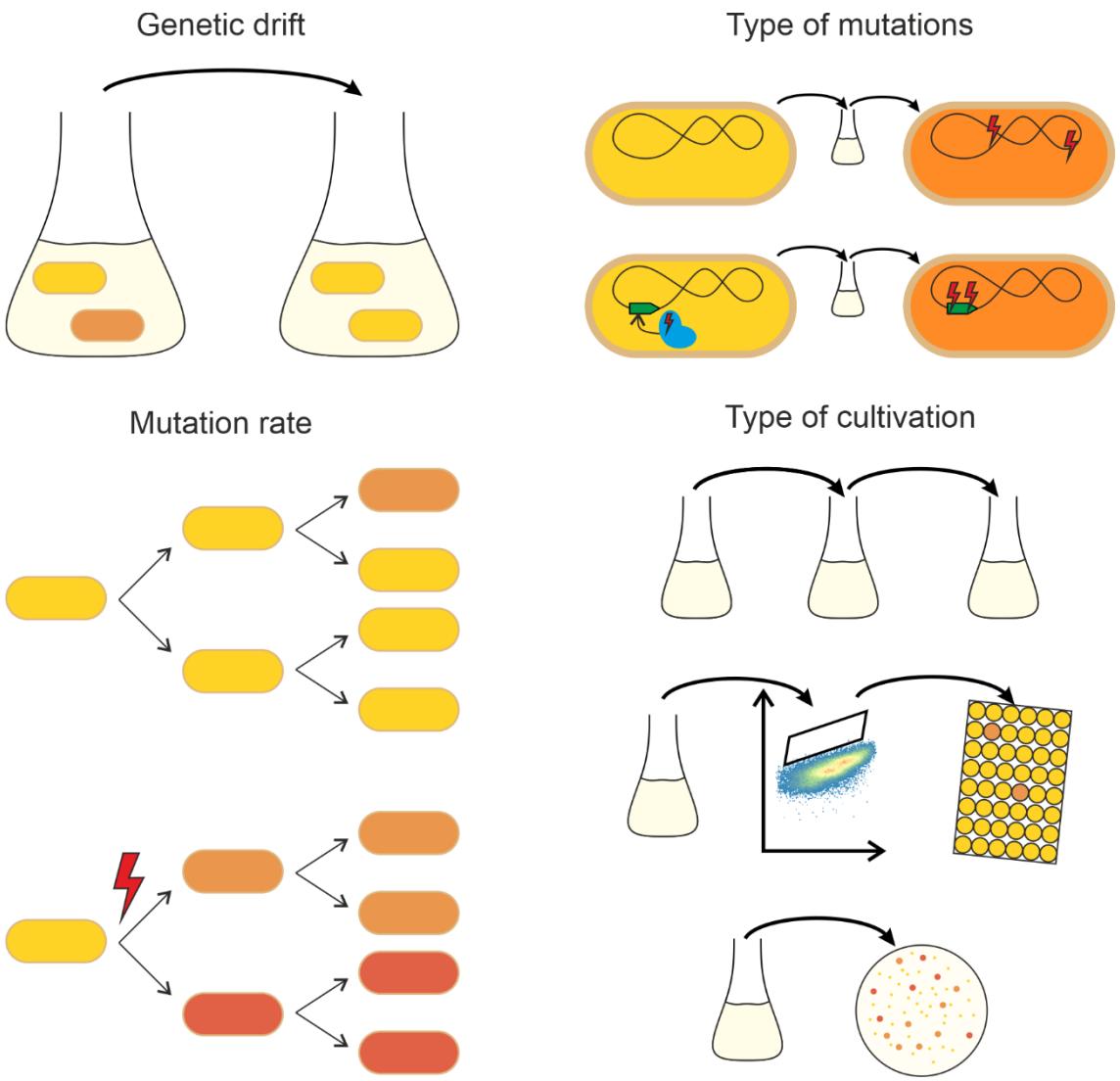

***Figure 3: Overview of important aspects of evolutionary engineering experiments**. Genetic drift demonstrates the loss of mutant cells (colored orange) by sampling. Mutation rate demonstrates the effect of the addition of mutagens on the occurrence of mutant cells (colored orange and red). Type of mutations demonstrates the difference between experiments where mutations occur at random in the genome (top), and experiments where targeted mutation-inducing agents such as CRISPR-AID* (Ma et al., 2016) *are used, which results in mutations occurring most frequently at a specific location. Type of cultivations shows different type of evolutionary cultivation systems, such as liquid cultivations (top), FACS-based selections (middle) and plate-based cultivations (bottom).*

Next to the rate of mutations and their effects, one needs to consider the effects of genetic drift on laboratory evolution experiments. Genetic drift is the effect that random sampling has on the frequency of mutants in a population (Masel, 2011). In typical laboratory evolution experiments, microbes are grown in liquid media or on solid media, starting with a single or a small number of cells, and ending with a number of cells orders of magnitude larger. If a second cultivation is desired, typically a fraction of the final population of the first cultivation is taken to start the next culture with. This can lead to genetic drift: if multiple mutants are present in small fractions in the population, transferring only a small fraction of this culture can lead to the loss of certain variants. This loss is even higher when one considers that microbes grow by doubling, and the effect that this has on mutation occurrence. As previously discussed, we can assume that the mutation rate of a strain is constant during an evolutionary experiment, and during every replication there is only a small chance of a mutation (~10^{-3} per genome per replication). Ergo, if we start a hypothetical experiment with one cell, when it replicates into two cells, the likelihood of a mutation is low, and the same holds for the next couple of replications. When a million cells replicate, the chance of a mutation per cell per replication is still the same, but since the replication is done a million times, there is a high chance that at least some of the cells obtain mutations. Thus, the chance that a mutation event happens is dependent on the amount of cells. Therefore, in lab cultures where cell numbers increase by doubling, most mutation events will happen during the end of the cultivation, since the absolute number of cell duplications is the highest at this point. Thus, genetic drift is an even more important phenomenon in laboratory evolution, because most of the diversity is generated at the final growth stage, but can easily be lost due to genetic drift originating from sampling. Therefore, genetic drift is the third aspect to keep in mind when designing laboratory experiments (Figure 3).

Finally, we come to the 'core' of laboratory evolution, the applied selective pressure. Ultimately, this will decide the outcome of an evolutionary experiment, as "you get what you screen for" (Schmidt-Dannert and Arnold, 1999). In the lab, selective pressure is applied by setting the cultivation conditions. Next to the selection of the type of media, nutrients, stressors, acidity, and more, also the type of screening or selection system has an influence on the evolutionary pressure. Multiple different systems have been described, such as solid media (agar plate) based cultivation, repetitive batch cultivations in liquid media (also know as serial transfer cultivations), and continuous cultivations (Barrick and Lenski, 2013; Fernández-Cabezón et al., 2019; Mans et al., 2018). Furthermore, more specialized selection systems have been described in the form of growth in droplets in water in oil emulsions, and FACS-based selection systems, which have been used to evolve cells for increased biomass yields, and for increased small molecule production using TF-based biosensors, respectively (Bachmann et al., 2013; Mahr et al., 2015). To consider the different evolutionary dynamics in the different systems, a distinction has to be made between systems in which cells compete against each other and systems in which cells are able to growth separated from each other. In cultivations systems with competition, known as adaptive evolution, there is a difference in the mutation rate and the observed mutation rate, which is know as the substitution rate. The mutation rate has been discussed previously, and is independent of the type of experiment. The substitution rate is defined as the rate at which new mutations accumulate in an evolving lineage over time (Barrick and Lenski, 2013). This depends on the mutation rate, but also on the fitness effect of the mutation. If a mutation leads to a fitness increase, the mutant will outgrow its competitors and quickly 'take over' the culture. Thus, to the experimenter it appears as if the rate of this mutation is higher, because the mutants quickly increase in frequency. The dynamics in bacterial adaptive laboratory evolution (ALE) usually follow the steps of: i) initial growth and occurrence of mutants; ii) mutant outcompetes parental strain and possibly other mutants, and; iii) possible repetition. A major benefit of this type of systems is the relatively easy way in which a small number of beneficial mutations can be acquired in a single evolved

strain. However, a problem in such systems can be clonal interference, which is what happens when two mutants arise in a population with different but both beneficial mutations, but due to a (small) fitness advantage of the one of the mutants, the other mutant will be outcompeted and this beneficial mutation is 'lost' (Barrick and Lenski, 2013). When cells are grown in spatial separation, which is possible when cells are grown on solid media or in small droplets, clonal interference does not play a role. In these systems a number of strains with one or a few, different, mutations can be obtained. However, it can be more challenging to obtain the 'best' mutant, as there is no competition between the mutants. The type of cultivation system is therefore the important final aspect to consider in laboratory evolution experiments (Figure 3).

Evolutionary engineering has been applied to improve several aspects of microbial production strains, which can be separated into four categories: increasing growth rate, increasing tolerance, improving substrate utilization and improving production (Sandberg et al., 2019; Stella et al., 2019), see also Chapter 3.1 of this thesis. Growth rate increase can be done for its own purpose (Pfeifer et al., 2017), but also to restore the growth rate of rationally engineered strains back towards the levels of the parental strain. Evolution for increased tolerance is often desired to improve the performance of strains under industrial conditions, which often feature high substrate and product concentrations and presence of stressors such as high acidity, temperature, or inhibitors (Sandberg et al., 2019; Stella et al., 2019). Evolution for improved substrate utilization is often done with strains that have been metabolically engineered to utilize carbon sources present in industrial substrate streams, such as pentose sugars (Radek et al., 2017; Wouter Wisselink et al., 2009). Finally, evolution can be applied to improve microbial production, which will be further discussed in the next section.

2.4.2. Evolutionary engineering to improve microbial production

An evolutionary experiment can only work if the desired mutant has a fitness advantage under the applied selective pressure. This proves to be challenging for most production phenotypes. For some products, it is possible to modify the cultivation conditions to create an appropriate selective pressure. Examples are fermentation products that are natively coupled to growth under anaerobic conditions, in which selection for increased growth leads to increased production (*e.g.* ethanol, lactic acid, acetic acid). For some other molecules, it is possible to utilize their intrinsic properties in selection schemes, such as antioxidant properties in combination with applying oxidative stress (Reyes et al., 2014), an increase in buoyancy in combination with a cultivation method to retain floating cells (Liu et al., 2015), or intrinsic fluorescence in combination with selection for fluorescent cells (An et al., 1991). However, most of the molecules of interest do not have any intrinsic property that can be exploited in evolution experiments and methods to couple production to a fitness advantage are required (Figure 4).

Especially for primary metabolites, the use of media supplements such as antimetabolites has been historically successful to screen for strains with improved production (Figure 4) (Eggeling and Bott, 2005; Fiedurek et al., 2017), such as improved amino acid production (Adrio and Demain, 2006; Tani et al., 1988). This is based on the microbial regulation of these molecules, as their production is usually allosterically controlled by the product concentration (*i.e.* negative feedback regulation). Screening for auxotrophic strain is another historically successful strategy (Adrio and Demain, 2006; Fiedurek et al., 2017), which is based on competition between pre-cursors of different pathways (*i.e.* inactivation of one pathway leads to overexpression of the other), often in combination with the removal of feedback inhibition from the inactivated pathway-product. For example, this has been shown for a *Brevibacterium ammoniagenes* guanine auxotrophic mutant that showed increased production of 5'-inosinic acid (Teshiba and Furuya, 1983).

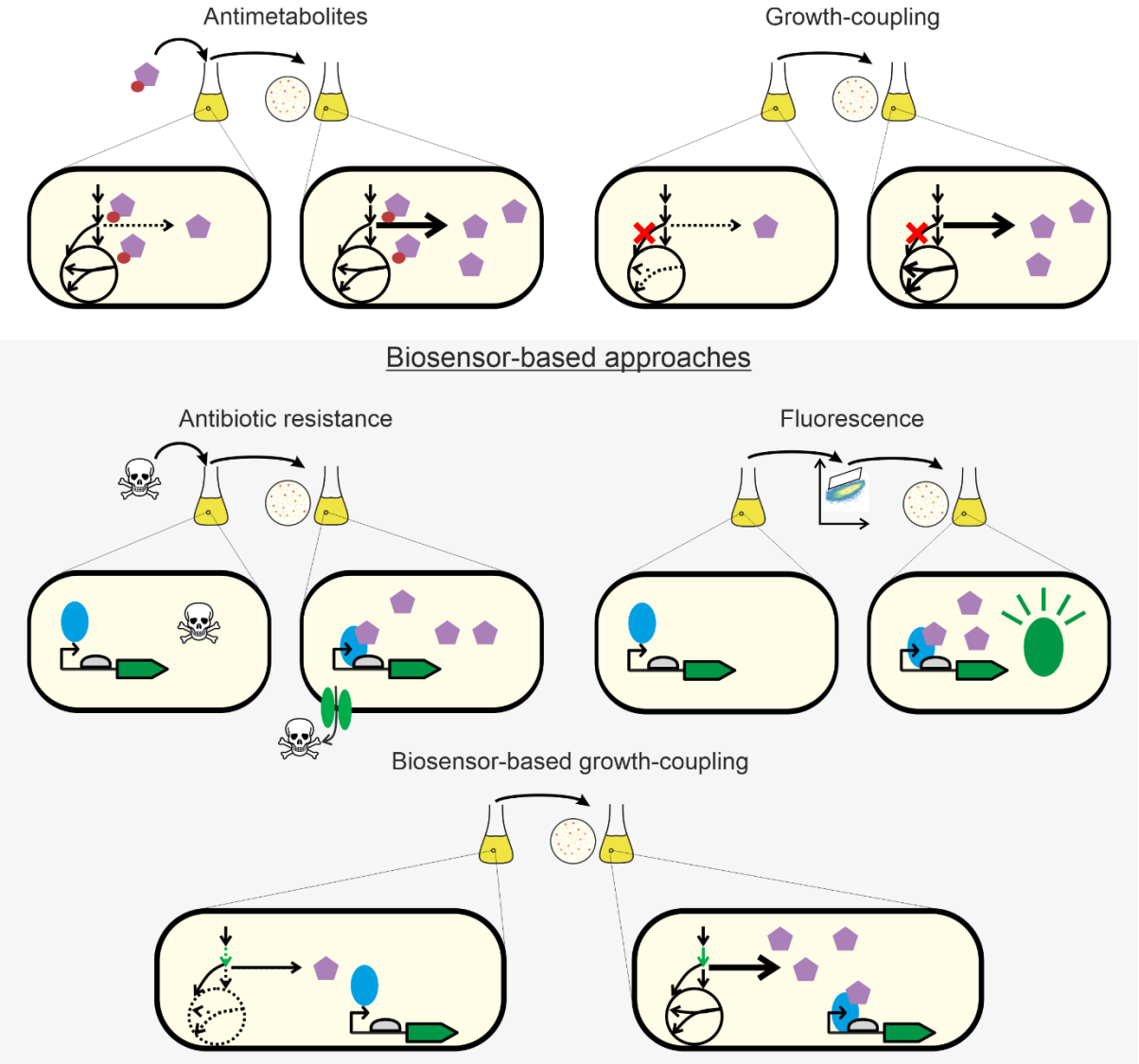

Figure 4: Comparison of main production-to-fitness coupling strategies used for evolutionary engineering. *The shake flask and agar plate are shown to indicate different possible cultivation strategies; products are shown as pink pentagons, antimetabolites are shown as pink pentagon-red circle combinations, antibiotics are shown as skull-and-bones, transcription factors are shown as blue oval shapes, fluorescent proteins are shown as green oval shapes.*

Targeted modification of the microbial strain forms another type of strategy to link production to fitness. Multiple studies describe metabolic engineering strategies, in which metabolism is 'rewired' to make the growth rate dependent of the intracellular concentration, and the production, of a specific molecule (Figure 4) (Buerger et al., 2019; Sandberg et al., 2019; Shepelin et al., 2018). An example is the genetic engineering of an *E. coli* strain to make L-alanine the sole fermentation product, followed by evolution under anaerobic conditions to increase L-alanine production (Zhang et al., 2007). In another study, growth was made dependent on *S*-adenosylmethionine(SAM)–dependent methylation (Luo et al., 2019). In the constructed strain, improvement of the rate of any SAM-dependent methyltransferase would lead to an increased growth rate, and this could lead to increased production of chemicals which require SAM-dependent methylation for their biosynthesis (Luo et al., 2019). Other interesting examples are the modification of the isoleucyl-tRNA synthetase to decrease its affinity to isoleucine, thereby coupling isoleucine production to growth (Sun et al., 2021), and the use of co-

cultivation of two strains to obtain improved producers on the basis of cooperation (Saleski et al., 2019), or competition (Charusanti et al., 2012) between the strains.

In contrast to metabolic engineering strategies, TF-based biosensors can be used to create synthetic regulatory circuits that couple the concentration of molecule of interest to production of a specific protein (Figure 4) (Lin et al., 2017; Mahr and Frunzke, 2016; Williams et al., 2016). In principle, expression of any gene that provides a selectable phenotype can be used as biosensor-output. The most frequently described are genes encoding fluorescent proteins or genes encoding antibiotic resistance genes. When production is coupled to expression of a gene conferring antibiotic resistance, cultivation in media containing a fixed or increasing amount of antibiotic can be used to enrich mutants with increased production, as non-producers are inhibited or killed under these conditions (Figure 4) (Leavitt et al., 2017; Raman et al., 2014; Snoek et al., 2018). When a gene conferring fluorescence is used as output, spatial separation-based cultivations can be used (*e.g.* growing cells on agar plates) to separate mutants, and screen for cells with increased fluorescence (Chou and Keasling, 2013). However, the amount of mutants that can be screened in this type of cultivations is rather limited and FACS-based screenings form a high-throughput alternative (Figure 4). FACS-based screening and selections have been demonstrated in this thesis using the LysG sensor in *V. natriegens* (Chapter 3.3), and multiple other examples have been described (Binder et al., 2012; Flachbart et al., 2019; Mahr et al., 2015). Coupling production to expression, or repression, of other types of genes is also possible, such as the expression of genes encoding a specific substrate transporter (Liu et al., 2017) or repression of a gene conferring toxicity under specific cultivation conditions (Xu et al., 2020).

While all above described approaches have successfully been applied to obtain improved producer strains, they require extensive genetic engineering and/or complex selection methods (Figure 4). A generally applicable method that couples production directly to growth, without requiring media additions, would have a great potential for application in evolutionary engineering. In the next section, such a strategy is presented, which has been developed as part of this thesis (Chapter 3.2).

2.4.3. Coupling amino acids production to growth in *Corynebacterium glutamicum* using Lrp

To enable direct coupling of production to growth, we designed a biosensor-based genetic circuit to couple production to the expression of an essential gene (Figure 4). To this end, the 'growth-regulating' genes *pfkA* and *hisD* were placed under control of the Lrp-based regulatory circuit in the *C. glutamicum* ATCC 13032 WT strain (Figure 5A). A dose-response experiment demonstrated the relationship between L-valine concentration and the maximum specific growth rate (μ_{max}) of the two strains (Figure 5B), which was done with a dipeptide feeding strategy (addition of ala-val) that was described previously (Vrljic et al., 1996). For P_{brnF}-*hisD* the growth rate was already restored to WT-like levels with addition of 1 mM ala-val, while P_{brnF}-*pfkA* required 3 mM ala-val to restore growth to WT levels. Thus, while the biosensor-base synthetic regulatory circuit was identical for both strains, the relation to growth was very dependent on the target growth-regulating gene. This was also observed in other studies, for example when the protocatechuic acid-responsive PcaQ sensor was coupled to the expression of nine different growth-regulating genes in *S. cerevisiae* (D'Ambrosio et al., 2020). Differences in growth were observed between all different strains. It is likely that engineering of the promoter region upstream of *hisD* or *pfkA* could also change the growth dynamics, as this was the case in *E. coli*, where intracellular arabinose concentration was coupled to expression of the *folP-glmM* operon (Rugbjerg et al., 2018). The growth rate was highly dependent on the promoter and RBS used. Nevertheless, growth-coupling was successful in *C. glutamicum* using the Lrp biosensor, and this enabled the use of evolutionary engineering strategies to improve amino acid production in these strains.

2.4.4. Exploring different cultivation strategies to evolve growth-coupled *Corynebacterium glutamicum*

Taking the two growth coupled strains, P_{brnF}-*pfkA* and P_{brnF}-*hisD*, we set out to investigate different selection strategies to isolate cells with improved amino acid production. All strategies were based on selection for improved growth rate. Initially, we evolved both strains in repetitive batch cultivations (*i.e.* we performed repetitive batch adaptive laboratory evolutions; rbALEs) with the aim to accumulate mutations that improved production, by growing 22 parallel cultures for each strain. First, a cultivation under unselective conditions was done, followed by multiple cultivations under selective conditions. In the selective cultivations, all cultures showed a rapid increase in growth rate, but none of the evolved strains showed any amino acid production, as measured by HPLC. Sequencing of six evolved strains found mutations in the integrated Lrp-based regulatory circuit, indicating that these strains were 'cheaters' rather than producers (*i.e.* they escaped the evolutionary pressure by cheating).

Going back to the aspects of evolutionary engineering as discussed previously, we considered the possible explanations for the obtained results. It could be that more mutations were possible that led to a cheater strain than to a producer strain, in the growth-coupled strains. Alternatively, mutations that led to a cheater strain could occur at a higher frequency. In both cases, we could assume that the effective mutation rate of a cheater mutation was higher than that of a producer mutation. Furthermore, the impact of the different mutations on the growth rate was likely different. Cheater mutations might completely restore the growth rate to that of the WT *C.* glutamicum strain, while a mutation leading to a small increase in production might only result in a small increase of growth rate. Modelling of the rbALE revealed that a cheater mutant was likely already present at the beginning of the selective cultivation, which is reasonable as the absolute amount of mutations is highest at high cell densities. Mutations were more likely to occur at the end of the first, nonselective batch cultivation, than at the beginning of the selective cultivation. Furthermore, multiple, possibly different, cheater cells were likely already present, as otherwise some cultures would have lost them in the first selective cultivation due to genetic drift. Using this information, we modelled the outcomes of rbALE experiments, with different ratios of cheater to producer cells at the start of the selective cultivations, and with different 'strengths' of producer mutations (*i.e.* producer mutations that had a small effect on growth rate, and producer mutations that led to almost WT-like growth rates). The result was that, in an rbALE, producer strains would only be enriched if strong producer mutants were present at a higher number than cheater cells at the beginning of the selective cultivations. In other words, we have a special case of clonal interference, in which cheater mutants prevent enrichment of producer mutants. To solve this problem, we could either try to influence the occurrence of cheater or producer mutations, or change the selection system. We investigated the latter, and tested evolutionary strategies based on spatial separation, to prevent the competition between cheater and producer cells.

A challenge for spatial separation strategies is the amount of cells to screen. While many mutants are likely to be present at the end of a typical unselective *C. glutamicum* batch cultivation, their ratio is still low compared to non-mutant cells (*i.e.* this comes from the high number of cells, typically in the order of billions, and a mutation rate in the order of 10^{-3} mutations per cell per replication). However, with our growth-coupled strain design, we could simply spread a high concentration of cells on agar plates containing selective media. Subsequently, we could pick the earliest observable or largest colonies, which were grown from mutants with an improved growth rate (Figure 5C, see also Chapter 3.2). We observed roughly one large colony per 10^4 total colonies. When we grew 96 of these colonies in selective media, all showed an increased growth rate compared to the parental, growth-coupled

strain. Furthermore, about 30 % were identified as producer strains, producing L-valine, L-leucine and/or L-isoleucine, while no product was measured for the remaining 70% (Figure 5D). Thus, by utilizing a cultivation based on spatial separation, we could successfully isolate producer strains.

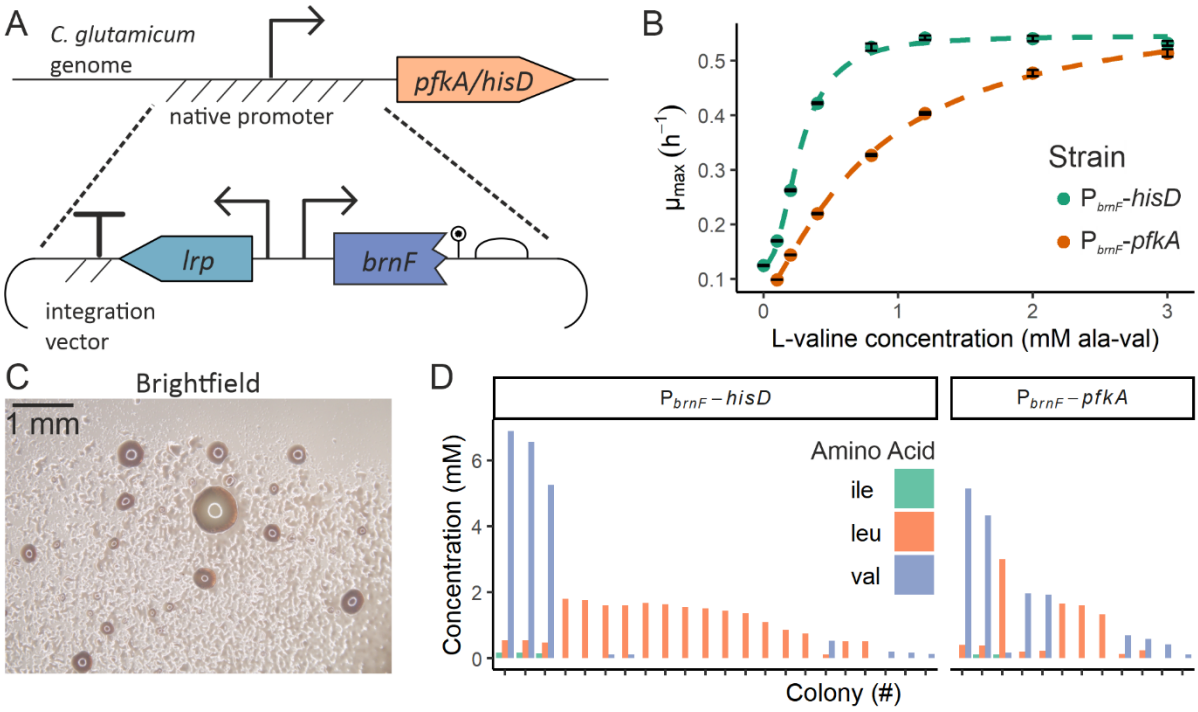

Figure 5: Overview of* C. glutamicum *biosensor-based growth coupling and evolution. *(Adapted from Chapter 3.3) A) Schematic overview of the* lrp-P_{brnF} *integration, upstream from* C. glutamicum *genes. The integration cassette consists of a terminator to block possible promoter activity of upstream regions,* lrp*, the* lrp-brnF *intergenic region, and the first 30 bp of* brnF*, followed by a stop codon, RBS and linker. B) Maximum specific growth rates (*μ_{max}*) of* P_{brnF}-hisD *and* P_{brnF}-pfkA *cultures supplemented with different amounts of ala-val dipeptide, grown in CGXII medium with 2% glucose. Average and standard deviation of three biological replicates are shown. Overview of results from plate-based selection strategy of* C. glutamicum *growth-coupled strains. C) Micrograph of* C. glutamicum*::*P_{brnF}-pfkA*, showing the appearance of larger mutant clones on CGXII. D) Amino acid production of 48 cultures of each strain started from large clones on CGXII plates, sorted by total amino acid production. Results are shown for clones that produced detectable amounts of L-valine, L-isoleucine or L-leucine.*

Next to plate-based cultivation, we also applied FACS to separate single growth-coupled cells. To this end, the plasmid pJC1-*lrp-brnF'-eyfp* was introduced into the growth-coupled strains. Thus, producer mutants would also show a fluorescent output. The strains were grown under non-selective conditions (*i.e.* in BHI medium), before FACS. Single cells of the top fluorescent population were sorted on a non-selective BHI agar plate, before starting a rbALE from 42 clones. Using this strategy, only one of the P_{brnF}-*pfkA* evolution-cultures showed high extracellular L-valine concentrations (> 1.0 mM). Compared to the plate based approach, the FACS approach had a lower effectivity. Furthermore, its use is more complicated than a plate-based approach. In conclusion, using a plate-based cultivation for spatially-separated growth is recommended.

Finally, sequencing of 15 L-valine producer mutations revealed that all contained mutations in either of the two genes encoding the acetohydroxyacid synthase (AHAS), *ilvB* or *ilvN*. AHAS catalyzes the first step in the biosynthesis of L-valine and related amino acids. We further investigated the functional impact of these mutations by constructing an in-silico model of the AHAS enzyme (see also Chapter 3.2). All obtained mutations are likely to result in a decreased negative feedback inhibition of this

enzyme, which would explain the producer phenotype. Multiple other studies also report the effect of mutations in AHAS on L-valine production (Guo et al., 2015; Liu et al., 2019; Vogt et al., 2014). Thus, the growth-coupled evolutionary engineering resulted in the isolation of strains with specific, causal mutations.

2.4.5. Future improvements of biosensors-based evolution

Biosensor-based growth coupling is a promising strategy to enable the application of evolutionary engineering to isolate mutants with increased production. The simple design and the straightforward selection phenotype (*i.e.* increased growth) result in a good tradeoff between the complexity of strain engineering and the complexity of the selection strategy. Furthermore, due to the relative modularity of biosensors, this strategy can be applied for a wide range of products, and in different hosts.

One of the major factors for improvement is dealing with the occurrence of cheaters, which is a known phenomenon in biosensor-based evolution. With our Lrp-based regulatory circuit, we observed different mutations that led to a cheater phenotype. Both mutations in the promoter (P_{brnF}), in the transcription factor (Lrp) and a duplication event in the *pfkA* gene-region were obtained, which resulted in strains escaping the selective pressure. Only a few other studies clearly reported the occurrence of cheater mutations and described them; in a study describing coupling of vanillic acid production to *GLN1* expression in *S. cerevisiae* using the transcriptional repressor VanR, a deletion mutation of the VanR binding site was described (D'Ambrosio et al., 2020). We showed that one method to address cheater mutations is to prevent competition between cheater mutants and producer mutants. It is unlikely that producer strains will outcompete cheater strains in direct competition, as there is always a direct trade-off between growth rate and production, due to resource allocation by the cell (*i.e.* cellular resources can either be used for growth, or for production; an increase in one leads to a decrease of the other). Therefore, cheater strains, which do not have to produce the product, will always have a (small) growth advantage. An alternative strategy to deal with cheaters is to modify the biosensor-based growth-coupling design, to either decrease the cheater mutation rate, or increase the producer mutation rate. Several biosensor modifications were previously shown to reduce the escape rate of strains in which biosensors were used to couple production to expression of an antibiotic marker (Raman et al., 2014). The described modifications where: i) addition of a degradation tag to the transcription factor; ii) modification of the cognate promoter of the transcription factor (*i.e.* the promoter of the antibiotic resistance marker; iii) expression of two gene copies of the transcription factor, and; iv) expression of two different antibiotic markers (Raman et al., 2014). However, no sequencing of the 'escapees' was done, and it is not clear if the modifications lowered the escape rate due to lower cheater mutations, or due to non-genetic variations, as the latter has been shown to have a large effect on growth-coupled strains (Xiao et al., 2016). Furthermore, these strategies complicate the design, and depending on the application, modification of the selection strategy might be more suitable.

To further improve the presented biosensor-based growth-coupled evolution, and to improve evolutionary strategies in general, modelling should be further applied and improved. We developed a very straightforward model, which is essentially based on the difference in growth rate of the parental strain, cheater strain and producer strain. With this model, we could simulate the behavior of evolution in rbALE experiments, which helped us to find a better selection strategy. Many evolutionary workflows to improve strain performance have been described, but few incorporate modelling of the evolutionary workflows. Some evolutionary models for strain improvement have been described, but they are not yet widely applied (LaCroix et al., 2017). Improvement of our model would essentially comprise the incorporation of the factors that are important to design evolutionary engineering experiments, which were discussed previously. First, mutation rates could be

incorporated, with different rates for different mutations (*i.e.* cheater mutations and producer mutations), which would be updated based on experimental results. Mutation is per definition a random process, therefore a model including mutation rates would likely be stochastic rather than deterministic (LaCroix et al., 2017). Furthermore, the mutation rates will probably be very dependent on the strain, product and biosensor used. Second, modelling of the mutation rate should be extended with incorporation of cell numbers and replications. Ideally, mutations could be 'tracked' over a cultivation; when a mutation occurs (modelled as a random event with a set chance of occurring), the mutant is modelled as a new cell type in the cultivation, which replicates at a certain rate, and is able to further mutate. The use of deep sequencing could be applied to provide experimental validation for such a model (Rugbjerg et al., 2018). Third, the effect of genetic drift should be added, in combination with different cultivation/selection strategies. This allows the experimenter to simulate expected results based on different evolutionary strategies, and only execute the most promising ones. Data on the (average) growth rate of different cheater and producer mutations would improve the model. Taking genetic drift into account could even lead to strategies using only liquid cultivations to isolate producers from growth-coupled strains, because culture transferring strategies could be designed that maximize the chance of only one type of mutant transferring to the next cultivation. This would lead to the separation of cheaters and producers in liquid cultures.

Finally, to further improve the production of the isolated strains, or the production of established production strain, modification of the Lrp-based regulatory circuit would be required. The presented evolutionary experiments showed the upper limit of the operational range at L-valine concentrations of 15 mM. Therefore, modifications of the Lrp-based biosensor were investigated, which are described in the next section.

2.5. Using lab automation to improve biosensors

The process of rational strain engineering (*i.e.* molecular biology workflows) usually consists of multiple steps that have to be performed in the lab, such as PCR, plasmid assembly and transformation (Figure 6). In addition, for less genetically tractable hosts such as *C. glutamicum,* which do not easily take up DNA, additional steps are required. These include plasmid preparation from the cloning host (*e.g. E. coli*) followed by *C. glutamicum* transformation (*e.g.* by electroporation). Especially when multiple strains have to be created in parallel, this can be very time-consuming, and would highly benefit from automation (Chao et al., 2017). In this section, the automation of a complete, standard cloning workflow for *C. glutamicum* engineering is described, which was developed as part of this thesis. This workflow was then used to construct and characterize different variants of the Lrp biosensor. These results are further described in Chapter 3.4, and have been published (Tenhaef et al., 2021).

With the advent of synthetic biology at the start of the current century (Cameron et al., 2014; Endy, 2005), the amount of strains that could be rationally designed quickly increased. This was aided by a plethora of software tools that have been developed to enable the design of many strains (Appleton et al., 2017b; Carbonell et al., 2016). This placed the bottleneck at the actual construction of the designed strains, the molecular cloning workflows (Ellis et al., 2011). To increase the throughput of molecular biology workflows, automation is required. Multiple studies described the automation of (part of) molecular cloning workflows using liquid handling robots (Chao et al., 2017; Hughes et al., 2007; Jiang et al., 2020; Yehezkel et al., 2011). Other studies highlight the application of microfluidics to integrate and automate strain construction on microfluidic chips (Moore et al., 2017; Shih et al., 2015). In recent years, multiple biofoundries have been developed in different countries, aiming for a complete integration of laboratory automation in biotechnology (Hillson et al., 2019). Biofoundries aim to "accelerate and enhance both academic and translational research in engineering/synthetic

biology by promoting and enabling the beneficial use of automation and high-throughput equipment including process scale-up, computer-aided design software, and other new workflows and tools" (Hillson et al., 2019). Still, most studies have focused on *E. coli*, and not on genetically less tractable host such as *C. glutamicum*. While some studies describe automation of *C. glutamicum* cloning workflows, the transformation step is still done manually (Wang et al., 2018). Therefore, we aimed to integrate this step into an automated cloning workflow for *C. glutamicum*.

2.5.1. Automated construction and characterization of Lrp biosensor variants

First, we set out to design and validate all the steps of a complete workflow to construct and express plasmids in *C. glutamicum*, using standard liquid handling systems (*i.e.* robots capable of pipetting and plate movement) (Figure 6). The construction workflow consists of PCR, Gibson assembly, *E. coli* heat shock transformation followed by conjugation to *C. glutamicum* (Figure 6). Furthermore, colony PCR and plasmid sequencing were performed to validate the constructs.

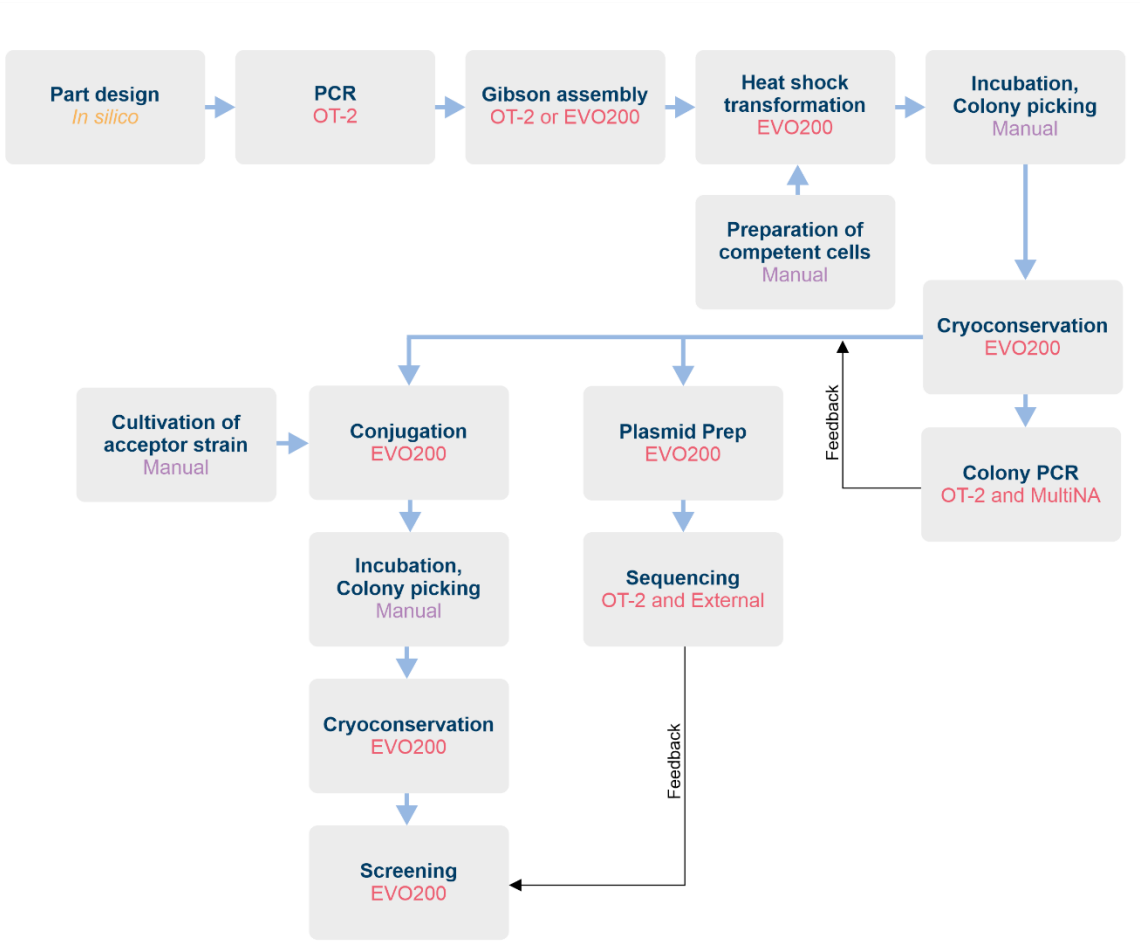

Figure 6: Overview of the automated genetic engineering workflow. *(Adapted from (Tenhaef et al., 2021), see Chapter 3.4). Each box describes one unit operation and informs about the device or entity used for performing this operation. OT-2: Opentrons OT-2 liquid handling system. EVO200: Tecan EVO200 liquid handling system. MultiNA: Shimadzu MCE-202 MultiNA chip electrophoresis system.*

We started the automated cloning workflow to construct 96 different variants of the Lrp biosensors, by combining different versions of the *lrp* start codon, the *lrp* RBS, the *brnF* promoter and the *eYFP* RBS (Figure 7A). Multiple constructs were lost especially after the *E. coli* heat shock (30 out of 96) and conjugation (19 out of 55) step. With future improvement of the workflow, these numbers should be decreased. However, it should be noted that during a manual workflow, 100% efficiency is rarely the

case. Furthermore, by analyzing the time needed for the workflow, we could conclude that the automated workflow could drastically reduce the hands-on time of the experimenter spent on strain construction. Additionally, a higher throughput can be achieved, which largely increases the quantity of constructs that can be produced in time. While the process has to be further improved, automation introduces standardization of the process, as all steps are documented and workflow variation is independent of differences between human scientists, which also makes it easier to find room for improvement.

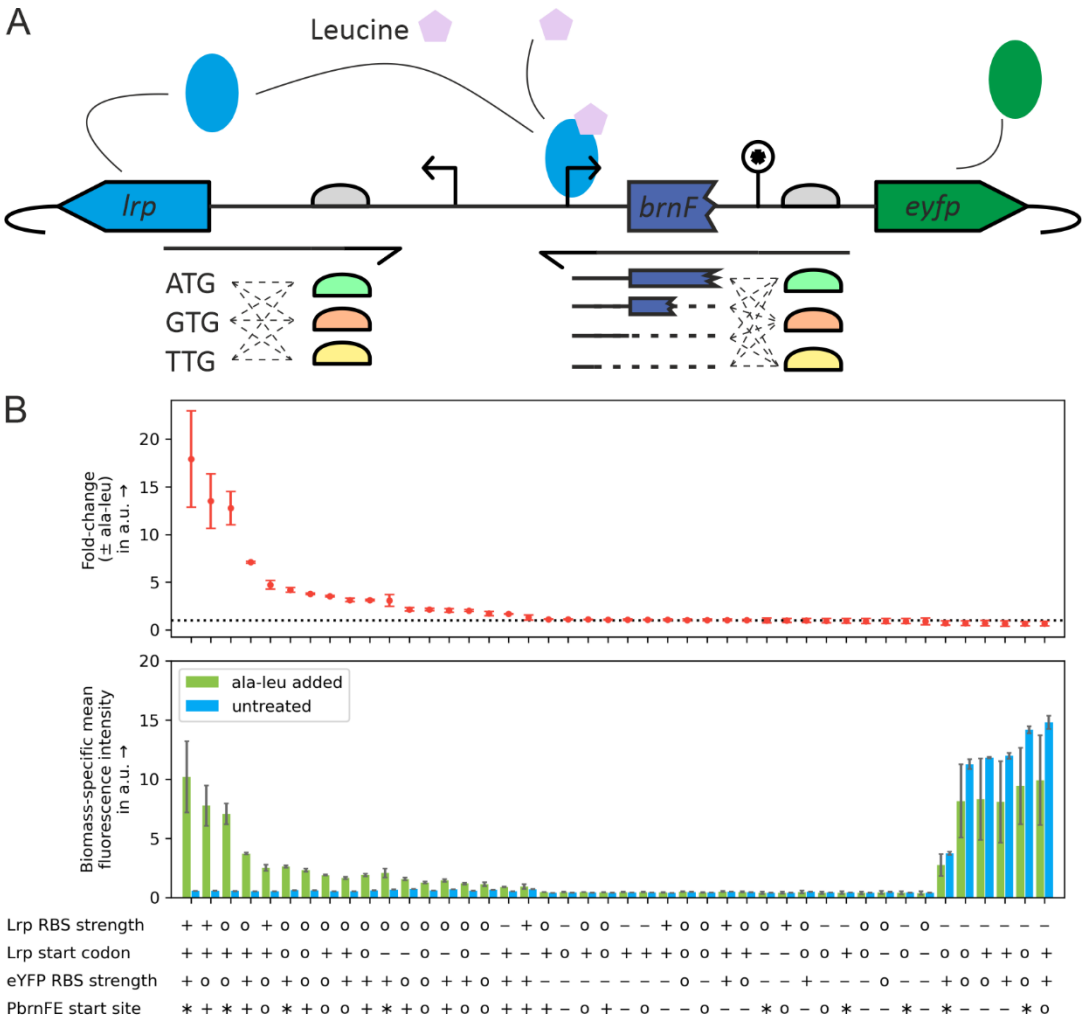

Figure 7: Design and analysis of Lrp biosensor variants. *(Adapted from (Tenhaef et al., 2021), see Chapter 3.4).A) Graphical overview of the different Lrp biosensor variants that were designed for construction and expression in* C. glutamicum. *On the left side, 9 different primers were designed, containing combinations of different* lrp *start codons and* lrp *RBSs. On the right side, 12 different primers were designed, containing combinations of different* brnF *promoter sequences and* eYFP *RBSs. B) Screening results of 44 Lrp biosensor variants. Fold-change of each strain is calculated by dividing the biomass-specific fluorescence after 20 h of growth with inducer (3 mM alanine-leucine dipeptide) by the biomass-specific fluorescence after 20 h of growth without inducer. Dashed line indicates a fold-change of one. Higher values indicate a higher dynamic range of the sensor. Symbols used for strain characteristics:* lrp *RBS strength: – = weak, o = average (native), + = strong;* lrp *start codon: – = weak, o = average, + = strong (native);* eyfp *RBS strength: – = weak, o = average (native), + = strong;* P_{brnFE} *start site: – = -15, o = 0, + = +15, ∗ = +30. Mean and standard deviation of three biological replicates are shown.*

Using the automated cloning workflow, we obtained 44 different variants of the Lrp biosensor. To characterize these variants, the sensor output was measured by growing the strains in microtiter

plates in the presence or absence of 3 mM alanine−leucine dipeptide (Figure 7B). The highest fold-change was observed for the sensors with the strongest *lrp* RBS and start codon, *eyfp* RBS, and the longest promoter containing the first 30 bp of *brnF*. Fold-change was relatively high when a strong *lrp* RBS and start codon was used in combination with a strong *eyfp* RBS. While the 'strongest' expression led to the highest dynamic range, this is not always the case, as high transcription factor expression can lead to expression of the reporter in absence of ligand binding (Sonntag et al., 2020). When either an *lrp* RBS or *eyfp* RBS with a low strength was used, hardly any sensor functionality was observed. For sensors that had an *lrp* RBS with low strength in combination with an *eyfp* RBS with strong or medium strength, an interesting result was observed. These sensors showed a high fluorescence output both in the presence and in the absence of the ligand. It could be that low expression of *lrp* relieved Lrp-based regulation of *eyfp*, and in combination with an *eyfp* RBS with medium or strong effect this resulted in Lrp-independent expression of *eyfp*. This would suggest that Lrp functions both as an activator and a repressor, which has previously been shown for the transcription factor AraC (Ogden et al., 1980). In contrast, a previous study showed that *lrp* deletion reduced export of L-isoleucine, likely due to lower Lrp-based activation of *brnFE* expression (Kennerknecht et al., 2002). To conclude, the regulatory mechanism of Lrp has not been completely elucidated yet, and should be further investigated.

Biosensor-modification strategies can be categorized into targeted and untargeted engineering approaches. We have described a targeted approach to modify the Lrp biosensors, as variants were created following a rational design. Multiple other studies have described targeted modifications of TF-based biosensor to improve their characteristics (Lin et al., 2017; Mahr and Frunzke, 2016), including engineering of the TF-based biosensor cognate promoter region (Zhang et al., 2012), addition of a degradation tag to the transcription factor and modification of the number of transcription factors used (Raman et al., 2014). In contrast, untargeted approaches use evolutionary engineering to isolate sensors with improved characteristics, by creating and screening a randomly mutated sensor library. For example, multiple sensor variants can quickly be created using error-prone PCR, and a library of clones each harboring one of the sensor variants can be screened to find sensors with improved characteristics (Chou and Keasling, 2013). Furthermore, some studies also describe a combination of both approaches, using targeted engineering to create a few variants, and then further improve their characteristics by creation and screening of randomly mutated derivates (Meyer et al., 2019). The advantage of untargeted strategies is the higher amount of throughput that can be achieved. A disadvantage is that knowledge is only obtained from variants that were first created and subsequently isolated. By chance, good variants might not be created, for example difficult to construct variants, and are therefore not obtained and characterized. This is not a problem for rationally designed variants, as the information on the created and characterized variants is available. However, the available throughput is lower with this strategy, especially when construction and characterization have to be performed manually. Therefore, the use of laboratory automation is highly beneficial to further the improvement and functional understanding of biosensors.

2.6. Conclusions and outlook

To foster the transition of our current economy into a sustainable bioeconomy, we need biotechnology. However, biotechnology is not yet ready to completely take over the role of the fossil industry. In this thesis, different ways to speed up strain construction using TF-based biosensors were investigated, covering development of novel hosts, evolutionary engineering strategies and lab automation. First, we showed the successful transfer of the LysG TF-based biosensor to *V. natriegens*, and applied a mutagenesis and screening protocol to isolate mutants producing L-lysine, L-histidine or L-arginine. This work demonstrates the benefit of TF-based biosensors for novel strain

development. Second, a novel evolutionary strategy was presented, based on coupling production to growth using TF-based biosensors. This strategy can be used to enable straightforward selection of producer strains, likely for a wide range of products, and in different microbial hosts. Finally, we transferred a complete *C. glutamicum* cloning workflow to liquid handling robots, to enable the automated, high-throughput construction of Lrp biosensor variants. This workflow can be adapted for most *C. glutamicum* cloning workflows, speeding up engineering workflow in general. Furthermore, an up-to-date overview of evolutionary engineering using *C. glutamicum* was presented in a review article.

While TF-based biosensors are promising and, for multiple applications, proven tools for microbial strain development, they have some limitations that should be addressed in future work. First, TF-based biosensors have been evolved to function under physiological conditions. Therefore, their operational range covers concentrations that are usually well below the product concentrations required in industrial processes. This is clear for the work presented in this thesis, as the top *V. natriegens* isolate produced 1 mM of L-lysine, and the top *C. glutamicum* isolate produced 15 mM of L-valine. Both concentrations are well below the industrial requirements. Therefore, future work should focus on shifting the operational range upwards. This can likely be achieved by a combination of targeted sensor engineering and screening of sensor libraries (Meyer et al., 2019). This would allow the application of screening and selection workflows using TF-based biosensors with strains that already produce high amounts of the target molecule, further improving them. Furthermore, by using an iterative workflow with biosensors working in different operational ranges, a non-producer strain could quickly be developed into a high-producing strain. Second, while the relative modularity of TF-factor based is one of their strengths, this modularity can still be improved. For example, we were able to express LysG in *V. natriegens*, but Lrp could not be functionally expressed. It would be ideal to have a 'plug-and-play' set of biosensors, for which one can easily 'pick' the detected molecule, the operation and dynamic range, and a reporter output. Some work has been done in this regard, by modifying transcription factors with clearly distinct ligand binding domains and DNA binding domains (Chou and Keasling, 2013), but this is still largely *ad hoc* engineering. Further research is required for widespread application and standardization. Third, for industrial processes the ideal producer strain would produce a lot of extracellular, and not intracellular, product. However, most TF-based biosensors function intracellularly, which can limit their application to isolate strong extracellular producers. This is especially the case when very high concentrations are required, as intracellular concentrations in the molar range are physiologically very unlikely to be achievable. In our work, we might have also isolated strain with mutations in amino acid exporters, as such strains would show an increased sensor output without an increased extracellular product concentration. However, we did not investigate this. Some studies report co-cultivation strategies (Saleski et al., 2019) or droplet cultivations (Abatemarco et al., 2017) to enable screening or selection of improved extracellular producer strains. Such strategies could also be implemented with biosensor or growth-coupled strains. Still, there are some issues that need to be addressed, such as the problem of cross-talk in liquid cultivations (Flachbart et al., 2019), and the fact that the sensor strain must be able to take up the product. In conclusion, TF-biosensors and their applications need to be further developed so they can be applied to directly improve industrial processes.

If there is one development that has the promise to revolutionize biotechnology, it is automation. In the lab, liquid handling robots coupled to specialized equipment are already capable of taking over most manual tasks. Still, application of robotics is not yet widely integrated, especially in academic labs. One of the (likely) reasons are the relatively high investment costs, including that for the robotic systems themselves, but also the time and costs of training people and establishing workflows. More affordable robotic systems have been developed in the last years. While starting with robotics will

require an initial investment phase, scientists would later be able to shift their time away from repetitive laboratory work. Instead, they could focus more on the design, analysis and learning from experiments. Considering the projects discussed in this thesis, (further) automation would benefit each of them. When transferring the TF-based biosensor to *V. natriegens*, only a few variants were constructed, mainly because of the additional hands-on construction time that would be required to construct 100 instead of 10 variants. When automated workflows are implemented, as was shown for the Lrp variants expressed in *C. glutamicum*, laboratory time is no longer an important consideration. For evolutionary workflows, implementing automated cultivation, culture transferring, clone picking and mutant characterization would enable a much higher throughput, which can be leveraged to isolate and analyze more producer mutants. This would in turn increase the chance of isolating a better producer, but also increase our knowledge on biology. Finally, laboratory automation could be implemented to optimize evolutionary workflows by deriving and modelling the important parameters, including mutation rate and type of mutations, and picking the best selection system by considering genetic drift and clonal interference. While our automation workflow for *C. glutamicum* cloning provides a good first step in general lab automation for strain engineering, there were still some manual steps that should be integrated (Figure 6). Furthermore, improvements would include optimization of each workflow, by systematically changing the workflow parameters to improve efficiency (*e.g.* minimize amount of expensive enzyme solutions required), effectiveness (*e.g.* maximize throughput by scheduling workflows) and minimize the amount of hands-on time required. A transition to completely automated workflows will also require another look at experimental design and analysis. Here, steps should be implemented to automate rational strain design, by abstracting standard processes for the user (*e.g.* design and ordering of primers needed to construct the desired strain), in a similar fashion to what has been done in the semiconductor industry (SYNTHACE, 2018). Instead of considering *how* a certain strain should be constructed and analyzed, the scientist should only be concerned with *which* strains should be constructed and the type of analyses that have to be performed, and leave the implementation to the automation process. Data streams stemming from each process in the construction and analysis workflow should be automatically processed, to provide the scientist with a clear overview of strains designed and their measured and calculated characteristics, again freeing time for the thinking, and not the doing, process. Multiple labs over the world have recently bundled their efforts to foster the transition from manual to automated laboratories, in the form of biofoundries (Hillson et al., 2019). Developments in laboratory automation will hopefully lead to an exponential increase in both the understanding and application of biotechnology.

2.7. References

Abatemarco, J., Sarhan, M.F., Wagner, J.M., Lin, J.L., Liu, L., Hassouneh, W., Yuan, S.F., Alper, H.S., Abate, A.R., 2017. RNA-aptamers-in-droplets (RAPID) high-throughput screening for secretory phenotypes. Nat. Commun. 8, 1–9. https://doi.org/10.1038/s41467-017-00425-7

Adelberg, E.A., Mandel, M., Ching Chen, G.C., 1965. Optimal conditions for mutagenesis by N-methyl-N'-nitro-N-nitrosoguanidine in *Escherichia coli* K12. Biochem. Biophys. Res. Commun. 18, 788–795. https://doi.org/10.1016/0006-291X(65)90855-7

Adrio, J.L., Demain, A.L., 2006. Genetic improvement of processes yielding microbial products. FEMS Microbiol. Rev. 30, 187–214. https://doi.org/10.1111/j.1574-6976.2005.00009.x

Aiyar, S.E., Gaal, T., Gourse, R.L., 2002. rRNA promoter activity in the fast-growing bacterium *Vibrio natriegens*. J. Bacteriol. 184, 1349–1358. https://doi.org/10.1128/JB.184.5.1349-1358.2002

Ambri, F., D'ambrosio, V., Di Blasi, R., Maury, J., Jacobsen, S.A.B., Mccloskey, D., Jensen, M.K., Keasling, J.D., 2020. High-resolution scanning of optimal biosensor reporter promoters in yeast. ACS Synth. Biol. 9, 218–226. https://doi.org/10.1021/acssynbio.9b00333

An, G.H., Bielich, J., Auerbach, R., Johnson, E.A., 1991. Isolation and characterization of carotenoid hyperproducing mutants of yeast by flow cytometry and cell sorting. Nat. Biotechnol. 9, 70–73. https://doi.org/10.1038/nbt0191-70

Anderson, J.C., 2006. Anderson promoter library [WWW Document]. URL http://parts.igem.org/Promoters/Catalog/Anderson

Appleton, E., Densmore, D., Madsen, C., Roehner, N., 2017a. Needs and opportunities in bio-design automation: four areas for focus. Curr. Opin. Chem. Biol. 40, 111–118. https://doi.org/10.1016/j.cbpa.2017.08.005

Appleton, E., Madsen, C., Roehner, N., Densmore, D., 2017b. Design automation in synthetic biology. Cold Spring Harb. Perspect. Biol. 9, a023978. https://doi.org/10.1101/cshperspect.a023978

Austin, B., Zachary, A., Colwell, R.R., 1978. Recognition of *Beneckea natriegens* (Payne et al.) Baumann et al. as a member of the genus *Vibrio*, as previously proposed by Webb and Payne. Int. J. Syst. Bacteriol. 28, 315–317. https://doi.org/10.1099/00207713-28-2-315

Bachmann, H., Fischlechner, M., Rabbers, I., Barfa, N., Branco dos Santos, F., Molenaar, D., Teusink, B., 2013. Availability of public goods shapes the evolution of competing metabolic strategies. Proc. Natl. Acad. Sci. 110, 14302–14307. https://doi.org/10.1073/pnas.1308523110

Baritugo, K., Kim, H.T., David, Y., Choi, J.H., Hong, S.H., Jeong, K.J., Choi, J.H., Joo, J.C., Park, S.J., Park, S.J., 2018. Metabolic engineering of *Corynebacterium glutamicum* for fermentative production of chemicals in biorefinery. Appl. Microbiol. Biotechnol. 102, 3915–3937. https://doi.org/10.1007/s00253-018-8896-6

Barrick, J.E., Lenski, R.E., 2013. Genome dynamics during experimental evolution. Nat. Rev. Genet. 14, 827–839. https://doi.org/10.1038/nrg3564

Baumann, P., Baumann, L., Mandel, M., 1971. Taxonomy of Marine Bacteria: the Genus *Beneckea*. J. Bacteriol. 107, 268–294.

Becker, J., Rohles, C.M., Wittmann, C., 2018. Metabolically engineered *Corynebacterium glutamicum* for bio-based production of chemicals, fuels, materials, and healthcare products. Metab. Eng. 50, 122–141. https://doi.org/10.1016/j.ymben.2018.07.008

Becker, J., Wittmann, C., 2016. Industrial Microorganisms: *Corynebacterium glutamicum*, in: Industrial Biotechnology: Microorganisms. Wiley Online Library, pp. 183–220. https://doi.org/10.1002/9783527807796.ch6

Becker, J., Wittmann, C., 2012. Systems and synthetic metabolic engineering for amino acid production - the heartbeat of industrial strain development. Curr. Opin. Biotechnol. 23, 718–726. https://doi.org/10.1016/j.copbio.2011.12.025

Bellman, A., Vrljić, M., Pátek, M., Sahm, H., Krämer, R., Eggeling, L., 2001. Expression control and specificity of the basic amino acid exporter lysE of *Corynebacterium glutamicum*. Microbiology 147, 1765–1774. https://doi.org/10.1099/00221287-147-7-1765

Binder, S., Schendzielorz, G., Stäbler, N., Krumbach, K., Hoffmann, K., Bott, M., Eggeling, L., 2012. A high-throughput approach to identify genomic variants of bacterial metabolite producers at the single-cell level. Genome Biol. 13, R40. https://doi.org/10.1186/gb-2012-13-5-r40

Binder, S., Siedler, S., Marienhagen, J., Bott, M., Eggeling, L., 2013. Recombineering in

Corynebacterium glutamicum combined with optical nanosensors: A general strategy for fast producer strain generation. Nucleic Acids Res. 41, 6360–6369. https://doi.org/10.1093/nar/gkt312

Blount, Z.D., Barrick, J.E., Davidson, C.J., Lenski, R.E., 2012. Genomic analysis of a key innovation in an experimental *Escherichia coli* population. Nature 489, 513–518. https://doi.org/10.1038/nature11514

Blount, Z.D., Borland, C.Z., Lenski, R.E., 2008. Historical contingency and the evolution of a key innovation in an experimental population of *Escherichia coli*. Proc. Natl. Acad. Sci. 105, 7899–7906. https://doi.org/10.1073/pnas.0803151105

Bolivar, F., Rodriguez, R.L., Greene, P.J., Betlach, M.C., Heyneker, H.L., Boyer, H.W., Crosa, J.H., Falkow, S., 1977. Construction and characterization of new cloning vehicle. II. A multipurpose cloning system. Gene 2, 95–113.

Browning, D.F., Busby, S.J.W., 2016. Local and global regulation of transcription initiation in bacteria. Nat. Rev. Microbiol. 14, 638–650. https://doi.org/10.1038/nrmicro.2016.103

Buerger, J., Gronenberg, L.S., Genee, H.J., Sommer, M.O.A., 2019. Wiring cell growth to product formation. Curr. Opin. Biotechnol. 59, 85–92. https://doi.org/10.1016/j.copbio.2019.02.014

Cameron, D.E., Bashor, C.J., Collins, J.J., 2014. A brief history of synthetic biology. Nat. Rev. Microbiol. 12, 381–390. https://doi.org/10.1038/nrmicro3239

Carbonell, P., Currin, A., Jervis, A.J., Rattray, N.J.W., Swainston, N., Yan, C., Takano, E., Breitling, R., 2016. Bioinformatics for the synthetic biology of natural products: Integrating across the Design-Build-Test cycle. Nat. Prod. Rep. 33, 925–932. https://doi.org/10.1039/c6np00018e

Chao, R., Mishra, S., Si, T., Zhao, H., 2017. Engineering biological systems using automated biofoundries. Metab. Eng. 42, 98–108. https://doi.org/10.1016/j.ymben.2017.06.003

Charusanti, P., Fong, N.L., Nagarajan, H., Pereira, A.R., Li, H.J., Abate, E.A., Su, Y., Gerwick, W.H., Palsson, B.O., 2012. Exploiting adaptive laboratory evolution of *streptomyces clavuligerus* for antibiotic discovery and overproduction. PLoS One 7, e33727. https://doi.org/10.1371/journal.pone.0033727

Chou, H.H., Keasling, J.D., 2013. Programming adaptive control to evolve increased metabolite production. Nat. Commun. 4, 1–8. https://doi.org/10.1038/ncomms3595

Cleto, S., Jensen, J.V.K., Wendisch, V.F., Lu, T.K., 2016. *Corynebacterium glutamicum* Metabolic Engineering with CRISPR Interference (CRISPRi). ACS Synth. Biol. 5, 375–385. https://doi.org/10.1021/acssynbio.5b00216

Crick, F., Watson, J., 1953. Molecular Strucutre of Nucleic Acids. Nature 171, 737–738.

Currie, J., 1917. The citric acid fermentation of *Aspergillus niger*. J. Biol. Chem. 31, 15–37.

D'Ambrosio, V., Dore, E., Di Blasi, R., van den Broek, M., Sudarsan, S., Horst, J. ter, Ambri, F., Sommer, M.O.A., Rugbjerg, P., Keasling, J.D., Mans, R., Jensen, M.K., 2020. Regulatory control circuits for stabilizing long-term anabolic product formation in yeast. Metab. Eng. 61, 369–380. https://doi.org/10.1016/j.ymben.2020.07.006

Dahl, R.H., Zhang, F., Alonso-Gutierrez, J., Baidoo, E., Batth, T.S., Redding-Johanson, A.M., Petzold, C.J., Mukhopadhyay, A., Lee, T.S., Adams, P.D., Keasling, J.D., 2013. Engineering dynamic pathway regulation using stress-response promoters. Nat. Biotechnol. 31, 1039–1046. https://doi.org/10.1038/nbt.2689

Dalia, T.N., Hayes, C.A., Stolyar, S., Marx, C.J., McKinlay, J.B., Dalia, A.B., 2017. Multiplex Genome Editing by Natural Transformation (MuGENT) for Synthetic Biology in *Vibrio natriegens*. ACS Synth. Biol. 6, 1650–1655. https://doi.org/10.1021/acssynbio.7b00116

Darwin, C., 1859. On the origin of species. Routledge.

Dawkins, R., 1986. The Blind Watchmaker. Norton & Company, Inc.

Demain, A.L., Vandamme, E.J., Collins, J., Buchholz, K., 2010. History of Industrial Biotechnology, in: Industrial Biotechnology: Microorganisms. Wiley Online Library, pp. 3–84. https://doi.org/10.1002/9783527630233.ch1

Des Soye, B.J., Davidson, S.R., Weinstock, M.T., Gibson, D.G., Jewett, M.C., 2018. Establishing a High-Yielding Cell-Free Protein Synthesis Platform Derived from *Vibrio natriegens*. ACS Synth. Biol. 7, 2245–2255. https://doi.org/10.1021/acssynbio.8b00252

Diethard, M., Gasser, B., Egermeier, M., Marx, H., Sauer, M., 2017. Industrial Microorganisms: *Saccharomyces cerevisiae* and other Yeasts, in: Industrial Biotechnology: Microorganisms. Wiley Online Library, pp. 673–686.

Dietrich, J.A., McKee, A.E., Keasling, J.D., 2010. High-Throughput Metabolic Engineering: Advances in Small-Molecule Screening and Selection. Annu. Rev. Biochem. 79, 563–590. https://doi.org/10.1146/annurev-biochem-062608-095938

Dietrich, J.A., Shis, D.L., Alikhani, A., Keasling, J.D., 2013. Transcription factor-based screens and synthetic selections for microbial small-molecule biosynthesis. ACS Synth. Biol. 2, 47–58. https://doi.org/10.1021/sb300091d

Dobzhansky, T., 1973. Nothing in Biology Makes Sense except in the Light of Evolution. Am. Biol. Teach. 35, 125–129. https://doi.org/10.2307/4444260

Drake, J.W., 1991. A constant rate of spontaneous mutation in DNA-based microbes. Proc. Natl. Acad. Sci. U. S. A. 88, 7160–7164. https://doi.org/10.1073/pnas.88.16.7160

Eagon, R.G., 1962. *Pseudomonas natriegens*, a marine bacterium with a generation time of less than 10 minutes. J. Bacteriol. 83, 736–737.

Eggeling, L., Bott, M., 2015. A giant market and a powerful metabolism: L-lysine provided by *Corynebacterium glutamicum*. Appl. Microbiol. Biotechnol. 99, 3387–3394. https://doi.org/10.1007/s00253-015-6508-2

Eggeling, L., Bott, M., 2005. Handbook of *Corynebacterium glutamicum*. CRC press.

Ellis, G.A., Tschirhart, T., Spangler, J., Walper, S.A., Medintz, I.L., Vora, G.J., 2019. Exploiting the Feedstock Flexibility of the Emergent Synthetic Biology Chassis *Vibrio natriegens* for Engineered Natural Product Production. Mar. Drugs 17, 1–21. https://doi.org/10.3390/md17120679

Ellis, T., Adie, T., Baldwin, G.S., 2011. DNA assembly for synthetic biology: From parts to pathways and beyond. Integr. Biol. 3, 109–118. https://doi.org/10.1039/c0ib00070a

Endy, D., 2005. Foundations for engineering biology. Nature 438, 449–453. https://doi.org/10.1038/nature04342

Erian, A.M., Freitag, P., Gibisch, M., Pflügl, S., 2020. High rate 2,3-butanediol production with *Vibrio natriegens*. Bioresour. Technol. Reports 10. https://doi.org/10.1016/j.biteb.2020.100408

Failmezger, J., Scholz, S., Blombach, B., Siemann-Herzberg, M., 2018. Cell-free protein synthesis from fast-growing *Vibrio natriegens*. Front. Microbiol. 9, 1–10.

https://doi.org/10.3389/fmicb.2018.01146

Fernández-Cabezón, L., Cros, A., Nikel, P.I., 2019. Evolutionary approaches for engineering industrially-relevant phenotypes in bacterial cell factories. Biotechnol. J. 14, 1800439. https://doi.org/10.1002/biot.201800439

Fiedurek, J., Trytek, M., Szczodrak, J., 2017. Strain improvement of industrially important microorganisms based on resistance to toxic metabolites and abiotic stress. J. Basic Microbiol. 57, 445–459. https://doi.org/10.1002/jobm.201600710

Flachbart, L.K., Sokolowsky, S., Marienhagen, J., 2019. Displaced by Deceivers: Prevention of Biosensor Cross-Talk Is Pivotal for Successful Biosensor-Based High-Throughput Screening Campaigns. ACS Synth. Biol. 8, 1847–1857. https://doi.org/10.1021/acssynbio.9b00149

Goeddel, D. V., Kleid, D.G., Bolivar, F., 1979. Expression in *Escherichia coli* of chemically synthesized genes for human insulin. Proc. Natl. Acad. Sci. U. S. A. 76, 106–110. https://doi.org/10.1073/pnas.76.1.106

Guo, Y., Han, M., Xu, J., Zhang, W., 2015. Analysis of acetohydroxyacid synthase variants from branched-chain amino acids-producing strains and their effects on the synthesis of branched-chain amino acids in *Corynebacterium glutamicum*. Protein Expr. Purif. 109, 106–112. https://doi.org/10.1016/j.pep.2015.02.006

Hillson, N., Caddick, M., Cai, Y., Carrasco, J.A., Chang, M.W., Curach, N.C., Bell, D.J., Le Feuvre, R., Friedman, D.C., Fu, X., Gold, N.D., Herrgård, M.J., Holowko, M.B., Johnson, J.R., Johnson, R.A., Keasling, J.D., Kitney, R.I., Kondo, A., Liu, C., Martin, V.J.J., Menolascina, F., Ogino, C., Patron, N.J., Pavan, M., Poh, C.L., Pretorius, I.S., Rosser, S.J., Scrutton, N.S., Storch, M., Tekotte, H., Travnik, E., Vickers, C.E., Yew, W.S., Yuan, Y., Zhao, H., Freemont, P.S., 2019. Building a global alliance of biofoundries. Nat. Commun. 10, 2040. https://doi.org/10.1038/s41467-019-10079-2

Hoff, J., Daniel, B., Stukenberg, D., Thuronyi, B.W., Waldminghaus, T., Fritz, G., 2020. *Vibrio natriegens*: an ultrafast-growing marine bacterium as emerging synthetic biology chassis. Environ. Microbiol. 22, 4394–4408. https://doi.org/10.1111/1462-2920.15128

Hoffart, E., Grenz, S., Lange, J., Nitschel, R., Müller, F., Schwentner, A., Feith, A., Lenfers-Lücker, M., Takors, R., Blombach, B., 2017. High substrate uptake rates empower *Vibrio natriegens* as production host for industrial biotechnology. Appl. Environ. Microbiol. 83, e01614–e01617. https://doi.org/10.1128/AEM.01614-17

Hughes, S.R., Dowd, P.F., Hector, R.E., Riedmuller, S.B., Bartolett, S., Mertens, J.A., Qureshi, N., Liu, S., Bischoff, K.M., Li, X.L., Jackson, J.S., Sterner, D., Panavas, T., Rich, J.O., Farrelly, P.J., Butt, T., Cotta, M.A., 2007. Cost-Effective High-Throughput Fully Automated Construction of a Multiplex Library of Mutagenized Open Reading Frames for an Insecticidal Peptide Using a Plasmid-Based Functional Proteomic Robotic Workcell with Improved Vacuum System. J. Assoc. Lab. Autom. 12, 202–212. https://doi.org/10.1016/j.jala.2007.04.007

Jacob, F., Monod, J., 1961. Genetic regulatory mechanisms in the synthesis of proteins. J. Mol. Biol. 3, 318–356. https://doi.org/10.1016/S0022-2836(61)80072-7

Jiang, X., Palazzotto, E., Wybraniec, E., Munro, L.J., Zhang, H., Kell, D.B., Weber, T., Lee, S.Y., 2020. Automating Cloning by Natural Transformation. ACS Synth. Biol. 9, 3228–3235. https://doi.org/10.1021/acssynbio.0c00240

Jiang, Y., Qian, F., Yang, J., Liu, Y., Dong, F., Xu, C., Sun, B., Chen, B., Xu, X., Li, Y., Wang, R., Yang, S., 2017. CRISPR-Cpf1 assisted genome editing of *Corynebacterium glutamicum*. Nat. Commun. 8, 1–11. https://doi.org/10.1038/ncomms15179

Jinek, M., Chylinski, K., Fonfara, I., Hauer, M., Doudna, J.A., Charpentier, E., 2012. A Programmable Dual-RNA – Guided DNA Endonuclease in Adaptive Bacterial Immunity. Science 337, 816–822. https://doi.org/10.1126/science.1225829

Kalinowski, J., Bathe, B., Bartels, D., Bischoff, N., Bott, M., Burkovski, A., Dusch, N., Eggeling, L., Eikmanns, B.J., Gaigalat, L., Goesmann, A., Hartmann, M., Huthmacher, K., Krämer, R., Linke, B., McHardy, A.C., Meyer, F., Möckel, B., Pfefferle, W., Pühler, A., Rey, D.A., Rückert, C., Rupp, O., Sahm, H., Wendisch, V.F., Wiegräbe, I., Tauch, A., 2003. The complete *Corynebacterium glutamicum* ATCC 13032 genome sequence and its impact on the production of L-aspartate-derived amino acids and vitamins. J. Biotechnol. 104, 5–25. https://doi.org/10.1016/S0168-1656(03)00154-8

Kennerknecht, N., Sahm, H., Yen, M.R., Pátek, M., Saier, M.H., Eggeling, L., 2002. Export of L-isoleucine from *Corynebacterium glutamicum*: A two-gene-encoded member of a new translocator family. J. Bacteriol. 184, 3947–3956. https://doi.org/10.1128/JB.184.14.3947-3956.2002

Kinoshita, S., Udaka, S., Shimono, S., 1957. Studies on the Amino Acid Fermentation. J. Gen. Appl. Microbiol. 3, 193–205. https://doi.org/10.2323/jgam.3.193

Kiviet, D.J., Nghe, P., Walker, N., Boulineau, S., Sunderlikova, V., Tans, S.J., 2014. Stochasticity of metabolism and growth at the single-cell level. Nature 514, 376–379. https://doi.org/10.1038/nature13582

Kojima, R., Aubel, D., Fussenegger, M., 2020. Building sophisticated sensors of extracellular cues that enable mammalian cells to work as “doctors” in the body. Cell. Mol. Life Sci. 77, 3567–3581. https://doi.org/10.1007/s00018-020-03486-y

LaCroix, R.A., Palssona, B., Feista, A., 2017. A Model for Designing Adaptive Laboratory Evolution Experiments. Appl. Environ. Microbiol. 83, 1–14.

Lamarck, J.-B., 1809. Philosophie zoologique.

Lange, C., Mustafi, N., Frunzke, J., Kennerknecht, N., Wessel, M., Bott, M., Wendisch, V.F., 2012. Lrp of *Corynebacterium glutamicum* controls expression of the brnFE operon encoding the export system for L-methionine and branched-chain amino acids. J. Biotechnol. 158, 231–241. https://doi.org/10.1016/j.jbiotec.2011.06.003

Leavitt, J.M., Wagner, J.M., Tu, C.C., Tong, A., Liu, Y., Alper, H.S., 2017. Biosensor-Enabled Directed Evolution to Improve Muconic Acid Production in *Saccharomyces cerevisiae*. Biotechnol. J. 12, 1600687. https://doi.org/10.1002/biot.201600687

Lee, H., Popodi, E., Tang, H., Foster, P.L., 2012. Rate and molecular spectrum of spontaneous mutations in the bacterium *Escherichia coli* as determined by whole-genome sequencing. Proc. Natl. Acad. Sci. 109, E2774–E2783. https://doi.org/10.1073/pnas.1210309109

Lee, H.H., Ostrov, N., Wong, B.G., Gold, M.A., Khalil, A.S., Church, G.M., 2019. Functional genomics of the rapidly replicating bacterium *Vibrio natriegens* by CRISPRi. Nat. Microbiol. 4, 1105–1113. https://doi.org/10.1038/s41564-019-0423-8

Lee, J.Y., Na, Y.A., Kim, E., Lee, H.S., Kim, P., 2016. The actinobacterium *Corynebacterium glutamicum*, an industrial workhorse. J Microbiol Biotechnol 26, 807–822. https://doi.org/10.4014/jmb.1601.01053

Lenski, R.E., 2017. Experimental evolution and the dynamics of adaptation and genome evolution in microbial populations. ISME J. 11, 2181–2194. https://doi.org/10.1038/ismej.2017.69

Lin, J.L., Wagner, J.M., Alper, H.S., 2017. Enabling tools for high-throughput detection of metabolites:

Metabolic engineering and directed evolution applications. Biotechnol. Adv. 35, 950–970. https://doi.org/10.1016/j.biotechadv.2017.07.005

Liu, S. De, Wu, Y.N., Wang, T.M., Zhang, C., Xing, X.H., 2017. Maltose Utilization as a Novel Selection Strategy for Continuous Evolution of Microbes with Enhanced Metabolite Production. ACS Synth. Biol. 6, 2326–2338. https://doi.org/10.1021/acssynbio.7b00247

Liu, L., Pan, A., Spofford, C., Zhou, N., Alper, H.S., 2015. An evolutionary metabolic engineering approach for enhancing lipogenesis in *Yarrowia lipolytica*. Metab. Eng. 29, 36–45. https://doi.org/10.1016/j.ymben.2015.02.003

Liu, Y., Wang, X., Zhan, J., Hu, J., 2019. The 138th residue of acetohydroxyacid synthase in *Corynebacterium glutamicum* is important for the substrate binding specificity. Enzyme Microb. Technol. 129, 109357. https://doi.org/10.1016/j.enzmictec.2019.06.001

Locey, K.J., Lennon, J.T., 2016. Scaling laws predict global microbial diversity. Proc. Natl. Acad. Sci. U. S. A. 113, 5970–5975. https://doi.org/10.1073/pnas.1521291113

Luo, H., Hansen, A.S.L., Yang, L., Schneider, K., Kristensen, M., Christensen, U., Christensen, H.B., Du, B., Özdemir, E., Feist, A.M., Keasling, J.D., Jensen, M.K., Herrgård, M.J., Palsson, B.O., 2019. Coupling S-adenosylmethionine–dependent methylation to growth: Design and uses. PLoS Biol. 17, 1–13. https://doi.org/10.1371/journal.pbio.2007050

Ma, Y., Zhang, J., Yin, W., Zhang, Z., Song, Y., Chang, X., 2016. Targeted AID-mediated mutagenesis (TAM) enables efficient genomic diversification in mammalian cells. Nat. Methods 13, 1029–1035. https://doi.org/10.1038/nmeth.4027

Mahr, R., Frunzke, J., 2016. Transcription factor-based biosensors in biotechnology: current state and future prospects. Appl. Microbiol. Biotechnol. 100, 79–90. https://doi.org/10.1007/s00253-015-7090-3

Mahr, R., Gätgens, C., Gätgens, J., Polen, T., Kalinowski, J., Frunzke, J., 2015. Biosensor-driven adaptive laboratory evolution of L-valine production in *Corynebacterium glutamicum*. Metab. Eng. 32, 184–194. https://doi.org/10.1016/j.ymben.2015.09.017

Maida, I., Bosi, E., Perrin, E., Papaleo, M.C., Orlandini, V., Fondi, M., Fani, R., Wiegel, J., Bianconi, G., Canganella, F., 2013. Draft Genome Sequence of the Fast-Growing Bacterium *Vibrio natriegens* Strain DSMZ 759. Genome Announc. 1, 1–2. https://doi.org/10.1186/1471-2164-9-75.9.

Mans, R., Daran, J.M.G., Pronk, J.T., 2018. Under pressure: evolutionary engineering of yeast strains for improved performance in fuels and chemicals production. Curr. Opin. Biotechnol. 50, 47–56. https://doi.org/10.1016/j.copbio.2017.10.011

Masel, J., 2011. Genetic drift. Curr. Biol. 21, R837–R838. https://doi.org/10.1016/j.cub.2011.08.007

Maslowska, K.H., Makiela-Dzbenska, K., Mo, J.Y., Fijalkowska, I.J., Schaaper, R.M., 2018. High-accuracy lagging-strand DNA replication mediated by DNA polymerase dissociation. Proc. Natl. Acad. Sci. U. S. A. 115, 4212–4217. https://doi.org/10.1073/pnas.1720353115

McNutt, M.K., Bradford, M., Drazen, J.M., Hanson, B., Howard, B., Jamieson, K.H., Kiermer, V., Marcus, E., Pope, B.K., Schekman, R., Swaminathan, S., Stang, P.J., Verma, I.M., 2018. Transparency in authors' contributions and responsibilities to promote integrity in scientific publication. Proc. Natl. Acad. Sci. U. S. A. 115, 2557–2560. https://doi.org/10.1073/pnas.1715374115

Meyer, A.J., Segall-Shapiro, T.H., Glassey, E., Zhang, J., Voigt, C.A., 2019. *Escherichia coli* "Marionette" strains with 12 highly optimized small-molecule sensors. Nat. Chem. Biol. 15, 196–204. https://doi.org/10.1038/s41589-018-0168-3

Moore, J.A., Nemat-Gorgani, M., Madison, A.C., Sandahl, M.A., Punnamaraju, S., Eckhardt, A.E., Pollack, M.G., Vigneault, F., Church, G.M., Fair, R.B., Horowitz, M.A., Griffin, P.B., 2017. Automated electrotransformation of *Escherichia coli* on a digital microfluidic platform using bioactivated magnetic beads. Biomicrofluidics 11, 1–18. https://doi.org/10.1063/1.4975391

Mustafi, N., Grünberger, A., Kohlheyer, D., Bott, M., Frunzke, J., 2012. The development and application of a single-cell biosensor for the detection of L-methionine and branched-chain amino acids. Metab. Eng. 14, 449–457. https://doi.org/10.1016/j.ymben.2012.02.002

Mustafi, N., Grünberger, A., Mahr, R., Helfrich, S., Nöh, K., Blombach, B., Kohlheyer, D., Frunzke, J., 2014. Application of a genetically encoded biosensor for live cell imaging of L-valine production in pyruvate dehydrogenase complex-deficient *Corynebacterium glutamicum* strains. PLoS One 9, e85731. https://doi.org/10.1371/journal.pone.0085731

Nanda, A.M., Thormann, K., Frunzke, J., 2015. Impact of spontaneous prophage induction on the fitness of bacterial populations and host-microbe interactions. J. Bacteriol. 197, 410–419. https://doi.org/10.1128/JB.02230-14

Nielsen, J., Keasling, J.D., 2016. Engineering Cellular Metabolism. Cell 164, 1185–1197. https://doi.org/10.1016/j.cell.2016.02.004

Ogden, S., Haggerty, D., Stoner, C.M., Kolodrubetz, D., Schleif, R., 1980. The *Escherichia coli* L-arabinose operon: Binding sites of the regulatory proteins and a mechanism of positive and negative regulation. Proc. Natl. Acad. Sci. U. S. A. 77, 3346–3350. https://doi.org/10.1073/pnas.77.6.3346

Paddon, C.J., Westfall, P.J., Pitera, D.J., Benjamin, K., Fisher, K., McPhee, D., Leavell, M.D., Tai, a, Main, a, Eng, D., Polichuk, D.R., Teoh, K.H., Reed, D.W., Treynor, T., Lenihan, J., Fleck, M., Bajad, S., Dang, G., Dengrove, D., Diola, D., Dorin, G., Ellens, K.W., Fickes, S., Galazzo, J., Gaucher, S.P., Geistlinger, T., Henry, R., Hepp, M., Horning, T., Iqbal, T., Jiang, H., Kizer, L., Lieu, B., Melis, D., Moss, N., Regentin, R., Secrest, S., Tsuruta, H., Vazquez, R., Westblade, L.F., Xu, L., Yu, M., Zhang, Y., Zhao, L., Lievense, J., Covello, P.S., Keasling, J.D., Reiling, K.K., Renninger, N.S., Newman, J.D., 2013. High-level semi-synthetic production of the potent antimalarial artemisinin. Nature 496, 528–32. https://doi.org/10.1038/nature12051

Payne, W.J., 1960. Effects of sodium and potassium ions on growth and substrate penetration of a marine pseudomonad. J. Bacteriol. 80, 696–700.

Payne, W.J., 1958. Studies on bacterial utilization of uronic acids. III. Induction of oxidative enzymes in a marine isolate. J. Bacteriol. 76, 301–307.

Payne, W.J., Eagon, R.G., Williams, A.K., 1961. Some Observations on the Physiology of *Psuedomonas natriegens* nov. Spec. Antonie Van Leeuwenhoek 27, 121–128.

Pfeifer-Sancar, K., Mentz, A., Rückert, C., Kalinowski, J., 2013. Comprehensive analysis of the *Corynebacterium glutamicum* transcriptome using an improved RNAseq technique. BMC Genomics 14, 1–23. https://doi.org/10.1186/1471-2164-14-888

Pfeifer, E., Gätgens, C., Polen, T., Frunzke, J., 2017. Adaptive laboratory evolution of *Corynebacterium glutamicum* towards higher growth rates on glucose minimal medium. Sci. Rep. 7, 16780. https://doi.org/10.1038/s41598-017-17014-9

Pfeifer, E., Michniewski, S., Gätgens, C., Münch, E., Müller, F., Polen, T., Millard, A., Blombach, B., Frunzke, J., 2019. Generation of a Prophage-Free Variant of the Fast-Growing Bacterium *Vibrio natriegens*. Appl. Environ. Microbiol. 85, e00853-19. https://doi.org/10.1128/aem.00853-19

Radek, A., Tenhaef, N., Müller, M.F., Brüsseler, C., Wiechert, W., Marienhagen, J., Polen, T., Noack, S.,

2017. Miniaturized and automated adaptive laboratory evolution: Evolving *Corynebacterium glutamicum* towards an improved d-xylose utilization. Bioresour. Technol. 245, 1377–1385. https://doi.org/10.1016/j.biortech.2017.05.055

Raman, S., Rogers, J.K., Taylor, N.D., Church, G.M., 2014. Evolution-guided optimization of biosynthetic pathways. Proc. Natl. Acad. Sci. 111, 17803–17808. https://doi.org/10.1073/PNAS.1409523111

Reyes, L.H., Gomez, J.M., Kao, K.C., 2014. Improving carotenoids production in yeast via adaptive laboratory evolution. Metab. Eng. 21, 26–33. https://doi.org/10.1016/j.ymben.2013.11.002

Rogers, J.K., Church, G.M., 2016. Genetically encoded sensors enable real-time observation of metabolite production. Proc. Natl. Acad. Sci. 113, 2388–2393. https://doi.org/10.1073/pnas.1600375113

Roggo, C., van der Meer, J.R., 2017. Miniaturized and integrated whole cell living bacterial sensors in field applicable autonomous devices. Curr. Opin. Biotechnol. 45, 24–33. https://doi.org/10.1016/j.copbio.2016.11.023

Rugbjerg, P., Sarup-Lytzen, K., Nagy, M., Sommer, M.O.A., 2018. Synthetic addiction extends the productive life time of engineered *Escherichia coli* populations. Proc. Natl. Acad. Sci. 115, 2347–2352. https://doi.org/10.1073/pnas.1718622115

Saleski, T.E., Kerner, A.R., Chung, M.T., Jackman, C.M., Khasbaatar, A., Kurabayashi, K., Lin, X.N., 2019. Syntrophic co-culture amplification of production phenotype for high-throughput screening of microbial strain libraries. Metab. Eng. 54, 232–243. https://doi.org/https://doi.org/10.1016/j.ymben.2019.04.007

Sambrook, J., MacCallum, P., Russell, D.W., 2001. Molecular cloning: a laboratory manual. Cold Spring Harbor Laboratory, Cold Spring Harbor, NY.

Sandberg, T.E., Salazar, M.J., Weng, L.L., Palsson, B.O., Feist, A.M., 2019. The emergence of adaptive laboratory evolution as an efficient tool for biological discovery and industrial biotechnology. Metab. Eng. 56, 1–16. https://doi.org/10.1016/j.ymben.2019.08.004

Schaaper, R.M., 1993. Base selection, proofreading, and mismatch repair during DNA replication in *Escherichia coli*. J. Biol. Chem. 268, 23762–23765. https://doi.org/10.1016/s0021-9258(20)80446-3

Schallmey, M., Frunzke, J., Eggeling, L., Marienhagen, J., 2014. Looking for the pick of the bunch: High-throughput screening of producing microorganisms with biosensors. Curr. Opin. Biotechnol. 26, 148–154. https://doi.org/10.1016/j.copbio.2014.01.005

Schendzielorz, G., Dippong, M., Grünberger, A., Kohlheyer, D., Yoshida, A., Binder, S., Nishiyama, C., Nishiyama, M., Bott, M., Eggeling, L., 2014. Taking control over control: Use of product sensing in single cells to remove flux control at key enzymes in biosynthesis pathways. ACS Synth. Biol. 3, 21–29. https://doi.org/10.1021/sb400059y

Schleif, R., 2000. Regulation of the L-arabinose operon of *Escherichia coli*. Trends Genet. 16, 559–565. https://doi.org/10.1016/S0168-9525(00)02153-3

Schmidt-Dannert, C., Arnold, F.H., 1999. Directed evolution of industrial enzymes. Trends Biotechnol. 17, 135–136. https://doi.org/10.1016/S0167-7799(98)01283-9

Schröder, J., Tauch, A., 2010. Transcriptional regulation of gene expression in *Corynebacterium glutamicum*: the role of global, master and local regulators in the modular and hierarchical gene regulatory network. FEMS Microbiol. Rev. 34, 685–737. https://doi.org/10.1111/j.1574-6976.2010.00228.x

Shepelin, D., Hansen, A.S.L., Lennen, R., Luo, H., Herrgård, M.J., 2018. Selecting the best: Evolutionary engineering of chemical production in microbes. Genes (Basel). 9, 249. https://doi.org/10.3390/genes9050249

Shih, S.C.C., Goyal, G., Kim, P.W., Koutsoubelis, N., Keasling, J.D., Adams, P.D., Hillson, N.J., Singh, A.K., 2015. A Versatile Microfluidic Device for Automating Synthetic Biology. ACS Synth. Biol. 4, 1151–1164. https://doi.org/10.1021/acssynbio.5b00062

Siedler, S., Schendzielorz, G., Binder, S., Eggeling, L., Bringer, S., Bott, M., 2014. SoxR as a single-cell biosensor for NADPH-consuming enzymes in *Escherichia coli*. ACS Synth. Biol. 3, 41–47. https://doi.org/10.1021/sb400110j

Simon, A.J., d'Oelsnitz, S., Ellington, A.D., 2019. Synthetic evolution. Nat. Biotechnol. 37, 730–743. https://doi.org/10.1038/s41587-019-0157-4

Skjoedt, M.L., Snoek, T., Kildegaard, K.R., Arsovska, D., Eichenberger, M., Goedecke, T.J., Rajkumar, A.S., Zhang, J., Kristensen, M., Lehka, B.J., Siedler, S., Borodina, I., Jensen, M.K., Keasling, J.D., 2016. Engineering prokaryotic transcriptional activators as metabolite biosensors in yeast. Nat. Chem. Biol. 12, 951–958. https://doi.org/10.1038/nchembio.2177

Smith, H.O., Welcox, K.W., 1970. A Restriction enzyme from *Hemophilus influenzae*. I. Purification and general properties. J. Mol. Biol. 51, 379–391. https://doi.org/10.1016/0022-2836(70)90149-X

Snoek, T., Romero-Suarez, D., Zhang, J., Ambri, F., Skjoedt, M.L., Sudarsan, S., Jensen, M.K., Keasling, J.D., 2018. An Orthogonal and pH-Tunable Sensor-Selector for Muconic Acid Biosynthesis in Yeast. ACS Synth. Biol. 7, 995–1003. https://doi.org/10.1021/acssynbio.7b00439

Sonntag, C.K., Flachbart, L.K., Maass, C., Vogt, M., Marienhagen, J., 2020. A unified design allows fine-tuning of biosensor parameters and application across bacterial species. Metab. Eng. Commun. 11, e00150. https://doi.org/10.1016/j.mec.2020.e00150

Steffen, V., Otten, J., Engelmann, S., Radek, A., Limberg, M., Koenig, B.W., Noack, S., Wiechert, W., Pohl, M., 2016. A toolbox of genetically encoded FRET-based biosensors for rapid L-lysine analysis. Sensors 16, 1604. https://doi.org/10.3390/s16101604

Stella, R.G., Wiechert, J., Noack, S., Frunzke, J., 2019. Evolutionary engineering of *Corynebacterium glutamicum*. Biotechnol. J. 14, 1800444. https://doi.org/10.1002/biot.201800444

Stukenberg, D., Hensel, T., Hoff, J., Daniel, B., Inckemann, R., Tedeschi, J.N., Nousch, F., Fritz, G., 2021. The Marburg Collection: A Golden Gate DNA Assembly Framework for Synthetic Biology Applications in *Vibrio natriegens*. bioRxiv 2021.03.26.437105.

Sun, X., Li, Q., Wang, Y., Zhou, W., Guo, Y., Chen, J., Zheng, P., Sun, J., Ma, Y., 2021. Isoleucyl-tRNA synthetase mutant based whole-cell biosensor for high-throughput selection of isoleucine overproducers. Biosens. Bioelectron. 172, 112783. https://doi.org/10.1016/j.bios.2020.112783

SYNTHACE, 2018. Computer Aided Biology.

Tani, Y., Lim, W.J., Yang, H.C., 1988. Isolation of l-methionine-enriched mutant of a methylotrophic yeast, *Candida biodinii* No. 2201. J. Ferment. Technol. 66, 153–158. https://doi.org/10.1016/0385-6380(88)90041-6

Tenhaef, N., Stella, R., Frunzke, J., Noack, S., 2021. Automated Rational Strain Construction Based on High-Throughput Conjugation. ACS Synth. Biol. 10, 589–599. https://doi.org/10.1021/acssynbio.0c00599

Teshiba, S., Furuya, A., 1983. Mechanisms of 5'-inosinic acid accumulation by permeability mutants of Brevibacterium ammoniagenes. II. Sensitivities of a series of mutants to various drugs. Agric. Biol.

Chem. 47, 1035–1041. https://doi.org/10.1080/00021369.1983.10865777

Theisen, M., Liao, J.C., Becker, J., Wittmann, C., Diethard, M., Gasser, B., Egermeier, M., Marx, H., Sauer, M., 2017. Industrial Biotechnology: *Escherichia coli* as a Host. Ind. Biotechnol. Microorg., Wiley Online Books. https://doi.org/https://doi.org/10.1002/9783527807796.ch5

Thoma, F., Blombach, B., 2021. Metabolic engineering of *Vibrio natriegens*. Essays Biochem. 14048, 1–12. https://doi.org/10.1042/ebc20200135

Thykaer, J., Nielsen, J., 2003. Metabolic engineering of β-lactam production. Metab. Eng. 5, 56–69. https://doi.org/10.1016/S1096-7176(03)00003-X

Tschirhart, T., Shukla, V., Kelly, E.E., Schultzhaus, Z., Newringeisen, E., Erickson, J.S., Wang, Z., Garcia, W., Curl, E., Egbert, R.G., Yeung, E., Vora, G.J., 2019. Synthetic Biology Tools for the Fast-Growing Marine Bacterium *Vibrio natriegens*. ACS Synth. Biol. 8, 2069–2079. https://doi.org/10.1021/acssynbio.9b00176

Vogt, M., Haas, S., Klaffl, S., Polen, T., Eggeling, L., Van Ooyen, J., Bott, M., 2014. Pushing product formation to its limit: Metabolic engineering of *Corynebacterium glutamicum* for l-leucine overproduction. Metab. Eng. 22, 40–52. https://doi.org/10.1016/j.ymben.2013.12.001

Vrljic, M., Sahm, H., Eggeling, L., 1996. A new type of transporter with a new type of cellular function: L-lysine export from *Corynebacterium glutamicum*. Mol. Microbiol. 22, 815–826. https://doi.org/10.1046/j.1365-2958.1996.01527.x

Wang, H.H., Isaacs, F.J., Carr, P.A., Sun, Z.Z., Xu, G., Forest, C.R., Church, G.M., 2009. Programming cells by multiplex genome engineering and accelerated evolution. Nature 460, 894–898. https://doi.org/10.1038/nature08187

Wang, Y., Liu, Y., Liu, J., Guo, Y., Fan, L., Ni, X., Zheng, X., Wang, M., Zheng, P., Sun, J., Ma, Y., 2018. MACBETH: multiplex automated *Corynebacterium glutamicum* base editing method. Metab. Eng. 47, 200–210. https://doi.org/10.1016/j.ymben.2018.02.016

Wang, Z., Lin, B., Hervey IV, W.J., Vora, G.J., 2013. Draft Genome Sequence of the Fast-Growing Marine Bacterium *Vibrio natriegens* Strain ATCC 14048. Genome Announc. 1, 736–737. https://doi.org/10.1128/genomeA.00589-13.Copyright

Wang, Z., Tschirhart, T., Schultzhaus, Z., Kelly, E.E., Chen, A., Oh, E., Nag, O., Glaser, E.R., Kim, E., Lloyd, P.F., Charles, P.T., Li, W., Leary, D., Compton, J., Phillips, D.A., Dhinojwala, A., Payne, G.F., Vora, G.J., 2020. Melanin produced by the fast-growing marine bacterium *Vibrio natriegens* through heterologous biosynthesis: Characterization and application. Appl. Environ. Microbiol. 86, e02749-19. https://doi.org/10.1128/AEM.02749-19

Watve, M.G., Tickoo, R., Jog, M.M., Bhole, B.D., 2001. How many antibiotics are produced by the genus *Streptomyces*? Arch. Microbiol. 176, 386–390. https://doi.org/10.1007/s002030100345

Webb, C.D., Payne, W.J., 1971. Influence of Na+ on synthesis of macromolecules by a marine bacterium. Appl. Microbiol. 21, 1080–8.

Weinstock, M.T., Hesek, E.D., Wilson, C.M., Gibson, D.G., 2016. *Vibrio natriegens* as a fast-growing host for molecular biology. Nat. Methods 13, 849–851. https://doi.org/10.1038/nmeth.3970

Weizmann, C., 1919. Improvements in the Bacterial Fermentation of Carbohydrates and in Bacterial Cultures for the same. GBD191504845 19150329.

Wendisch, V.F., 2014. Microbial production of amino acids and derived chemicals: Synthetic biology approaches to strain development. Curr. Opin. Biotechnol. 30, 51–58. https://doi.org/10.1016/j.copbio.2014.05.004

Wiegand, D.J., Lee, H.H., Ostrov, N., Church, G.M., 2018. Establishing a Cell-Free *Vibrio natriegens* Expression System. ACS Synth. Biol. 7, 2475–2479. https://doi.org/10.1021/acssynbio.8b00222

Williams, T.C., Pretorius, I.S., Paulsen, I.T., 2016. Synthetic Evolution of Metabolic Productivity Using Biosensors. Trends Biotechnol. 34, 371–381. https://doi.org/10.1016/j.tibtech.2016.02.002

Wouter Wisselink, H., Toirkens, M.J., Wu, Q., Pronk, J.T., Van Maris, A.J.A., 2009. Novel evolutionary engineering approach for accelerated utilization of glucose, xylose, and arabinose mixtures by engineered *Saccharomyces cerevisiae* strains. Appl. Environ. Microbiol. 75, 907–914. https://doi.org/10.1128/AEM.02268-08

Xiao, Y., Bowen, C.H., Liu, D., Zhang, F., 2016. Exploiting nongenetic cell-to-cell variation for enhanced biosynthesis. Nat. Chem. Biol. 12, 339–344. https://doi.org/10.1038/nchembio.2046

Xu, M., Liu, P., Chen, J., Peng, A., Yang, T., Zhang, X., Xu, Z., Rao, Z., 2020. Development of a Novel Biosensor-Driven Mutation and Selection System via in situ Growth of *Corynebacterium crenatum* for the Production of L-Arginine. Front. Bioeng. Biotechnol. 8, 175. https://doi.org/10.3389/fbioe.2020.00175

Yehezkel, T. Ben, Nagar, S., Mackrants, D., Marx, Z., Linshiz, G., Shabi, U., Shapiro, E., 2011. Computer-aided high-throughput cloning of bacteria in liquid medium. Biotechniques 50, 124–127. https://doi.org/10.2144/000113514

Zhang, F., Carothers, J.M., Keasling, J.D., 2012. Design of a dynamic sensor-regulator system for production of chemicals and fuels derived from fatty acids. Nat. Biotechnol. 30, 354–359. https://doi.org/10.1038/nbt.2149

Zhang, F., Keasling, J., 2011. Biosensors and their applications in microbial metabolic engineering. Trends Microbiol. 19, 323–329. https://doi.org/10.1016/j.tim.2011.05.003

Zhang, J., Jensen, M.K., Keasling, J.D., 2015. Development of biosensors and their application in metabolic engineering. Curr. Opin. Chem. Biol. 28, 1–8. https://doi.org/10.1016/j.cbpa.2015.05.013

Zhang, X., Jantama, K., Moore, J.C., Shanmugam, K.T., Ingram, L.O., 2007. Production of L-alanine by metabolically engineered *Escherichia coli*. Appl. Microbiol. Biotechnol. 77, 355–366. https://doi.org/10.1007/s00253-007-1170-y

3. Publications

To determine author contributions for the publications and manuscripts presented in the following sections of this thesis, the "Contributor Roles Taxonomy" (CRediT) methodology was used (McNutt et al., 2018). The author roles and role definitions are summarized in the table below.

Contributor role	Role definition
Conceptualization	Ideas; formulation or evolution of overarching research goals and aims.
Formal analysis	Application of statistical, mathematical, computational, or other formal techniques to analyse or synthesize study data.
Investigation/Experiments	Conducting a research and investigation process, specifically performing the experiments, or data/evidence collection.
Methodology	Development or design of methodology; creation of models.
Project administration	Management and coordination responsibility for the research activity planning and execution.
Software	Programming, software development; designing computer programs; implementation of the computer code and supporting algorithms; testing of existing code components.
Supervision	Oversight and leadership responsibility for the research activity planning and execution, including mentorship external to the core team.
Visualization	Preparation, creation and/or presentation of the published work, specifically visualization/data presentation.
Writing – original draft	Preparation, creation and/or presentation of the published work, specifically writing the initial draft (including substantive translation).
Writing – review & editing	Preparation, creation and/or presentation of the published work by those from the original research group, specifically critical review, commentary or revision – including pre- or post-publication stages.

3.1. Evolutionary engineering of *Corynebacterium glutamicum*

Stella, R. G., Wiechert, J., Noack, S. and Frunzke, J.

Published in *Biotechnology Journal*, 2019.

Contributor role	Role definition
Conceptualization	RS 35%, JW 10%, SN 10%, JF 45%
Formal analysis	-
Investigation/Experiments	-
Methodology	-
Project administration	RS 50%, JW 5%, JF 45%
Software	-
Supervision	RS 50%, JF 50%
Visualization	RS 100%
Writing – original draft	RS 60%, JW 10%, SN 10%, JF 20%
Writing – review & editing	RS 45%, JW 5%, SN 5%, JF 45%

Overall contribution RS: 60%

Robert Stella wrote the main part of this review, and contributed to its conceptualization. More specifically, Sections 1, 3, 6 and 7 were written by RS. All visualizations were created by RS.

REVIEW

Biotechnology Journal
www.biotechnology-journal.com

Evolutionary engineering of *Corynebacterium glutamicum*

*Roberto G. Stella, Johanna Wiechert, Stephan Noack, and Julia Frunzke**

A unique feature of biotechnology is that we can harness the power of evolution to improve process performance. Rational engineering of microbial strains has led to the establishment of a variety of successful bioprocesses, but it is hampered by the overwhelming complexity of biological systems. Evolutionary engineering represents a straightforward approach for fitness-linked phenotypes (e.g., growth or stress tolerance) and is successfully applied to select for strains with improved properties for particular industrial applications. In recent years, synthetic evolution strategies have enabled selection for increased small molecule production by linking metabolic productivity to growth as a selectable trait. This review summarizes the evolutionary engineering strategies performed with the industrial platform organism *Corynebacterium glutamicum*. An increasing number of recent studies highlight the potential of adaptive laboratory evolution (ALE) to improve growth or stress resistance, implement the utilization of alternative carbon sources, or improve small molecule production. Advances in next-generation sequencing and automation technologies will foster the application of ALE strategies to streamline microbial strains for bioproduction and enhance our understanding of biological systems.

1. Introduction

The Gram-positive actinomycete *Corynebacterium glutamicum* has a long-standing history in microbial biotechnology, following its isolation in 1957 by Kinoshita et al.[1] due to its potential to secrete large amounts of L-glutamate.[2] In the last few decades, *C. glutamicum* has been engineered for the production of a variety of value-added products, including amino acids, organic acids, polymer precursors, aromatic chemicals, and proteins. These achievements are mainly the result of classical metabolic engineering and have been summarized in a number of recent reviews.[3–6]

Systems biology and metabolic engineering take a rational approach at strain development and are aided by the high level of information available for *C. glutamicum*, including a comprehensive overview on the transcriptomic map and detailed information on metabolic pathways and their regulation.[5,7,8] Strain construction is accelerated by an ever-increasing amount of synthetic biology tools, such as CRISPR/Cpf1[9] and CRISPRi,[10] which has been covered by several reviews.[5,11,12] Transcription factor-based biosensors, which enable the visualization of cellular productivity at the single-cell level, have proven to be a powerful tool for the high-throughput screening of strain or enzyme libraries and for single-cell analysis of producer strains.[13–16]

While rational approaches are indispensable for the development of industrial platform strains in general, their application is often hampered by the overwhelming complexity of biological systems. Even for well-established model systems, like *C. glutamicum* or *Escherichia coli*, we are still not able to quantitatively predict responses to environmental changes or genetic perturbations. However, nature itself provides us with the most powerful approach for the optimization of biological systems: evolution. Evolutionary engineering, also known as adaptive laboratory evolution (ALE), has a long-standing history in the development of microbial production strains and has been heavily applied to improve growth rates, stress, or product tolerance.[17,18] ALE requires microbial growth, which is usually facilitated by repetitive batch cultivations or continuous cultivations, which can be simple (e.g., shake flasks) or more advanced (e.g., pH auxostats).[17,19] When combined with next-generation sequencing and comprehensive omics analysis, ALE strategies can be used to not only obtain better production strains, but also to identify non-intuitive targets for strain engineering, and ultimately to gain a comprehensive understanding of biological pathway regulation. Furthermore, advances in automation of laboratory workflows and microbial phenotyping are fostering a tremendous increase in throughput and efficiency.

This review gives an overview of evolutionary engineering of *C. glutamicum*, including approaches to improve growth on glucose or alternative carbon sources, stress tolerance, or small molecule production by growth coupling strategies and biosensor-guided evolution (**Figure 1**, examples summarized in **Table 1**). We conclude by highlighting the potential of a smart combination of synthetic biology and workflow automation for next-generation evolutionary engineering approaches.

R. G. Stella, J. Wiechert, Dr. S. Noack, Prof. J. Frunzke
Institute of Bio- and Geosciences, IBG-1: Biotechnology,
Forschungszentrum Jülich
Wilhelm-Johnen-Straße
52428, Jülich, Germany
E-mail: j.frunzke@fz-juelich.de

DOI: 10.1002/biot.201800444

2. Accelerating Growth on Glucose

The time needed for biomass production represents a key factor in the economic success of biotechnological processes. While ALE approaches have been intensively explored to accelerate the growth of *E. coli*,[37,38] so far, only two recent studies have reported on the evolution of *C. glutamicum* towards higher growth rates on glucose minimal medium (Table 1).[20,21] Interestingly, these studies revealed similar key targets for enhancing metabolic flux and increasing substrate uptake rates for both species, indicating that microorganisms follow similar principles to adapt to fast growth.

Among the key targets for improving growth on glucose, mutations in the *pyk* gene, encoding the pyruvate kinase (PK), were recently described. Reintroduction of the identified single-nucleotide polymorphism (SNPs) into the parental strain caused a significant decrease in PK activity (T12A, and A20V).[20] Furthermore, a mutation of alanine 271 to threonine (A271T) was enriched in one cell line. Intriguingly, a PK enzyme carrying this mutation was previously described as being desensitized toward the allosteric activator fructose 1,6-bisphosphate (FBP), resulting in reduced PK activity upon accumulation of the glycolytic intermediate FBP.[39] Mutations in the *pyk* gene were also identified in the prominent *E. coli* long-term evolution experiment that lasted for more than 25 years,[40] and in a recent study by LaCroix et al.[41] where cells were evolved towards fast growth on glucose. It is interesting to note that fast proliferating eukaryotic cells, like embryonic stem cells and cancer cells, also harbor a less active PKM2 isoform of the PK enzyme.[42,43] From these findings, we can conclude that lowering the PK activity appears to be a conserved strategy of fast-growing cells that need to exploit large amounts of glucose for anabolic pathways.

Robert Stella is a Ph.D. student in the group of Prof. Julia Frunzke at Forschungszentrum Jülich, Germany. He received his Master of Science degree in Life Science and Technology from the Delft University of Technology, The Netherlands in 2017. After a research internship at Synthetic Genomics Inc., San Diego, USA in 2017, he started his PhD studies in 2018. His research interests comprise transcription factor-based biosensors, synthetic evolution strategies, lab automation methods, and the intersection of those fields.

Julia Frunzke studied Biology at the University of Marburg. From 2004 to 2007 she did her doctoral studies at Forschungszentrum Jülich and obtained her Ph.D. in 2007 from Heinrich Heine University in Düsseldorf, Germany. Subsequently, she was a postdoctoral fellow at the Institute for Microbiology, ETH Zurich, Switzerland. In 2009 she started her own lab at the Institute of Bio- and Geosciences, IBG-1, at Forschungszentrum Jülich where she held her own Helmholtz Young Investigators Group (2011 to 2016) and was Assistant Professor at the HHU. Since 2017 she holds a position as an Associate Professor in Microbiology at HHU.

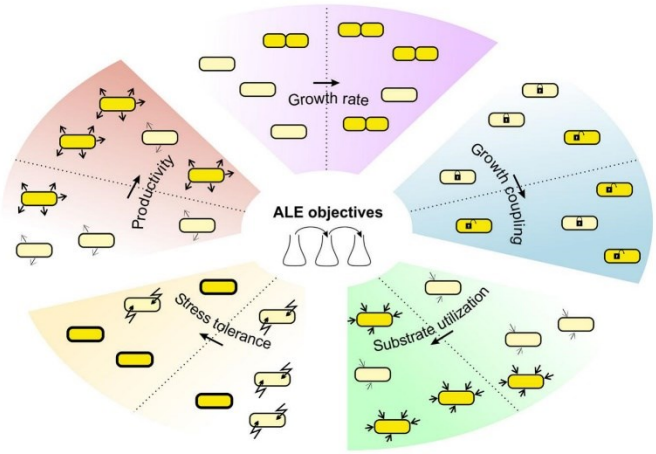

Figure 1. Overview of different objectives in *C. glutamicum* ALE studies. ALE has successfully been applied to increase the growth rate,[20,21] substrate utilization,[22] stress tolerance,[23,24] and small molecule production.[25] Growth coupling strategies have been used to increase precursor supply and small molecule production.[26]

Table 1. Overview of ALE studies with *C. glutamicum*.

ALE target	Experimental setup	ALE duration	Phenotype of evolved strain	Sequencing/ transcriptomics	Proven causal mutations	References
Growth						
Accelerating growth on glucose minimal media	Repetitive batch in minimal media containing glucose as sole carbon source	Approximately 630 generations	26% higher growth rate ($0.67 \pm 0.01\ h^{-1}$)	WGS of two independently evolved cell lines, 70 mutations	Mutational hotspots in *pyk*, *fruK*, and *corA*	[20]
Accelerating growth on glucose minimal media	Repetitive batch in minimal media containing glucose as sole carbon source	7 months, approximately 1500 generations	42% higher growth rate ($0.64 \pm 0.01\ h^{-1}$)	WGS after different ALE times, seven mutations and one genomic deletion (CGP3 element)	*gntR1*-E70K and *ramA*-A52V	[21]
Stress tolerance						
Increased growth at high temperatures	Repetitive batch in rich media, a gradual increase in process temperature	65 days	Better performance at suboptimal temperatures, increased T_{max} (41.5 °C)	WGS of three evolved isolates, deletion of two genomic regions, 295 total point mutations	*glmU*-E295K and *otsA*-R328H	[27]
Increased tolerance to inhibitors in corn stover hydrolysate	Repetitive batch in minimal media with corn stover hydrolysate	128 days	Higher degradation rate of several inhibitors, higher growth rate on media containing corn stover hydrolysate	WGS of evolved and parental culture, seven mutations; transcriptome comparison between evolved and parental strain	Not determined	[23]
Increased tolerance to methanol	Repetitive batch in minimal media containing methanol	50 generations	Improved growth rate on minimal media with 500–2000 mM methanol	WGS of single isolate, 29 mutations found; transcriptome analysis using DNA microarrays	*metY*-A165T and *cat*-Q342*	[24]
Increased tolerance to H_2O_2	Chemostat with a dilution rate of $0.15\ h^{-1}$, growth on minimal media containing glucose, gradual increase of H_2O_2 concentration to 10 mM	1900 h (approximately 411 generations)	Better performance in media containing 10 mM H_2O_2	No sequencing performed; transcriptome analysis using RNAseq	Not determined	[28]
Substrate expansion						
Improved growth on cellobiose	Repetitive batch in minimal media containing cellobiose	25 days	Improved growth on cellobiose	WGS of two differently evolved strains, ten shared mutations identified; transcriptome analysis using DNA microarrays	Not determined	[29]
Improved growth on D-xylose	Automated repetitive batch in minimal media containing D-xylose	13 days (35 generations)	Twofold increase in growth rate on D-xylose ($0.26 \pm 0.02\ h^{-1}$)	WGS of multiple evolved strains	Upregulation of *iolT1*	[22,30]
Co-utilization of xylose and methanol	Repetitive batch in minimal media with xylose and methanol	206 days (approximately 27 generations)	20-fold increase in growth rate ($0.03\ h^{-1}$)	WGS of three evolved isolates, six missense mutations; ^{13}C flux analysis	Not determined	[31]
Metabolic engineering to guide evolution						
Evolution of a PEP and	Repetitive batch in media containing	13, 15 or 33 days			*icd*-A94D, *icd*-R453C,	[26]

(*Continued*)

Table 1. (*Continued*)

ALE target	Experimental setup	ALE duration	Phenotype of evolved strain	Sequencing/ transcriptomics	Proven causal mutations	References
pyruvate carboxylase-deficient strain towards growth on glucose	yeast extract and glucose		Improved growth rate to 59% of WT ($0.23 \pm 0.01\ h^{-1}$)	WGS of three independently evolved mutants	and *icd*-G407S	
Increasing small molecule production						
Increased fatty acid production	Sequential selection for suppressor mutants on agar plates containing Tween40 or cerulenin	Multiple days	Increased fatty acid production ($322.23 \pm 15.09\ mg\ L^{-1}$)	WGS of best-producing isolate, a total of four mutations	*fasR*-S20D, *fasA*^{HP}-C63G, *fasA*-A2623V and *accD3*-A433T	[32,33]
Increased putrescine production	Repetitive batch in rich media containing putrescine, after random mutagenesis	11 days	Increased putrescine titer (111.42 ± 2.56 mM)	WGS of best-producing isolate, 78 SNPs	Not determined	[34]
Increased L-ornithine production	Repetitive batch in media containing glucose and L-ornithine	70 days	20% higher L-ornithine titer ($13.6 \pm 0.5\ g\ L^{-1}$)	Not performed	Not determined	[35]
Biosensor-guided evolution						
Increased L-valine production	Repetitive batch in minimal media containing glucose and acetate, selection via biosensor mediated FACS	6 days	Higher growth rate ($0.41 \pm 0.02\ h^{-1}$) and 63% increased L-valine titer (57 mM)	WGS of evolved culture and two isolates	*glxR*-T93S, *prpD*-T201I, *rpsP*-D30D, and *ureD*-E188*	[25]
Plasmid-based protein production	Repetitive batch in minimal media containing glucose, selection via biosensor mediated FACS	8 days	Higher plasmid copy number	Sequencing of plasmid backbone	Several inactivating mutations in *parB*	[36]

Further key targets identified by Pfeifer et al.[20] were mutations in *fruK*, which encodes for 1-phosphofructokinase (Pfk1). In a previous study, deletion of the *fruK* gene was actually reported to enhance glucose uptake of *C. glutamicum*.[44] The authors speculated that this was the result of an accumulation of F1P relieving *ptsG* repression via the SugR regulator. However, further analyses are required to understand the impact of Pfk1 on the sugar phosphate pool and its impact on regulatory networks in these strains.

The *corA* gene, coding for a putative Mg^{2+}/Co^{2+} transport protein,[45] represented an unexpected mutational hotspot in the *C. glutamicum* long-term evolution and was also identified, but not discussed, in the *E. coli* experiment of LaCroix et al.[20,41] Mg^{2+} limitation was previously described to increase glucose consumption rates and metabolic flux of *E. coli* in the stationary phase. Here, the authors assumed that reduced Mg^{2+} levels might cause a block in pyruvate dehydrogenase (PDH) activity, leading to an accumulation of upstream intermediates like 2-phosphoenolpyruvate (PEP), which stimulate glucose uptake.[46] However, the availability of magnesium ions is known to affect a variety of different enzymes and to have an impact on the stability of polyphosphates.[45] For example, the biologically active form of ATP is a complex with Mg^{2+}. Based on these findings, we can conclude that mutation of *corA* linked to magnesium limitation appears to be a prime target to enhance glucose uptake, but the underlying mechanism is not fully understood and requires further theoretical and experimental attention.

In another recent ALE experiment, *C. glutamicum* cultures were evolved for about 1500 generations in defined media with glucose.[21] The evolved cell line was found to lack large parts of the CGP3 element. Deletion of the prophage CGP3 was also revealed as a competitive fitness advantage in the other *C. glutamicum* ALE study, where a competitive growth experiment showed that a prophage-free strain (MB001) outcompetes the wild type.[20] Besides the lack of the prophage element, the authors found mutations in the *gntR1* gene, encoding a repressor of

gluconate catabolism and an activator of *ptsG*,[47] and in *ramA*, encoding a LuxR-type regulator, which inherits a global role in the coordination of the central metabolism.[48] Re-introduction into the wild-type background revealed that both mutations significantly increased the growth rate and glucose consumption rate (Table 1).[21] Metabolomic flux and transcriptome analysis showed an increased flux through the pentose phosphate pathway but did not indicate significant rewiring of the central metabolic network, which is in agreement with similar studies on *E. coli*.[49]

3. Improving Performance under Industrial Conditions

Evolutionary engineering provides an efficient means to improve the performance of microbial strains under harsh industrial conditions and/or to realize the utilization of second and third generation feedstock.[50,51] Recent studies have employed ALE strategies for both aspects, and while the division is not always clear (e.g., in the case of methanol tolerance and utilization), they will be discussed separately in this section (Table 1).

3.1. Improving Stress Tolerance

In an economically optimized bioprocess, microorganisms should be able to grow on low-purity feedstock (lower substrate costs) and at favorable process conditions (e.g., at a higher temperature, to reduce cooling costs). An improved heat tolerance was reported for *C. glutamicum* after a repetitive batch ALE (rbALE) of 65 days, in which the temperature was gradually increased from 38 °C to 41.5 °C.[27] Sequencing of three evolved isolates revealed a surprisingly high amount of 295 point mutations and two genomic deletions in total. This was caused by an acquired mutator phenotype, which resulted in a mutation rate 40- to 80-fold higher than that of the parental strain. A genetic basis for this phenotype was not found. However, the combined reengineering of the mutations *glmU* (E295K) and *otsA*(R328H) resulted in an improved heat tolerance and increased the maximum specific growth rate at 40.7 °C from $0.27 \pm 0.02\ h^{-1}$ to $0.33 \pm 0.03\ h^{-1}$.

Two different studies applied rbALE to increase tolerance for inhibitors present in corn stover hydrolysate[23] and for methanol, which is an impurity found in certain glycerol waste streams.[24] A fixed amount of inhibitor was added, and cells were selected for growth. The corn stover evolved strain showed a higher degradation rate of the inhibitors furfural, HMF, vanillin, syringaldehyde, 4-hydroxybenzaldehyde, and acetic acid.[23] When grown on corn stover hydrolysate, the evolved strain also showed a 68% higher glutamic acid titer and 35% higher yield than the parental strain. The increased glucose consumption rate probably resulted from a higher *ptsI* expression, which codes for a component of the phosphotransferase system (PTS). In the methanol study, tolerance was increased by using media with 50 mM methanol.[24] The evolved strain showed a higher growth rate under methanol concentrations between 500 mM and 2000 mM. Sequencing identified 29 mutations and combined engineering of two of them, *metY* (A165T) and *cat*(Q342*), increased the methanol tolerance of the parental strain to that of the evolved strain. Interestingly, both the reverse engineered strain and the evolved strain lost the ability to grow on ethanol. This showed that, in contrast to an observed beneficial cross-tolerance for isobutanol after ALE for increased temperatures,[27] a single-target ALE approach is typically associated with significant negative trade-off effects.

3.2. Increasing Feedstock Flexibility

The utilization of alternative, non-native carbon sources is key to the implementation of non-glucose based second or third generation processes in modern biotechnology, which provides a strong incentive to engineer industrial strains that utilize most of the components present in these substrate feeds. Attractive targets to realize a flexible feedstock concept are, for example, carbon sources derived from complex polymers (e.g., starch, cellulose, or xylan), di- and monosaccharides (e.g., arabinose or xylose), and C1 compounds, such as methanol.[50,51] If a microbe has no native capacity to consume the particular substrate of interest, targeted engineering can provide an initial, nonoptimal strain, which can subsequently be improved by ALE. This combinatorial strategy was applied in three recent publications that describe improved growth on xylose, cellobiose, and methanol (Table 1).[22,29,31]

Two different rbALE approaches were described for the co-utilization of xylose and methanol[31] or xylose and cellobiose.[29] In the xylose and methanol study, targeted engineering was first applied to obtain a strain that required both xylose and ribose for growth. After the first ALE, this strain showed an increased maximum specific growth rate, from $0.03\ h^{-1}$ to $0.15\ h^{-1}$. Then, the evolved strain was rationally engineered for the co-utilization of xylose and methanol and submitted to another round of ALE. After 206 days, the evolved strain was able to grow, but the reported growth rate of $0.03\ h^{-1}$ is still far away from industrial applications. Interestingly, the authors describe the *metY*(G1256A) mutation; another mutation in the same gene (*metY*(A165T)) was also found in the methanol tolerance study.[24] An elegant approach to realize methanol-essential growth was recently reported for *E. coli*.[52] The assimilation of methanol and gluconate was stoichiometrically coupled in a strain that had the ribulose monophosphate cycle. This study highlights the potential of metabolic rerouting for the successful implementation of synthetic methylotrophy in established industrial platform organisms.

In the xylose and cellobiose study, targeted engineering was first applied to obtain two different strains that could grow on cellobiose as the sole carbon source.[29] ALE was performed until growth and cellobiose consumption did not improve anymore. Sequencing analysis revealed a high number of mutations (36 and 300), which could not be explained. After the ALE for cellobiose, a xylose consumption pathway was introduced and co-utilization of xylose and cellobiose was shown.

An improved growth rate on only D-xylose was shown by Radek et al.,[22] using a rationally engineered strain that was subsequently evolved by high-throughput rbALE for 35 generations in only 13 days. A best performer showed more than a doubling of the maximum specific growth rate, compared to the

parental strain ($0.26 \pm 0.02\ h^{-1}$ and $0.10 \pm 0.02\ h^{-1}$, respectively). Sequencing analysis revealed putative loss-of-function mutations in the transcriptional regulator IolR, involved in myo-inositol uptake and degradation, and cg3388, which encodes a putative transcriptional regulator. In a subsequent study, the functional loss of IolR was shown to result in an upregulation of the gene *iolT1* (encoding the myo-inositol/proton symporter IolT1), and additional reengineering could prove the importance of IolT1 for xylose uptake.[30] Interestingly, the identified mutations are different from those identified by the xylose–methanol ALE study.[31] Altogether, these examples once more highlight the importance of subsequent reengineering of key mutations to expand our knowledge of biological systems.

4. Metabolic Engineering to Guide Evolution

Combining evolutionary engineering with rationally engineered system perturbations is a promising approach for the identification of metabolic traits that can be beneficial for target molecule production.[53] Gene knockouts are frequently used to not only investigate the metabolic and regulatory function of gene products,[54,55] but also for predefining the cell's metabolic network with regard to precursor supply for biotechnological applications (**Figure 2**).[56] Growth defects that result from system perturbations by introduction of gene knockouts provide a guided selection pressure toward fitness recovery. This can lead to alternative reoptimized metabolic states, for example by harnessing the underground metabolism by building on promiscuous enzyme activity of the particular species.[54,57]

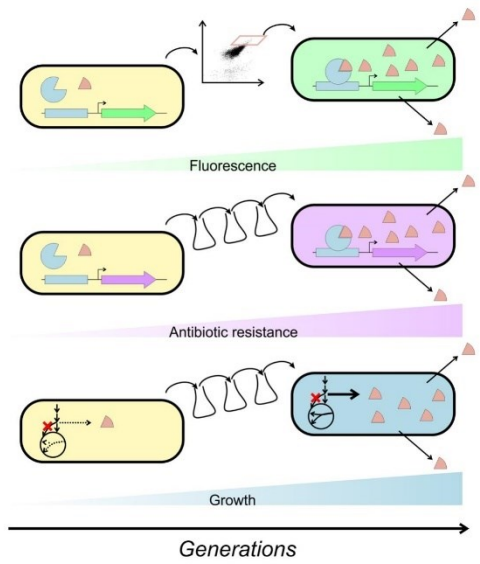

Figure 2. Overview of different synthetic evolution approaches to select for increased small molecule production. Synthetic regulatory circuits can be constructed to couple intracellular product concentration to a selectable output, for example to fluorescent protein synthesis,[25] which can be selected for by FACS, or to synthesis of an antibiotic or auxotrophic marker.[58] Metabolic engineering to guide evolution can be applied to increase small molecule production by selecting for growth rate.[26]

Schwentner et al.[26] used the inactivation of anaplerotic reactions to evolve an alternative producer platform for the amino acid L-valine. This effort was motivated by the fact that metabolic engineering of *C. glutamicum* for L-valine production is typically based on complete inactivation or downregulation of the pyruvate dehydrogenase complex (PDHC).[59,60] Schwentner et al. evolutionary engineered an alternative route for increased pyruvate supply by inactivating the genes encoding the PEP and pyruvate carboxylase (*ppc* and *pyc*). The resulting strain was unable to grow on glucose as the sole carbon source since the replenishment of the oxaloacetate pool was impaired.[61] Whole genome sequencing of the evolved strains revealed *icd*, encoding isocitrate dehydrogenase (ICD), as a consistent mutation target in all evolved strains. Re-engineering of the identified key mutations in *icd* revealed an upregulation of the glyoxylate shunt[62] as an alternative route to replenish the oxaloacetate pool in the Δ*pyc* Δ*ppc* background.[26] However, further studies are necessary to identify the molecular mechanisms underlying the activation of the glyoxylate shunt as a secondary effect of reduced ICD activity. In accordance with assumptions of Baumgart et al.,[63] the authors postulated that the reduced ICD activity and the resulting accumulation of isocitrate promote activation of the glyoxylate shunt.[26] Based on a 1.9-fold increased intracellular L-valine level and a predicted increased flux through the PDHC, Schwentner et al. suggested that the re-engineered strains represent promising candidates for L-valine producers. Indeed, plasmid-based overexpression of L-valine biosynthesis genes (pJC4*ilvBNCE*) led to a fourfold-enhanced L-valine product yield in comparison to the wild type.[26]

The study of Schwentner and co-workers demonstrated the potential of guided evolution strategies to improve glucose conversion to value-added compounds like L-valine. In contrast, the previously discussed guided evolution approaches of Lee et al.[29] and Tuyishime et al.[31] resulted in strains showing efficient co-utilization of the alternative substrates xylose and methanol or xylose and cellobiose, demonstrating the broad application spectrum of guided evolution strategies (Table 1).

McCloskey and colleagues intensively studied growth recovery of different *E. coli* knockout strains during ALE at the systems level. The combination of ALE and multiomics technologies provided deep insights into the versatile pathways allowing rebalancing of the metabolite and redox state.[54,55] Furthermore, growth coupling approaches with *E. coli* used the strong evolutionary driving force towards redox homeostasis for increasing fermentative production of lactic acid,[56] 1-butanol,[64] and linear higher alcohols[65] by inactivating competing NADH oxidizing enzymes. These examples highlight that not only the experimental conditions but also the genetic strain background need to be streamlined for the particular aim of the ALE.

5. The Benefit of Automation

A number of different ALE approaches are already established that can roughly be classified according to the cultivation conditions (i.e., chemostat vs repetitive batch culture), experimental throughput (i.e., lab-scale vs microscale bioreactor systems), and degree of automation (i.e., manual vs autonomous operation). See Dragosits et al.[17] and Gresham et al.[66] for a detailed discussion of the advantages and disadvantages of the chemostat and repetitive batch approach.

In recent years, the rbALE approach has become more popular due to its lower costs for operation, simpler experimental implementation, and easier expandability. In short, individual cultivation batches are sequentially inoculated until a termination point (e.g., no further improvement in fitness criterion) is reached. Adaptation and diversification of cells during rbALE depends on the applied selection pressure, which can greatly vary between conditions of feast (i.e., exponential growth) and famine (i.e., stationary phase).

In many cases, selection focuses on higher maximum growth rates, which are best supported by keeping the cells under balanced growth conditions throughout the whole rbALE experiment. The time window of exponential growth depends on the inoculation density, the lag-phase and the specific growth rate, and should become smaller with increasing number of beneficial mutations leading to faster cell population growth and earlier consumption of the usually fixed nutrient resources. Therefore, the application of conventional shaking flasks and offline OD measurements for monitoring biomass growth does not interface with appropriate standardization.

To overcome this limitation, several microbioreactor systems are available that are based on shaken microtiter plates (MTPs), e.g., "GrowthProfiler" (EnzyScreen), "Bioscreen C" (Oy Growth Curves) or "BioLector" (m2p-labs), which employ (quasi)-continuous biomass measurement via integrated image analysis, optical density, or backscatter (see Hemmerich et al.[67] for an comprehensive overview). In addition, MTPs enable a higher throughput to perform replicate ALE experiments under identical conditions[22,68] and thus provide access to important quantities for analyzing the evolutionary process, e.g., in terms of beneficial mutation rates and the occurrence of fixed or converged mutations.[69] It is noteworthy that the typical 1 mL working volume of standard MTPs is also sufficient to carry out further in-depth characterizations of evolved strains using available spectrophotometric assays[70] and quantitative omics technologies.[71]

However, when applied as stand-alone devices for rbALE, the above systems still require the manual passaging of cells from one MTP-well to another. Consequently, there is a high demand for automation to optimally balance available resources (i.e., personnel, material, and time) with the expected outcomes (i.e., strains with improved properties, new knowledge on cellular metabolism, and targets for rational strain design).

As a first step in this direction, a recently established a workflow was reported, which enables the performance of rbALE experiments in an automated manner.[22] By building on an existing microbial phenotyping platform (i.e., Mini Pilot Plant integrating a BioLector system with liquid handling robotics[72]), the workflow covers essential steps for autonomous rbALE, including preparation of different media compositions, their cool temporary storage and the repeated inoculation of individual MTP-cavities in the BioLector. The latter is supported by various online measurements (i.e., backscatter, pO^2, pH, and fluorescence) and ensures an instantaneous recording of metabolic adaptation events during ALE experimentation (**Figure 3.2**). Moreover, the setup not only enables dynamic adjustments of passage sizes for keeping genetic diversity, but (if required) also provides access to the full spectrum of applicable selection pressures.

6. Evolutionary Engineering of Small Molecule Production

Redirecting cellular metabolism toward the production of small molecules is challenging, because metabolic pathways have been evolved for tight control and our understanding of their regulation is incomplete.[73] For ALE approaches, the difficulty lies in applying a pressure that selects for production of the compound of interest. While traditional approaches select for

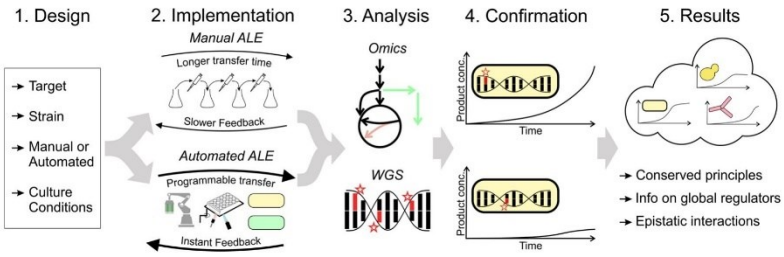

Figure 3. Outlook on future ALE strategies. Future ALE studies could implement multiple selection pressures, to optimize industrial performance of microbial strains. Automated approaches allow for simultaneous cultivation of multiple cultures, programmable transfer-time points and instant feedback, especially in combination with biosensors. ALE should be followed by whole genome sequencing analysis and confirmation of causal mutations via re-engineering approaches. Finally, online databases can be used to gather ALE results for different microbial organisms to ultimately increase our knowledge on biological systems.

suppressor mutants, the development of transcription factor-based biosensors enabled a direct coupling of product formation to an easily selectable output, which resulted in the first reports of "synthetic evolution."[16,74–76] For *C. glutamicum*, ALE for increased small molecule production has been shown for fatty acids, L-ornithine, putrescine, plasmid-based proteins, and L-valine (Table 1).

6.1. Selection for Suppressor Mutants

Early efforts on the improvement of small molecule production focused on the application of random mutagenesis (UV- or chemical mutagenesis) and on selection schemes based on the resistance to antimetabolites or product analogs inhibiting growth. Key enzymes of biosynthetic pathways (e.g., amino acid biosynthesis) are typically feedback-inhibited by the particular end-product of the pathway. Application of product analogous antimetabolites enabled the efficient isolation of mutations causing feedback-resistance of key enzymes.[2]

Two groups have recently published work on improving small molecule production by selecting suppressor mutants. Takeno et al.[32] used two different chemicals, Tween40 and cerulenin, to select for mutants with a higher fatty acid production, using multiple selection steps on agar plates. Jiang et al.[35] applied rbALE in media containing the desired product, L-ornithine, to select for mutants resistant to product inhibition. In both studies, the final product titer could be improved with the evolved strain, from $3.21 \pm 0.06\ mg\ L^{-1}$ to $279.95 \pm 8.50\ mg\ L^{-1}$ for fatty acids,[32] and from $10.2 \pm 0.2\ g\ L^{-1}$ to $13.6 \pm 0.5\ g\ L^{-1}$ for L-ornithine.[35] While Jiang et al. did not perform whole genome sequencing, Takeno et al. reported three mutations in the genes responsible for fatty acid synthesis. Takeno et al.[33] repeated the selection step on cerulenin plates and identified one additional mutation. Re-engineering of this mutation in the previously evolved strain resulted in a 1.2-fold higher oleic acid titer. This shows how iterative selection of a parental strain can be used to find different mutations that have an additive effect on productivity. The L-ornithine evolved strain was further engineered for putrescine production.[34] Random mutagenesis in combination with rbALE in media containing putrescine resulted in a strain showing a twofold higher final putrescine titer (111.42 ± 2.56 mM). Sequencing analysis revealed 78 SNPs; further analysis suggested that a decrease in the activity of the α-ketoglutarate decarboxylase OdhA and an increase in the major facilitator superfamily permease CgmA, a putative putrescine permease, contributed to a higher putrescine production.

6.2. Biosensor-Guided Evolution

Biosensors can greatly increase the throughput and selectivity for ALE, and thereby accelerate strain development (Figure 2). Initially, two studies reported on transcription factor-based biosensors that were designed to induce *eyfp* expression in response to higher intracellular amino acid concentrations in *C. glutamicum*. The pSenLys biosensor detects amino acids with a basic side chain[13] and the Lrp biosensor detects L-methionine and branched chain amino acids.[14] Both studies showed that random mutagenesis coupled to FACS could be used to select for cells with higher productivity, illustrating the use of biosensors to screen for producers strains. However, applying random mutagenesis results in many mutations. Binder et al.[13] reported 268 SNPs and a similar study reported 83 SNPs.[77] This high number of mutations complicates the identification of causal ones.

In a recent study, Mahr et al.[25] described a biosensor-guided ALE approach based on the native mutagenesis rate, by applying multiple rounds of selection using the Lrp biosensor (Table 1). The L-valine producer strain *C. glutamiucm* Δ*ace*, which produces valine in the stationary phase, was used as the parental strain. Five iterative evolution steps were performed and, in each step, the top 10% fluorescent cells were transferred by FACS. After only five iterations, a single isolate showed a twofold increase in L-valine production compared to the parental strain. Only seven mutations were identified after whole genome sequencing. This is in large contrast to the higher number of mutations found when random mutagenesis is applied. The identified *ureD*(E188*) mutation resulted in a truncated version of the urease accessory protein and was shown to increase the final L-valine titer (44.2 mM for evolved strain) by more than 100%.[25] A low amount of mutations was also the result of a simple biosensor ALE experiment, in which iterative FACS selection was done with a strain containing a plasmid-based *egfp*. Only one mutation was identified, a loss of function of *parB*, which resulted in tenfold higher plasmid copy numbers.[36] Further examples for biosensor-guided evolution approaches in *E. coli* are the coupling of mutation rate to small molecule production[76] and the selection of improved producers via an antibiotic-based positive and negative selection strategy.[58]

The mutations identified by ALE can be further investigated by targeted mutagenesis followed by biosensor mediated screening, which was shown for the *argB* gene using pSenLys[78] and for the RBS sequence in *tktA* using the ShiR-based shikimate sensor.[79] An interesting method was described by Binder et al.,[80] who designed a rapid recombineering and screening approach, based on the RectT recombinase from prophage Rac and the pSenLys sensor, which was applied to screen for mutations in *murE* with an impact on L-lysine production.[80] Furthermore, studies in *E. coli* have demonstrated the use of multiplexed genome engineering in combination with barcoding to increase mutation rates and enable tracking of mutations.[81,82] Altogether, these approaches demonstrate the potential of transcription factor-based biosensors for the design of synthetic evolution schemes to enable the improvement of microbial small molecule production.

7. Conclusions

In engineering disciplines, the possibility of process improvement via evolution is a feature unique to biotechnology. But what do we learn from the comparison of different ALE endeavors? Evolution of living organisms is shaped by the particular environmental conditions (like media composition, gas supply, etc.), the genetic background, and by the mode of cultivation (batch, chemostat, solid media), including passage time and culture volume. For example, LaCroix et al.[41]

achieved a significant increase of growth rates in a shorter time compared to the Lenski experiment, because batch cultures where propagated during the exponential phase rather than inoculated from stationary phase cultures. These examples demonstrate that an ALE setup must be efficiently tailored to the particular scientific aim. However, most studies only focus on one aspect of industrial performance (e.g., productivity or stress tolerance). A more integrative approach could combine several improvement targets into one experiment. Especially, the development of biosensors could aid in this field, as they allow for coupling of producers to a selectable output under industrial conditions. This could even be extended with high-throughput technologies enabling the design of novel ALE strategies (Figure 3).

Several recent examples highlight the fact that ALE or untargeted selection strategies should be complemented by sequencing, and possibly by transcriptome analyses and re-engineering to obtain novel information on enzyme properties or pathway regulation. Especially in the absence of a random mutagenesis step, the amount of mutations is most of the times low enough to allow for reverse engineering and an in-depth characterization of specific mutations. This is in contrast to classical genome breeding approaches where a high number of induced mutations (e.g., via UV radiation) may result in the accumulation on non-beneficial side mutations having a negative impact on genome stability. Often, different mutations found in different studies can result in an additive effect, but it can be hard to keep track of all described mutations. Recent database efforts such as the AleDB could aid in improving our understanding of metabolic regulations.[69] A more systemic analysis of ALE experiments combined with sophisticated data management will accelerate the identification of causative key mutations and epistatic interactions resulting in improved strain properties.

Acknowledgements

The authors acknowledge funding from the Helmholtz Association (grant W2/W3-096). Further funding was obtained from Bioeconomy Science Center (BioSC, Grant. No. 325-40000213) as part of the Focus FUND project "HyImPAct—Hybrid processes for important precursor and active pharmaceutical ingredients."

Conflict of Interest

The authors declare no conflict of interest.

Keywords

adaptive laboratory evolution (ALE), biosensors, *Corynebacterium glutamicum*, evolutionary engineering, laboratory automation

Received: November 29, 2018
Revised: January 23, 2019
Published online:

[1] S. Kinoshita, S. Udaka, M. Shimono, *J. Gen. Appl. Microbiol.* **1957**, *3*, 193.
[2] L. Eggeling, M. Bott, *Handbook of Corynebacterium glutamicum*, CRC press, Boca Raton, FL **2005**.
[3] J. Becker, C. Wittmann, *Curr. Opin. Biotechnol.* **2012**, *23*, 718.
[4] V. F. Wendisch, J. M. P. Jorge, F. Pérez-García, E. Sgobba, *World J. Microbiol. Biotechnol.* **2016**, *32*, 105.
[5] J. Becker, C. M. Rohles, C. Wittmann, *Metab. Eng.* **2018**, *50*, 122.
[6] K-.A. G. Baritugo, H. T. Kim, Y. C. David, J. H. Choi, J. Choi, T. W. Kim, C. Park, S. H. Hong, J-.G. Na, K. J. Jeong, J. C. Joo, S. J. Park, *Biofuels, Bioprod. Biorefin.* **2018**, *12*, 899.
[7] K. Pfeifer-Sancar, A. Mentz, C. Rückert, J. Kalinowski, *BMC Genomics* **2013**, *14*, 888.
[8] J. Kalinowski, B. Bathe, D. Bartels, N. Bischoff, M. Bott, A. Burkovski, N. Dusch, L. Eggeling, B. J. Eikmanns, L. Gaigalat, A. Goesmann, M. Hartmann, K. Huthmacher, R. Krämer, B. Linke, A. C. McHardy, F. Meyer, B. Möckel, W. Pfefferle, A. Pühler, D. A. Rey, C. Rückert, O. Rupp, H. Sahm, V. F. Wendisch, I. Wiegräbe, A. Tauch, *J. Biotechnol.* **2003**, *104*, 5.
[9] Y. Jiang, F. Qian, J. Yang, Y. Liu, F. Dong, C. Xu, B. Sun, B. Chen, X. Xu, Y. Li, R. Wang, S. Yang, *Nat. Commun.* **2017**, *8*, 15179.
[10] S. Cleto, J. V. Jensen, V. F. Wendisch, T. K. Lu, *ACS Synth. Biol.* **2016**, *5*, 375.
[11] K-. A. Baritugo, H. T. Kim, Y. David, J. Choi, S. H. Hong, K. J. Jeong, J. H. Choi, J. C. Joo, S. J. Park, *Appl. Microbiol. Biotechnol.* **2018**, *102*, 3915.
[12] V. F. Wendisch, *Curr. Opin. Biotechnol.* **2014**, *30*, 51.
[13] S. Binder, G. Schendzielorz, N. Stäbler, K. Krumbach, K. Hoffmann, M. Bott, L. Eggeling, *Genome Biol.* **2012**, *13*, R40.
[14] N. Mustafi, A. Grünberger, D. Kohlheyer, M. Bott, J. Frunzke, *Metab. Eng.* **2012**, *14*, 449.
[15] N. Mustafi, A. Grünberger, R. Mahr, S. Helfrich, K. Nöh, B. Blombach, D. Kohlheyer, J. Frunzke, *PLoS One* **2014**, *9*, e85731.
[16] R. Mahr, J. Frunzke, *Appl. Microbiol. Biotechnol.* **2016**, *100*, 79.
[17] M. Dragositz, D. Mattanovich, *Microb. Cell Fact.* **2013**, *12*, 64.
[18] V. A. Portnoy, D. Bezdan, K. Zengler, *Curr. Opin. Biotechnol.* **2011**, *22*, 590.
[19] R. Mans, J-. M. G. Daran, J. T. Pronk, *Curr. Opin. Biotechnol.* **2018**, *50*, 47.
[20] E. Pfeifer, C. Gätgens, T. Polen, J. Frunzke, *Sci. Rep.* **2017**, *7*, 16780.
[21] Z. Wang, J. Liu, L. Chen, A. P. Zeng, C. Solem, P. R. Jensen, *Metab. Eng.* **2018**, *48*, 1.
[22] A. Radek, N. Tenhaef, M. F. Müller, C. Brüsseler, W. Wiechert, J. Marienhagen, T. Polen, S. Noack, *Bioresour. Technol.* **2017**, *245*, 1377.
[23] X. Wang, I. Khushk, Y. Xiao, Q. Gao, J. Bao, *Appl. Microbiol. Biotechnol.* **2018**, *102*, 377.
[24] L. Leßmeier, V. F. Wendisch, *BMC Microbiol.* **2015**, *15*, 216.
[25] R. Mahr, C. Gätgens, J. Gätgens, T. Polen, J. Kalinowski, J. Frunzke, *Metab. Eng.* **2015**, *32*, 184.
[26] A. Schwentner, A. Feith, E. Münch, T. Busche, C. Rückert, J. Kalinowski, R. Takors, B. Blombach, *Metab. Eng.* **2018**, *47*, 31.
[27] S. Oide, W. Gunji, Y. Moteki, S. Yamamoto, M. Suda, T. Jojima, H. Yukawa, M. Inui, *Appl. Environ. Microbiol.* **2015**, *81*, 2284.
[28] J.-Y. Lee, J. Seo, E.-S. Kim, H.-S. Lee, P. Kim, *Biotechnol. Lett.* **2013**, *35*, 709.
[29] J. Lee, J. N. Saddler, Y. Um, H. M. Woo, *Microb. Cell Fact.* **2016**, *15*, 20.
[30] C. Brüsseler, A. Radek, N. Tenhaef, K. Krumbach, S. Noack, J. Marienhagen, *Bioresour. Technol.* **2018**, *249*, 953.
[31] P. Tuyishime, Y. Wang, L. Fan, Q. Zhang, Q. Li, P. Zheng, J. Sun, Y. Ma, *Metab. Eng.* **2018**, *49*, 220.
[32] S. Takeno, M. Takasaki, A. Urabayashi, A. Mimura, T. Muramatsu, S. Mitsuhashi, M. Ikeda, *Appl. Environ. Microbiol.* **2013**, *79*, 6775.
[33] S. Takeno, N. Murata, M. Kura, M. Takasaki, M. Hayashi, M. Ikeda, *Appl. Microbiol. Biotechnol.* **2018**, *102*, 10603.
[34] Z. Li, Y. P. Shen, X. L. Jiang, L. S. Feng, J. Z. Liu, *J. Ind. Microbiol. Biotechnol.* **2018**, *45*, 123.
[35] L. Y. Jiang, S. G. Chen, Y. Y. Zhang, J. Z. Liu, *BMC Biotechnol.* **2013**, *13*, 47.

[36] J. W. Choi, S. S. Yim, K. J. Jeong, *Appl. Microbiol. Biotechnol.* **2018**, *102*, 873.
[37] J. E. Barrick, R. E. Lenski, *Nat. Rev. Genet.* **2013**, *14*, 827.
[38] R. E. Lenski, *ISME J.* **2017**, *11*, 2181.
[39] G. Valentini, L. Chiarelli, R. Fortin, M. L. Speranza, A. Galizzi, A. Mattevi, *J. Biol. Chem.* **2000**, *275*, 18145.
[40] R. Woods, D. Schneider, C. L. Winkworth, M. A. Riley, R. E. Lenski, *Proc. Natl. Acad. Sci.* **2006**, *103*, 9107.
[41] R. A. LaCroix, T. E. Sandberg, E. J. O'brien, J. Utrilla, A. Ebrahim, G. I. Guzman, R. Szubin, B. O. Palsson, A. M. Feist, *Appl. Environ. Microbiol.* **2015**, *81*, 17.
[42] G. Dong, Q. Mao, W. Xia, Y. Xu, J. Wang, L. Xu, F. Jiang, *Oncol. Lett.* **2016**, *11*, 1980.
[43] M. A. Iqbal, V. Gupta, P. Gopinath, S. Mazurek, R. N. K. Bamezai, *FEBS Lett.* **2014**, *588*, 2685.
[44] Z. Wang, S. H. J. Chan, S. Sudarsan, L. M. Blank, P. R. Jensen, C. Solem, *Metab. Eng.* **2016**, *38*, 344.
[45] E. a Groisman, K. Hollands, M. A. Kriner, E. J. Lee, S. Y. Park, M. H. Pontes, *Annu. Rev. Genet.* **2014**, *47*, 625.
[46] V. Chubukov, U. Sauer, *Appl. Environ. Microbiol.* **2014**, *80*, 2901.
[47] J. Frunzke, V. Engels, S. Hasenbein, C. Gätgens, M. Bott, *Mol. Microbiol* **2008**, *67*, 305.
[48] A. Shah, B. Blombach, R. Gauttam, B. J. Eikmanns, *Appl. Microbiol. Biotechnol.* **2018**, *102*, 5901.
[49] C. P. Long, J. E. Gonzalez, A. M. Feist, B. O. Palsson, M. R. Antoniewicz, *Metab. Eng.* **2017**, *44*, 100.
[50] N. Buschke, R. Schäfer, J. Becker, C. Wittmann, *Bioresour. Technol.* **2013**, *135*, 544.
[51] V. F. Wendisch, L. F. Brito, M. Gil Lopez, G. Hennig, J. Pfeifenschneider, E. Sgobba, K. H. Veldmann, *J. Biotechnol.* **2016**, *234*, 139.
[52] F. Meyer, P. Keller, J. Hartl, O. G. Gröninger, P. Kiefer, J. A. Vorholt, *Nat. Commun.* **2018**, *9*, 1508.
[53] K. Tokuyama, Y. Toya, T. Horinouchi, C. Furusawa, F. Matsuda, H. Shimizu, *Biotechnol. Bioeng.* **2018**, *115*, 1542.
[54] D. McCloskey, S. Xu, T. E. Sandberg, E. Brunk, Y. Hefner, R. Szubin, A. M. Feist, B. O. Palsson, *Appl. Environ. Microbiol.* **2018**, *84*, e00823.
[55] D. McCloskey, S. Xu, T. E. Sandberg, E. Brunk, Y. Hefner, R. Szubin, A. M. Feist, B. O. Palsson, *Nat. Commun.* **2018**, *9*, 3796.
[56] S. S. Fong, A. P. Burgard, C. D. Herring, E. M. Knight, F. R. Blattner, C. D. Maranas, B. O. Palsson, *Biotechnol. Bioeng.* **2005**, *91*, 643.
[57] J. Rosenberg, F. M. Commichau, *Trends Biotechnol.* **2018**, *37*(1), 29.
[58] S. Raman, J. K. Rogers, N. D. Taylor, G. M. Church, *Proc. Natl. Acad. Sci. U. S. A.* **2014**, *111*, 17803.
[59] M. Oldiges, B. J. Eikmanns, B. Blombach, *Appl. Microbiol. Biotechnol.* **2014**, *98*, 5859.
[60] B. J. Eikmanns, B. Blombach, *J. Biotechnol.* **2014**, *192*, 339.
[61] P. G. Peters-wendisch, C. Kreutzer, J. Kalinowski, M. Patek, H. Sahm, B. J. Eikmanns, *Microbiology* **1998**, *144*, 915.
[62] V. F. Wendisch, M. Spies, D. J. Reinscheid, S. Schnicke, H. Sahm, B. J. Eikmanns, *Arch. Microbiol.* **1997**, *168*, 262.
[63] M. Baumgart, N. Mustafi, A. Krug, M. Bott, *J. Bacteriol.* **2011**, *193*, 6864.
[64] C. R. Shen, E. I. Lan, Y. Dekishima, A. Baez, K. M. Cho, J. C. Liao, *Appl. Environ. Microbiol.* **2011**, *77*, 2905.
[65] H. B. Machado, Y. Dekishima, H. Luo, E. I. Lan, J. C. Liao, *Metab. Eng.* **2012**, *14*, 504.
[66] D. Gresham, J. Hong, *FEMS Microbiol. Rev.* **2015**, *39*, 2.
[67] J. Hemmerich, S. Noack, W. Wiechert, M. Oldiges, *Biotechnol. J.* **2018**, *13*, 1700141.
[68] M. Baumgart, S. Unthan, R. Kloß, A. Radek, T. Polen, N. Tenhaef, M. F. Müller, A. Küberl, D. Siebert, N. Brühl, K. Marin, S. Hans, R. Krämer, M. Bott, J. Kalinowski, W. Wiechert, G. Seibold, J. Frunzke, C. Rückert, V. F. Wendisch, S. Noack, *ACS Synth. Biol.* **2018**, *7*, 132.
[69] P. V. Phaneuf, D. Gosting, B. O. Palsson, A. M. Feist, *Nucleic Acids Res* **2018**, gky983.
[70] J. Hemmerich, N. Tenhaef, C. Steffens, J. Kappelmann, M. Weiske, S. J. Reich, W. Wiechert, M. Oldiges, S. Noack, *Biotechnol. J* **2018**, 1800428.
[71] S. Noack, R. Voges, J. Gätgens, W. Wiechert, *J. Biotechnol.* **2017**, *258*, 13.
[72] S. Unthan, A. Radek, W. Wiechert, M. Oldiges, S. Noack, *Microb. Cell Fact.* **2015**, *14*, 32.
[73] J. Nielsen, J. D. Keasling, *Cell* **2016**, *164*, 1185.
[74] T. C. Williams, I. S. Pretorius, I. T. Paulsen, *Trends Biotechnol.* **2016**, *34*, 371.
[75] J. L. Lin, J. M. Wagner, H. S. Alper, *Biotechnol. Adv.* **2017**, *35*, 950.
[76] H. H. Chou, J. D. Keasling, *Nat. Commun.* **2013**, *4*, 2595.
[77] X. Zhang, X. Zhang, G. Xu, X. Zhang, J. Shi, Z. Xu, *Appl. Microbiol. Biotechnol.* **2018**, *102*, 5939.
[78] G. Schendzielorz, M. Dippong, A. Grünberger, D. Kohlheyer, A. Yoshida, S. Binder, C. Nishiyama, M. Nishiyama, M. Bott, L. Eggeling, *ACS Synth. Biol.* **2014**, *3*, 21.
[79] C. Liu, B. Zhang, Y. M. Liu, K. Q. Yang, S. J. Liu, *ACS Synth. Biol.* **2018**, *7*, 591.
[80] S. Binder, S. Siedler, J. Marienhagen, M. Bott, L. Eggeling, *Nucleic Acids Res.* **2013**, *41*, 6360.
[81] A. D. Garst, M. C. Bassalo, G. Pines, S. A. Lynch, A. L. Halweg-Edwards, R. Liu, L. Liang, Z. Wang, R. Zeitoun, W. G. Alexander, R. T. Gill, *Nat. Biotechnol.* **2017**, *35*, 48.
[82] J. R. Warner, P. J. Reeder, A. Karimpour-Fard, L. B. A. Woodruff, R. T. Gill, *Nat. Biotechnol.* **2010**, *28*, 856.

3.2. Biosensor-based growth-coupling and spatial separation as an evolution strategy to improve small molecule production of *Corynebacterium glutamicum*

Stella, R. G., Gertzen, C. G. W., Smits, S. H. J., Gätgens, C., Polen, T., Noack, S., & Frunzke, J.

Published in *Metabolic Engineering,* 2021

Contributor role	Role definition
Conceptualization	RS 45%, JF 45%, SN 10%
Formal analysis	RS 90%, TP 10%
Investigation/Experiments	RS 90%, CGä 10%
Methodology	RS 20%, SN 30%, CGe 25%, SS 25%
Project administration	RS 50%, JF 50%
Software	RS 70%, SN 10%, CGe 10%, SS 10%
Supervision	RS 50%, JF 50%
Visualization	RS 95%, SS 5%
Writing – original draft	RS 90%, SS 5%, SN 5%
Writing – review & editing	RS 40%, JF 35%, SN 10%, CGe 5%, SS 5%, TP 5%

Overall contribution RS: 80%

This work forms the main body of this thesis. Robert Stella performed all laboratory experiments, except for strain construction experiments, which were done in collaboration with CGä. RS analyzed all data, except for the raw sequencing data, which were processed and analyzed by TP. All visualizations were done by RS, except for the enzyme model, which was created by SS and CGe. RS wrote the main part of the manuscript. The Results and M&M part concerning the enzyme model was written by SS and CGe. The M&M part concerning the ALE modelling was written by SN.

Metabolic Engineering 68 (2021) 162–173

Contents lists available at ScienceDirect

Metabolic Engineering

journal homepage: www.elsevier.com/locate/meteng

Biosensor-based growth-coupling and spatial separation as an evolution strategy to improve small molecule production of *Corynebacterium glutamicum*

Roberto G. Stella [a], Christoph G.W. Gertzen [b,c], Sander H.J. Smits [b,d], Cornelia Gätgens [a], Tino Polen [a], Stephan Noack [a,e], Julia Frunzke [a,*]

[a] Institute of Bio- and Geosciences, IBG-1: Biotechnology, Forschungszentrum Jülich GmbH, Wilhelm-Johnen-Straße, Jülich D-52425, Germany
[b] Center for Structural Studies (CSS), Heinrich Heine University Düsseldorf, Universitätsstr. 1, 40225, Düsseldorf, Germany
[c] Institute for Pharmaceutical and Medicinal Chemistry, Heinrich Heine University Düsseldorf, Universitätsstr. 1, 40225, Düsseldorf, Germany
[d] Institute of Biochemistry, Heinrich Heine University Düsseldorf, Universitätsstr. 1, 40225, Düsseldorf, Germany
[e] Bioeconomy Science Center (BioSC), Forschungszentrum Jülich GmbH, Wilhelm-Johnen-Straße, Jülich D-52425, Germany

ARTICLE INFO

Keywords:
Transcription factor-based biosensors
Growth-coupling
Adaptive evolution
Amino acid production

ABSTRACT

Evolutionary engineering is a powerful method to improve the performance of microbial cell factories, but can typically not be applied to enhance the production of chemicals due to the lack of an appropriate selection regime. We report here on a new strategy based on transcription factor-based biosensors, which directly couple production to growth. The growth of *Corynebacterium glutamicum* was coupled to the intracellular concentration of branched-chain amino acids, by integrating a synthetic circuit based on the Lrp biosensor upstream of two growth-regulating genes, *pfkA* and *hisD*. Modelling and experimental data highlight spatial separation as key strategy to limit the selection of 'cheater' strains that escaped the evolutionary pressure. This approach facilitated the isolation of strains featuring specific causal mutations enhancing amino acid production. We envision that this strategy can be applied with the plethora of known biosensors in various microbes, unlocking evolution as a feasible strategy to improve production of chemicals.

1. Introduction

Microorganisms enable the conversion of renewable carbon sources into a large variety of chemicals, but usually have to be engineered to increase production towards industrially viable numbers (Nielsen and Keasling, 2016). Evolutionary engineering is a proven strategy to optimize the performance of microbial strains (Dragosits and Mattanovich, 2013; Fernández-Cabezón et al., 2019; Mans et al., 2018; Portnoy et al., 2011; Sandberg et al., 2019; Stella et al., 2019), but the production of most chemicals is not natively linked to a selectable fitness phenotype. Thus, strategies to couple production to a selectable output are of great interest, and a variety of ways to implement this coupling have been described (Buerger et al., 2019; Shepelin et al., 2018; Yang et al., 2019).

Traditional methods include the application of antimetabolites and auxotrophic strains to screen for improved producers (Fiedurek et al., 2017). Some strategies exploit specific characteristics of the product for selection, such as intrinsic fluorescence (An et al., 1991), antioxidant properties (Reyes et al., 2014), or an increase in buoyancy (Liu et al., 2015). Co-cultures have been used to obtain improved producers on the basis of cooperation (Saleski et al., 2019), or competition (Charusanti et al., 2012). Furthermore, a variety of metabolic engineering strategies have been described that target specific pathways or enzymes to create strains in which growth is coupled to the production of a specific molecule or an enzymatic reaction, but often under specific conditions (*e.g.* anaerobic cultivation) (Otero et al., 2013; Shepelin et al., 2018; Sun et al., 2021).

Biosensors provide an alternative strategy to link production to a selectable fitness phenotype, by creating synthetic regulatory circuits responsive to the molecule of interest. Biosensors have multiple applications, for example they have been used to dynamically regulate production pathways (Dahl et al., 2013) and for (online) monitoring of product formation in both single cells and cell cultures (Lin et al., 2017; Mahr and Frunzke, 2016; Mustafi et al., 2014). Especially transcription factor(TF)-based biosensors have recently been successfully

* Corresponding author.
E-mail address: j.frunzke@fz-juelich.de (J. Frunzke).

https://doi.org/10.1016/j.ymben.2021.10.003
Received 22 July 2021; Received in revised form 27 September 2021; Accepted 3 October 2021
Available online 8 October 2021

implemented in evolutionary experiments (Williams et al., 2016). Multiple studies report their application to couple the production of a specific chemical to the expression of a measurable and selectable output, for example by coupling production to expression of a gene encoding antibiotic resistance (Dietrich et al., 2013; Leavitt et al., 2017; Raman et al., 2014; Snoek et al., 2018), to expression of a gene encoding a fluorescent reporter (Chou and Keasling, 2013; Mahr et al., 2015), to expression of a specific substrate transporter (Liu et al., 2017) or repression of a gene conferring toxicity under specific cultivation conditions (Xu et al., 2020).

In combination with an appropriate selection regime, such coupling strategies can lead to isolation of improved producer strains. In *Corynebacterium glutamicum*, production of L-valine was coupled to the production of the fluorescent protein eYFP and an iterative FACS-based selection of the most fluorescent cells resulted in the isolation of strains with an improved production of L-valine (Mahr et al., 2015). In *E. coli*, production of naringenin and glutaric acid was coupled to expression of an antibiotic resistance marker encoding TolC, which confers resistance to sodium dodecyl-sulfate and susceptibility to colicin E1 (Raman et al., 2014). This enabled the establishment of a dual selection strategy to deal with the problem of 'cheaters'. Cheaters are strains, which escape the evolutionary pressure, for example, by mutating the biosensor circuit. Cheaters are an important concern in biosensor-based approaches. The occurrence of cheaters was prevented by repetitive cultivations under positive and negative selection, while strains with improved production were isolated (Raman et al., 2014). However, a dual selection approach is only possible if the production pathway is inducible (*i.e.* production can be stopped before the negative selection).

All above-described approaches require either significant strain engineering that is often *ad hoc*, the use of specialized equipment for selection strategies (*e.g.* FACS), and/or medium amendments that will alter the selective pressure (*e.g.* antibiotics). We argue that the most straightforward growth coupling system consist of a simple regulatory system that does not require medium amendments and which is, by design, generally applicable in different microbial production hosts and for a wide variety of products.

In this study, we present a new evolutionary engineering strategy that satisfies these requirements, which is based on biosensors. By placing the expression of essential genes under control of a TF-based biosensor, the native regulatory circuitry of the host was rewired to couple production directly to cellular growth, without requiring the introduction of heterologous genetic material (*e.g.* by introducing heterologous regulatory circuits or reporter genes). Comparative analysis and modelling of different selective cultivation conditions revealed spatial separation as a key strategy to prevent the enrichment of cheaters. This approach does not require any media additives or specialized cultivation conditions and its general design principle has a high potential for use in industrial and biofoundry applications.

2. Results

2.1. Design of growth-coupled strains

To provide the basis for our envisaged synthetic evolution strategy, we coupled production to growth using a TF-based biosensor. The growth-coupled strain should have a lower biomass-specific growth rate (μ_{max}) than the parental strain (*i.e.* 0.05–0.40 h^{-1}), to allow for growth-based selection. To demonstrate our approach, a *C. glutamicum* ATCC 13032 WT strain was chosen in combination with the Lrp biosensor. The Lrp biosensor displays the highest sensitivity for L-methionine followed by L-leucine, L-isoleucine and L-valine and the intracellular concentration of these amino acids in *C. glutamicum* WT is low (<0.1 mM) (Mustafi et al., 2012). Furthermore, the system requires a gene of which the expression level has a direct influence on μ_{max} (*i.e.* when the expression of this gene is reduced, μ_{max} is reduced). Therefore, different potential "growth-regulating" genes were placed under control of the Lrp-based regulatory circuit, and the influence on μ_{max} was determined.

The Lrp-based regulatory circuit consists of the *lrp* gene, the *lrp-brnF* intergenic region, and the first 30 bp of *brnF* followed by a stop codon, a ribosomal binding site (RBS) and a linker (Mustafi et al., 2012). In the presence of its effector molecules, Lrp induces the expression of the selected growth-regulating gene downstream of P_{brnF}. To prevent potential interference from the native promoter of the growth-regulating gene, a region of about 100 bp upstream from the target gene was replaced with the regulatory circuit, and a terminator part was added upstream, to prevent any read-through activity (Fig. 1A, Suppl. Data 1, 2).

Potential growth-regulating genes were selected based on previous studies (Li et al., 2016; Rugbjerg et al., 2018) and by considering essential enzymatic reactions for growth on minimal media (*e.g.* DNA replication or amino acid synthesis; excluding biosynthesis pathways for Lrp effector amino acids). Integration of the regulatory circuit was tried for multiple genes, and five strains were obtained. Three strains (P_{brnF}-*mrsA*, P_{brnF}-*folP1* and P_{brnF}-*dnaE1*) showed WT-like growth in the absence of Lrp effector molecules (data not shown). Successful growth coupling was achieved with *pfkA* and *hisD; pfkA* encodes phosphofructokinase, which catalyzes the conversion of fructose-6-phosphate to fructose1,6-bisphosphate and *hisD* encodes histidinol dehydrogenase, which catalyzes the final steps in the *C. glutamicum* L-histidine biosynthesis pathway. When grown on glucose-based minimal media (CGXII), a reduced expression of *pfkA* should lower μ_{max} due to the lower flux through the Embden-Meyerhof-Parnas pathway, while a reduced expression of *hisD* should lower the μ_{max} due to the limited availability of L-histidine, without interference with the biosynthesis of the Lrp effector molecules. Both strains (P_{brnF}-*pfkA* and P_{brnF}-*hisD*) showed slower growth in defined glucose medium, compared to the WT strain (Fig. 1B). To activate Lrp, we increased the intracellular concentration of L-valine by a dipeptide feeding strategy (addition of ala-val) that was described previously (Vrljic et al., 1996). The addition resulted in a complete growth recovery of both strains. Furthermore, a dose-response experiment demonstrated the relationship between L-valine concentration and μ_{max} of the two strains (Figs. 1C and S1). The operational range for P_{brnF}-*hisD* was shorter. Here, the growth rate was already restored to WT-like levels with addition of 1 mM ala-val, while P_{brnF}-*pfkA* showed a more linear response and higher L-valine requirements, as 3 mM ala-val were required to restore growth to WT levels. This effect was likely due to the higher cellular demand for PfkA compared to HisD, during exponential growth on glucose minimal media. No effect on growth and μ_{max} was observed when strains were grown in BHI complex medium (Fig. 2B). In conclusion, two engineered strains were obtained that could be subjected to biosensor-based growth-coupled evolution towards higher amino acid production.

2.2. Adaptive laboratory evolution of growth-coupled strains

To evolve the two growth-coupled strains P_{brnF}-*pfkA* and P_{brnF}-*hisD* towards higher production of effector amino acids, a straightforward repetitive batch adaptive laboratory evolution (rbALE) was performed. For both strains, 22 clones were independently evolved. Cultures were grown in microtiter plates in CGXII minimal medium supplemented with 2% glucose, after a first cultivation starting from single clones grown in BHI. Cultures were transferred to fresh media once a day, or after stationary phase was reached. Growth was monitored for all cultivations and the biomass specific growth rates were calculated (Fig. 2).

All P_{brnF}-*pfkA* cultures showed a rapid recovery in growth. The growth rates of the first CGXII cultures (culture 1) were still low (average 0.12 h^{-1}), but after two more repetitive cultivations growth was already recovered to WT-like levels. For all P_{brnF}-*hisD* cultures, the growth rate declined from the first to the second CGXII cultures (average 0.14 h^{-1}), which could be due to carry-over of amino acids or other growth supplements (histidine) from the BHI culture to the first CGXII culture. Also, for these cultures, growth was eventually restored to WT-

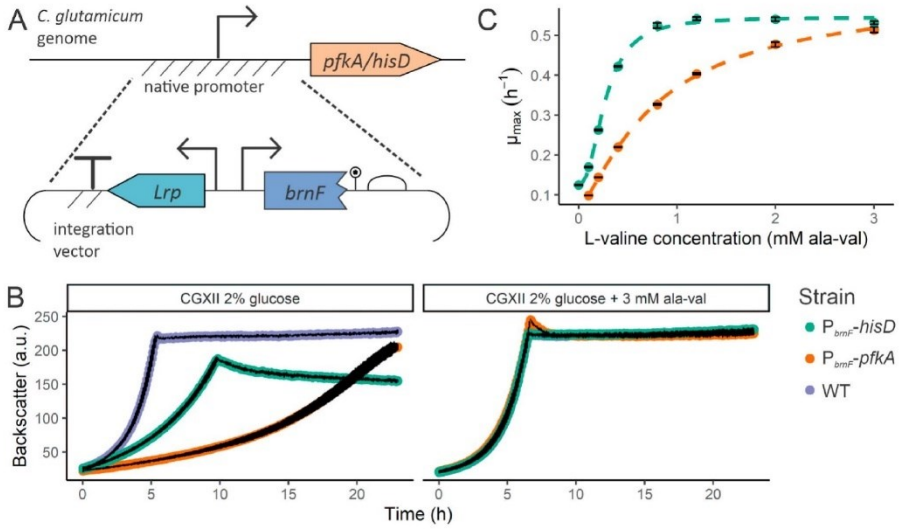

Fig. 1. Design and growth characteristics of Lrp-based growth-coupled *C. glutamicum* strains. A) Schematic overview of the Lrp-P_{brnF} integration, upstream from *C. glutamicum* genes. The integration cassette consists of a terminator to block possible promoter activity of upstream regions, *lrp*, the *lrp-brnF* intergenic region, and the first 30 bp of *brnF*, followed by a stop codon, RBS and linker. B) *C. glutamicum* microscale cultivation showing the effect of chromosomal expression of *pfkA* and *hisD* under control of the *brnF* promoter, compared to WT. Cultures were grown in standard CGXII 2% (w/v) glucose medium under non-induced (left) and induced (3 mM ala-val added, right) conditions. C) Maximum specific growth rates (μ_{max}) of P_{brnF}-*hisD* and P_{brnF}-*pfkA* cultures supplemented with different amounts of ala-val dipeptide, grown in CGXII medium with 2% (w/v) glucose. Average and standard deviation of three biological replicates are shown. (Two-column figure. Figure should be printed in color).

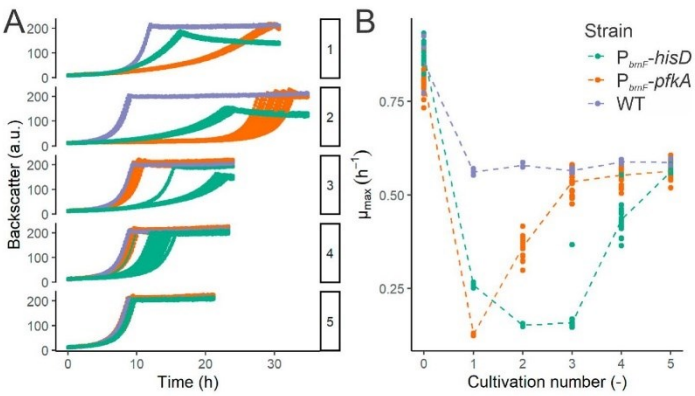

Fig. 2. Microscale rbALE of *C. glutamicum* growth-coupled strains. A) Backscatter values of five *C. glutamicum* repetitive batch cultivations, covering 22 P_{brnF}-*pfkA* and P_{brnF}-*hisD* cultures and three *C. glutamicum* WT controls. B) Maximum specific growth rates (μ_{max}) of each independent culture per repetitive batch, the line represents average per culture per strain. Culture 0 (pre-culture) was grown under non-selective conditions (in BHI media); subsequent cultures were grown under selective conditions (in CGXII medium containing 2% (w/v) glucose). (Two-column figure. Figure should be printed in color).

like levels, but only after 5 repetitive cultivations. To rule out that the observed increase in maximum specific growth rate was not due to adaptation to the media, evolved strains were grown on BHI and afterwards transferred to CGXII 2% glucose. Growth rates were still similar to WT for all evolved strains (data not shown).

While the growth rate was restored to WT-like levels for all evolved cell lines, there were no detectable amounts (>10 μM) of extracellular amino acids measured in any of the cultures as analyzed by HPLC. Whole genome sequencing was performed on three evolved P_{brnF}-*pfkA* and three evolved P_{brnF}-*hisD* strains. Mutations were found in the integrated Lrp-based regulatory circuit, indicating evolution by 'cheating' rather than by increased levels of effector amino acids. Examples of found mutations were changes in the P_{brnF} promoter region, amino acid substitutions in Lrp, and a duplication of the region containing the *pfkA* gene (Table S1).

Thus, for all six evolution lines, the evolved strains did not have any improved producer phenotype, but were 'cheater' cells that mutated the regulatory control circuit. These results indicated that, during evolution for higher production, cells easily escape the selection pressure by single point mutations in the synthetic promoter region.

2.3. Theoretical evaluation of growth-coupled ALE cultivations

Due to the relatively fast accumulation of cheater strains, we speculated that mutant cells were already present at the start of the selective cultivation. To further elucidate the potential dynamics of both cheater and producer mutants during repetitive cultivations, we developed a suitable process model. To simulate the phenotypes of growth-coupled strains, the model builds on the standard Monod description for biomass growth, extended with an 'activator' term, which captures the Lrp-based regulatory circuit. Growth is dependent on the amount of Lrp-based induction (activator concentration (A) and a strain-specific affinity (K_A) for this activator (Fig. 3). Following this approach, a producer is allowed to grow faster as a consequence of an increased induction of the Lrp-based regulatory circuit, followed by an increase in A. In turn, a cheater is modelled as a strain with $K_A = 0$, effectively removing the growth-coupled part from the equation. The model allows for the simulation of repetitive cultivations starting with different amounts of producer and cheater cells, and for simulating different producer strains (i.e. strong producers having a high induction by Lrp and weaker producers having a lower induction by Lrp).

When the simulated rbALE was started with cheater cells already present at the start of the selective cultivation, the resulting growth profiles were very similar to the experimental growth profiles observed before (Fig. 3A). Combined with the fact that the chance of a single mutation event happening is directly proportional to the amount of cells dividing, cheater mutations probably occur at the end of a batch cultivation, when cell numbers are highest. Thus, it is reasonable to assume that cheater mutations already happened during the first, unselective cultivation and that cheaters were already present at the start of the selective cultivations (here in BHI medium). Following the same reasoning, we argue that a producer mutant could also be present at the start of the selective cultivation. While the ratio of producer to cheater mutant is dependent on biology (which mutations lead to a cheater, and which to a producer) and a certain amount of randomness, we can capture these events in the model by modifying the starting ratio of producer to cheater ratio. We thus simulated multiple rbALEs, starting with different ratios of producer to cheater mutants, and varying the level of Lrp induction (Fig. 3B). If producer to cheater ratio is low, but the producer mutant strongly induces the Lrp-based regulatory circuit, some accumulation of the producer strain occurred, but the producers were not able to take over the culture in the rbALE. Only with a high producer to cheater ratio, the model predicts the enrichment of producer cells.

Following these results, a spatial separation of cheater and producer mutants right at the start of the evolution experiment would be required to efficiently enrich producer strains. Therefore, we investigated two different evolutionary selection strategies, one based on fluorescence-activated cell sorting (FACS), and the other one following a plate-based selection of producer strains (Fig. 3C).

2.4. Spatial separation of producer mutants by FACS

The first selection strategy implementing spatial separation was based on FACS. To enable selective sorting of potential producer mutants present at the end of the first non-selective cultivation, the plasmid pJC1-*lrp-brnF^r-eyfp* was introduced into the growth-coupled strains, P_{brnF}-*pfkA* and P_{brnF}-*hisD*, respectively. This sensor plasmid couples a high intracellular concentration of Lrp effector molecules to production of eYFP (Mahr et al., 2015). Here, both strains were grown under non-selective conditions (*i.e.* in BHI medium), before cell sorting. Single cells of the top fluorescent population were sorted on a non-selective BHI agar plate (Fig. 4A). Then, the rbALE was started from 42 single clones of each strain, as well as from 3 *C. glutamicum* WT clones, under selective conditions (CGXII medium) (Figs. 4B and S2).

The change in growth rate per repetitive cultivation was very similar to that of the previous rbALE (starting from liquid media precultures),

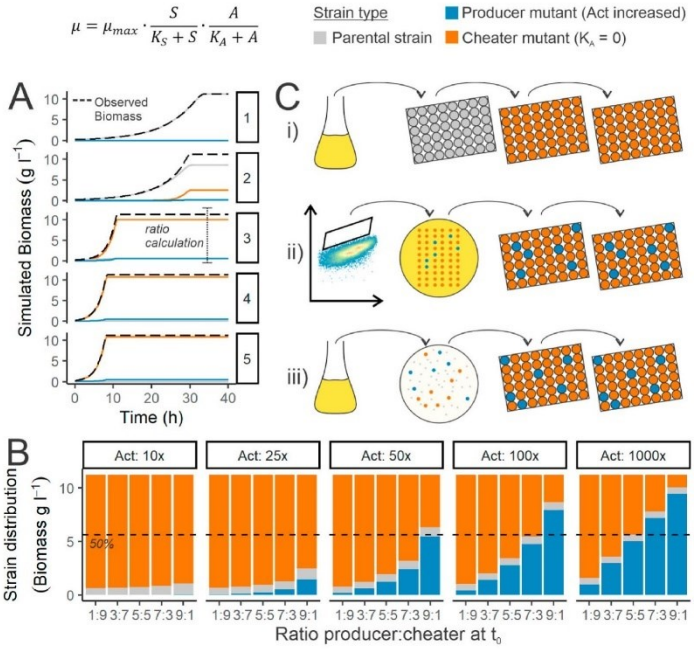

Fig. 3. Theoretical evaluation of cheater and producer dynamics in an evolutionary experiment. A) Simulated microscale rbALE, starting from arbitrarily picked values of 3 producer mutants and 7 cheater mutants at t = 0, with producer mutants having a 50x higher induction of the Lrp-based circuit compared to the parental strain. B) Strain distribution of P_{brnF}-*pfkA* parental, producer and cheater cells at the stationary phase of the third repetitive batch, for different strain ratios at t = 0, and different producer strengths (multitude of A compared to parental strain). C) Schematic overview of different evolutionary cultivation strategies; i) liquid culture rbALE, ii) FACS-based pre-selection of cells, followed by liquid rb cultivations, iii) plate-based selection followed by liquid rb cultivations. (Two-column figure. Figure should be printed in color).

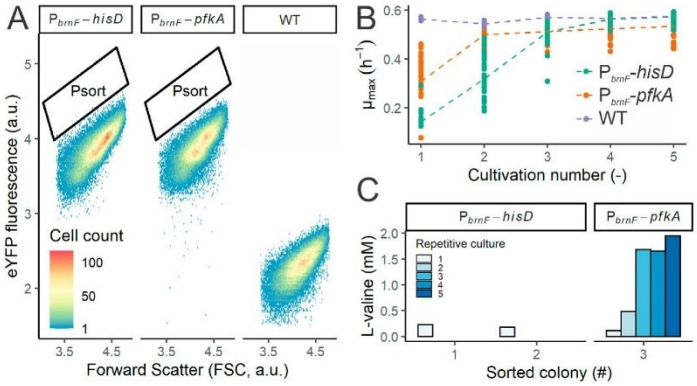

Fig. 4. Spatial separation of growth-coupled *C. glutamicum* strains using FACS followed by rbALE. A) Fluorescence intensity per cell for the P_{brnF}-*pfkA*/pJC1-*lrp-brnF'-eyfp*, P_{brnF}-*hisD*/pJC1-*lrp-brnF'-eyfp* and WT strains. Sorting gate indicates the gate used to sort only the top-fluorescent (~0.01% most fluorescent) cells. B) Maximum specific growth rates of the cultures per repetitive batch. Dots show μ_{max} of each culture of 42 P_{brnF}-*pfkA* and 42 P_{brnF}-*hisD* cultures and three *C. glutamicum* WT cultures; the lines represents average per culture, per strain. C) Extracellular L-valine concentration of three evolved clones that produced detectable amounts of extracellular amino acids. (Two-column figure. Figure should be printed in color).

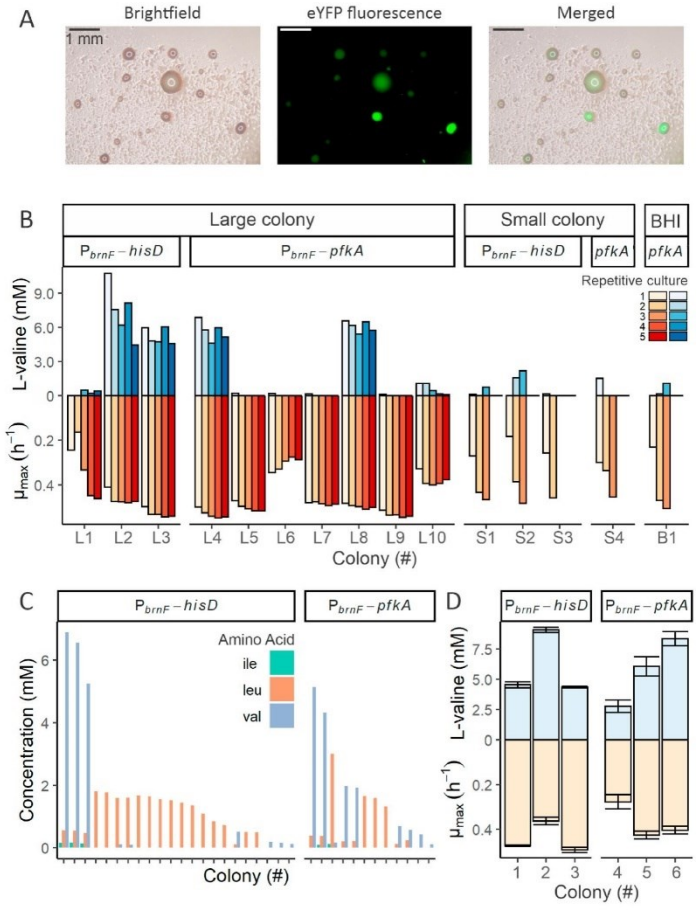

Fig. 5. Overview of results from plate-based selection strategy of *C. glutamicum* growth-coupled strains. A) Micrographs of *C. glutamicum*::P_{brnF}-*pfkA*/pJC1-*lrp-brnF'-eyfp*, showing the appearance of larger mutant clones on CGXII, which also displayed a high eYFP fluorescence intensity. B) L-valine production and growth rates of cultures started from colonies. Cultures were started from large colonies on CGXII plates, small colonies on CGXII plates, and from normal colonies on BHI plates (non-selective condition). Fifteen colonies were picked for each plate-strain combination. Results are shown for clones that produced detectable amounts of L-valine (>0.1 mM) in at least one repetitive culture. Color scales indicate results for a maximum of five repetitive cultures. C) Amino acid production of 48 cultures of each strain started from large clones on CGXII plates, sorted by total amino acid production. Results are shown for clones that produced detectable amounts of L-valine, L-isoleucine or L-leucine. D) L-valine production and growth rates of the second repetitive cultivation of the three best L-valine producing cultures (shown in C) of P_{brnF}-*pfkA* and P_{brnF}-*hisD*. Mean values and standard deviations of three biological replicates are shown. For further information, see also Figs. S7–9). (Two-column figure. Figure should be printed in color).

with the μ_{max} of the P_{brnF}-*pfkA* cultures recovering faster than that of the P_{brnF}-*hisD* cultures. Especially for the P_{brnF}-*pfkA* strains, an increased μ_{max} was already observed during the first cultivation, which could be due to successful FACS of cells with an increased amino acid production. However, only one of the P_{brnF}-*pfkA* evolution-cultures showed extracellular L-valine, with amounts increasing with higher μ_{max} over the repetitive cultivations (Fig. 4C). Two P_{brnF}-*hisD* cultures showed L-valine production, but only after the first cultivation. In conclusion, the FACS-based evolution strategy resulted in the isolation of a producer strain, but a high fraction of false positive cells was selected via this approach.

2.5. Spatial separation of producer mutants by growth on agar plates

An alternative, straightforward selection strategy is based on growth on solid media (agar-plates), enabling the separated, non-competitive growth of individual cells into colonies. When grown on selective media, mutants with an improved growth should outgrow the parental growth-coupled cells and be visible as earlier appearing and larger colonies. After a pre-cultivation in non-selective media (BHI), different dilutions of the two growth-coupled strains, P_{brnF}-*pfkA* and P_{brnF}-*hisD*, were streaked out on selective (CGXII) plates (Figs. S3–5). For a *C. glutamicum* WT strain, colonies are clearly visible on CGXII or BHI plates after just one day of incubation. For the growth-coupled strains, more time was needed on selective (CGXII) plates, due to the lower growth rate, while colonies on BHI plates were also clearly visible after just one day of incubation. After two to three days of incubation on selective plates, larger colonies were visible on plates with higher cell concentration, with an estimate of one large colony per 10^4 total colonies (Table S2). To confirm the faster growing phenotype on solid media, 8 large and small colonies of P_{brnF}-*hisD* were streaked on a fresh selective and non-selective plate; after one day colonies were only visible on the selective plate with large colonies (Fig. S6). Thus, a plate-based selection approach could successfully be applied to screen for strains that appear to have a faster growth rate. Furthermore, when growth-coupled strains harboring the plasmid pJC1-*lrp-brnF'-eyfp* were plated, a clear relationship between colony size and activation of the Lrp-based regulatory circuit could be visualized, with larger clones showing high eYFP fluorescence intensity (Fig. 5A).

The amino acid production of the different colonies was quantified in repetitive cultivations in CGXII medium. Cultures were started from three types of colonies; from the large colonies on the CGXII plates, which were expected to be evolved strains; from the small colonies on the CGXII plates, which were cultivated under selective pressure but might show only low productivity; and from BHI colonies, which were grown under non-selective conditions and were not expected to be evolved (Figs. S3–5). For each growth-coupled strain, fifteen cultures were started from each type of colony (90 cultures in total). L-valine producing strains were obtained from both growth-coupled strains and the best results were obtained from the large colonies (Fig. 5B, S7-9). Four cultures from large colonies showed extracellular L-valine concentrations above 5 mM, with the highest measured concentration above 10 mM, while the highest concentration measured for cultures from other small colonies or one clone isolated from the BHI control was less than 2.5 mM. In total, 10 out of 30 cultures from large colonies produced detectable amounts of L-valine (>0.1 mM) in at least one repetitive cultivation. For the cultures from small colonies, this was only true for four out of 30 cultures, and only one culture from a BHI-plate clone showed detectable amounts of L-valine. The growth rates of most cultures originating from the large colonies were already relatively high in the first cultivation and remained stable during subsequent cultivations, while the cultures originating from the small colonies and BHI colonies showed a relatively low initial growth rate with a sharp increase in subsequent cultivations. Thus, the larger colonies on the CGXII plate were indeed strains with an improved growth rate.

Four strains were obtained that produced extracellular L-valine in concentrations above 5 mM, with production remaining stable over all five repetitive batch cultivations (Fig. 5B, S7-9). For the other cultures that produced L-valine, two opposite trends were observed. For some cultures, L-valine was detected in the first cultivations, but not during later cultivations. This could indicate a mixed population with both producer and cheater mutants in which the cheater eventually outgrows the producers. In other cultures, no L-valine was detected during the first cultivations, but increasing concentrations were measured in the later cultivations. This increase in production was always coupled to an increase in growth rate, indicating enrichment of a producer mutant during the repetitive cultivation. Most of the L-valine producers also secreted lower amounts of L-leucine and L-isoleucine (<1.0 mM, Fig. S9), but no sole L-leucine, L-isoleucine or L-methionine producers were obtained. In conclusion, the plate-based selection strategy was successful, and especially the selection of large clones on selective media seems a good strategy to obtain high-producing mutants.

To increase the throughput of this strategy, the plate-based selection of large colonies on selective media was repeated, but the first cultivation was performed in microtiter plates with smaller wells, to increase throughput. Per strain, 48 large colonies were picked into selective media (CGXII), and extracellular amino acids were quantified after one day of cultivation (Fig. 5C). A total of 34 out of 96 cultures produces significant amounts of L-valine (15 cultures) or L-leucine (19 cultures). A second repetitive cultivation was done starting from three single clones of the top 6 L-valine and L-leucine producer cultures (Fig. 5D). Surprisingly, no extracellular L-leucine was detected for all L-leucine producers. The reason for this result is not clear, but it could be due to the differences in aeration between the different micro-cultivation systems. In contrast, the top three L-valine producers of each strain showed similar L-valine concentrations in both cultivations (Fig. 5D).

2.6. Whole genome sequencing revealed mutations in the acetohydroxyacid synthase genes ilvN and ilvB

Whole genome sequencing was performed for 15 isolated L-valine producer strains: the top producer from the FACS-based evolution (Fig. 4C), strains L1-4,8, S1,2 and B1 from the first plate-based evolution (Fig. 5B) and the top six L-valine producers from the second, HT plate-based evolution (Fig. 5D). Genomic DNA was isolated from the final repetitive batch culture. All strains had only two or less high frequency mutations (>35%), which were not present in the respective parental strain (Table S1). Remarkably, all strains had a mutation in either *ilvB* or *ilvN*, which encode the large and small subunit of the acetohydroxyacid synthase (AHAS, also known as acetolactate synthase), respectively (Fig. 6A). AHAS catalyzes the first step in the biosynthesis of L-valine and related amino acids (Fig. 6B). Mutations clustered in one region within *ilvB* and two regions within *ilvN*, but the effect on L-valine production was more dependent on the mutation than on the location (Figs. 6C and S10). An amino acid substitution of the 29th residue of *ilvN* was obtained in 5 strains, with F29L found in four strains, three of which produced the same amount of L-valine (Fig. 6C). One strain, *ilvN* (F29L) #4, produced only halve the amount of L-valine, which fits to the observation that this SNP showed only a 50% occurrence in the evolved population (Table S1). There seems to be a correlation between mutation occurrence in *ilvBN* and the evolutionary strategy applied, with cultures started from large colonies on selective plates showing high occurrences of the mutations (88–100%, except for *ilvN* D17E, which was a low frequency causal mutation), while the cultures started after FACS-based selection, from small colonies on selective plates, or from colonies on non-selective plates showed lower occurrences of the mutations (40–64%) (Table S1). Since no cheater mutations were obtained in any of the strains, it is possible that the non-evolved parental strain was still present in the cultures with a lower than 100% mutation occurrence.

To assess the possible impact of the SNPs onto the structure of the *C. glutamicum* AHAS complex, we constructed a homology model of the heterotetrameric complex consisting of two IlvB and two IlvN protomers

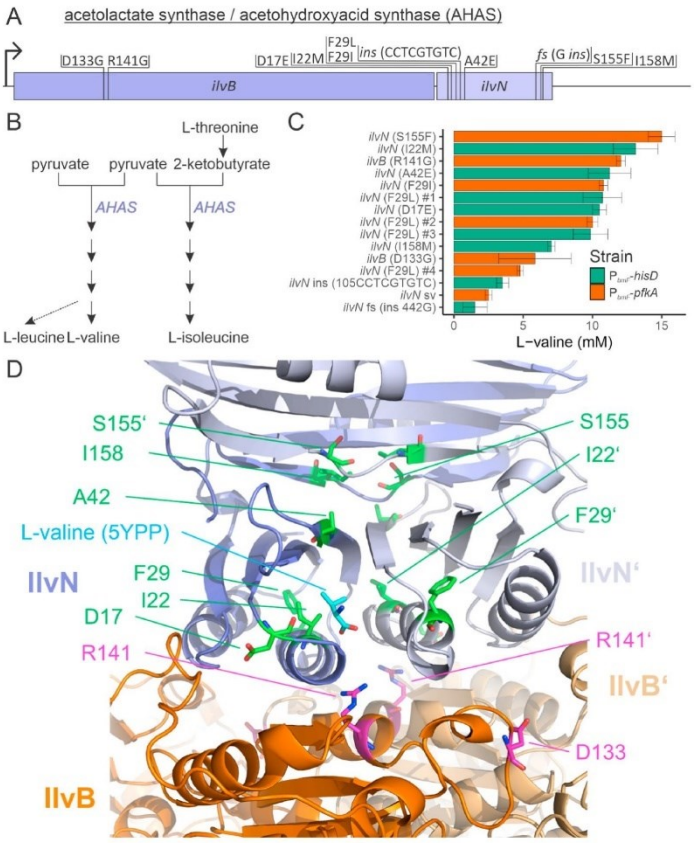

Fig. 6. Overview of mutations identified in 15 L-valine producer mutants and their effect on L-valine production. A) Schematic overview of *ilvB* and *ilvN*, indicating identified mutations at the corresponding locations (see also Table S1). B) Biosynthesis pathway of L-valine and related amino acids. C) Extracellular L-valine concentrations of 15 L-valine producer mutants, measured at the end of exponential phase. Mean values and standard deviations of three biological replicates are shown; *fs*: frameshift mutation, *sv*: structural variant, *ins*: insertion. D) Homology model of the heterotetrameric AHAS complex consisting of two IlvB protomers (orange and light orange) and two IlvN protomers (navy and blueish white) of *C. glutamicum, showing* the residues targeted by SNPs (sticks; green and magenta in IlvN and IlvB, respectively). Valine (cyan) bound to IlvN has been taken from an X-ray crystal structure of *E. coli* IlvN (PDB-ID: 5YPP (Bansal et al., 2019)) after structural alignment to the homology model. The mutated residues leading to a higher L-valine production in IlvB cluster around the L-valine binding site in IlvN and are in the first (IlvN: D17, I22, F29, and A42) or second (IlvN: S155 and I158) shell of the binding site of L-valine or are in the interface between IlvB and IlvN (IlvB: R141; IlvN: D17). (Two-column figure. Figure should be printed in color).

each (Fig. 6D). To identify the L-valine binding site in the homology model, we aligned the valine-bound *E. coli* IlvN X-ray crystal structure (PDB-ID: 5YPP (Bansal et al., 2019)), which is structurally identical to our homology model regarding the tertiary structure comprising the L-valine binding site. In the homology model, L-valine could form hydrophobic interactions with I22 and hydrogen bonds to T30′, N35', and N50 of the respective binding site in IlvN. The residues targeted by SNPs, which increase L-valine production, cluster around the L-valine binding site in IlvN (Fig. 6D) and are in the first (IlvN: D17, I22, F29, and A42) or second (IlvN: S155 and I158) shell of the binding site of L-valine, or are in the interface between IlvB and IlvN (IlvB: R141; IlvN: D17). Mutation of the residues in the first interaction shell could directly decrease the affinity of IlvN towards L-valine. As such, the IlvN I22M variant, which is the second-best L-valine producer, could sterically hinder the interaction between I22 and L-valine (Fig. 6D) by increasing the size of the sidechain. Affected residues in the second interaction shell, particularly the size increase of the side chain in the IlvN S155F variant, could affect the formation of the IlvN homodimer or disturb the shape of the L-valine binding site. Lastly, mutation of IlvB/IlvN interface residues (*e.g.*, in the IlvB R141G variant) could disrupt the crosstalk between and thus negative regulation of IlvN on IlvB. Taken together, our homology model shows that the mutation of the residues in the improved producer phenotypes could directly and indirectly affect the binding of L-valine to IlvN or disrupt the crosstalk between IlvN and IlvB and thus decrease the negative regulation of IlvN on IlvB. Taken together, the presented evolutionary strategies resulted in the isolation of strains with very specific, causal mutations.

3. Discussion

In the present study, we demonstrate the direct coupling of production to growth using TF-based biosensors as a promising strategy to enable selection for microbial production. Compared to metabolic engineering or other biosensor-based coupling strategies, our approach enabled the efficient isolation of producers starting from wild type strains and it does not require significant re-design of strains, specialized cultivation, analysis equipment, or media additives. Furthermore, no methods to increase the mutation rate are required (*e.g.* mutagen addition or UV-radiation), which results in few mutations simplifying the search for causal ones.

For our growth-coupled strains, the relationship between product concentration and growth rate was very dependent on the selected gene, as *hisD* and *pfkA* showed a different dose-response relation and no growth-regulation effect was found with *mrsA*, *folP1* and *dnaE1*. Such differences were also observed in studies demonstrating biosensor-based growth-coupling to maintain production in metabolically engineered *E. coli* and *S. cerevisiae* producer strains (D'Ambrosio et al., 2020; Rugbjerg et al., 2018). When the protocatechuic acid-responsive PcaQ

sensor was coupled to the expression of nine different growth-regulating genes in *S. cerevisiae*, differences in growth between almost all strains were observed (D'Ambrosio et al., 2020). In *E. coli*, intracellular arabinose concentration was coupled to expression of the *folP-glmM* operon, using AraC and different combinations of P_{BAD} variants and RBS variants (Rugbjerg et al., 2018). Growth was highly dependent on the promoter and RBS used. Sensor modification has also been applied to tune the expression of antibiotic resistance-markers, to optimize the selection pressure (Leavitt et al., 2017; Raman et al., 2014), and could be a good strategy to enable Lrp-based expression of more growth-regulating genes. Modification of the Lrp biosensor would also be required to apply growth-coupling-based evolution to engineered producer strains, to enable further increase of production by evolution. This will require an upward shift in the operational range of the Lrp biosensor, as the current evolutionary experiments show the upper limit at L-valine concentrations of 15 mM. Different studies have already shown suitable sensor modifications for Lrp, which could be applied in this regard (Han et al., 2020; Tenhaef et al., 2021). The recently reported 'OptCouple' approach simultaneously identifies combinations of gene knockouts, insertions and medium components coupling growth to production of a target compound and may also aid in the design of more efficient growth-coupling circuits (Jensen et al., 2019).

The occurrence of cheaters in biosensor-based screenings is a known phenomenon and major hurdle in synthetic evolution approaches. In our work, we observed some versatility in cheater mutations, as both mutations in the promoter (P_{brnF}), in the transcription factor (Lrp) and a duplication event in the *pfkA* gene-region were obtained that resulted in strains escaping the selective pressure (Table S1). In a study with *S. cerevisiae*, in which the production of vanillic acid was coupled to *GLN1* expression using the transcriptional repressor VanR, one cheater mutant was described which had a deletion of the VanR binding site in the promoter upstream of *GLN1* (D'Ambrosio et al., 2020). Several biosensor modifications were previously shown to reduce the escape rate of strains in which biosensors were used to couple production to expression of an antibiotic marker (Raman et al., 2014). These modifications included adding a degradation tag to the sensors, modification of the promoter of the antibiotic resistance marker, and using two copies of the sensors or two different antibiotic markers. Furthermore, incorporating a negative selection step against cheaters mutations prevented cheater occurrence. However, all strategies require significant strain redesign and a negative selection step cannot be used in whole cell evolution, in which the production pathway cannot simply be 'switched off'. In our work, we focused on generally applicable modifications of process conditions rather than sensor modifications to prevent the enrichment of cheaters. The applied modelling approach is in line with the hypothesis that clonal interference of cheater mutants prevents selective enrichment of producers in liquid cultures (Barrick and Lenski, 2013). By enabling initial spatial separation between the mutants under selective conditions, we could prevent the enrichment of only cheater mutants. The stability of the producer phenotype probably depends on the molecule of interest and the particular mutation. In this study, FACS- and plate-base pre-selection were followed by five repetitive batch cultivations confirming the stability of the producer phenotype in most cases. A similar regulatory circuit was applied in previous studies to establish a 'synthetic addiction' to mevalonate production of *E. coli* (Rugbjerg et al., 2018). Here, the authors reported stable productivity over >90 generations. While the accumulation of cheaters remains a challenge to synthetic evolution approaches, the strength of the reported growth-coupling strategy lies in the rapid identification of beneficial mutations enhancing target product formation. Application of this strategy will not result in the isolation of strains with superior producer phenotypes – ready for industry. This will rather be achieved through a smart combination of rational approaches with evolutionary engineering and/or HT screenings. The reported strategy is probably not suitable for long-term evolution approaches, since only cheaters will achieve maximum fitness in the long run as they since they do not invest resources for production.

The influence of the cultivation strategy on the evolutionary outcome has been extensively described and tested before (Barrick and Lenski, 2013; Mans et al., 2018; Strauss et al., 2019). A good example of the effect of spatial separation on evolutionary outcome was described for evolution of *Lactococcus lactis* (Bachmann et al., 2013). When no spatial structuring was applied, selection in liquid cultures would favor the strain with the highest growth rate. In contrast, when spatial structuring was applied based on growth in water-in-oil droplets, selection favored the strain with the highest yield and, as a consequence, a lower growth rate. In our work, different methods were used to apply spatial separation; by using FACS and by growing cells on solid media rather than in liquid media. By growing cells under selective pressure on solid media, colony size could be used to select the best producer mutants, as the highest producers were obtained from large colonies on selective plates.

Sequencing of 15 L-valine producer mutations revealed the genes encoding AHAS as a mutational hotspot. Furthermore, the presented homology model clearly points at a decreased negative feedback inhibition as result of these mutations. This is further supported by multiple studies that report the effect of different AHAS muteins on L-valine production. The small subunit, IlvN, has a regulatory function and multiple mutations (G20N, I21N, I22F, S41V, G156V) have been described that are at similar locations as the ones found in our strains (Guo et al., 2015; Vogt et al., 2014). For IlvB, one study reported the importance of the 138th residue for binding of pyruvate, and we found two mutations at the same site (Liu et al., 2019). Mutations in AHAS did not result in high L-leucine or L-isoleucine production. Possible solutions to evolve L-isoleucine or L-leucine producing strains could be to start with engineered producer strains to evolve for pathway optimization rather than innovation, or to modify the Lrp sensor to focus ligand specificity towards only one amino acid, which was recently shown for the LysG biosensor of *C. glutamicum* (Della Corte et al., 2020). Furthermore, it is possible that a fraction of the cheater mutants are actually exporter mutants that result in a higher intracellular concentration of Lrp-effector molecules, and for which no extracellular amino acids are observed as measured by HPLC. The potential isolation of such exporter mutants was previously discussed in a study where L-lysine producing mutants were obtained via biosensor-based FACS screening that showed a high fluorescence output, but low L-lysine production, in contrast other isolates showing a high production but low fluorescence output (Binder et al., 2012). Nevertheless, the fact that each isolated L-valine producer showed a single causal mutation shows the strength of evolutionary engineering to improve production.

Finally, different biosensor-based coupling strategies have successfully been applied in evolutionary experiments (Williams et al., 2016), and it would therefore be interesting to directly compare the effect of each strategy on the evolutionary outcome. For example, a recent study compared the effect of different evolutionary strategies when *E. coli* and *S. cerevisiae* were evolved for cold-tolerance, which showed large differences in the final outcome based on the applied selection (Strauss et al., 2019). Such an approach could quantify the differences between biosensor-based selection strategies and the robustness of the particular evolutionary strategy.

In conclusion, we presented direct coupling of production to growth using TF-based biosensors. While we mainly focused on the application of this principle for evolutionary engineering, it has previously been shown that growth-coupling can also increase production during fermentations, by preventing accumulation of detrimental mutations or growth of non-genetic low producing variants (D'Ambrosio et al., 2020; Rugbjerg et al., 2018; Xiao et al., 2016). Furthermore, the principle of non-conditional coupling in combination with selection solely based on growth allows for integration of further selection schemes for other (industrially) interesting characteristics, such as robustness and growth on non-native substrates and interfaces well with laboratory automation workflows (Radek et al., 2017; Wong et al., 2018). Therefore, we

envision widespread application of biosensor-based growth-coupling systems to both evolve and maintain production under industrially relevant conditions.

4. Materials and methods

4.1. Media, plasmids and strains

All strains and plasmids used in this study are listed in Table S3. *E. coli* DH5α was used for plasmid storage and propagation (Invitrogen, Karlsruhe, Germany). *E. coli* cells were grown in lysogeny broth (LB: 10 g/l tryptone, 5 g/l yeast extract, 10 g/l NaCl) or on LB agar plates (LB supplemented with 15 g/l agar), at 37 °C. If not indicated otherwise, media were supplemented with kanamycin (50 mg/l).

All *C. glutamicum* strains used in this work were derived from C. *glutamicum* ATCC 13032 (Kalinowski et al., 2003). *C. glutamicum* cells were grown in liquid Brain Heart Infusion (BHI, Difco Laboratories, Detroit, USA) or liquid CGXII minimal medium(Keilhauer et al., 1993) (1 g/l K_2HPO_4, 1 g/l KH_2PO_4, 5 g/l urea, 42 g/l MOPS, 13.25 mg/l $CaCl_2 \cdot 2\,H_2O$, 0.25 g/l $MgSO_4 \cdot 7\,H_2O$, 10 mg/l $FeSO_4 \cdot 7\,H_2O$, 10 mg/l $MnSO_4 \cdot H_2O$, 0.02 mg/l $NiCl_2 \cdot 6\,H_2O$, 0.313 mg/l $CuSO_4 \cdot 5\,H_2O$, 1 mg/l $ZnSO_4 \cdot 7\,H_2O$, 0.2 mg/l biotin, 30 mg/l 3,4-dihydroxybenzoate (PCA), 20 g/l d-glucose, pH 7.0), or on BHI agar plates (BHI supplemented with 17.5 g/l agar, or an CGXII agar plates (CGXII supplemented with 17.5 g/l agar). When indicated, the medium was supplemented with alanine-valine dipeptide (Bachem, Switzerland), or kanamycin (25 mg/l).

All plasmids constructed in this work were based on the pK19-*mobsacB* integration vector (Schäfer et al., 1994).

4.2. Molecular biology methods

Standard molecular biology methods, including PCR and DNA restriction, were carried out according to established protocols (Sambrook et al., 2001). Primers were ordered as custom DNA oligonucleotides (Eurofins Genomics, Ebersberg, Germany) (Table S4). PCR reactions were performed using Q5® High-Fidelity 2X Master Mix (New England Biolabs GmbH, Frankfurt am Main, Germany). Plasmid assembly was performed using Gibson Assembly (Gibson et al., 2009).

The integration cassettes pK19-*mobsacB-pfkA-lrp-brnF'* and pK19-*mobsacB-hisD-lrp-brnF'* were created by Gibson assembly of an upstream homology part (of *pfkA* or *hisD*), a terminator part, a part containing *lrp*, the *lrp-brnF* intergenic region, and the first 30 bp of *brnF* followed by a stopcodon, RBS and linker, and a downstream homology part (of *pfkA* or *hisD*) into an *Eco*RI and *Bam*HI digestion pK19-*mobsacB* vector (Suppl. Data 1,2). The homology parts were PCR amplified from *C. glutamicum* genomic DNA, using primers hisD_up_fw and hisD_up_rv (*hisD* upstream), hisD_down_fw and hisD_down_rv (*hisD* downstream), pfkA_up_fw and pfkA_up_rv (*pfkA* upstream), pfkA_down_fw and pfkA_down_rv (*pfkA* downstream). The terminator part was PCR amplified from pJC1-Venus-term (Baumgart et al., 2013), using primers term_fw and term_rv. The lrp-brnF part was PCR amplified from pJC1-lrp-brnF'-eyfp (Mustafi et al., 2012), using primers lrp_fw and lrp_rv. Successful plasmid assembly was verified by Sanger sequencing (Eurofins Genomics, Ebersberg, Germany).

E. coli was transformed using the Rubidium Chloride method (Hanahan, 1983). Preparation of plasmids from *E.coli* was done with the QIAprep spin miniprep kit (Qiagen, Hilden, Germany). Plasmid integration into *C. glutamicum* and second recombination were performed as described previously (Niebisch and Bott, 2001), *C. glutamicum* transformation was done by electroporation (van der Rest et al., 1999). Successful integration was verified by Sanger sequencing (Eurofins Genomics, Ebersberg, Germany).

4.3. Standard cultivation conditions

Growth characterization of *C. glutamicum* cultures was done with the BioLector® microcultivation system (m2p-labs, Germany) as described previously (Mustafi et al., 2012). Cultures were grown in 800 µl media in 48-well FlowerPlates® (m2p-labs, Germany), at 30 °C, 80% humidity and 1200 rpm shaking frequency. Culture growth was measured as the backscatter of light with a wavelength of 620 nm (signal gain factor of 20). When indicated, fluorescence was measured by excitation with light with a wavelength of 510 nm and emission was measured at 532 nm (signal gain factor of 60). Measurements were taken in 10 or 15 min intervals.

When no online measurement was required, cultures were grown in 1 ml media in 96-well deep-well plates (VWR, USA) in a microtron cultivation system (Infors HT), at 30 °C and 900 rpm shaking frequency.

For dipeptide addition experiments, cultures were started in BHI medium from frozen stocks of the parental strain. Cultures were washed twice (in 15 ml CGXII media without glucose and centrifuged at 3000 rpm for 10 min). Cultures were started with a stable minimum of preculture; for growth curve comparisons, cultures were started at optical density (OD_{600}) 0.1; for growth rate determinations, cultures were started at OD_{600} 0.005. This was done to manage the tradeoff between effector molecule carry-over (taken up intracellularly from the complex media) and evolutionary pressure. Starting with OD_{600} 0.1, growth was slower but effects from carry-over were measurable (increased μ_{max}). Starting with OD_{600} 0.005, no effects of carry over were measurable (stable low μ_{max}), but cheater growth was observed for the P_{brnF}-*pfkA* strain when no effector was added. For L-valine determination experiments of evolved isolates, precultures were started in CGXII 2% (w/v) glucose medium from frozen stocks and grown overnight. Main cultures were started at OD_{600} 1.0.

4.4. Evolutionary experiments

For rbALE experiments, cells from frozen stocks were streaked on BHI agar-plates. Single colonies were picked into BHI medium to start the rbALE, at each transfer 12.5 µl culture were transferred to 787.5 µl of fresh media.

For FACS-based evolution experiments, cultures were started in BHI medium from frozen stocks of the parental strain. After overnight cultivation, 10 µl were transferred to 1 ml sterile filtered (0.20 µm syringe-driven filter unit, Millex, Darmstadt, Germany) CGXII media without glucose, incubated for 10 min at room temperature, and filtered using a 30 µm filter (Sysmex, Goerlitz, Germany) before FACS analysis and sorting. After sorting, plates were incubated overnight and single colonies were picked into selective media (CGXII) to start the repetitive cultivations.

For plate-based evolution experiments, cultures were started in BHI medium from frozen stocks of the parental strain. After overnight cultivation, a series of 10X dilutions was made in sterile filtered (0.20 µm syringe-driven filter unit, Millex, Darmstadt, Germany) PBS, and 100 µl of diluted cultures were spread on agar plates. After overnight cultivation, single colonies were picked into selective media (CGXII) to start the repetitive cultivations. The first repetitive cultivation was either started in 48-well FlowerPlates® (m2p-labs, Germany), or, for the high-throughput selective cultivations, in 96-well deep-well plates.

4.5. HPLC analysis

Amino acids were quantified as ortho-phthaldialdehyde derivatives by uHPLC using an Agilent 1290 Infinity LC ChemStation (Agilent, Santa Clara, USA) equipped with automatic pre-column derivatization and a fluorescence detector. A Kinetex® 2.6 µm EVO C18 100 Å 30 × 2.1 column (Phenomenex®, Aschaffenburg, Germany) was used in combination with a SecurityGuard™ guard column (SecurityGuard™ ULTRA cartridge for EV0-C18 UHPLC, sub-2µm and core-shell columns with 2.1

mm internal diameters, Phenomenex®, Aschaffenburg, Germany) and elution was performed using a gradient of Na-borate buffer (10 mM Na_2HPO_4; 10 mM$Na_2B_4O_7$, pH 8.2) and methanol, adapted to operator's guide.

HPLC samples were prepared from cultures by centrifugation for 10 min at 1,500 g and 4 °C, followed by sterile filtration of the supernatant using a 0.2 µm filter (AcroPrep™ Advance, 96-well plate with 0,2 µm wwPTFE membrane, VWR, USA). Different sample dilutions in ddH_2O were prepared before measurement.

4.6. Whole genome sequencing

C. glutamicum genomic DNA was purified using a NucleoSpin Microbial DNA Mini kit (MACHEREY-NAGEL, Dueren, Germany) from an overnight BHI culture. DNA concentration was measured using the Qubit 2.0 fluorometer (Thermo Fisher Scientific, Waltham, USA). Afterwards, 1 µg of DNA was used for library preparation using the NEBNext® Ultra™ II DNA Library Prep Kit for Illumina® (NEB, Frankfurt am Main, Germany). The library was evaluated by qPCR using the KAPA library quantification kit (Peqlab, Erlangen, Germany). Afterwards, normalization for pooling was done and paired-end sequencing with a read length of 2 × 150 bases was performed by Genewiz (Leipzig, Germany). Sequencing output (base calls) were recieved as demultiplexed fastq files. The data (*e.g.* trimming, mapping, coverage extraction) were processed using the CLC Genomic Workbench software (Qiagen Aarhus A/S, Aarhus, Denmark). For mapping, modified versions of the *C. glutamicum* ATCC 13032 genome were used that included the genomic integrations. The relevance of identified mutations was assessed manually.

4.7. Flow cytometry

Cell sorting and analysis by flow cytometry were performed on a FACSAria Fusion flow cytometer (Becton Dickinson, San Jose, USA) equipped a 488 nm excitation laser and a 70 µm nozzle. Forward scatter was filtered using a 1.5 neutral density (ND) filter, side scatter was measured using a 488/10 nm band-pass filter. Fluorescence (eYFP) was measured using a 530/30 band-pass filter. FACS-Diva software version 8.0.2 was used to record and export the measurements. For cell sorting, the single-cell precision mode was used. The sort gate was set such that only a few cells per 10,000 cells fell into the gate. Sorted cells were collected on BHI agar plates.

4.8. Microscopy

Micrographs were made using an SMZ-18 stereo microscope (Nikon, Tokio, Japan), equiped with a P2-SHR Plan Apo 1x N.A. objective (Nikon), a P2-DBL LED plain base for transmitted light (Nikon), and a DS-Fi3 digital microscope camera (Nikon). For fluorescence measurements, a SOLA SM II LED light engine (LUMENCOR, Beaverton, OR, USA) was used in combination with an F46-003SMZ YFP ET optical filter set (Ex: 500/20, Em: 535/30) (Chroma Technology Corp., Bellows Falls, VT, USA). Subsequent image processing was performed using NIS-Elements BR software version 5.20.00 (Nikon).

4.9. Modelling microscale rbALE experiments

To describe the dynamics of the growth-coupled strains in microscale rbALE experiments a five species process model was formulated:

$$\dot{X}_i = \mu_i(S(t), A, K_A) n X_i(t) X_i(t=0) = X_0 \frac{-b \pm \sqrt{b^2 - 4ac}}{2a} \quad (1)$$

$$X^{tot}(t) = \sum_i X_i(t) \quad (2)$$

$$\dot{S} = -\sum_i q_{S,i} n X_i(t) S(t=0) = S_0 \quad (3)$$

with

$$X_1 = X^{ori} X_2 = X^{-} X_3 = X^{-}$$

$$\mu_i = \mu_{max} \frac{S}{K_S + S} \frac{A}{K_A + A}$$

$$q_{S,i} = \frac{\mu_i}{Y_{XS}}$$

where X^{ori}, X^{+}, and X^{-} denote the time-dependent concentrations of original (non-evolved), producer (positively evolved), and cheater (negatively evolved) cells, respectively. X^{tot} and S denote the time-dependent concentrations of the total (observed) biomass and the limiting substrate. The specific growth rate μ is modelled by using standard Monod kinetics where μ_{max} and K_S denote the maximum specific growth rate and the subtrate affinity constant. To capture the interaction with the synthetic biosensor the equation is further modulated by an activation term with A and K_A denoting the activator concentration and affinity, respectively. The substrate consumption rate q_S is related to biomass growth by the yield coefficient Y_{XS}.

For the simulation of the consecutive repetitive batches of the ALE experiment, a predefined number j of time-dependent events ($t_{tf,j}$) were formulated to describe the transfer of biomass from one batch to another (modelled as dilution by factor f_{dil}) as well as the addition of fresh substrate:

$$X_i(t) = \begin{cases} X_i f_{dil} & t = t_{tf,j} \\ X_i & otherwise \end{cases}$$

$$S(t) = \begin{cases} S f_{dil} + S_0 & t = t_{tf,j} \\ S & otherwise \end{cases}$$

The process model was implemented using the pyFOOMB tool (Hemmerich et al., 2021). For details on model validation using experimental data from microscale experiments see Suppl. Data 3.

4.10. Protein modelling

The homology models of *C. glutamicum* IlvN and IlvB were made using the Phyre2 web services (Kelley et al., 2015) and yielded a satisfactory quality when analyzed with TopScore (Mulnaes and Gohlke, 2018). The resulting models were subsequently aligned onto the X-ray crystal structure of an *E. coli* AHAS holo-complex (PDB-ID: 6LPI (Zhang et al., 2020)) to form the heterotetrameric complex using Pymol v2.4 (DeLano, 2002). The valine-bound X-ray structure of *E. coli* IlvN (PDB-ID: 5YPP (Bansal et al., 2019)) was aligned similarly and the coordinates of valine were adopted. The resulting valine-bound *C. glutamicum* AHAS complex was subsequently structurally relaxed using UCSF ChimeraX (Goddard et al., 2018).

4.11. Data analysis and visualization

Analysis and visualization of model, growth, HPLC and fluorescence data was done using R v3.6.3 (R Core Team, 2020) and tidyverse (Wickham et al., 2019). Fluorescence data was parsed using flowcore (Ellis et al., 2021), hill curve fitting for dose response curves was done using drc (Ritz et al., 2015). Calculation of growth rates was done by fitting a linear model to the log-transformed backscatter values. The start and end of the exponential phase were determined by eye (*i.e.* low backscatter values in the lag phase and high backscatter values in the stationary phase were removed).

Data availability

All relevant data supporting the findings of this manuscript are provided in the manuscript and the supplementary information; further raw data will be provided from the corresponding author upon reasonable request.

Author contributions

R.G.S., S.N., and J.F. conceived and designed the study. R.G.S., and C.G. performed all strain construction experiments, R.G.S. performed all other biological experiments. R.G.S. analyzed all data. T.P. processed and analyzed raw sequencing data. C.G.W.G, and S.H.J.S. performed the computational enzyme modelling experiments. S.N. and R.G.S. performed the computational evolution modelling experiments. R.G.S, S.N., and J.F. wrote the manuscript with input from all authors.

Declaration of competing interest

The authors have declared no conflicts of interest.

Acknowledgements

Funding was received by the German Federal Ministry of Education and Research (BMBF, projects: "BioökonomieREVIER_INNO: Entwicklung der Modellregion BioökonomieREVIER Rheinland", grant no. 031B0918A) and by the Helmholtz Association (grant W2/W3-096). Further funding was received by the Deutsche Forschungsgemeinschaft (priority program SPP 2170, grant NO 427904493). The Center for Structural Studies is funded by the Deutsche Forschungsgemeinschaft (DFG Grant number 417919780 to S.S.). We would like to thank Max Hünnefeld for assistance with microscopy, and Astrid Wirtz for assistance with HPLC.

Appendix A. Supplementary data

Supplementary data to this article can be found online at https://doi.org/10.1016/j.ymben.2021.10.003.

References

An, G.H., Bielich, J., Auerbach, R., Johnson, E.A., 1991. Isolation and characterization of carotenoid hyperproducing mutants of yeast by flow cytometry and cell sorting. Nat. Biotechnol. 9, 70–73. https://doi.org/10.1038/nbt0191-70.

Bachmann, H., Fischlechner, M., Rabbers, I., Barfa, N., Branco dos Santos, F., Molenaar, D., Teusink, B., 2013. Availability of public goods shapes the evolution of competing metabolic strategies. Proc. Natl. Acad. Sci. U.S.A 110, 14302–14307. https://doi.org/10.1073/pnas.1308523110.

Bansal, A., Karanth, N.M., Demeler, B., Schindelin, H., Sarma, S.P., 2019. Crystallographic structures of IlvN-Val/ile complexes: conformational selectivity for feedback inhibition of aceto hydroxy acid synthases. Biochemistry 58, 1992–2008. https://doi.org/10.1021/acs.biochem.9b00050.

Barrick, J.E., Lenski, R.E., 2013. Genome dynamics during experimental evolution. Nat. Rev. Genet. 14, 827–839. https://doi.org/10.1038/nrg3564.

Baumgart, M., Luder, K., Grover, S., Gätgens, C., Besra, G.S., Frunzke, J., 2013. IpsA, a novel LacI-type regulator, is required for inositol-derived lipid formation in *Corynebacteria* and *Mycobacteria*. BMC Biol. 11, 1–14. https://doi.org/10.1186/1741-7007-11-122.

Binder, S., Schendzielorz, G., Stäbler, N., Krumbach, K., Hoffmann, K., Bott, M., Eggeling, L., 2012. A high-throughput approach to identify genomic variants of bacterial metabolite producers at the single-cell level. Genome Biol. 13, R40. https://doi.org/10.1186/gb-2012-13-5-r40.

Buerger, J., Gronenberg, L.S., Genee, H.J., Sommer, M.O.A., 2019. Wiring cell growth to product formation. Curr. Opin. Biotechnol. 59, 85–92. https://doi.org/10.1016/j.copbio.2019.02.014.

Charusanti, P., Fong, N.L., Nagarajan, H., Pereira, A.R., Li, H.J., Abate, E.A., Su, Y., Gerwick, W.H., Palsson, B.O., 2012. Exploiting adaptive laboratory evolution of *streptomyces clavuligerus* for antibiotic discovery and overproduction. PLoS One 7, e33727. https://doi.org/10.1371/journal.pone.0033727.

Chou, H.H., Keasling, J.D., 2013. Programming adaptive control to evolve increased metabolite production. Nat. Commun. 4, 1–8. https://doi.org/10.1038/ncomms3595.

D'Ambrosio, V., Dore, E., Di Blasi, R., van den Broek, M., Sudarsan, S., Horst, J. ter, Ambri, F., Sommer, M.O.A., Rugbjerg, P., Keasling, J.D., Mans, R., Jensen, M.K., 2020. Regulatory control circuits for stabilizing long-term anabolic product formation in yeast. Metab. Eng. 61, 369–380. https://doi.org/10.1016/j.ymben.2020.07.006.

Dahl, R.H., Zhang, F., Alonso-Gutierrez, J., Baidoo, E., Batth, T.S., Redding-Johanson, A. M., Petzold, C.J., Mukhopadhyay, A., Lee, T.S., Adams, P.D., Keasling, J.D., 2013. Engineering dynamic pathway regulation using stress-response promoters. Nat. Biotechnol. 31, 1039–1046. https://doi.org/10.1038/nbt.2689.

DeLano, W.L., 2002. Pymol: an open-source molecular graphics tool. CCP4 Newsl. Protein Crystallogr. 40, 82–92.

Della Corte, D., van Beek, H.L., Syberg, F., Schallmey, M., Tobola, F., Cormann, K.U., Schlicker, C., Baumann, P.T., Krumbach, K., Sokolowsky, S., Morris, C.J., Grünberger, A., Hofmann, E., Schröder, G.F., Marienhagen, J., 2020. Engineering and application of a biosensor with focused ligand specificity. Nat. Commun. 11, 1–11. https://doi.org/10.1038/s41467-020-18400-0.

Dietrich, J.A., Shis, D.L., Alikhani, A., Keasling, J.D., 2013. Transcription factor-based screens and synthetic selections for microbial small-molecule biosynthesis. ACS Synth. Biol. 2, 47–58. https://doi.org/10.1021/sb300091d.

Dragosits, M., Mattanovich, D., 2013. Adaptive laboratory evolution – principles and applications for biotechnology. Microb. Cell Factories 12, 1–17. https://doi.org/10.1186/1475-2859-12-64.

Ellis, B., Haaland, P., Hahne, F., Le Meur, N., Gopalakrishnan, N., Spidlen, J., Jiang, M., Finak, G., 2021. flowCore: flowCore: Basic Structures for Flow Cytometry Data (R Packag. version).

Fernández-Cabezón, L., Cros, A., Nikel, P.I., 2019. Evolutionary approaches for engineering industrially-relevant phenotypes in bacterial cell factories. Biotechnol. J. 14, 1800439 https://doi.org/10.1002/biot.201800439.

Fiedurek, J., Trytek, M., Szczodrak, J., 2017. Strain improvement of industrially important microorganisms based on resistance to toxic metabolites and abiotic stress. J. Basic Microbiol. 57, 445–459. https://doi.org/10.1002/jobm.201600710.

Gibson, D.G., Young, L., Chuang, R.-Y., Venter, J.C., Hutchison, C.A., Smith, H.O., 2009. Enzymatic assembly of DNA molecules up to several hundred kilobases. Nat. Methods 6, 343–345. https://doi.org/10.1038/nmeth.1318.

Goddard, T.D., Huang, C.C., Meng, E.C., Pettersen, E.F., Couch, G.S., Morris, J.H., Ferrin, T.E., 2018. UCSF ChimeraX: meeting modern challenges in visualization and analysis. Protein Sci. 27, 14–25. https://doi.org/10.1002/pro.3235.

Guo, Y., Han, M., Xu, J., Zhang, W., 2015. Analysis of acetohydroxyacid synthase variants from branched-chain amino acids-producing strains and their effects on the synthesis of branched-chain amino acids in *Corynebacterium glutamicum*. Protein Expr. Purif. 109, 106–112. https://doi.org/10.1016/j.pep.2015.02.006.

Han, G., Xu, N., Sun, X., Chen, J., Chen, C., Wang, Q., 2020. Improvement of L-valine production by atmospheric and room temperature plasma mutagenesis and high-throughput screening in *Corynebacterium glutamicum*. ACS Omega 5, 4751–4758. https://doi.org/10.1021/acsomega.9b02747.

Hanahan, D., 1983. Studies on transformation of *Escherichia coli* with plasmids. J. Mol. Biol. 166, 557–580. https://doi.org/10.1016/S0022-2836(83)80284-8.

Hemmerich, J., Tenhaef, N., Wiechert, W., Noack, S., 2021. pyFOOMB: Python framework for object oriented modeling of bioprocesses. Eng. Life Sci. 21, 242–257. https://doi.org/10.1002/elsc.202000088.

Jensen, K., Broeken, V., Hansen, A.S.L., Sonnenschein, N., Herrgård, M.J., 2019. OptCouple: joint simulation of gene knockouts, insertions and medium modifications for prediction of growth-coupled strain designs. Metab. Eng. Commun. 8 https://doi.org/10.1016/j.mec.2019.e00087.

Kalinowski, J., Bathe, B., Bartels, D., Bischoff, N., Bott, M., Burkovski, A., Dusch, N., Eggeling, L., Eikmanns, B.J., Gaigalat, L., Goesmann, A., Hartmann, M., Huthmacher, K., Krämer, R., Linke, B., McHardy, A.C., Meyer, F., Möckel, B., Pfefferle, W., Pühler, A., Rey, D.A., Rückert, C., Rupp, O., Sahm, H., Wendisch, V.F., Wiegräbe, I., Tauch, A., 2003. The complete *Corynebacterium glutamicum* ATCC 13032 genome sequence and its impact on the production of L-aspartate-derived amino acids and vitamins. J. Biotechnol. 104, 5–25. https://doi.org/10.1016/S0168-1656(03)00154-8.

Keilhauer, C., Eggeling, L., Sahm, H., 1993. Isoleucine synthesis in *Corynebacterium glutamicum*: molecular analysis of the *ilvB-ilvN-ilvC* operon. J. Bacteriol. 175, 5595–5603. https://doi.org/10.1128/jb.175.17.5595-5603.1993.

Kelley, L.A., Mezulis, S., Yates, C.M., Wass, M.N., Sternberg, M.J., 2015. The Phyre2 web portal for protein modeling, prediction and analysis. Nat. Protoc. 10, 845–858. https://doi.org/10.1038/nprot.2015-053.

Leavitt, J.M., Wagner, J.M., Tu, C.C., Tong, A., Liu, Y., Alper, H.S., 2017. Biosensor-enabled directed evolution to improve muconic acid production in *Saccharomyces cerevisiae*. Biotechnol. J. 12, 1600687 https://doi.org/10.1002/biot.201600687.

Li, S., Jendresen, C.B., Grünberger, A., Ronda, C., Jensen, S.I., Noack, S., Nielsen, A.T., 2016. Enhanced protein and biochemical production using CRISPRi-based growth switches. Metab. Eng. 38, 274–284. https://doi.org/10.1016/j.ymben.2016.09.003.

Lin, J.L., Wagner, J.M., Alper, H.S., 2017. Enabling tools for high-throughput detection of metabolites: metabolic engineering and directed evolution applications. Biotechnol. Adv. 35, 950–970. https://doi.org/10.1016/j.biotechadv.2017.07.005.

Liu, S. De, Wu, Y.N., Wang, T.M., Zhang, C., Xing, X.H., 2017. Maltose utilization as a novel selection strategy for continuous evolution of microbes with enhanced metabolite production. ACS Synth. Biol. 6, 2326–2338. https://doi.org/10.1021/acssynbio.7b00247.

Liu, L., Pan, A., Spofford, C., Zhou, N., Alper, H.S., 2015. An evolutionary metabolic engineering approach for enhancing lipogenesis in *Yarrowia lipolytica*. Metab. Eng. 29, 36–45. https://doi.org/10.1016/j.ymben.2015.02.003.

Liu, Y., Wang, X., Zhan, J., Hu, J., 2019. The 138th residue of acetohydroxyacid synthase in *Corynebacterium glutamicum* is important for the substrate binding specificity.

Enzym. Microb. Technol. 129, 109357. https://doi.org/10.1016/j.enzmictec.2019.06.001.
Mahr, R., Frunzke, J., 2016. Transcription factor-based biosensors in biotechnology: current state and future prospects. Appl. Microbiol. Biotechnol. 100, 79–90. https://doi.org/10.1007/s00253-015-7090-3.
Mahr, R., Gätgens, C., Gätgens, J., Polen, T., Kalinowski, J., Frunzke, J., 2015. Biosensor-driven adaptive laboratory evolution of L-valine production in *Corynebacterium glutamicum*. Metab. Eng. 32, 184–194. https://doi.org/10.1016/j.ymben.2015.09.017.
Mans, R., Daran, J.M.G., Pronk, J.T., 2018. Under pressure: evolutionary engineering of yeast strains for improved performance in fuels and chemicals production. Curr. Opin. Biotechnol. 50, 47–56. https://doi.org/10.1016/j.copbio.2017.10.011.
Mulnaes, D., Gohlke, H., 2018. TopScore: using deep neural networks and large diverse data sets for accurate protein model quality assessment. J. Chem. Theor. Comput. 14, 6117–6126. https://doi.org/10.1021/acs.jctc.8b00690.
Mustafi, N., Grünberger, A., Kohlheyer, D., Bott, M., Frunzke, J., 2012. The development and application of a single-cell biosensor for the detection of L-methionine and branched-chain amino acids. Metab. Eng. 14, 449–457. https://doi.org/10.1016/j.ymben.2012.02.002.
Mustafi, N., Grünberger, A., Mahr, R., Helfrich, S., Nöh, K., Blombach, B., Kohlheyer, D., Frunzke, J., 2014. Application of a genetically encoded biosensor for live cell imaging of L-valine production in pyruvate dehydrogenase complex-deficient *Corynebacterium glutamicum* strains. PLoS One 9, e85731. https://doi.org/10.1371/journal.pone.0085731.
Niebisch, A., Bott, M., 2001. Molecular analysis of the cytochrome *bc1-aa3* branch of the *Corynebacterium glutamicum* respiratory chain containing an unusual diheme cytochrome c1. Arch. Microbiol. 175, 282–294. https://doi.org/10.1007/s002030100262.
Nielsen, J., Keasling, J.D., 2016. Engineering cellular metabolism. Cell 164, 1185–1197. https://doi.org/10.1016/j.cell.2016.02.004.
Otero, J.M., Cimini, D., Patil, K.R., Poulsen, S.G., Olsson, L., Nielsen, J., 2013. Industrial systems biology of *Saccharomyces cerevisiae* enables novel succinic acid cell factory. PLoS One 8, e54144. https://doi.org/10.1371/journal.pone.0054144.
Portnoy, V.A., Bezdan, D., Zengler, K., 2011. Adaptive laboratory evolution-harnessing the power of biology for metabolic engineering. Curr. Opin. Biotechnol. 22, 590–594. https://doi.org/10.1016/j.copbio.2011.03.007.
R Core Team, 2020. R: A Language and Environment for Statistical Computing. R Found. Stat. Comput., Vienna, Austria.
Radek, A., Tenhaef, N., Müller, M.F., Brüsseler, C., Wiechert, W., Marienhagen, J., Polen, T., Noack, S., 2017. Miniaturized and automated adaptive laboratory evolution: evolving *Corynebacterium glutamicum* towards an improved d-xylose utilization. Bioresour. Technol. 245, 1377–1385. https://doi.org/10.1016/j.biortech.2017.05.055.
Raman, S., Rogers, J.K., Taylor, N.D., Church, G.M., 2014. Evolution-guided optimization of biosynthetic pathways. Proc. Natl. Acad. Sci. U.S.A 111, 17803–17808. https://doi.org/10.1073/PNAS.1409523111.
Reyes, L.H., Gomez, J.M., Kao, K.C., 2014. Improving carotenoids production in yeast via adaptive laboratory evolution. Metab. Eng. 21, 26–33. https://doi.org/10.1016/j.ymben.2013.11.002.
Ritz, C., Baty, F., Streibig, J.C., Gerhard, D., 2015. Dose-response analysis using R. PLoS One 10, e0146021.
Rugbjerg, P., Sarup-Lytzen, K., Nagy, M., Sommer, M.O.A., 2018. Synthetic addiction extends the productive life time of engineered *Escherichia coli* populations. Proc. Natl. Acad. Sci. U.S.A 115, 2347–2352. https://doi.org/10.1073/pnas.1718622115.
Saleski, T.E., Kerner, A.R., Chung, M.T., Jackman, C.M., Khasbaatar, A., Kurabayashi, K., Lin, X.N., 2019. Syntrophic co-culture amplification of production phenotype for high-throughput screening of microbial strain libraries. Metab. Eng. 54, 232–243.
Sambrook, J., MacCallum, P., Russell, D.W., 2001. Molecular Cloning: a Laboratory Manual. Cold Spring Harbor Laboratory, Cold Spring Harbor, NY.
Sandberg, T.E., Salazar, M.J., Weng, L.L., Palsson, B.O., Feist, A.M., 2019. The emergence of adaptive laboratory evolution as an efficient tool for biological discovery and industrial biotechnology. Metab. Eng. 56, 1–16. https://doi.org/10.1016/j.ymben.2019.08.004.
Schäfer, A., Tauch, A., Jäger, W., Kalinowski, J., Thierbach, G., Pühler, A., 1994. Small mobilizable multi-purpose cloning vectors derived from the *Escherichia coli* plasmids pK18 and pK19: selection of defined deletions in the chromosome of *Corynebacterium glutamicum*. Gene 145, 69–73. https://doi.org/10.1016/0378-1119(94)90324-7.
Shepelin, D., Hansen, A.S.L., Lennen, R., Luo, H., Herrgård, M.J., 2018. Selecting the best: evolutionary engineering of chemical production in microbes. Genes (Basel). 9, 249. https://doi.org/10.3390/genes9050249.
Snoek, T., Romero-Suarez, D., Zhang, J., Ambri, F., Skjoedt, M.L., Sudarsan, S., Jensen, M.K., Keasling, J.D., 2018. An orthogonal and pH-tunable sensor-selector for muconic acid biosynthesis in yeast. ACS Synth. Biol. 7, 995–1003. https://doi.org/10.1021/acssynbio.7b00439.
Stella, R.G., Wiechert, J., Noack, S., Frunzke, J., 2019. Evolutionary engineering of *Corynebacterium glutamicum*. Biotechnol. J. 14, 1800444 https://doi.org/10.1002/biot.201800444.
Strauss, S.K., Schirman, D., Jona, G., Brooks, A.N., Kunjapur, A.M., Nguyen Ba, A.N., Flint, A., Solt, A., Mershin, A., Dixit, A., Yona, A.H., Csörgő, B., Busby, B.P., Hennig, B.P., Pál, C., Schraivogel, D., Schultz, D., Wernick, D.G., Agashe, D., Levi, D., Zabezhinsky, D., Russ, D., Sass, E., Tamar, E., Herz, E., Levy, E.D., Church, G.M., Yelin, I., Nachman, I., Gerst, J.E., Georgeson, J.M., Adamala, K.P., Steinmetz, L.M., Rübsam, M., Ralser, M., Klutstein, M., Desai, M.M., Walunjkar, N., Yin, N., Hefetz, N.A., Jakimo, N., Snitser, O., Adini, O., Kumar, P., Smith, R.S.H., Zean, R., Hazan, R., Rak, R., Kishony, R., Johnson, S., Nouriel, S., Vonesch, S.C., Foster, S., Dagan, T., Wein, T., Karydis, T., Wannier, T.M., Stiles, T., Olin-Sandoval, V., Mueller, W.F., Bar-On, Y.M., Dahan, O., Pilpel, Y., 2019. Evolthon: a community endeavor to evolve lab evolution. PLoS Biol. 17, e3000182 https://doi.org/10.1371/journal.pbio.3000182.
Sun, X., Li, Q., Wang, Y., Zhou, W., Guo, Y., Chen, J., Zheng, P., Sun, J., Ma, Y., 2021. Isoleucyl-tRNA synthetase mutant based whole-cell biosensor for high-throughput selection of isoleucine overproducers. Biosens. Bioelectron. 172, 112783. https://doi.org/10.1016/j.bios.2020.112783.
Tenhaef, N., Stella, R., Frunzke, J., Noack, S., 2021. Automated rational strain construction based on high-throughput conjugation. ACS Synth. Biol. 10, 589–599. https://doi.org/10.1021/acssynbio.0c00599.
van der Rest, M.E., Lange, C., Molenaar, D., 1999. A heat shock following electroporation induces highly efficient transformation of *Corynebacterium glutamicum* with xenogeneic plasmid DNA. Appl. Microbiol. Biotechnol. 52, 541–545. https://doi.org/10.1007/s002530051557.
Vogt, M., Haas, S., Klaffl, S., Polen, T., Eggeling, L., Van Ooyen, J., Bott, M., 2014. Pushing product formation to its limit: metabolic engineering of *Corynebacterium glutamicum* for l-leucine overproduction. Metab. Eng. 22, 40–52. https://doi.org/10.1016/j.ymben.2013.12.001.
Vrljic, M., Sahm, H., Eggeling, L., 1996. A new type of transporter with a new type of cellular function: L-lysine export from *Corynebacterium glutamicum*. Mol. Microbiol. 22, 815–826. https://doi.org/10.1046/j.1365-2958.1996.01527.x.
Wickham, H., Averick, M., Bryan, J., Chang, W., McGowan, L.D., François, R., Grolemund, G., Hayes, A., Henry, L., Hester, J., et al., 2019. Welcome to the tidyverse. J. Open Source Softw. 4, 1686.
Williams, T.C., Pretorius, I.S., Paulsen, I.T., 2016. Synthetic evolution of metabolic productivity using biosensors. Trends Biotechnol. 34, 371–381. https://doi.org/10.1016/j.tibtech.2016.02.002.
Wong, B.G., Mancuso, C.P., Kiriakov, S., Bashor, C.J., Khalil, A.S., 2018. Precise, automated control of conditions for high-throughput growth of yeast and bacteria with eVOLVER. Nat. Biotechnol. 36, 614–623. https://doi.org/10.1038/nbt.4151.
Xiao, Y., Bowen, C.H., Liu, D., Zhang, F., 2016. Exploiting nongenetic cell-to-cell variation for enhanced biosynthesis. Nat. Chem. Biol. 12, 339–344. https://doi.org/10.1038/nchembio.2046.
Xu, M., Liu, P., Chen, J., Peng, A., Yang, T., Zhang, X., Xu, Z., Rao, Z., 2020. Development of a novel biosensor-driven mutation and selection system via in situ growth of *Corynebacterium crenatum* for the production of L-arginine. Front. Bioeng. Biotechnol. 8, 175. https://doi.org/10.3389/fbioe.2020.00175.
Yang, J., Kim, B., Kim, G.Y., Jung, G.Y., Seo, S.W., 2019. Synthetic biology for evolutionary engineering: from perturbation of genotype to acquisition of desired phenotype. Biotechnol. Biofuels 12, 113. https://doi.org/10.1186/s13068-019-1460-5.
Zhang, Y., Li, Y., Liu, X., Sun, J., Li, X., Lin, J., Yang, X., Xi, Z., Shen, Y., 2020. Molecular architecture of the acetohydroxyacid synthase holoenzyme. Biochem. J. 477, 2439–2449. https://doi.org/10.1042/BCJ20200292.

3.3. Biosensor-based isolation of amino acid-producing *Vibrio natriegens* strains

Stella, R. G., Baumann, P., Lorke, S., Münstermann, F., Wirtz, A., Wiechert, J., Marienhagen, J., & Frunzke, J.

Published in *Metabolic Engineering Communications,* 2021

Contributor role	Role definition
Conceptualization	RS 40%, PF 10%, JM 10%, JF 40%
Formal analysis	RS 100%
Investigation/Experiments	RS 50%, PB 10%, SL 17.5%, FM 17.5%, JW 5%
Methodology	RS 60%, PB 20%, AW 20%
Project administration	RS 40%, JF 60%
Software	RS 100%
Supervision	RS 50%, JF 50%
Visualization	RS 100%
Writing – original draft	RS 100%
Writing – review & editing	RS 30%, PB 15%, JM 15%, JF 40%

Overall contribution RS: 75%

Robert Stella performed most experiments. Molecular cloning experiments were done by RS, partly in collaboration with SL. The second FACS enrichment was done in collaboration with FM. Mutagenesis experiments were performed by PB. All other experiments were performed by RS. All data was analyzed by RS. RS wrote the manuscript and created all figures.

Metabolic Engineering Communications 13 (2021) e00187

Contents lists available at ScienceDirect

Metabolic Engineering Communications

journal homepage: www.elsevier.com/locate/mec

Biosensor-based isolation of amino acid-producing *Vibrio natriegens* strains

Roberto Giuseppe Stella [a], Philipp Baumann [a], Sophia Lorke [a], Felix Münstermann [a], Astrid Wirtz [a], Johanna Wiechert [a], Jan Marienhagen [a,b], Julia Frunzke [a,*]

[a] Institute of Bio- and Geosciences, IBG-1: Biotechnology, Forschungszentrum Jülich, Jülich, Germany
[b] Institute of Biotechnology, RWTH Aachen University, Worringer Weg 3, D-52074, Aachen, Germany

ARTICLE INFO

Keywords:
Transcription factor-based biosensors
Metabolic engineering
Amino acid production
High-throughput screening

ABSTRACT

The marine bacterium *Vibrio natriegens* has recently been demonstrated to be a promising new host for molecular biology and next generation bioprocesses. *V. natriegens* is a Gram-negative, non-pathogenic slight-halophilic bacterium, with a high nutrient versatility and a reported doubling time of under 10 min. However, *V. natriegens* is not an established model organism yet, and further research is required to promote its transformation into a microbial workhorse.

In this work, the potential of *V. natriegens* as an amino acid producer was investigated. First, the transcription factor-based biosensor LysG, from *Corynebacterium glutamicum*, was adapted for expression in *V. natriegens* to facilitate the detection of positively charged amino acids. A set of different biosensor variants were constructed and characterized, using the expression of a fluorescent protein as sensor output. After random mutagenesis, one of the LysG-based sensors was used to screen for amino acid producer strains. Here, fluorescence-activated cell sorting enabled the selective sorting of highly fluorescent cells, *i.e.* potential producer cells. Using this approach, individual L-lysine, L-arginine and L-histidine producers could be obtained producing up to 1 mM of the effector amino acid, extracellularly. Genome sequencing of the producer strains provided insight into the amino acid production metabolism of *V. natriegens*.

This work demonstrates the successful expression and application of transcription factor-based biosensors in *V. natriegens* and provides insight into the underlying physiology, forming a solid basis for further development of this promising microbe.

1. Introduction

Development of *Vibrio natriegens* as a new host for molecular biology and bioprocesses has seen a recent surge in interest. *V. natriegens* was first described in 1958, as a sodium ('natrium') requiring bacterium isolated from marsh mud (Payne, 1958). *V. natriegens* is a non-pathogenic, Gram-negative, slight halophile with a high nutrient versatility, which was previously classified as *Pseudomonas natriegens* and later *Beneckea natriegens* (Baumann et al., 1971; Payne et al., 1961). The most remarkable property of *V. natriegens* is its very short doubling time, which is below 10 min under optimal conditions (Eagon, 1962; Hoffart et al., 2017).

Recent work has highlighted the application of *V. natriegens* in several different areas of biotechnology (Hoff et al., 2020; Thoma and Blombach, 2021). Weinstock et al. demonstrated that *V. natriegens* can be used as an alternative for *Escherichia coli* for standard molecular biology procedures, shortening the time of standard workflows (Weinstock et al., 2016). *V. natriegens* high capacity for translation makes it an attractive platform for cell free protein production (Des Soye et al., 2018; Failmezger et al., 2018; Wiegand et al., 2018). Furthermore, several studies contributed to improving the available toolbox for engineering *V. natriegens*, describing protocols for natural (Dalia et al., 2017) and artificial (Weinstock et al., 2016) transformation, characterization of genetic parts and tools (e.g. promoters, plasmids) (Tschirhart et al., 2019), use of CRISPRi (Lee et al., 2019), which are summarized in recent review articles (Hoff et al., 2020; Thoma and Blombach, 2021).

V. natriegens was also shown to be a potential production host for biotechnology, because of its high biomass specific substrate consumption rate, which is at least two fold higher than the biomass specific substrate consumption rate of *E. coli*, *Pseudomonas putida*, *Corynebacterium glutamicum* and yeast, under both anaerobic and aerobic conditions

* Corresponding author.
E-mail address: j.frunzke@fz-juelich.de (J. Frunzke).

https://doi.org/10.1016/j.mec.2021.e00187
Received 11 June 2021; Received in revised form 19 October 2021; Accepted 7 November 2021
Available online 11 November 2021

(Hoffart et al., 2017). Recently, a *V. natriegens* platform strain was developed, which features the genomic removal of two prophage regions (Pfeifer et al., 2019). These prophages exhibited spontaneous activation under standard cultivation conditions. The prophage-free strain showed an improved tolerance to DNA-damaging conditions and hypo-osmotic conditions and outcompeted the wild type in a competitive growth experiment (Pfeifer et al., 2019). Furthermore, *V. natriegens* strains were successfully engineered for the production of chemicals, including L-alanine (Hoffart et al., 2017), poly-β-hydroxybutyrate (Dalia et al., 2017), 2,3-butanediol (Erian et al., 2020), melanin (Wang et al., 2020), violacein and β-carotene (Ellis et al., 2019). High natural PHB production was also described by a strain similar to *V. natriegens* (Chien et al., 2007). Development of *V. natriegens* into a production strain could be accelerated with the use of transcription factor (TF)-based biosensors. TF-based biosensors comprise a variety of proteins that enable the detection of specific cellular products (Dietrich et al., 2010; Lin et al., 2017; Mahr and Frunzke, 2016). They have multiple applications, including the dynamic regulation of production pathways (Dahl et al., 2013), monitoring of product formation in both single cells and cell cultures (Mustafi et al., 2014), and enabling screening and selection of cells with increased product formation (Chou and Keasling, 2013; Mahr et al., 2015; Raman et al., 2014). However, biosensors have not been established in *V. natriegens* yet.

Therefore, we aimed to establish TF-based biosensors in *V. natriegens*. In particular, we chose to express two biosensors from *C. glutamicum*, based on LysG and Lrp, which have been successfully applied in screenings and selections for amino acid production (Binder et al., 2012; Mahr et al., 2015; Schendzielorz et al., 2014). In this study, we adapted these sensors for expression in *V. natriegens*, and applied one of them in a mutagenesis and screening approach to obtain *V. natriegens* strains that produce positively charged amino acids.

2. Materials and methods

2.1. Bacterial strains and plasmids

All *V. natriegens* and *E. coli* strains and plasmids used in this study are listed in Table 1. *E. coli* DH5α was used for plasmid storage and propagation (Invitrogen, Karlsruhe, Germany). All *V. natriegens* strains used in this work were derived from *V. natriegens* ATCC 14048 (Payne, 1958). All plasmids constructed in this work were based on pBR322 (Bolivar et al., 1977).

2.2. Media and culture conditions

E. coli cells were grown in liquid lysogeny broth (LB: 10 g l^{-1} tryptone, 5 g l^{-1} yeast extract, 10 g l^{-1} NaCl) or on LB agar plates (LB with 15 g l^{-1} agar [Carl Roth, Karlsruhe, Germany]) at 37 °C. Carbenicillin (50 mg l^{-1}) was added, if not indicated otherwise.

For molecular cloning procedures and for first pre-cultures, *V. natriegens* strains were grown in BHIN (37 g l^{-1} brain heart infusion [Becton, Dickinson, Franklin Lakes, NJ] with additional 15 g l^{-1} NaCl). When minimal media was required, *V. natriegens* was grown in standard VN medium (5 g l^{-1} $(NH_4)_2SO_4$, 15 g l^{-1} NaCl, 1 g l^{-1}, KH_2PO_4,1 g l^{-1} K_2HPO_4, 0.25 g l^{-1} $MgSO_4$, 0.01 g l^{-1} $CaCl_2$, 16.4 mg l^{-1} $FeSO_4{\cdot}7H_2O$, 10 mg l^{-1} $MnSO_4{\cdot}H_2O$, 0.3 mg l^{-1} $CuSO_4{\cdot}5H_2O$, 1 mg l^{-1} $ZnSO_4{\cdot}7H_2O$, 0.02 mg l^{-1} $NiCl_2{\cdot}6H_2O$, 21 g l^{-1} 3-(N-morpholino)propanesulfonic acid (MOPS), pH set to 7.5 by addition of NaOH), or optimized VN, VNopt (VN with in total 42 g l^{-1} 3-(N-morpholino)propanesulfonic acid (MOPS), pH set to 8.0 by addition of NaOH).

Standard cultivations always followed the same procedure; a first preculture in BHIN medium, followed by a second preculture in VN medium, and finally the main cultivation in VN medium. If not specifically indicated, the optimized VN medium was used, supplemented with 15 g l^{-1} glucose. For biosensor experiments, medium was additionally supplemented with carbenicillin (50 mg l^{-1}). When indicated, media were supplemented with specific amino acids (Sigma Aldrich, USA), or glucose was replaced with the indicated amino acid (20 mM).

Table 1
Bacterial strains used in this study.

Strain/plasmid	Genotype and relevant characteristic	Reference
V. natriegens ATCC 14048; DSM 759	Wild type	German Collection of Microorganisms and Cell Cultures, (Payne, 1958)
E. coli DH5a	supE 44 ΔlacU169 (φ80lacZDM15) hsdR17 recA1 endA1 gyrA 96 thi-1 relA1	Invitrogen (Karlsruhe, Germany)
pBR322	AmpR, TetR,	Bolivar et al. (1977)
pBR322-eYFP	AmpR, pBR322 derived backbone used for LysG sensor construction	This study
pBR322-J23100-Lrp-P_{brnFE}-eYFP	AmpR, pBR322 derived Lrp biosensor, Lrp expressed under the J23100 promoter	This study
pBR322-J23101-Lrp-P_{brnFE}-eYFP	AmpR, pBR322 derived Lrp biosensor, Lrp expressed under the J23101 promoter	This study
pBR322-J23106-Lrp-P_{brnFE}-eYFP	AmpR, pBR322 derived Lrp biosensor, Lrp expressed under the J23106 promoter	This study
pBR322-J23108-Lrp-P_{brnFE}-eYFP	AmpR, pBR322 derived Lrp biosensor, Lrp expressed under the J23108 promoter	This study
pBR322-J23110-Lrp-P_{brnFE}-eYFP	AmpR, pBR322 derived Lrp biosensor, Lrp expressed under the J23110 promoter	This study
pBR322-J23100-LysG-P_{lysE}-eYFP	AmpR, pBR322 derived LysG biosensor, LysG expressed under the J23100 promoter	This study
pBR322-J23101-LysG-P_{lysE}-eYFP	AmpR, pBR322 derived LysG biosensor, LysG expressed under the J23101 promoter	This study
pBR322-J23104-LysG-P_{lysE}-eYFP	AmpR, pBR322 derived LysG biosensor, LysG expressed under the J23104 promoter	This study
pBR322-J23106-LysG-P_{lysE}-eYFP	AmpR, pBR322 derived LysG biosensor, LysG expressed under the J23106 promoter	This study
pBR322-J23108-LysG-P_{lysE}-eYFP	AmpR, pBR322 derived LysG biosensor, LysG expressed under the J23108 promoter	This study
pBR322-J23110-LysG-P_{lysE}-eYFP	AmpR, pBR322 derived LysG biosensor, LysG expressed under the J23110 promoter	This study

Growth characterization of main cultures was done using the BioLector® microcultivation system (m2p-labs, Germany) as described previously (Heyer et al., 2012). Cultures were grown in 800 μl in 48-well FlowerPlates® (m2p-labs, Germany), at 30 °C, 80% humidity and 1500 rpm shaking frequency. When required, FlowerPlates® containing optodes for the measurement of dissolved oxygen (DO) and pH were used. Typically, cultures were inoculated to a start OD_{600} of 0.5, unless specified otherwise. Culture growth was measured as the backscatter of light with a wavelength of 620 nm (signal gain factor of 20). When indicated, fluorescence was measured by excitation with light with a wavelength of 510 nm and emission was measured at 532 nm (signal gain factor of 60). For measurement of dissolved oxygen and pH, standard settings were used. Measurements were taken in 5 or 10 min intervals.

When no online measurement was required, cultures were grown in 1 ml medium in 96-well deep well plates (VWR, USA)), at 30 °C and 900 rpm shaking frequency, in an HT Microtron shaker (Infors HT, Bottmingen, Switzerland).

2.3. Molecular cloning

Standard cloning methods, including PCR and DNA restriction, were

carried out according to established protocols (Sambrook et al., 2001). PCR reactions were performed using Q5® High-Fidelity 2X Master Mix (New England Biolabs GmbH, Frankfurt am Main, Germany). Plasmid assembly was done using Gibson assembly (Gibson et al., 2009). Plasmid sequences were verified by Sanger sequencing, by Eurofins Genomics (Ebersberg, Germany). Primers were ordered as custom DNA oligonucleotides from Eurofins Genomics (Ebersberg, Germany). All primers are listed in Table S1.

Construction of the Lrp-based sensors was performed in one step assembly of *Eco*RV and NheI digested pBR322 and three inserts; a part containing *lrp*, a part containing *eyfp* and a part containing one of the Anderson promoter sequences and the *lrp-brnF* intergenic region with the first 30 bp of *brnF*. The *lrp* containing part was obtained by PCR from *C. glutamicum* genomic DNA with primers lrp_fw and lrp_rv. The *eyfp* containing part was obtained by PCR from plasmid pJC1-*lrp-brnF'-eyfp* (Mustafi et al., 2012) with primers lrp_eYFP_fw and lrp_eYFP_rv. The constitutive promoter parts were obtained by PCR from *C. glutamicum* genomic DNA with different P1xx_PbrnFE_fw primers and primer PbrnFE_rv.

Construction of the LysG-based sensors was performed in two steps. In the first step, the intermediate plasmid pBR322-eYFP was constructed by assembly of BamHI and NheI digested pBR322 and two PCR products, a part containing *eyfp* and a linker part. The *eyfp* containing part was obtained by PCR from plasmid pJC1-*lrp-brnF'-eyfp* (Mustafi et al., 2012) with primers lysG_eYFP_fw and lysG_eYFP_rv. The linker part was obtained by PCR from plasmid pDM4-*vnp2*-p*BAD-ccdB* (Pfeifer et al., 2019) with primers lysG_araC_fw and lysG_araC_rv. The LysG-based biosensor expression vectors were constructed by assembly of SmaI and BcuI digested pBR322-eYFP and three inserts, a part containing *lysG*, a part containing one of the Anderson promoter sequences, and a part containing the *lysG-lysE* intergenic region with the first 60 bp of *lysE*. The *lysG* containing part was obtained by PCR from *C. glutamicum* genomic DNA with primers lysG_fw and lysG_rv. The parts containing different Anderson promoter sequences were obtained by hybridization of two complementary oligonucleotides, P100_lysG_fw with P100_lysG_rv, P101_lysG_fw with P101_lysG_rv, etc. The parts containing the *lysG-lysE* intergenic region and an overlap sequence for assembly with a specific Anderson promoter sequence-containing part were obtained by PCR from *C. glutamicum* genomic DNA with different PlysE_1xx_fw primers and primer PlysE_rv.

For all biosensors plasmids, upstream of *eyfp* a stop codon was added followed by a ribosomal binding site (RBS) for *V. natriegens* (AAAGAGGAGAAA) and a 6 nucleotide spacer sequence (TAATCT), which was previously reported to enhance expression of fluorescent proteins (Lentini et al., 2013).

E. coli was transformed using the Rubidium Chloride method (Hanahan, 1983). Preparation of plasmids from *E. coli* was done with the QIAprep spin miniprep kit (Qiagen, Hilden, Germany). *V. natriegens* electroporation transformation was done following a previously established electroporation protocol (Weinstock et al., 2016).

2.4. HPLC analyses

Organic acids were quantified by high performance liquid chromatography (HPLC) using an Agilent 1100/1200 LC ChemStation combination (Agilent, Santa Clara, USA) equipped with a refractive index detector (RID). A Phenomenex rezex ROA-organic acid H+ 300 mm × 7.80 mm column (Phenomenex®, Germany) was used and isocratic elution was done with 5 mM H_2SO_4.

Amino acids were quantified as ortho-phthaldialdehyde derivatives by HPLC using an Agilent 1290 Infinity LC ChemStation (Agilent, Santa Clara, USA) equipped with automatic pre-column derivatization and a fluorescence detector. A Zorbax Eclipse AAA 3.5 μm 4.6 × 7.5 mm column (Agilent, Santa Clara, USA) was used and elution was performed using a gradient of Na-borate buffer (10 mM Na_2HPO_4; 10 mM$Na_2B_4O_7$, pH 8.2) and methanol, adapted to operator's guide.

HPLC samples were prepared from cultures by centrifugation for 15 min at 4000 g and 4 °C, followed by 1:10 dilution in ddH_2O, and filtration using a 0.2 μM filter. For amino acid determination, samples were prepared once cultures were at the end of the first exponential phase (after approximately 4 h of growth).

2.5. MNNG mutagenesis

For mutagenesis, methyl nitronitrosoguanidine (MNNG) was dissolved in DMSO to a concentration of 3 g l^{-1}. From that, working solutions were prepared from 3 g l^{-1} to 1 g l^{-1} in 0.5 stepwise increments. Cell cultures were grown in BHIN supplemented with 50 mg l^{-1} carbenicillin in 500 ml shake flasks for 4 h to a final OD_{600} of 4.6 and left in stationary phase for 30 min prior to mutagenesis. Upon addition of 250 μl MNNG solution (or DMSO as control) to 5 ml of culture volume, cell cultures were incubated for 15 min in 50 ml centrifuge tubes in a 37 °C rotary shaker, including handling time. Immediately afterwards, 45 ml 0.9% NaCl was added before culture harvest by centrifugation was performed (20 °C, 4000 rpm, 7 min, Heraeus X3R, Thermo Scientific, Waltham, USA). Cells were washed twice with 0.9% NaCl and transferred to BHIN, supplemented with 50 mg l^{-1} carbenicillin, for 1 h regeneration at 37 °C.

Afterwards, for each different MNNG concentration-culture, 160 cells were sorted on BHIN agar plates supplemented with 50 mg l^{-1} carbenicillin, using a FACSAria Fusion flow cytometer (Becton Dickinson, San Jose, USA). After one day, viability of the cultures was determined by counting the number of clones on each plates.

2.6. Flow cytometry analysis and sorting

Characterization of sensor performance was done by flow cytometry using a MACSQuant® (Miltenyi Biotec, Germany) equipped with a 488 nm excitation laser and a 525/50 nm band-pass detection filter. Cultures were grown for one day, diluted 1:100 into sterile VNopt medium and incubated for 30 min on room temperature before measurement.

Cell sorting experiments by flow cytometry were performed on a FACSAria Fusion flow cytometer (Becton Dickinson, San Jose, USA) equipped with a 488 nm excitation laser and a 85 μm nozzle. Forward scatter was filtered using a 1.5 neutral density (ND) filter, side scatter was measured using a 488/10 nm band-pass filter. Fluorescence (eYFP) was measured using a 530/30 nm band-pass filter. FACS-Diva software version 8.0.2 was used to record and export the measurements. For cell sorting, the single-cell precision mode was used. Prior to flow cytometry analysis, cultures were diluted 500 times in VNopt medium without glucose, filtered using a 30 μm filter (Sysmex, Goerlitz, Germany) and incubated for 30 min on room temperature to allow for eYFP protein maturation. A hierarchical gating strategy was used for sorting. Non-bacterial particles were excluded using forward scatter and side scatter values, and doublet discrimination (avoiding sorting of multiple cells in one droplet) was done using side scatter and forward scatter area and width values. A rectangular gate was used to sort the top 5% most fluorescent cells. For bulk sorting experiments, cells were collected in a 15 ml tube prefilled with 5 ml sterile filtered VNopt medium without glucose. Afterwards, tubes were centrifuged at 1500 rpm for 5 min, excess medium was removed and the remainder was resuspended in VNopt medium to a total volume of 800 μl.

Cultures were grown until stationary phase overnight. In the morning, a 10x dilution in fresh medium was done and the FACS sorting procedure was started once cultures were at the end of the first exponential phase (after approximately 4 h of growth).

2.7. Data analysis and visualization

Analysis and visualization of growth, HPLC and fluorescence data was done using R v3.6.3 (R Core Team, 2020) and tidyverse (Wickham et al., 2019). Fluorescence data was parsed using flowcore (Ellis et al.,

2021), hill curve fitting for dose response curves was done using drc (Ritz et al., 2015).

2.8. Whole genome sequencing

V. natriegens genomic DNA was purified using a NucleoSpin Microbial DNA Mini kit (MACHEREY-NAGEL, Dueren, Germany) from an overnight BHIN culture. DNA concentration was measured using the Qubit 2.0 fluorometer (Thermo Fisher Scientific, Waltham, USA). Afterwards, 1 µg of DNA was used for library preparation using the NEBNext® Ultra™ II DNA Library Prep Kit for Illumina® (NEB, Frankfurt am Main, Germany). Library evaluation was done by qPCR using the KAPA library quantification kit (Peqlab, Erlangen, Germany). Afterwards, normalization for pooling was done and paired-end sequencing was performed using a Miseq (Illumina, San Diego, CA), with a read length of 2 × 150 bases. Sequencing output (base calls) were stored as demultiplexed fastq files. Processing of the data (e.g. trimming, mapping, coverage extraction) was done with the CLC Genomic Workbench software (Qiagen Aarhus A/S, Aarhus, Denmark). Reads were mapped against the *V. natriegens* ATCC 14048 genome (RefSeq replicon entries NZ_CP009977.1 and NZ_CP009978.1). The relevance of identified mutations was assessed manually. Only SNPs with a frequency higher than 50% were considered.

3. Results and discussion

3.1. Optimizing a defined medium for repetitive-batch cultivation

A *V. natriegens* medium that supports repetitive-batch cultivations is required for iterative screening experiments, such as fluorescence activated cell sorting (FACS) based enrichments and adaptive laboratory evolution (ALE) experiments. Therefore, initial microtiter growth cultivations were performed with *V. natriegens* to find a medium that supports repetitive-batch cultivations (*i.e.*, in which iterative cultivations show nearly identical growth behavior). Several different growth media have been described for *V. natriegens*, which are generally adapted

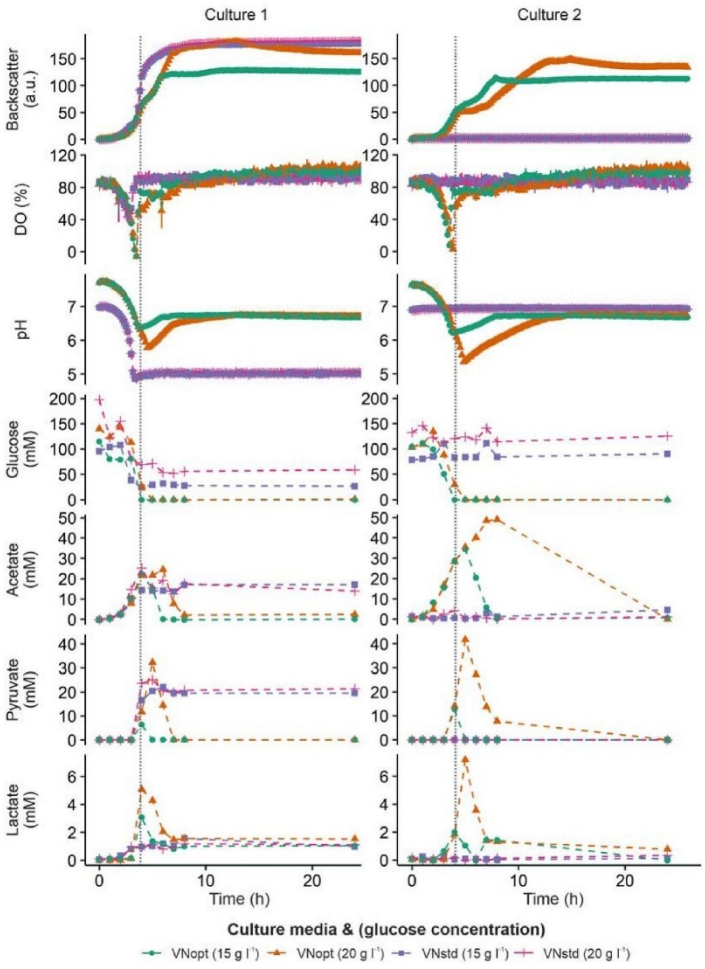

Fig. 1. Optimization of a *V. natriegens* growth medium suitable for repetitive-batch cultivation. *V. natriegens* growth in standard VN (VNstd) with 15 g l^{-1} glucose or 20 g l^{-1} glucose, and optimized VN (VNopt) with 15 g l^{-1} glucose or 20 g l^{-1} glucose. For two repetitive cultivations, backscatter (indicates biomass), dissolved oxygen and pH were measured online (n = 3, mean and standard deviation are shown), and samples were taken for measurement of glucose, acetate, pyruvate and lactate concentrations (n = 1 representative culture). Vertical grey lines indicate end of first exponential phase of culture in VNopt with 15 g l^{-1} glucose.

media originally used to grow other bacteria (e.g., *E. coli* or *C. glutamicum*), usually with increased sodium chloride concentrations; examples are M9-based (Weinstock et al., 2016) and VN (CGXII-based) (Hoffart et al., 2017) media. When *V. natriegens* was grown in VN medium with 20 g l^{-1} glucose using the BioLector® cultivation system, growth was severely hampered when repetitive cultivations where performed (Fig. 1). It was hypothesized that a low pH, reached during stationary phase in the first culture, could be the reason, as it was previously shown that *V. natriegens* converts glucose to organic acids such as acetate, pyruvate and lactate during batch cultivations in VN medium (Hoffart et al., 2017; Payne et al., 1961).

To enable stable repetitive growth in VN medium, the initial pH was increased from 7.5 to 8.0, and the amount of buffer (MOPS) was doubled to 42 g l^{-1}. *V. natriegens* was grown in the standard VN medium and in the new, optimized medium, with different glucose concentrations, and extracellular concentrations of glucose, acetate, pyruvate and lactate were measured over time by HPLC (Fig. 1).

When grown in the standard medium with normal (20 g l^{-1}) or lowered (15 g l^{-1}) glucose concentrations, only the first culture showed growth. In the second culture no change in any of the measured parameters was observed. In contrast, for cultivations in the optimized medium with both glucose concentrations, growth was observed in both the first and second cultivation. Thus, in standard VN medium the *V. natriegens* cultures seemed to lose their viability during the first cultivation. This was likely due to the low pH values that were reached after approximately 4 h, due to production of the organic acids acetate, pyruvate and lactate. After reaching a pH value of 5, no more decrease in glucose concentration was observed and the stable dissolved oxygen (DO) values indicated no respiratory activity. The backscatter measurement did not represent worse growth in standard VN medium, compared to optimized VN medium, but this was likely an artefact of the backscatter measurement; final optical density values (OD_{600}) were 10.0 ± 0.2 (20 g l^{-1} glucose) and 10.3 ± 0.1 (15 g l^{-1} glucose) for standard VN medium, and 20.6 ± 0.0 (20 g l^{-1} glucose) and 18.0 ± 0.2 (15 g l^{-1} glucose) for optimized VN medium. These values support the hypothesis that the *V. natriegens* cultures were inhibited by low pH values, which led to growth arrest. This effect was also found in a previous study that reported a negative effect on growth when pH values dropped below 7, when *V. natriegens* was grown on trypticase-based medium (Payne et al., 1961).

When *V. natriegens* was grown in optimized VN medium, two distinct growth phases were observed. First, an exponential growth phase in which all glucose was consumed and acetate, pyruvate and lactate were produced (Fig. 1). During this phase the DO values and pH rapidly decreased. Then, a second growth phase started, in which the concentrations of acetate, pyruvate and lactate decreased to below the detection limit, and the pH value increased. The lowered DO values during this phase indicate respiration of organic acids. The second cultivation in optimized VN medium showed the same trend as the first one, but especially for the higher glucose concentration (20 g l^{-1}), more acetate, pyruvate and lactate were produced and a lower pH value was reached, compared to the first cultivation. Previous studies also reported the production of organic acids, especially under anaerobic conditions (Hoffart et al., 2017; Long et al., 2017; Payne et al., 1961; Thiele et al., 2021).

Repetitive cultivations, showing a similar growth profile, could be done in optimized VN medium with both 20 g l^{-1} glucose and 15 g l^{-1} glucose for at least 8 cultivations (data not shown). Because of the faster cultivation time and lower organic acid production, all remaining experiments were carried out using VN medium with a pH initially set to 8.0, with 42 g l^{-1} MOPS and 15 g l^{-1} glucose.

3.2. Orthogonal transfer of TF-based biosensors to V. natriegens

To establish biosensors in *V. natriegens*, two transcription factor-based biosensors previously used in *C. glutamicum* were adapted for expression in *V. natriegens*; LysG and Lrp. Both are used for the detection of amino acids: Lrp for L-methionine, L-leucine, L-isoleucine and L-valine; LysG for L-histidine, L-arginine and L-threonine (Binder et al., 2012; Mustafi et al., 2012).

For both Lrp and LysG, a set of sensor variants were designed, following a similar design principle (Fig. 2A). The fluorescent protein eYFP was chosen as the sensor reporter. The Lrp sensor consists of the *C. glutamicum lrp* gene, the *lrp-brnF* intergenic region and the first part of *brnF* (Mustafi et al., 2012). The LysG sensor consists of the *C. glutamicum lysG* gene, the *lysG-lysE* intergenic region and the first part of *lysE* (Binder et al., 2012). The first part of *brnF* or *lysG* were added, because these genes are transcribed as a leaderless transcripts (Pfeifer-Sancar et al., 2013). Therefore, the first parts of *brnF* or *lysG* probably have regulatory functions and are important for Lrp or LysG binding. For each sensor, an in-frame stop codon, RBS and linker fragment was added upstream of *eyfp*. For both sensors, a small sensor library was constructed by expressing the *lrp* or *lysG* gene under different promoters from the Anderson promoter library, which was previously shown to be functional in *V. natriegens* (Anderson, 2006; Stukenberg et al., 2021; Tschirhart et al., 2019).

Functionality of each sensor set was tested with each sensor inducer, by measuring the reporter output in presence and absence of inducer (Fig. 2B). The sensor variants with different promoters showed different outputs, both in the presence or absence of inducers. Interestingly, the relative maximum output did not necessarily correspond to the promoter strength measured in previous studies (Stukenberg et al., 2021; Tschirhart et al., 2019), but this could be due to the different reporter or media used. Cultivation media were shown to have an influence on promoter functioning in *V. natriegens* (Wu et al., 2020). Another explanation could be the lack of promoter insulation, since the Anderson promoter sequences are relatively short (35bp), and only a short RBS was added (21bp). Lack of promoter insulation and different RBSs have been shown to influence expression levels (Mutalik et al., 2013). Only for the LysG sensor induced with L-lysine, a clear difference between background and induced expression was observed, with all sensor variants (up to 5-fold for P106). However, some constructs exhibited a high background level in the absence of the inducer (P101 and P108), which would have a negative implication for their application in screening procedures. To rule out that low induction levels for the other sensor-inducer combinations were due to inhibited uptake of amino acids, *V. natriegens* was grown on amino acids as sole carbon and energy source. Growth was possible on L-leucine, L-histidine and L-arginine (data not shown), growth on L-histidine and L-arginine was also shown in previous studies (Baumann et al., 1971; Ellis et al., 2019), ruling out uptake problems for these amino acids. When the LysG-based biosensor was used in *C. glutamicum*, the fluorescence-output was higher with addition of L-arginine and L-histidine than with L-lysine (Binder et al., 2012). Thus, the reason for the low response with these biosensor-inducer combinations in *V. natriegens* cannot be explained. A LysG variant that is not responsive to L-lysine anymore was recently described, and could be an interesting alternative for use in *V. natriegens* for the specific isolation of histidine producers (Della Corte et al., 2020).

For the Lrp-based sensor, none of the added inducers resulted a measurable difference in output. It is therefore likely that correct expression or functioning of this protein was not possible in *V. natriegens*.

To further characterize the LysG sensor induced with L-lysine, the dose-response relationship was measured (Fig. 2C). All sensor variants could be used to detect differences in the lower millimolar ranges, the different promoters resulted in differences in the background output and dynamic range of the sensors.

3.3. Mutagenesis and FACS-based enrichment

To demonstrate the application of transcription factor-based biosensors for the development of *V. natriegens*, the LysG-based sensor strain was used to screen for amino acid producer strains. Production of

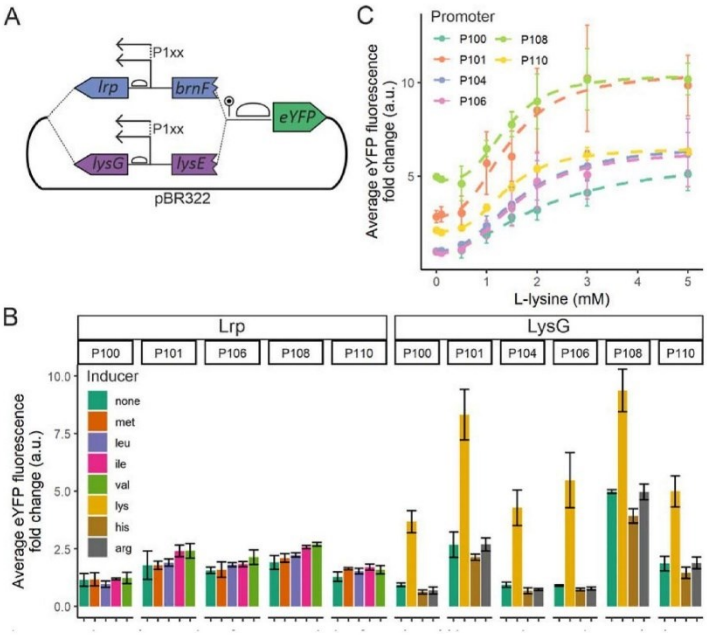

Fig. 2. Design and expression of two transcription factor-based biosensors in *V. natriegens* A) Schematic overview of LysG and Lrp biosensor design for expression in *V. natriegens*. Different sensor variants were created using promoters from the Anderson promoter library to express lrp or lysG. The first part of brnF or lysG were added to the respective construct, because these genes are transcribed as a leaderless transcripts. After the first part of brnF/lysE, a stop codon (pin) and an additional RBS (bubble) were added (for further details, see supplementary data 2 and 3). B) Sensor response of the Lrp and LysG based biosensor variants. Strains were induced with 3 mM of the indicated inducer, or no inducer was added. C) Dose-reponse signal of the LysG based biosensor variants and L-lysine. A hill-curve was fitted to the measured values. For all fluorescence measurements, fluorescence per cell of 10,000 cells per culture were measured and averaged, and fold change over background was calculated. Average and standard deviation of three cultures are shown (n = 3). Promoters from the Anderson promoter library are shown as abbreviations (P100 = J23100, etc.).

positively charged amino acids has not been shown for *V. natriegens*, and the WT strain does not produce measurable quantities of these components (Fig. 3). Using fluorescence-activated cell sorting (FACS), mutant cells with increased production can be selected, based on the higher fluorescence output (Binder et al., 2012; Mahr et al., 2015). The sensor harboring promoter P106 (J23106) was used for this experiment, because it has a low basal fluorescence output in combination with a good dynamic range (Fig. 2C) reducing the selection of false positive cells (*i.e.* fluorescent cells that are not producer cells).

To generate genotypic diversity, a culture carrying the P106-LysG-biosensor was subjected to the mutagen MNNG (N-methyl-N′-nitro-N-nitrosoguanidine) (Adelberg et al., 1965). Because the effect of MNNG on *V. natriegens* has not been described yet, the cultures were subjected to different concentrations (1.0, 1.5, 2.0, 2.5 and 3.0 g l^{-1}). The viability was calculated after MNNG treatment, which ranged from 55% to 20% (Fig. 3A). Enrichment of potential producer strains was done for each mutagenized culture, by repetitive sorting of 300,000 of the top 5% fluorescent strains followed by an overnight cultivation in optimized VN medium described in section 3.1 (Fig. 3B). Each MNNG treated culture showed an upward shift in fluorescence after three to four enrichment steps (Fig. 3C). After the fourth enrichment step, single cells were sorted on plates for the top 5% fluorescent cells, from each MNNG treated culture. Cells that formed colonies were grown in microtiter plates and the concentration of extracellular positively charged amino acids was quantified by HPLC measurement (Fig. 3D). From 245 measured strains, 37 (15%) produced more than 10 μM extracellular amino acids, and producers were isolated from cultures treated with each different MNNG concentration. Single producers of each amino acid were obtained, as well as strains that produced two or all three positively charged amino acids. In *C. glutamicum*, the LysG-based biosensor has been used in FACS-based screenings to isolate L-lysine and L-arginine producers, but not L-histidine producers (Binder et al., 2012; Schendzielorz et al., 2014). As a control experiment, we isolated eight clones from a gate covering the whole population; none of them produced any of the effector amino acids. As a further control, we randomly picked 89 MNNG-treated clones from plates. Among these, a total of only 3 clones produced more than 10 μM of the LysG effector amino acids (one clone produced 128 μM L-arginine and two clones produced 70 and 22 μM L-lysine, respectively). These controls confirm the functionality of the biosensor-based FACS-screening approach.

During growth of the cultures from the isolates, the sensor output was also measured as bulk culture fluorescence. The strongest producer strains did not show the highest fluorescence (Fig. 3D). This only confirms that the sensor output cannot directly provide information about the efficiency of amino acid secretion. While the TF-based biosensor detects the intracellular amino acid concentration, the extracellular concentration is measured by HPLC in the secondary screening. This means that, for example, a strain with very good secretion properties may feature a low intracellular amino acid level. This was also observed previously when a similar analysis was performed on isolated *C. glutamicum* L-lysine producers (Binder et al., 2012). There, the authors identified two clusters of isolates based on L-lysine production and fluorescence output: one cluster of low-fluorescent, high L-lysine producing strains, and one cluster of highly fluorescent, low-producing strains (false-positives). We observe a similar result, with a high variation in fluorescence for the non-producing isolates, and a low variation in fluorescence for the producer-isolates. This effect could be due to mutations in amino acid exporters, or due to mutations in the biosensors. Sequencing of the sensor region of two false-positive strains revealed mutations in *lysG* (E76K and S270F), which likely increased the fluorescence output without requiring an increase in amino acid production. In conclusion, the LysG sensor could be successfully applied in a high-throughput screening to isolate positively charged amino acid producing *V. natriegens* strains.

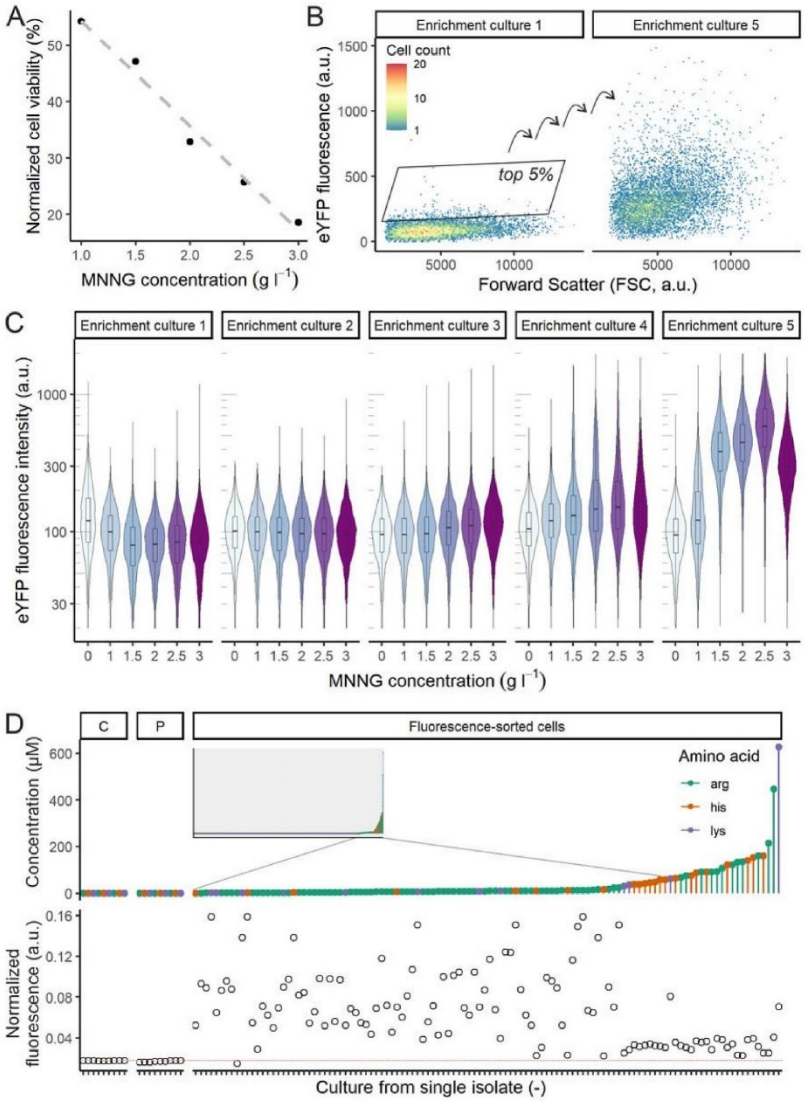

Fig. 3. Mutagenesis and FACS-based screening of *V. natriegens* harboring a LysG-based biosensor to isolate amino acid producing strains. A) Viability of *V. natriegens* cells after treatment with different MNNG concentrations. Values are normalized based on the viability of a control that was not subjected to MNNG. B) FACS scatterplots showing distribution of single cells treated with 3.0 g l^{-1} MNNG for the first and final enrichment culture (n = 10,000). C) Fluorescence per cell distribution per enrichment step (n = 10,000). Boxplots show median and first and third quartiles (lower and upper hinges). For the MNNG treated strains, the 300,000 cells of the top 5% fluorescent cells were sorted after each cultivation. For the non-MNNG treated control, 300,000 cells of the main population (no selection) were sorted after each cultivation. D) Overview of amino acid production and fluorescence of single isolates. C denotes control strain (non-MNNG treated, main population sorted), P denotes parental strain. Small frame shows amino acid concentrations of all fluorescence-sorted cells, selection shows strains for which more than 10 µM extracellular amino acid was measured. The concentration of each amino acid is shown separately for each culture (i.e. up to 3 amino acids concentrations for each). Fluorescence values are based on normalized bulk fluorescence measurements of the culture, red line indicates average fluoresce value of parental and control strains. (For interpretation of the references to colour in this figure legend, the reader is referred to the Web version of this article.)

3.4. FACS-based enrichment for improved L-lysine production

Analysis of the cultures from single isolates after the FACS enrichment revealed that the strongest producers did not show the highest fluorescence output. This indicates that the production in these mutants did not lead to maximum sensor induction. Therefore, the best producer, which produced more than 600 μM L-lysine, was subjected to another series of FACS-based enrichments. No additional mutagen was applied. After five new enrichments, an increase in fluorescence was observed (Fig. 4A). During the FACS-based enrichment, a population of low-fluorescent cells was observed at each sorting step (Fig. 4A), which was not observable during the first enrichment (Fig. 3D). A possible explanation for this observation is plasmid instability, as one study reported a low plasmid maintenance for the pBR322 backbone in *V. natriegens* (Tschirhart et al., 2019).

After the seventh enrichment, single cells of the top 5% fluorescent population were sorted. Cultures from 96 colonies were grown in microtiter plates and the concentration of extracellular L-lysine was quantified by HPLC measurement (Fig. 4B). Almost all cultures showed similar levels of L-lysine, in higher amounts than the parental strain (max. 1.1 mM). Therefore, it is likely that this approach resulted in the efficient enrichment of the most competitive clones under the chosen selection regime, suggesting a low genetic diversity of the population at the end of the enrichment workflow.

3.5. Identification of causal mutations in producer strains

Whole genome sequencing of the parental strain and the single top L-lysine, L-histidine and L-arginine producers after the first 5-round FACS enrichment (Fig. 3) was performed to identify causal mutations for the producer phenotype (Table 2, Suppl. Data 1). Overall, 81 single nucleotide polymorphisms (SNPs) could be identified, of which 68 (84%) were in coding regions, and 50 (62%) resulted in amino acid exchanges. Furthermore, all but one mutations were G to A (32, 40%) or C to T (48, 59%) mutations, which was expected since MNNG is known to predominantly induce G to A conversions. For the L-histidine producer, 23 SNPs were found, of which three could be related to L-histidine metabolism based on gene annotations and predicted metabolic networks. The first, a mutation in a gene encoding a serine ammonia-lyase (V395I) which catalyzes the conversion of serine to pyruvate, could result in an indirect increase of L-histidine. A lower activity of this enzyme would increase the reaction of serine to glycine. This reaction yields methyl tetrahydrofolate (mTHF) as a cofactor, which is needed to remove the toxic intermediate 5-aminoimidazole-4-carboxamide ribonucleotide (AICAR) in the L-histidine synthesis pathway (Schwentner et al., 2019). Two other mutations were found, one in a gene encoding IMP dehydrogenase (L433F) and one in a *carA* (P358L), encoding carbamoyl phosphate synthetase, which are both involved in nucleotide biosynthesis pathways, which are linked to L-histidine biosynthesis.

Table 2
Relevant mutations of isolated V. natriegens amino acid producer strains. Total SNPs for each strain are indicated in brackets.

#	Phenotype	Relevant mutations
H1	L-histidine producer (23 SNPs)	serine ammonia-lyase (V395I) IMP dehydrogenase (L433F) *carA*, carbamoyl phosphate synthetase (P358L)
A1	L-arginine producer (35 SNPs)	agmatine deiminase (P77L) *potD*, ABC transporter substrate-binding protein (L15F) acetolactate synthase large subunit (Y296C and W486*) threonine synthase (A186V) upstream of glutamate synthase (G to A and G to A)
L1	L-lysine producer (23 SNPs)	*dapA*, 4-hydroxy-tetrahydrodipicolinate synthase (H56Y) DUF1338 domain-containing protein (V92I)
L2	L-lysine improved producer (2 SNPs)	*All mutations of L1* DNA topoisomerase I (S500P)

For the L-arginine producer, 35 SNPs were identified, seven of which could be related to positively charged amino acid metabolism. Two mutations could reduce the conversion of L-arginine to other compounds, thereby increasing the L-arginine concentration. The first of these mutations was found in the gene encoding an agmatine deiminase (P77L), which catalyzes a step in an L-arginine degradation pathway. The other mutation was found in *potD*, encoding an ABC transporter substrate-binding protein (L15F) that transports spermidine and putrescine, which are compounds that are produced from L-arginine. A possible decrease in transport could increase their concentration, leading to an increase in L-arginine concentrations due to lower conversion requirements. Another set of mutations were all involved in metabolism of other amino acids, which are connected to L-arginine biosynthesis by biochemical pathways. Two mutations were found in a gene encoding the large subunit of acetolactate synthase (Y296C and W486*), and one mutation was found in a gene encoding threonine synthase (A186V). Both enzymes are involved in L-threonine and branched chain amino acid biosynthesis. Furthermore, two mutations were found upstream of the gene encoding glutamate synthase (two G to A mutations), which could alter the expression of this gene. The multiple mutations in genes involved in amino acids biosynthesis and degradation found in the L-arginine producers could indicate an intricate rewiring of metabolism to increase the production of L-arginine.

A total of 23 SNPs were found in the L-lysine producer isolated after the first round of FACS enrichment, of which two could be related to L-lysine metabolism. The first is a mutation in *gapA* (H56Y), which encodes 4-hydroxy-tetrahydrodipicolinate synthase. This is the third enzyme in the L-lysine biosynthesis pathway, which is known to be feedback-inhibited by L-lysine, and mutation could result in a lower

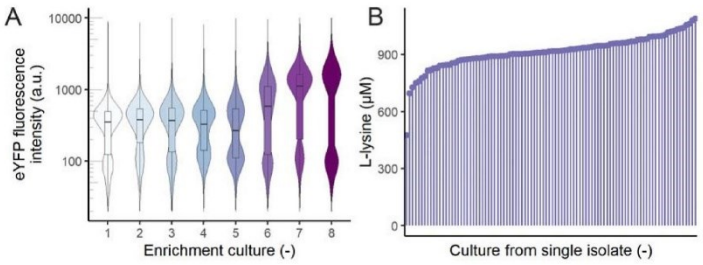

Fig. 4. FACS-based enrichment of *V. natriegens* L-lysine producers harboring a LysG-based biosensor. A) Fluorescence per cell distribution per enrichment step (n = 10,000). Boxplots show median and first and third quartiles (lower and upper hinges); 300,000 cells of the top 5% fluorescent cells were sorted after each cultivation. B) Extracellular L-lysine concentration of 96 cultures from sorted single isolates.

inhibition leading to an increased L-lysine production. Another mutation was found in a gene encoding an enzyme active in a putative L-lysine degradation pathway, identified as a DUF1338 domain-containing protein (V92I). In *P. putida*, a homologue of this protein catalyzes the conversion of 2-oxoadipate to 2-hydroxyglutarate, in a pathway that leads to the conversion of L-lysine to 2-ketoglutarate (Thompson et al., 2019). While this pathway has not been described in *V. natriegens*, this mutation could result in a lower L-lysine degradation rate. Furthermore, SNPs in several ABC transporters were found. While these could influence amino acid transport, their specific function still need to be elucidated.

Finally, the genome of the improved L-lysine production strain, isolated after the second FACS enrichment, was analyzed and compared to the parental L-lysine producer. Only two additional SNPs were found, this low number is likely because no additional mutagenesis was done on this strain. The first mutation was in a gene encoding DNA topoisomerase I (S500P), the second one was a C to G mutation in the intergenic region between a hypothetical protein and phosphate ABC transporter substrate-binding protein. It is possible that the mutation in the DNA topoisomerase has pleiotropic effects that potentially affect the expression of genes involved in L-lysine biosynthesis.

4. Conclusion

V. natriegens is a promising host for next-generation bioprocesses. A recent study showed a high volumentric productivity of engineered *V. natriegens* for L-alanine production (0.56 ± 0.10 g L-alanine liter^{-1} min^{-1}) using resting cells under anaerobic conditions (Hoffart et al., 2017). These results impressively emphasize *V. natriegens* as a potential production host for amino acid production.

In this work, we describe the first expression of transcription factor-based biosensors in *V. natriegens*, and use them in a high-throughput screening to isolate producer strains. Individual L-lysine, L-arginine and L-histidine were obtained, but all showed relatively low productivity in the high micro molar range. This is in stark contrast to the results of screenings with the same sensor in the established amino acid producer *C. glutamicum*. Here, FACS screenings resulted in the isolation of clones secreting up to 40 mM L-lysine (Binder et al., 2012; Schendzielorz et al., 2014), but no L-histidine producers were obtained. These clones carried mutations leading to a loss of feedback inhibition of the aspartate kinase – a key target for engineering L-lysine production in these strains. Nevertheless, the successful isolation of *V. natriegens* clones secreting low amounts of LysG effector amino acids demonstrates the functionality of this approach. FACS screening enables the rapid isolation of positive clones from a large library (Dietrich et al., 2010). The high rate of false-positive clones - a typical characteristic of such an approach - naturally requires the examination of the isolates with regard to their production properties by means of HPLC. Results shown in Fig. 3D indicate that the initial FACS screening provides qualitative information, but may not provide quantitative information on the overall productivity of the strain, since the sensor acts intracellularly. Here, mutation of the sensor construct itself or mutation in exporters may drastically affect the sensor output. The high-throughput character of the overall approach does, nevertheless, enable the identification of potential causal mutations, demonstrating the power of this approach. The mutated genes provide information about the *V. natriegens* amino acid metabolism and regulation and could be targeted in future engineering work to further improve *V. natriegens* as a host for amino acid production. Multiplexed re-engineering of the identified genetic variants, e.g. by using the MuGent approach (Dalia et al., 2017), could identify novel and non-intuitive beneficial mutations and provide insights in epistatic interactions.

Declaration of competing interest

The authors declare that they have no known competing financial interests or personal relationships that could have appeared to influence the work reported in this paper.

Acknowledgements

This project has received funding from the European Research Council (ERC) under the European Union's Horizon 2020 research and innovation program (grant agreement no 638718) and the Helmholtz Association (grant number W2/W3-096). The authors would like to thank Tino Polen for help with the analysis of sequencing data.

Appendix A. Supplementary data

Supplementary data to this article can be found online at https://doi.org/10.1016/j.mec.2021.e00187.

Author contributions

Roberto Giuseppe Stella: Conceptualization, Methodology, Software, Validation, Formal analysis, Investigation, Data Curation, Writing – Original Draft, Visualization, Supervision, Project administration. **Philipp Baumann**: Conceptualization, Methodology, Investigation, Writing – Review & Editing. **Sophia Lorke**: Investigation. **Felix Münstermann**: Investigation. **Astrid Wirtz**: Methodology. **Jan Marienhagen**: Conceptualization, Resources, Writing – Review & Editing, Funding acquisition. **Julia Frunzke**: Conceptualization, Resources, Writing – Review & Editing, Supervision, Project administration, Funding acquisition.

References

Adelberg, E.A., Mandel, M., Ching Chen, G.C., 1965. Optimal conditions for mutagenesis by N-methyl-N′-nitro-N-nitrosoguanidine in *Escherichia coli* K12. Biochem. Biophys. Res. Commun. 18, 788–795. https://doi.org/10.1016/0006-291X(65)90855-7.

Anderson, J.C., 2006. Anderson promoter library [WWW Document]. URL. http://parts.igem.org/Promoters/Catalog/Anderson.

Baumann, P., Baumann, L., Mandel, M., 1971. Taxonomy of marine bacteria: the genus *Beneckea*. J. Bacteriol. 107, 268–294.

Binder, S., Schendzielorz, G., Stäbler, N., Krumbach, K., Hoffmann, K., Bott, M., Eggeling, L., 2012. A high-throughput approach to identify genomic variants of bacterial metabolite producers at the single-cell level. Genome Biol. 13, R40. https://doi.org/10.1186/gb-2012-13-5-r40.

Bolivar, F., Rodriguez, R.L., Greene, P.J., Betlach, M.C., Heyneker, H.L., Boyer, H.W., Crosa, J.H., Falkow, S., 1977. Construction and characterization of new cloning vehicle. II. A multipurpose cloning system. Gene 2, 95–113.

Chien, C.-C., Chen, C.-C., Choi, M.-H., Kung, S.-S., Wei, Y.-H., 2007. Production of poly-β-hydroxybutyrate (PHB) by *Vibrio* spp. isolated from marine environment. J. Biotechnol. 132, 259–263.

Chou, H.H., Keasling, J.D., 2013. Programming adaptive control to evolve increased metabolite production. Nat. Commun. 4, 1–8. https://doi.org/10.1038/ncomms3595.

Dahl, R.H., Zhang, F., Alonso-Gutierrez, J., Baidoo, E., Batth, T.S., Redding-Johanson, A. M., Petzold, C.J., Mukhopadhyay, A., Lee, T.S., Adams, P.D., Keasling, J.D., 2013. Engineering dynamic pathway regulation using stress-response promoters. Nat. Biotechnol. 31, 1039–1046. https://doi.org/10.1038/nbt.2689.

Dalia, T.N., Hayes, C.A., Stolyar, S., Marx, C.J., McKinlay, J.B., Dalia, A.B., 2017. Multiplex genome editing by natural transformation (MuGENT) for synthetic biology in *Vibrio natriegens*. ACS Synth. Biol. 6, 1650–1655. https://doi.org/10.1021/acssynbio.7b00116.

Della Corte, D., van Beek, H.L., Syberg, F., Schallmey, M., Tobola, F., Cormann, K.U., Schlicker, C., Baumann, P.T., Krumbach, K., Sokolowsky, S., Morris, C.J., Grünberger, A., Hofmann, E., Schröder, G.F., Marienhagen, J., 2020. Engineering and application of a biosensor with focused ligand specificity. Nat. Commun. 11, 1–11. https://doi.org/10.1038/s41467-020-18400-0.

Des Soye, B.J., Davidson, S.R., Weinstock, M.T., Gibson, D.G., Jewett, M.C., 2018. Establishing a high-yielding cell-free protein synthesis platform derived from *Vibrio natriegens*. ACS Synth. Biol. 7, 2245–2255. https://doi.org/10.1021/acssynbio.8b00252.

Dietrich, J.A., McKee, A.E., Keasling, J.D., 2010. High-throughput metabolic engineering: advances in small-molecule screening and selection. Annu. Rev. Biochem. 79, 563–590. https://doi.org/10.1146/annurev-biochem-062608-095938.

Eagon, R.G., 1962. *Pseudomonas natriegens*, a marine bacterium with a generation time of less than 10 minutes. J. Bacteriol. 83, 736–737.

Ellis, B., Haaland, P., Hahne, F., Le Meur, N., Gopalakrishnan, N., Spidlen, J., Jiang, M., Finak, G., 2021. flowCore: flowCore: basic structures for flow cytometry data, 2017 R Packag. version, 2.4.0.

Ellis, G.A., Tschirhart, T., Spangler, J., Walper, S.A., Medintz, I.L., Vora, G.J., 2019. Exploiting the feedstock flexibility of the emergent synthetic biology chassis *Vibrio natriegens* for engineered natural product production. Mar. Drugs 17, 1–21. https://doi.org/10.3390/md17120679.

Erian, A.M., Freitag, P., Gibisch, M., Pflügl, S., 2020. High rate 2,3-butanediol production with *Vibrio natriegens*. Bioresour. Technol. Reports 10. https://doi.org/10.1016/j.biteb.2020.100408.

Failmezger, J., Scholz, S., Blombach, B., Siemann-Herzberg, M., 2018. Cell-free protein synthesis from fast-growing *Vibrio natriegens*. Front. Microbiol. 9, 1–10. https://doi.org/10.3389/fmicb.2018.01146.

Gibson, D.G., Young, L., Chuang, R.-Y., Venter, J.C., Hutchison, C.A., Smith, H.O., 2009. Enzymatic assembly of DNA molecules up to several hundred kilobases. Nat. Methods 6, 343–345. https://doi.org/10.1038/nmeth.1318.

Hanahan, D., 1983. Studies on transformation of *Escherichia coli* with plasmids. J. Mol. Biol. 166, 557–580. https://doi.org/10.1016/S0022-2836(83)80284-8.

Heyer, A., Gätgens, C., Hentschel, E., Kalinowski, J., Bott, M., Frunzke, J., 2012. The two-component system ChrSA is crucial for haem tolerance and interferes with HrrSA in haem-dependent gene regulation in *Corynebacterium glutamicum*. Microbiology 158, 3020–3031. https://doi.org/10.1099/mic.0.062638-0.

Hoff, J., Daniel, B., Stukenberg, D., Thuronyi, B.W., Waldminghaus, T., Fritz, G., 2020. *Vibrio natriegens*: an ultrafast-growing marine bacterium as emerging synthetic biology chassis. Environ. Microbiol. 22, 4394–4408. https://doi.org/10.1111/1462-2920.15128.

Hoffart, E., Grenz, S., Lange, J., Nitschel, R., Müller, F., Schwentner, A., Feith, A., Lenfers-Lücker, M., Takors, R., Blombach, B., 2017. High substrate uptake rates empower *Vibrio natriegens* as production host for industrial biotechnology. Appl. Environ. Microbiol. 83 https://doi.org/10.1128/AEM.01614-17 e01614–e01617.

Lee, H.H., Ostrov, N., Wong, B.G., Gold, M.A., Khalil, A.S., Church, G.M., 2019. Functional genomics of the rapidly replicating bacterium *Vibrio natriegens* by CRISPRi. Nat. Microbiol. 4, 1105–1113. https://doi.org/10.1038/s41564-019-0423-8.

Lentini, R., Forlin, M., Martini, L., Del Bianco, C., Spencer, A.C., Torino, D., Mansy, S.S., 2013. Fluorescent proteins and in vitro genetic organization for cell-free synthetic biology. ACS Synth. Biol. 2, 482–489. https://doi.org/10.1021/sb400003y.

Lin, J.L., Wagner, J.M., Alper, H.S., 2017. Enabling tools for high-throughput detection of metabolites: metabolic engineering and directed evolution applications. Biotechnol. Adv. 35, 950–970. https://doi.org/10.1016/j.biotechadv.2017.07.005.

Long, C.P., Gonzalez, J.E., Cipolla, R.M., Antoniewicz, M.R., 2017. Metabolism of the fast-growing bacterium *Vibrio natriegens* elucidated by13C metabolic flux analysis. Metab. Eng. 44, 191–197. https://doi.org/10.1016/j.ymben.2017.10.008.

Mahr, R., Frunzke, J., 2016. Transcription factor-based biosensors in biotechnology: current state and future prospects. Appl. Microbiol. Biotechnol. 100, 79–90. https://doi.org/10.1007/s00253-015-7090-3.

Mahr, R., Gätgens, C., Gätgens, J., Polen, T., Kalinowski, J., Frunzke, J., 2015. Biosensor-driven adaptive laboratory evolution of L-valine production in *Corynebacterium glutamicum*. Metab. Eng. 32, 184–194. https://doi.org/10.1016/j.ymben.2015.09.017.

Mustafi, N., Grünberger, A., Kohlheyer, D., Bott, M., Frunzke, J., 2012. The development and application of a single-cell biosensor for the detection of L-methionine and branched-chain amino acids. Metab. Eng. 14, 449–457. https://doi.org/10.1016/j.ymben.2012.02.002.

Mustafi, N., Grünberger, A., Mahr, R., Helfrich, S., Nöh, K., Blombach, B., Kohlheyer, D., Frunzke, J., 2014. Application of a genetically encoded biosensor for live cell imaging of L-valine production in pyruvate dehydrogenase complex-deficient *Corynebacterium glutamicum* strains. PLoS One 9, e85731. https://doi.org/10.1371/journal.pone.0085731.

Mutalik, V.K., Guimaraes, J.C., Cambray, G., Mai, Q.-A., Christoffersen, M.J., Martin, L., Yu, A., Lam, C., Rodriguez, C., Bennett, G., 2013. Quantitative estimation of activity and quality for collections of functional genetic elements. Nat. Methods 10, 347–353.

Payne, W.J., 1958. Studies on bacterial utilization of uronic acids. III. Induction of oxidative enzymes in a marine isolate. J. Bacteriol. 76, 301–307.

Payne, W.J., Eagon, R.G., Williams, A.K., 1961. Some observations on the physiology of *Psuedomonas natriegens* nov. Spec. Antonie Van Leeuwenhoek 27, 121–128.

Pfeifer-Sancar, K., Mentz, A., Rückert, C., Kalinowski, J., 2013. Comprehensive analysis of the *Corynebacterium glutamicum* transcriptome using an improved RNAseq technique. BMC Genom. 14, 1–23. https://doi.org/10.1186/1471-2164-14-888.

Pfeifer, E., Michniewski, S., Gätgens, C., Münch, E., Müller, F., Polen, T., Millard, A., Blombach, B., Frunzke, J., 2019. Generation of a prophage-free variant of the fast-growing bacterium *Vibrio natriegens*. Appl. Environ. Microbiol. 85 https://doi.org/10.1128/aem.00853-19 e00853-19.

R Core Team, 2020. R: A Language and Environment for Statistical Computing. R Found. Stat. Comput., Vienna, Austria. https://www.R-project.org/.

Raman, S., Rogers, J.K., Taylor, N.D., Church, G.M., 2014. Evolution-guided optimization of biosynthetic pathways. Proc. Natl. Acad. Sci. Unit. States Am. 111, 17803–17808. https://doi.org/10.1073/PNAS.1409523111.

Ritz, C., Baty, F., Streibig, J.C., Gerhard, D., 2015. Dose-response analysis using R. PLoS One 10, e0146021.

Sambrook, J., MacCallum, P., Russell, D.W., 2001. Molecular Cloning: a Laboratory Manual. Cold Spring Harbor Laboratory, Cold Spring Harbor, NY.

Schendzielorz, G., Dippong, M., Grünberger, A., Kohlheyer, D., Yoshida, A., Binder, S., Nishiyama, C., Nishiyama, M., Bott, M., Eggeling, L., 2014. Taking control over control: use of product sensing in single cells to remove flux control at key enzymes in biosynthesis pathways. ACS Synth. Biol. 3, 21–29. https://doi.org/10.1021/sb400059y.

Schwentner, A., Feith, A., Münch, E., Stiefelmaier, J., Lauer, I., Favilli, L., Massner, C., Öhrlein, J., Grund, B., Hüser, A., Takors, R., Blombach, B., 2019. Modular systems metabolic engineering enables balancing of relevant pathways for l-histidine production with *Corynebacterium glutamicum*. Biotechnol. Biofuels 12, 1–21. https://doi.org/10.1186/s13068-019-1410-2.

Stukenberg, D., Hensel, T., Hoff, J., Daniel, B., Inckemann, R., Tedeschi, J.N., Nousch, F., Fritz, G., 2021. The marburg collection: a golden gate DNA assembly framework for synthetic biology applications in *Vibrio natriegens*, 2021.03 bioRxiv 26, 437105.

Thiele, I., Gutschmann, B., Aulich, L., Girard, M., Neubauer, P., Riedel, S.L., 2021. High-cell-density fed-batch cultivations of *Vibrio natriegens*. Biotechnol. Lett. https://doi.org/10.1007/s10529-021-03147-5.

Thoma, F., Blombach, B., 2021. Metabolic engineering of *Vibrio natriegens*. Essays Biochem. 14048, 1–12. https://doi.org/10.1042/ebc20200135.

Thompson, M.G., Blake-Hedges, J.M., Cruz-Morales, P., Barajas, J.F., Curran, S.C., Eiben, C.B., Harris, N.C., Benites, V.T., Gin, J.W., Sharpless, W.A., Twigg, F.F., Skyrud, W., Krishna, R.N., Pereira, J.H., Baidoo, E.E.K., Petzold, C.J., Adams, P.D., Arkin, A.P., Deutschbauer, A.M., Keasling, J.D., 2019. Massively parallel fitness profiling reveals multiple novel enzymes in *Pseudomonas putida* lysine metabolism. mBio 10. https://doi.org/10.1128/mBio.02577-18 e02577-18.

Tschirhart, T., Shukla, V., Kelly, E.E., Schultzhaus, Z., Newringeisen, E., Erickson, J.S., Wang, Z., Garcia, W., Curl, E., Egbert, R.G., Yeung, E., Vora, G.J., 2019. Synthetic biology tools for the fast-growing marine bacterium *Vibrio natriegens*. ACS Synth. Biol. 8, 2069–2079. https://doi.org/10.1021/acssynbio.9b00176.

Wang, Z., Tschirhart, T., Schultzhaus, Z., Kelly, E.E., Chen, A., Oh, E., Nag, O., Glaser, E. R., Kim, E., Lloyd, P.F., Charles, P.T., Li, W., Leary, D., Compton, J., Phillips, D.A., Dhinojwala, A., Payne, G.F., Vora, G.J., 2020. Melanin produced by the fast-growing marine bacterium *Vibrio natriegens* through heterologous biosynthesis: characterization and application. Appl. Environ. Microbiol. 86 https://doi.org/10.1128/AEM.02749-19 e02749-19.

Weinstock, M.T., Hesek, E.D., Wilson, C.M., Gibson, D.G., 2016. *Vibrio natriegens* as a fast-growing host for molecular biology. Nat. Methods 13, 849–851. https://doi.org/10.1038/nmeth.3970.

Wickham, H., Averick, M., Bryan, J., Chang, W., McGowan, L.D., François, R., Grolemund, G., Hayes, A., Henry, L., Hester, J., et al., 2019. Welcome to the tidyverse. J. Open Source Softw. 4, 1686.

Wiegand, D.J., Lee, H.H., Ostrov, N., Church, G.M., 2018. Establishing a cell-free *Vibrio natriegens* expression system. ACS Synth. Biol. 7, 2475–2479. https://doi.org/10.1021/acssynbio.8b00222.

Wu, F., Chen, W., Peng, Y., Tu, R., Lin, Y., Xing, J., Wang, Q., 2020. Design and reconstruction of regulatory parts for fast-frowing *Vibrio natriegens* synthetic biology. ACS Synth. Biol. 9, 2399–2409. https://doi.org/10.1021/acssynbio.0c00158.

3.4. Automated Rational Strain Construction Based on High-Throughput Conjugation

Tenhaef, N.*, Stella, R.*, Frunzke, J., & Noack, S.

Published in *ACS Synthetic Biology*, 2021

**Authors contributed equally*

Contributor role	Role definition
Conceptualization	RS 30%, NT 30%, JF 15%, SN 25%
Formal analysis	RS 50%, NT 50%
Investigation/Experiments	RS 60%, NT 40%
Methodology	RS 40%, NT 60%
Project administration	RS 30%, NT 30%, JF 15%, SN 25%
Software	RS 50%, NT 50%
Supervision	RS 20%, NT 20%, JF 25%, SN 35%
Visualization	RS 50%, NT 50%
Writing – original draft	RS 50%, NT 50%
Writing – review & editing	RS 20%, NT 30%, JF 20%, SN 30%

Overall contribution RS: 40%

All experiments and data analyses were performed by RS and TN, in close collaboration. RS brought the molecular biology expertise, and TN the robotics expertise, to develop all automated workflows. All figure were created by RS and TN, RS created the major part of figure 2, 3 and 4, TN created the major part of figure 1, 5 and 7. RS and TN wrote the manuscript.

ACS SyntheticBiology

pubs.acs.org/synthbio Research Article

Automated Rational Strain Construction Based on High-Throughput Conjugation

Niklas Tenhaef,[¶] Robert Stella,[¶] Julia Frunzke, and Stephan Noack*

Cite This: *ACS Synth. Biol.* 2021, 10, 589−599 Read Online

ACCESS | Metrics & More | Article Recommendations | Supporting Information

ABSTRACT: Molecular cloning is the core of synthetic biology, as it comprises the assembly of DNA and its expression in target hosts. At present, however, cloning is most often a manual, time-consuming, and repetitive process that highly benefits from automation. The automation of a complete rational cloning procedure, *i.e.*, from DNA creation to expression in the target host, involves the integration of different operations and machines. Examples of such workflows are sparse, especially when the design is rational (*i.e.*, the DNA sequence design is fixed and not based on randomized libraries) and the target host is less genetically tractable (*e.g.*, not sensitive to heat-shock transformation). In this study, an automated workflow for the rational construction of plasmids and their subsequent conjugative transfer into the biotechnological platform organism *Corynebacterium glutamicum* is presented. The whole workflow is accompanied by a custom-made software tool. As an application example, a rationally designed library of transcription factor-biosensors based on the regulator Lrp was constructed and characterized. A sensor with an improved dynamic range was obtained, and insights from the screening provided evidence for a dual regulator function of *C. glutamicum* Lrp.

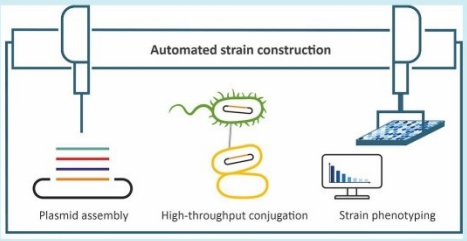

KEYWORDS: *laboratory automation, strain construction, molecular cloning, transcription factor-based biosensors, DNA assembly, high-throughput conjugation*

INTRODUCTION

Microbial production of bulk and fine chemicals is a vital part of a more sustainable global economy. To foster this development, both the fundamental understanding of microbial life and its engineering to fulfill society's needs must be advanced. In recent years, the employment of a design-build-test-learn (DBTL) cycle has been proposed as a tool to achieve this.[1] Molecular cloning plays an important role in this cycle since it allows for the generation of new genotypes with different properties to explore.

Multiple software tools have been developed to aid the *in silico* cloning of genotypes, in numbers that easily exceed the amount that could be manually made in the laboratory.[2] It is now feasible to design many hundreds of genotypes in a short amount of time. For example, a production pathway of five genes each with three different ribosomal binding sites (RBSs) already results in $3^5 = 243$ variants. However, the relatively easy design of such a project now shifts the bottleneck to the actual *in vitro* creation of these sequences and their expression in the desired industrial host.[3]

This problem can be addressed by using one-pot assembly and screening approaches, *i.e.*, to obtain many but not necessarily all variants and using a screening assay to select for the best performers.[4] However, these approaches have one drawback: Knowledge is only obtained from the few variants that were successfully constructed and isolated from the one-pot reaction. More difficult to construct variants are less abundant in such a reaction and are therefore less likely to be screened for their properties. For many fundamental biological questions, this is not an ideal solution. Here, rational strain construction with complete traceability of all varieties within all steps of the workflow is necessary, as is realized by classical molecular cloning.

At present, however, molecular cloning is most often a manual, time-consuming, and repetitive process that would highly benefit from automation.[5] The automation of a rational cloning workflow has multiple benefits. The hands-on time the experimenter spends on strain construction can be drastically reduced. Together with the higher throughput that can be realized, this largely increases the quantity of constructs that can be produced in time. Furthermore, automation introduces standardization of the process by removing random variations from the process. The processes can also be more easily

Received: November 26, 2020
Published: February 16, 2021

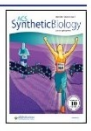

https://dx.doi.org/10.1021/acssynbio.0c00599
ACS Synth. Biol. 2021, 10, 589−599

ACS Synthetic Biology pubs.acs.org/synthbio Research Article

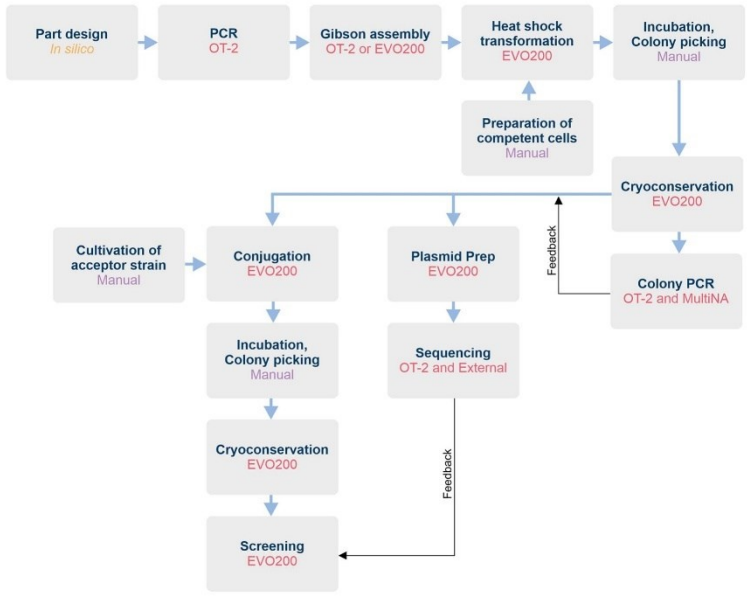

Figure 1. Overview of the automated genetic engineering workflow. Each box describes one unit operation and informs one about the device or entity used for performing this operation. OT-2: Opentrons OT-2 liquid handling system. EVO200: Tecan EVO200 liquid handling system. MultiNA: Shimadzu MCE-202 MultiNA chip electrophoresis system.

monitored and analyzed, making it easier to find room for improvement. Thus, automation can increase both the quantity and quality of cloning workflows.

In recent years, microfluidics has been used to automate cloning processes.[6,7] Here, tailor-made microfluidic chips are used to provide liquid separation for and liquid transfer in between the single unit operations. While this technique comes with the advantage of combining many unit operations in one device and the ability to scale up to a high number of experiments per chip, a highly specialized infrastructure and personnel are needed to fabricate the chips and to conduct the experiments.

A more modular and accessible solution is the employment of standard liquid handling systems and, if needed, auxiliary devices. Such a system can be rather complex and capable of performing a high number of experiments with varying tasks,[8−11] but also more cost-efficient solutions are available.[12] A recently presented strategy uses the natural transformation capacity of specific bacteria, resulting in a highly efficient and easy to use cloning method.[13] However, this approach is limited to the few organisms that actively take up exogenous DNA.

Most automated cloning workflows published so far focused on working with *Escherichia coli*.[14] *E. coli* is a well-established host for molecular cloning that is very genetically tractable. Many genetic tools have been developed and optimized for use in *E. coli*, and comprehensive omics data is available. However, *E. coli* is not always an ideal host for industrial processes due to its low stress tolerance and risk of phage infection.[15] Therefore, it would be beneficial to extend automation platforms to include the engineering of other microorganisms that are less genetically tractable.

Corynebacterium glutamicum is a widely used industrial bacterium[16] that is more difficult to engineer than *E. coli* due to its resistance to automation friendly transformation processes such as heat-shock transformation. While some steps have been taken in this direction,[17] they usually fall short in automating the process of transforming the actual target organism, most often because electroporation, which is the method of choice for such organisms, is not easily accessible for automation.

This study presents a complete workflow for automated rational strain construction of heat-shock resistant microorganisms. All work was carried out using standard liquid handling systems. PCR and Gibson assembly were used to construct a library of 96 plasmids. Automated protocols were developed for heat-shock transformation of *E. coli* as a shuttle system. Colony PCR and sequencing were used as quality controls. For the final step of transforming *C. glutamicum*, a novel high-throughput conjugation workflow was developed. Conjugation is a well-described and highly relevant technique for the transformation of bacteria.[18] High efficiency can be obtained, but the method is usually laborious because of the use of agar plates and filter papers. For this study, the operation was simplified and made accessible to automation by using centrifugation. The whole workflow was accompanied by

https://dx.doi.org/10.1021/acssynbio.0c00599
ACS Synth. Biol. 2021, 10, 589−599

a custom-made software tool to keep track of all constructs and their status within the process.

As an application example, the assembly and expression of different Lrp biosensor variants in *C. glutamicum* are shown. The Lrp biosensor was previously developed for the detection of L-methionine and branched-chain amino acids in *C. glutamicum*.[19] This sensor couples intracellular L-methionine and branched-chain amino acid concentrations to the expression of *eyfp*, encoding a fluorescent reporter protein. Increased intracellular concentration results in a higher fluorescent signal. In general, biosensors are relatively modular in their design; their characteristics can be changed by modifying, for example, ribosomal binding sites and promoter length.[20,21] Furthermore, by design, they provide a direct and easily measurable relationship between genotype and phenotype; *i.e.*, a change in Lrp sensor design will likely result in a different, measurable fluorescence output. Therefore, the rational design of different Lrp biosensors was chosen as an application example demonstrating the strength of our cloning automation approach.

RESULTS AND DISCUSSION

Workflow for Automated Genetic Engineering. The automated cloning workflow developed in this study (Figure 1) can be divided into two stages: plasmid assembly and amplification in *E. coli* and transfer of the plasmid to the target organism, in this case *C. glutamicum*. Plasmids were constructed by designing the parts *in silico*, building fragments by PCR, and integrating into a backbone vector by Gibson assembly. Gibson assembly was chosen because it allows for the scarless assembly of plasmids.[22] The subsequent transformation into *E. coli* was done by heat shock. The resulting clones were stored by cryoconservation, and a first quality control step was done by colony PCR. This method was chosen because of its cost efficiency and short run times. The results from this colony PCR influenced the next steps: Only *E. coli* clones with a positive colony PCR result, *i.e.*, with a resulting DNA fragment of the expected size, indicating the successful assembly of a fragment into the backbone, were considered for automated plasmid preparation and, in parallel, conjugation into *C. glutamicum*. Purified plasmids were used for sequencing as a final quality control. Afterward, the automatically constructed strains were screened to characterize the altered properties. Most importantly, each unit operation was designed to be self-contained, so it can be used when detached from the workflow.

Automated unit operations were carried out or supported by a low-cost liquid handling device, the Opentrons OT-2, and a more sophisticated liquid handling platform based on a Tecan EVO 200 described earlier.[23,24] Both systems are fundamentally different: The OT-2 uses a setup of two air displacement pipettes working with disposable tips. Available pipettes have a volume range similar to a manual pipet, and the operator has to select the ones suitable for the experiment. It does not have a robotic manipulator; therefore, it is not able to change the location of the plates, *e.g.*, to place a plate on a heating block or in a centrifuge. The deck can hold up to nine microtiter plates. The model used for this study was not equipped with an option to cool labware. A custom-made cooling rack that could be filled with ice and fitting adapters was designed and 3D printed (see the Supporting Information) to cool down reagents when necessary (*e.g.*, for Gibson assembly). The EVO 200, in the configuration used in this study, has a liquid-based liquid handling system, spanning a volume range of 3 to 990 μL. It is equipped with a centrifuge, a cooling carrier, and a heater/shaker unit, both accessible for the integrated robotic manipulator arm. The deck can hold 15 or more microtiter plates, depending on the carriers used. For spotting of bacterial cultures onto round 100 mm Petri dishes, a custom-made adapter was designed and 3D printed (see the Supporting Information).

The decision to use two different liquid handling systems was motivated by the need to use lab equipment most efficiently: Whenever possible, the OT-2 was used to carry out a unit operation. This saved time compared to the more expensive EVO 200, which thus could be used for more demanding experiments. The unit operation "colony picking" was done manually in this study. It can be automated by dedicated devices, but none of those were available at the time.

Rational Combinatorial Design of Transcription Factor-Based Biosensors. To demonstrate the applicability of our workflow, different versions of the Lrp biosensor were designed, constructed, and expressed in *C. glutamicum*. The Lrp biosensor couples intracellular L-methionine, L-leucine, L-isoleucine, and L-valine concentrations to expression of the fluorescent reporter protein eYFP. To construct different versions of the Lrp biosensor, different parts of the sensor were modified. The Lrp biosensor consists of the *lrp* gene, which encodes the Lrp transcription factor, the divergently expressed *eyfp* gene, which encodes the fluorescent reporter, and the intergenic region, which contains the *lrp* promoter and the *brnF* promoter upstream of *eyfp* and the *eyfp* RBS[19] (Figure 2). Different variants were designed for the *lrp* start codon and RBS, for the *brnF* promoter, and for the *eyfp* RBS.

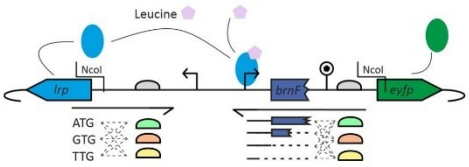

Figure 2. Graphical overview of the different Lrp biosensor variants that were designed for the construction and expression in *C. glutamicum*. On the left side, 9 different primers were designed, containing combinations of different *lrp* start codons and *lrp* RBSs. On the right side, 12 different primers were designed, containing combinations of different *brnF* promoter sequences and *eyfp* RBSs.

For the *lrp* start codon, three variants were chosen: the native start codon ATG, which should result in the highest expression, the start codon GTG, which should result in lower expression, and TGT, which should result in very low or no expression. Each of these start codon variants were combined with three different *lrp* RBSs, again ranging from the highest expression to the lowest expression: GCTAAAATGG (strongest), GCTATTGTGC (native, less strong), and CAATCCTACC (weakest). The combination of three start codons and three RBSs at the *lrp* side resulted in 3 × 3 = 9 different primers.

The *eyfp* gene was expressed under control of the *brnF* promoter, which contains binding sites for the Lrp protein.[25] Thus, when the promoter sequence was shortened or elongated, the binding site(s) can be included or removed. Because *brnF* is transcribed as a leaderless transcript and the

https://dx.doi.org/10.1021/acssynbio.0c00599
ACS Synth. Biol. 2021, 10, 589−599

first part of *brnF* probably has a regulatory function,[26] the *eyfp* promoter of the standard Lrp sensor includes the first 30 bp of *brnF*. In this study, four different variants were designed, starting at +30 (standard Lrp biosensor promoter) and shortened versions in steps of 15, *i.e.*, +15, 0, and −15. For the RBS of *eyfp*, three variants were chosen: AAAAGGAGAT (strongest), AGAAGGAGAT (native, less strong), and ATCCGACCAT (weakest). The combination of four promoter lengths and three RBSs at the *eyfp* side resulted in 4 × 3 = 12 different primers. This design strategy would include 9 × 12 = 108 different variants of the Lrp biosensor in total.

Each variant can be constructed by a single PCR reaction, and all PCR reactions can use the same PCR template, plasmid pJC1-*lrp-brnF′-eyfp*. To assemble the biosensor plasmids, each PCR reaction is followed by a two-fragment Gibson assembly, in which the PCR product is assembled into a pEC-Tmob18-*lrp-eyfp* backbone; all PCR products were designed so they could be assembled into the same backbone.

DNA Assembly and Transformation of *E. coli*. Before construction of the Lrp biosensor variants, a backbone plasmid was constructed by inserting *lrp* and *eyfp* into the mobilizable pEC-Tmob18 backbone. A short spacer that contained two NcoI restriction sites was inserted between the two genes. This sequence allowed for plasmid linearization and the insertion of different versions of the sequence variants containing different *lrp* start codons, *lrp* RBSs, *brnF* promoter lengths, and *eyfp* RBSs in the next step.

Out of the 108 variants, 96 were selected as an application example for the automated cloning workflow because most automation devices are designed for 96-well multititer plates. Variant constructions by PCR, Gibson assembly, and *E. coli* heat-shock transformation were performed directly after each other. The Opentrons OT-2 enabled automated pipetting of 96 PCR reactions in 85 min, after which the plate was manually transferred to a thermocycler. After thermocycling, the OT-2 was used to mix the 96 Gibson assembly reactions, which took 50 min. Incubation was done by manually transferring the plate to a thermocycler. Appropriate cooling of the Gibson master mix before the 50 °C incubation step turned out to be crucial; otherwise, no *E. coli* transformants were obtained. In our workflow, cooling was achieved by placing all labware in small 3D-printed boxes filled with ice. *E. coli* heat-shock transformation was performed on a TECAN EVO200 liquid handling robot, which enabled a completely hands-off process, starting with the Gibson assembly mixtures and competent cells and ending with the cells spotted on agar plates ready for overnight incubation. This process took 170 min. In total, PCR, Gibson assembly, and transformation of 96 constructs were achieved in 8 h with only 40 min of hands-on time.

A suitable way to implement the heat-shock step was to preheat a V-bottom 96-well plate on a heating device, transfer the 8 cell-plasmid mixtures one at a time from the cooling carrier to the heated plate, incubate them for 30 s, and transfer them back to the cooling carrier. While transferring a complete plate from the cooling carrier to the heating device is faster, this gives less reliable heat transfer results. The cell suspension was concentrated by centrifugation, resuspended in LB medium, and spotted on agar plates, *i.e.*, by pipetting 6 spots of 5 μL on the same row of a single agar plate.

Additionally, parameters for heat-shock transformation were tested using *E. coli* competent cells (NEB 5-alpha Competent *E. coli*) using a pUC19 standard vector. Heat-shock temperatures (37, 42, and 47 °C) and heat-shock durations (0 to 30 s, in steps of 5 s) were tested. Surprisingly, little difference in colony forming units was observed between the conditions with successful transformations for each condition. Eventually, conditions most similar to standard manual routines were chosen.

Transformed *E. coli* clones were counted after ∼16 h of plate incubation at 37 °C. A total of 273 clones were obtained with a maximum of 12 clones per construct. On average, 4.6 colonies were yielded per construct. The number of unique constructs for which a single clone was obtained was 60 out of 96 (*i.e.*, 36 constructs yielded no colony). Colony PCR was done on at most 4 clones of each construct to test if the PCR product was correctly inserted into the pEC-Tmob18-*lrp-eyfp* backbone in the Gibson assembly step. A total of 184 clones were tested, and results were analyzed on a MultiNA, which allowed for easy and high-throughput analysis of PCR band sizes for all constructs. From 184 clones, 172 had a PCR band with a length within 10 base pairs from the target length. If only unique constructs are considered, 55 out of 60 constructs were correct. To validate the results of the MultiNA, a classical agarose gel electrophoresis was done for 16 colony-PCR products and the result was compared to the MultiNA results (Figure 3). The obtained bands are highly comparable between the two methods, validating the use of the MultiNA as a replacement for classical gel electrophoresis.

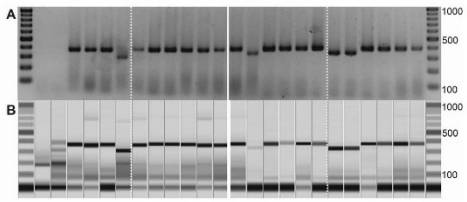

Figure 3. Comparison of standard gel electrophoresis and MultiNA capillary gel electrophoresis for colony PCR analysis. (A) Annotated gel image. GeneRuler 100 bp Plus DNA-Ladder was used as the marker. (B) Virtual gel image created from gel electrophoresis data. Linear DNA fragment sizes are shown on the right size in base pairs (bps). NEB 1 kb Plus DNA Ladder was used as the marker.

Transformation of *C. glutamicum* and Strain Validation. The automation of the transfer of plasmid into *C. glutamicum* provided a challenge because no chemical protocols (*e.g.*, heat shock) have been shown to work, and available high-throughput electroporation devices are not automation friendly. Conjugation is an alternative plasmid transfer method in which a donor cell (*e.g.*, *E. coli*) transfers a plasmid into an acceptor cell (*e.g.*, *C. glutamicum*). For conjugation, cells need to be in close contact to each other, which is typically achieved by mixing the donor and acceptor cultures and spreading the mixture on an agar plate. This is usually on top of a filter to allow for easy removal of the cells. Automated conjugation was implemented on the Tecan EVO200 by mixing the donor and acceptor cultures and performing a centrifugation step to avoid the plating step but keeping the cultures in close contact.

Initially, three different types of plasmid were considered for conjugation, pEC-Tmob18, pEC-Cmob18, and pEC-

https://dx.doi.org/10.1021/acssynbio.0c00599
ACS Synth. Biol. 2021, 10, 589−599

Smob18,[27,28] harboring a resistance marker for tetracycline, chloramphenicol, and streptomycin, respectively. Consistent successful conjugation results were only obtained for pEC-Tmob18, which was therefore used for all experiments. Two parameters were investigated to optimize the conjugation protocol. First, the effect of cell concentration was tested by combining different *C. glutamicum* starting culture optical densities (OD_{600}'s) with different *E. coli* starting culture OD_{600}'s (Figure 4). The effect of the *C. glutamicum* starting culture OD_{600} was much larger than that of the *E. coli* starting culture OD_{600}, with higher densities resulting in more clones. Furthermore, when using overnight cultures to conjugate the plasmids of 96 *E. coli* strains harboring different Lrp biosensor plasmids, it was found that older overnight cultures (more than 20 h) performed worse (47 clones, 38 unique) than fresh, high density cultures (233 clones, 84 unique). This effect was likely due to the starvation effects of the prolonged stationary phase. Finally, the effect of *C. glutamicum* growth media was investigated. The change to BHI media instead of LB media for *C. glutamicum* preculture growth gave the best results (995 clones, 96 unique, at least 4 clones per conjugation reaction).

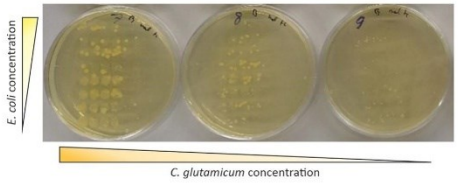

Figure 4. Effect of *E. coli* (donor) and *C. glutamicum* (acceptor) starting culture optical density on the conjugation results. Each row on a single BHI agar plate represents multiple cultures from the same conditions. Fewer clones are visible with decreasing *C. glutamicum* starting culture optical densities, while the effect of *E. coli* optical density does not have a large effect.

Using the Tecan EVO200 platform, 96 conjugation reactions could be performed in 70 min with less than 10 min hands-on time. To transfer the biosensor variants to *C. glutamicum*, 96 *E. coli* cultures harboring 55 unique constructs were used for the conjugation protocol. At least 4 *C. glutamicum* clones per construct were obtained (995 clones in total). However, not all clones could grow in liquid cultures after being picked from the agar plate, an effect that is probably backbone dependent. Picking 4 clones per construct into liquid BHI media resulted in 64 strains with one or more clones that could grow in liquid media, including 45 unique strains. Interestingly, at least some of the clones that were not able to grow in liquid BHI media did contain a plasmid, as confirmed with colony PCR. The reason for this unexpected growth behavior is not clear and should be investigated in the future.

Plasmid Preparation and Validation. After conjugation, 45 unique constructs were transferred to *C. glutamicum*. To validate the sequence of these sensor variants, the relevant plasmids were sequenced (externally) by Sanger sequencing. Sanger sequencing required purified plasmids. Using the TACO software (as described below), the location of the *E. coli* clones harboring the plasmids that were successfully transferred to *C. glutamicum* was retrieved, and these clones were picked for overnight growth and plasmid purification. When the Tecan platform was used, 45 plasmid purifications could be performed in 105 min. The measurement of 8 samples gave concentrations between 25 and 50 ng μL^{-1} (elution volume 100 μL), which is on par with plasmid amounts obtained with manual miniprep kits.

Sanger sequencing revealed that 36 out of the 45 plasmids had the expected sequence. From the 9 plasmids without a correct sequence, 4 were constructed using the same primer, and all missed a large part of the inset sequence. This could indicate a problem with this primer, but also correct constructs were obtained using the same primer. For the other mutations, no correlation was found. However, a result of ~80% of correct sequences is not below the results obtained using manual cloning procedures.

TACO. All molecular cloning workflows require a certain effort in the documentation of design ideas, results, and storage locations of DNA fragments, plasmids, clones, *etc.* With increased throughput, this task becomes increasingly difficult and cannot be handled anymore by standard techniques such as manually maintained (electronic) lab notebooks. To solve this problem, a Tool for Automated Cloning (TACO) was developed. Using Python 3.8 and building on top of the widely used libraries Pandas and NumPy, TACO provides the user with templates to keep track of different constructs, the

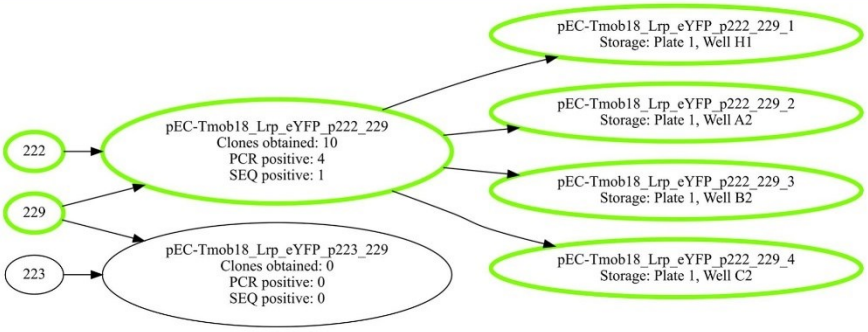

Figure 5. Part of the DAG for the conjugation stage of the application example. Initial fragments, constructs, conjugation events, and stored clones form nodes. Edges visualize their relationship. The user can choose to highlight successfully stored clones and their linage, as done here.

https://dx.doi.org/10.1021/acssynbio.0c00599
ACS Synth. Biol. 2021, 10, 589−599

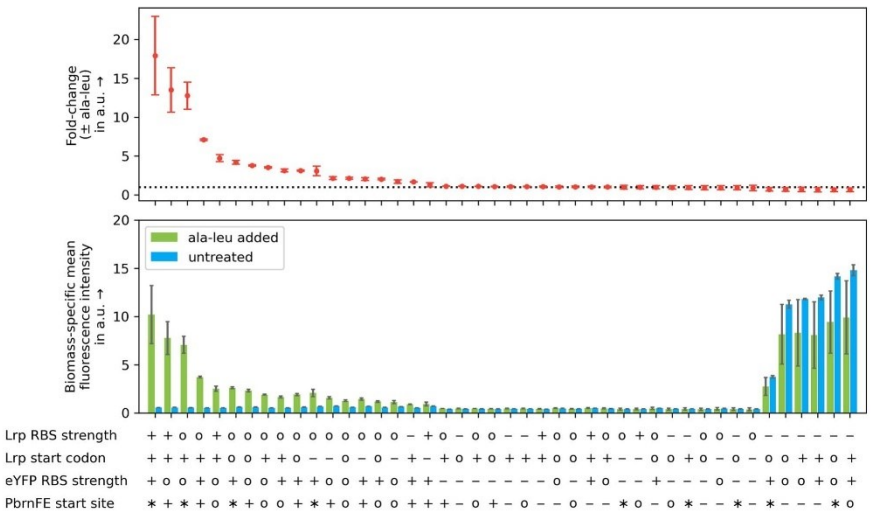

Figure 6. Screening results from the application example. Fold-change of each strain is calculated by dividing the biomass-specific fluorescence after 20 h of growth with the inducer (3 mM alanine−leucine dipeptide) by the biomass-specific fluorescence after 20 h of growth without the inducer. Dashed line indicates a fold-change of one. Higher values indicate a higher dynamic range of the sensor. Symbols used for strain characteristics: *lrp* RBS strength: −, weak; ○, average (native); +, strong; *lrp* start codon: −, weak; ○, average; +, strong (native); *eyfp* RBS strength: −, weak; ○, average (native); +, strong; *brnF* promoter start site: −, −15; ○, 0; +, +15; *, +30. The mean and standard deviation of three biological replicates are shown.

number of clones resulting from transformation experiments, and plate storage locations. All templates are provided as Microsoft Excel files for easy access and transfer to lab locations (*e.g.*, by printing). Submodules allow for the expansion of TACO. One submodule was developed to analyze data from the capillary gel electrophoresis device MultiNA, used for colony PCR in this workflow. Another submodule was made to assist with the conjugation part of the workflow. To provide visual aids for the user, Graphviz was used to create directed acyclic graphs (DAGs) from both plasmid assembly and conjugation stages of the workflow. An illustration of such graphs can be found in Figure 5.

Screening of Novel Biosensor Strains. After the complete cloning workflow, 36 *C. glutamicum* strains with different versions of the Lrp sensor were obtained. During the initial testing experiments, 8 more *C. glutamicum* strains with different, validated Lrp sensors were obtained, bringing the total to 44. The sensor response was measured by growing the strains in microtiter plates in the presence or absence of 3 mM inducer (alanine−leucine dipeptide). The inoculation of the main cultures and the automated measurement were carried out on the Tecan EVO200 platform. Fluorescence output was measured, and fold-change was calculated (Figure 6). The highest fold-change was observed for the sensors with the strongest *lrp* RBS and start codon, *eyfp* RBS, and the longest promoter containing the first 30 bp of *brnF*. In general, the fold-change was the highest when using a strong *lrp* RBS and start codon in combination with a strong *eyfp* RBS. When the strength of either of the four elements was lowered, a decrease in fold-change could be observed. In contrast, when the *lrp* RBS strength or the *eyfp* RBS strength was low, the fold-change was close to 1, meaning that these constructs hardly showed any sensor functionality. Six sensors with the lowest fold-change (below 1) showed a high fluorescence output both in the presence and in the absence of the inducer. This result was unexpected. These sensors had a low *lrp* RBS strength in combination with a strong or medium *eyfp* RBS strength. Thus, the results indicate that a low expression of *lrp* relieved the Lrp-based regulation of *eyfp*, resulting in the expression in both the presence and absence of the inducer. This observation suggests that Lrp might function as both an activator and a repressor. Such a dual-regulatory function is known for the transcription factor AraC.[29] However, previous results showed that the deletion of *lrp* reduced the export of L-isoleucine,[30] so the exact regulatory mechanism should be investigated further.

Considerations for the Automated Cloning Workflow. The automated cloning workflow presented in this study still features some manual parts.

1. The preparation of competent *E. coli* cells is necessary for heat-shock transformation. It has been shown that this procedure can be automated.[31] For the study presented here, this approach was not worthwhile since *E. coli* is only used as a shuttle system to carry the plasmid and perform conjugation into *C. glutamicum*. This task can be fulfilled by using a single *E. coli* strain, which can be manually prepared in bulk and stored by cryoconservation.
2. The targeted *C. glutamicum* culture was prepared manually in this study. The reasoning here is the same as before. Since only one strain is used, it is actually more efficient to use a simple shake flask culture than setting up a robot for automated cultivation. Of course, this changes when multiple target strains are to be transformed, which conjugation easily allows, or when

https://dx.doi.org/10.1021/acssynbio.0c00599
ACS Synth. Biol. 2021, 10, 589−599

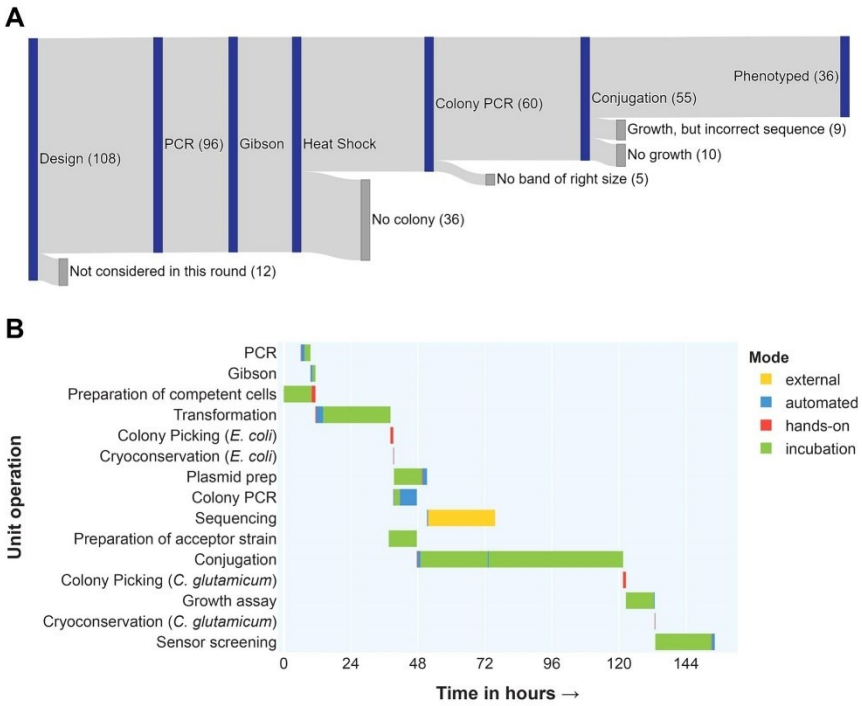

Figure 7. Efficiency of the automated cloning workflow. (A) Number of unique constructs passing each unit operation of the workflow. (B) Gantt chart of all unit operations.

one aims for a completely autonomous platform. Then, an automated cultivation can be realized, *e.g.*, by using microbioreactors or microtiter plate-based cultivation.[23]

3. The task of colony picking is done by hand. As discussed, dedicated devices are available for this operation.[32] They can be easily integrated into the existing workflow, further reducing the manual labor involved in molecular cloning.
4. The transfer of labware between the different devices used is done manually. Although not time-consuming, automated transfer and orchestration of the different unit operations are necessary for a completely autonomous workflow. In this study, this challenge was partly alleviated by the long incubation times, shifting the transfer of labware and start of operations into standard work hours.

Two different liquid handling systems were used for this publication: a low-cost device, the Opentrons OT-2, and a liquid handling platform based on a Tecan EVO200. To make the workflow as accessible as possible, it would be beneficial to only use the OT-2. For all the steps leading up to the conjugation, this can easily be realized by integrating the necessary modules provided by the manufacturer, *i.e.*, the temperature module, magnetic module, and thermocycler. Conjugation is more difficult to realize since it involves multiple steps using centrifugation. This cannot be done using the OT-2, which lacks a robotic manipulator arm, since labware must be moved in and out of a centrifuge. Simple sedimentation of *E. coli* and *C. glutamicum* did not yield any transformants (data not shown), presumably because the distance between donor and receptor organisms remained too large. A semiautomated procedure, where the OT-2 is responsible for liquid handling and the human operator for manual centrifugation, seems reasonable for this unit operation.

In regards to the efficiency of the presented workflow, two domains have to be discussed: the number of constructs successfully passing through each unit operation and the time necessary to perform the operations. Most constructs were lost after the heat-shock operation for the creation of transformed *E. coli* cells (Figure 7A). This could have multiple reasons, leaving room for further investigations: Either the heat-shock operation itself had low efficiency or the steps leading up to this operation did not work properly. Operations and reaction conditions were identical for all constructs except for the PCR reactions, where different primers were used to generate the biosensor variations. Thus, one can assume that this operation is responsible for the loss in constructs. This could possibly have been alleviated by introducing replicates, but since it is usually not possible to deal with all constructs in one pass of this workflow anyway, it would be most efficient to continue the workflow regardless of losses and queue the failed

https://dx.doi.org/10.1021/acssynbio.0c00599
ACS Synth. Biol. 2021, 10, 589−599

candidates for the next pass. This would work especially well when combined with scheduling approaches (see below).

Incubation times took most of the total workflow time (Figure 7B). This if mostly due to the relatively slow growth rate of the target organism, *C. glutamicum*, which is most prevalent in the conjugation step, but also *E. coli* operations are slowed by the necessary incubation times. The switch to an even faster organism as a tool for molecular cloning, *e.g.*, *Vibrio natrigens*,[33] might be an option here, provided that a strain that is able to perform conjugation can be obtained. To increase throughput, especially on a fully autonomous platform, one could employ scheduling to prepare one microtiter plate of constructs after the other and incubate them together. Since the whole workflow is designed for batches of 96 constructs, the development of such a scheduled workflow is straightforward. The Gantt chart also demonstrates the reasoning behind the different feedback levels within the workflow: colony PCR provides a quick first evaluation of the quality of the constructed *E. coli* strains, helping to use strains with a fully assembled plasmid for conjugation. Sequencing provides a detailed genotype but takes longer and is more costly. Therefore, this information is incorporated into the workflow at a later stage.

■ CONCLUSIONS

The presented study shows the development of an automated workflow for high-throughput rational construction of plasmids and their subsequent transfer into an industrial-relevant target organism by conjugation. The workflow is described and characterized in-depth to be used as a basis for further developments. One novel unit operation, the automated conjugation of *E. coli* and *C. glutamicum*, enables high-throughput genetic engineering of this otherwise laborious to engineer microorganism. Most importantly, this process is not specific to one target species. It can rather be used for any microorganism susceptible to horizontal gene transfer *via* conjugation with little to no effort for the preparation of the target strain. Furthermore, recent work has shown the potential of conjugation to genetically engineer a wide range of established and novel hosts.[34] The workflow presented here is accompanied by a custom-made software tool to keep track of the constructed variants and their status. By applying the operations described in this study, an Lrp-biosensor library was constructed and characterized, resulting in the identification of a sensor with an improved dynamic range. Furthermore, the fact that several sensor variants showed output in the absence of effector hints at a reassessment of the function of Lrp as both an inducer and a repressor, thus providing novel fundamental insights. When one builds upon this workflow and fills the remaining gaps, an autonomous biofoundry for engineering of industrial microbial strains is within reach.

■ MATERIAL AND METHODS

Bacterial Strains, Plasmids, Primers, and Growth Media. *E. coli* S17-1[35] was used for plasmid propagation, for storage, and as a donor strain for plasmid conjugation. Cultures were grown in Lysogeny Broth (LB) medium or on LB-agar plates at 37 °C. Supplementation with antibiotics was done, depending on the experiment, with 5 μg mL^{-1} tetracycline (Sigma-Aldrich, USA).

All *C. glutamicum* strains are derived from *C. glutamicum* ATCC 13032[36] and were grown aerobically at 30 °C on Brain Heart infusion (BHI) (Difco Laboratories, Detroit, USA) agar plates (with 1.8% (w v^{-1}) agar). Supplementation with antibiotics was done, depending on the experiment, with 5 μg mL^{-1} tetracycline (Sigma-Aldrich, USA).

Defined CGXII medium[37] contained (per liter of deionized water): 20 g of $(NH_4)_2SO_4$, 1 g of K_2HPO_4, 1 g of KH_2PO_4, 5 g of urea, 42 g of MOPS, 13.25 mg of $CaCl_2{\cdot}2H_2O$, 0.25 g of $MgSO_4{\cdot}7H_2O$, 10 mg of $FeSO_4{\cdot}7H_2O$, 10 mg of $MnSO_4{\cdot}H_2O$, 0.02 mg of $NiCl_2{\cdot}6H_2O$, 0.313 mg of $CuSO_4{\cdot}5H_2O$, 1 mg of $ZnSO_4$ $7H_2O$, 0.2 mg of biotin, 30 mg of 3,4 dihydroxybenzoate (PCA), and 20 g of D-glucose; 5 mg of tetracycline was used for the *C. glutamicum* phenotyping experiments. Supplementation with 3 g L^{-1} alanine−leucine dipeptide (Bachem, Switzerland) was done depending on the experiment.

All constructed plasmids were derived from pEC-T18mob2,[28] an *E. coli*−*C. glutamicum* shuttle vector that contains the *E. coli* oriV, the *C. glutamicum* pGA1 ori, and a tetracyline resistance marker. Plasmid pJC1-*lrp-brnE′-eyfp*[19] was used as template for all Lrp biosensor variant constructions. For initial conjugation testing experiments, plasmids pEC-C18mob2 and pEC-S18mob2 were used.[27] Primers were ordered as custom DNA oligonucleotides from Eurofins Genomics (Ebersberg, Germany). All primers are listed in Table S1.

Robotic Platforms and 3D Printing. In this study, two robotic platforms were used for the automation of genetic engineering workflows. The Opentrons OT-2 (Opentrons Inc., New York, NY, USA) is a benchtop liquid handling device, capable of transferring liquids using electronic pipettes and disposable tips. To keep reagents and plates cooled on the robot's deck, a rack that could be filled with ice and fitting adapters was designed and 3D printed (see Figure S1). Additionally, a BioShake 3000 elm (Quantifoil Instruments GmbH, Jena, Germany) was placed next to the system to provide quick access to shaking and heating capabilities by manually placing a microtiter plate on the device.

For more sophisticated processes, a customized Freedom EVO200 liquid handling system (Tecan, Männedorf, Switzerland) was used. The system provides the following capabilities: liquid handling access to up to 16 plates and/or tube racks, cooling of up to 3 microtiter plates down to 4 °C, heating and shaking (BioShake 3000 elm, Quantifoil Instruments GmbH, Jena, Germany), centrifugation (4-5KRL, Sigma Laborzentrifugen GmbH, Osterode am Harz, Germany or Rotanda 460 Robotic, Andreas Hettich GmbH & Co. KG, Tuttlingen, Germany), and photometric measurements (Infinite M200, Tecan, Männedorf, Switzerland). Additionally, the liquid handling arm has access to a microtiter plate cultivation device (BioLector, m2p-laboratories GmbH, Germany).

3D printing was realized by fused-filament fabrication using an Original Prusa MK3S (Prusa Research a.s., Prague, Czech Republic) with polylactic-acid filament (DAS FILAMENT, Emskirchen, Germany). The design of 3D models was done using SolidWorks 2016 (Dassault Systèmes, Vélizy-Villacoublay, France).

PCR. Automated polymerase chain reaction (PCR) was performed using the OT-2 liquid handling system and a qTOWER 2.2 (Analytic Jena, Jena, Germany) thermocycler. A microtiter plate holding the PCR reactions was prepared by distributing 15 μL of manually prepared PCR master mix, containing Q5 High-Fidelity 2× Master Mix (New England Biolabs GmbH, Frankfurt am Main, Germany) and plasmid

https://dx.doi.org/10.1021/acssynbio.0c00599
ACS Synth. Biol. 2021, 10, 589−599

pJC1-*lrp-brnF′-eyfp*[19] as template, to each well and adding 1 μL of each primer. All reagents were kept cool on ice during the pipetting process. The plate was then covered with foil (SILVERseal, Greiner Bio-One International GmbH, Kremsmünster, Austria) and placed into the thermocycler (qTOWER 2.2, Analytic Jena, Jena, Germany). Thermocycling was done according to the manufacturer's instructions.

Manual PCR was performed using a Biometra personal thermocycler (Analytic Jena, Jena, Germany) and the Q5 High-Fidelity 2× Master Mix (New England Biolabs GmbH, Frankfurt am Main, Germany) according to the manufacturer's instructions.

Gibson Assembly. Gibson assembly[22] was done by combining 2 μL of PCR product with 8 μL of manually prepared Gibson assembly Mastermix, containing 2 ng μL^{-1} NcoI-cleaved backbone (pEC-Tmob18-*lrp-eyfp*), in a microtiter plate using the OT-2 or EVO-200. All reagents were kept cool on ice or on the cooling carrier during the pipetting process. The plate was then covered with foil (SILVERseal, Greiner bio-one, Kremsmünster, Austria) and placed in a qTOWER 2.2 (Analytic Jena, Jena, Germany) thermocycler at 50 °C for 1 h.

Manual Gibson assembly of the pEC-Tmob18-*lrp-eyfp* backbone was done by combining 1 μL of each PCR product (*lrp* and *eyfp*) with 3 μL of *Eco*RI and *Bam*HI cleaved backbone (pEC-Tmob18) and 5 μL of Gibson assembly Mastermix. All reagents were kept cool on ice and placed in a Biometra personal thermocycler (Analytic Jena, Jena, Germany) at 50 °C for 1 h.

Heat-Shock Transformation of *E. coli*. *E. coli* S17-1[35] competent cells were prepared manually according to the rubidium chloride method.[38] Heat-shock transformation was done using the EVO200 liquid handling system. The heating device was set to 42 °C, and a V-Bottom plate (Greiner Bio-One International GmbH, Kremsmünster, Austria) was placed on it. Two μL per well of Gibson assembly product was distributed to a cooled (4 °C) microtiter plate. Twenty-five μL of competent *E. coli* S17-1 cells was added from a tube. The plate was incubated for 30 min. After incubation, the following procedure was done for each well of the microtiter plate, eight wells at a time: the complete volume of cell suspension was taken up by the liquid handler, pipetted into a well of the heated V-Bottom plate, incubated for 30 s, taken up again, and transferred back to the cooled plate. After this procedure was done for the whole plate, 200 μL of BHI medium was added to every well. Afterward, all wells were transferred to a 2 mL deep-well plate, and 600 μL of BHI medium was added. This plate was shaken at 800 rpm and 37 °C for 60 min to provide cell recovery. For plating, a spotting routine was employed: 12 round agar plates were placed on the robotic deck using a custom-made adapter (see the Supporting Information). For each well, 2 spots with 5 μL of the cell suspension were made. Afterwards, the deep-well plate was spun down using a centrifuge (4500 rpm, 5 min); the supernatant was removed, and the cells were resuspended in 50 μL of LB medium. From this solution, another 4 spots per well, again with 5 μL, were made.

Incubation and Colony Picking. Agar plates were incubated for 16 h at 37 °C. For each construct, at most, four colonies were picked by using a sterile toothpick: after carefully touching the colony, the toothpick was dipped into the master mix for Colony PCR and into LB medium for liquid culture.

Plasmid Preparation. For automated plasmid preparation, a ChargeSwitch NoSpin Plasmid Micro Kit (Thermo Fisher Scientific, Waltham, USA) was used on the EVO200 liquid handling system according to the manufacturer's instructions. A Magnetic-Ring Stand (Thermo Fisher Scientific, Waltham, USA) was used as the magnet. Plasmid DNA was eluted using 50 μL of elution buffer. The quality was checked by analyzing a random sample ($n = 8$) using a Implen NanoPhotometer P330 (Implen, Bayern, Germany). Sanger sequencing of plasmids was done by Eurofins Genomics (Ebersberg, Germany).

Colony PCR and Standard and Capillary Gel Electrophoresis. Colony PCR thermocycling was performed using a qTOWER 2.2 (Analytic Jena, Jena, Germany) thermocycler and the OneTaq 2× Master Mix with Standard Buffer (New England Biolabs GmbH, Frankfurt am Main, Germany) according to the manufacturer's instructions. PCR products were loaded on a 2% (w v^{-1}) agarose gel, and gel electrophoresis was done for 40 min at 100 V. GeneRuler 100 bp Plus DNA-Ladder (Thermo Fisher Scientific, Waltham, USA) was used for the quantification of PCR product sizes. Additionally, PCR products were analyzed by capillary gel electrophoresis using a MCE-202 MultiNA capillary gel electrophoresis device (Shimadzu Corp., Nakagyo-ku, Kyōto, Japan) according to the manufacturer's instructions.

Conjugation of *E. coli* and *C. glutamicum*. Conjugation was performed by preparing liquid cultivations of *E. coli* harboring the assembled plasmids and *C. glutamicum*. *E. coli* was cultivated using a deep well plate filled with 200 μL of LB medium per well and shaken at 900 rpm and 37 °C overnight. Prior to conjugation, 800 μL of LB medium was added per well (1:5 dilution), and the plate was shaken at 900 rpm and 37 °C for 3 h. For *C. glutamicum*, a preculture was prepared by using a 500 mL shake flask filled with 50 mL of BHI medium and shaken at 250 rpm and 30 °C overnight. Prior to conjugation, this culture was transferred to a 1000 mL shake flask filled with 50 mL of fresh BHI medium (1:2 dilution). This culture was shaken at 250 rpm and 30 °C for 3 h. Right before starting the conjugation procedure, the *C. glutamicum* culture was placed in a 48.5 °C water bath for 9 min to inhibit the restriction modification system.[39]

Both cultures were placed on the robotic deck of the EVO200 system. For *C. glutamicum*, a trough was used. From each *E. coli* culture, 250 μL was transferred to a 1 mL deep well plate, and 750 μL of *C. glutamicum* culture was added. The plate was then centrifuged (4500 rpm, 5 min); the supernatant was removed, and the pellet was resuspended in LB media by pipetting up and down 10 times with a 950 μL volume. The plate was then again centrifuged (4500 rpm, 5 min), and the supernatant was partly removed so that 300 μL was left on top of the pellet. The plate was covered with gas-permeable sealing foil (m2p-laboratories, Baesweiler, Germany) and placed in an incubator for 20 h. After incubation, each well was thoroughly mixed by pipetting up and down 10 times with 950 μL of BHI. From each well, two spots with 5 μL were plated on an BHI agar plate containing the antibiotics tetracylin (5 μg mL^{-1}) and nalidixin (50 μg mL^{-1}). The plate was centrifuged (4500 rpm, 5 min); the supernatant was removed, and each well was resuspended with 50 μL of BHI medium. From this concentrated suspension, four additional spots with 5 μL were prepared on agar plates. After approximately 40 h of incubation, single *C. glutamicum* clones were picked into BHI medium containing the antibiotics tetracylin (5 μg mL^{-1}) and nalidixin (50 μg mL^{-1}) for storage and phenotyping.

https://dx.doi.org/10.1021/acssynbio.0c00599
ACS Synth. Biol. 2021, 10, 589−599

Phenotyping of *C. glutamicum* Strain Variants. Cultivations for phenotyping of *C. glutamicum* strain variants were performed using specialized 48-well microtiter plates (FlowerPlate, m2p-laboratories GmbH, Baesweiler, Germany). The EVO200 system was used to distribute defined CGXII medium with or without the supplementation of 3 mM alanine−leucine dipeptide to the plates. Inoculation using 10 μL of thawed cryocultures per well was also done using this robot. Plates were then covered with gas-permeable sealing foil (m2p-laboratories GmbH, Baesweiler, Germany), transferred to an incubator (TiMix/TH 15, Edmund Bühler GmbH, Bodelshausen, Germany) set to 30 °C, and shaken at 1400 rpm.

After 20 h of incubation, a sample of 250 μL was drawn from each well and transferred to a multititer plate (PS, F-Bottom, transparent, Greiner Bio-One International GmbH, Kremsmünster, Austria) for subsequent measurements of absorption at 600 nm and fluorescence (excitation 488 nm, emission 525 nm).

Computational Methods and TACO. The whole workflow was accompanied by data management using a tailor-made toolbox named TACO (Tool for Automated Cloning). TACO is written in Python 3.8 and available to the general public under an MIT license. TACO uses Pandas[40] and NumPy[41] for most of its functionality. User input is done directly *via* Python or using Microsoft Excel (Microsoft Corp., Seattle, WA, USA). Graphviz[42] is used for visualization within TACO. matplotlib,[43] Seaborn,[44] and plotly (Plotly Inc., Montreal, Quebec, Canada) were used for additional plotting.

■ ASSOCIATED CONTENT

Supporting Information

The Supporting Information is available free of charge at https://pubs.acs.org/doi/10.1021/acssynbio.0c00599.

Further information on the primer design for the biosensor variants and the 3D printed devices (PDF)

■ AUTHOR INFORMATION

Corresponding Author

Stephan Noack − *Institute of Bio- and Geosciences − IBG-1: Biotechnology, Forschungszentrum Jülich GmbH, Jülich 52425, Germany; Bioeconomy Science Center (BioSC), Forschungszentrum Jülich, Jülich 52425, Germany;* orcid.org/0000-0001-9784-3626; Phone: +49 (0)2461 616044; Email: s.noack@fz-juelich.de; Fax: +49 (0)2461 613870

Authors

Niklas Tenhaef − *Institute of Bio- and Geosciences − IBG-1: Biotechnology, Forschungszentrum Jülich GmbH, Jülich 52425, Germany*

Robert Stella − *Institute of Bio- and Geosciences − IBG-1: Biotechnology, Forschungszentrum Jülich GmbH, Jülich 52425, Germany*

Julia Frunzke − *Institute of Bio- and Geosciences − IBG-1: Biotechnology, Forschungszentrum Jülich GmbH, Jülich 52425, Germany;* orcid.org/0000-0001-6209-7950

Complete contact information is available at: https://pubs.acs.org/10.1021/acssynbio.0c00599

Author Contributions

¶N.T. and R.S. contributed equally to this work.

Notes

The authors declare no competing financial interest.

The source code for the TACO package and data from this study as an application example are freely available at https://github.com/MicroPhen/taco. Additional data can be made available on request.

■ ACKNOWLEDGMENTS

Funding was received by the German Federal Ministry of Education and Research (BMBF, projects "BioökonomieREVIER_INNO: Entwicklung der Modellregion BioökonomieREVIER Rheinland", grant no. 031B0918A) and by the Helmholtz Association (grant W2/W3-096).

■ REFERENCES

(1) Opgenorth, P., Costello, Z., Okada, T., Goyal, G., Chen, Y., Gin, J., Benites, V., de Raad, M., Northen, T. R., Deng, K., et al. (2019) Lessons from Two Design-Build-Test-Learn Cycles of Dodecanol Production in *Escherichia coli* Aided by Machine Learning. *ACS Synth. Biol. 8*, 1337−1351.

(2) Appleton, E., Madsen, C., Roehner, N., and Densmore, D. (2017) Design Automation in Synthetic Biology. *Cold Spring Harbor Perspect. Biol. 9*, No. a023978.

(3) Ellis, T., Adie, T., and Baldwin, G. S. (2011) DNA assembly for synthetic biology: from parts to pathways and beyond. *Integrative Biology 3*, 109−118.

(4) Rogers, J. K., and Church, G. M. (2016) Multiplexed engineering in biology. *Trends Biotechnol. 34*, 198−206.

(5) Chao, R., Mishra, S., Si, T., and Zhao, H. (2017) Engineering biological systems using automated biofoundries. *Metab. Eng. 42*, 98−108.

(6) Linshiz, G., Jensen, E., Stawski, N., Bi, C., Elsbree, N., Jiao, H., Kim, J., Mathies, R., Keasling, J. D., and Hillson, N. J. (2016) End-to-end automated microfluidic platform for synthetic biology: from design to functional analysis. *J. Biol. Eng. 10*, 3.

(7) Patrick, W. G., Nielsen, A. A., Keating, S. J., Levy, T. J., Wang, C.-W., Rivera, J. J., Mondragón-Palomino, O., Carr, P. A., Voigt, C. A., Oxman, N., et al. (2015) DNA assembly in 3D printed fluidics. *PLoS One 10*, No. e0143636.

(8) Chao, R., Liang, J., Tasan, I., Si, T., Ju, L., and Zhao, H. (2017) Fully Automated One-Step Synthesis of Single-Transcript TALEN Pairs Using a Biological Foundry. *ACS Synth. Biol. 6*, 678−685.

(9) HamediRad, M., Chao, R., Weisberg, S., Lian, J., Sinha, S., and Zhao, H. (2019) Towards a fully automated algorithm driven platform for biosystems design. *Nat. Commun. 10*, 1−10.

(10) Si, T., Chao, R., Min, Y., Wu, Y., Ren, W., and Zhao, H. (2017) Automated multiplex genome-scale engineering in yeast. *Nat. Commun. 8*, 1−12.

(11) Leguia, M., Brophy, J., Densmore, D., and Anderson, J. C. (2011) *Methods in Enzymology*, Vol. *498*, pp 363−397, Elsevier.

(12) Storch, M., Haines, M. C., and Baldwin, G. S. (2020) DNA-BOT: A low-cost, automated DNA assembly platform for synthetic biology. *Synthetic Biology 5*, No. ysaa010.

(13) Jiang, X., Palazzotto, E., Wybraniec, E., Munro, L. J., Zhang, H., Kell, D. B., Weber, T., and Lee, S. Y. (2020) Automating Cloning by Natural Transformation. *ACS Synth. Biol. 9*, 3228−3235.

(14) Carbonell, P., Jervis, A. J., Robinson, C. J., Yan, C., Dunstan, M., Swainston, N., Vinaixa, M., Hollywood, K. A., Currin, A., Rattray, N. J., et al. (2018) An automated Design-Build-Test-Learn pipeline for enhanced microbial production of fine chemicals. *Communications Biology 1*, 1−10.

(15) Theisen, M., and Liao, J. C. (2016) Industrial biotechnology: *Escherichia coli* as a host. *Industrial Biotechnology: Microorganisms 1*, 149−181.

(16) Becker, J., Rohles, C. M., and Wittmann, C. (2018) Metabolically engineered *Corynebacterium glutamicum* for bio-based

production of chemicals, fuels, materials, and healthcare products. *Metab. Eng. 50*, 122−141.
(17) Wang, Y., Liu, Y., Liu, J., Guo, Y., Fan, L., Ni, X., Zheng, X., Wang, M., Zheng, P., Sun, J., et al. (2018) MACBETH: multiplex automated *Corynebacterium glutamicum* base editing method. *Metab. Eng. 47*, 200−210.
(18) Vertès, A. A., Inui, M., and Yukawa, H. (2005) Manipulating *Corynebacteria*, from Individual Genes to Chromosomes. *Appl. Environ. Microbiol. 71*, 7633−7642.
(19) Mustafi, N., Grünberger, A., Kohlheyer, D., Bott, M., and Frunzke, J. (2012) The development and application of a single-cell biosensor for the detection of L-methionine and branched-chain amino acids. *Metab. Eng. 14*, 449−457.
(20) Chou, H. H., and Keasling, J. D. (2013) Programming adaptive control to evolve increased metabolite production. *Nat. Commun. 4*, 1−8.
(21) Raman, S., Rogers, J. K., Taylor, N. D., and Church, G. M. (2014) Evolution-guided optimization of biosynthetic pathways. *Proc. Natl. Acad. Sci. U. S. A. 111*, 17803−17808.
(22) Gibson, D. G., Young, L., Chuang, R.-Y., Venter, J. C., Hutchison, C. A., and Smith, H. O. (2009) Enzymatic assembly of DNA molecules up to several hundred kilobases. *Nat. Methods 6*, 343−345.
(23) Hemmerich, J., Tenhaef, N., Steffens, C., Kappelmann, J., Weiske, M., Reich, S. J., Wiechert, W., Oldiges, M., and Noack, S. (2019) Less Sacrifice, More Insight: Repeated Low-Volume Sampling of Microbioreactor Cultivations Enables Accelerated Deep Phenotyping of Microbial Strain Libraries. *Biotechnol. J. 14*, 1800428.
(24) Jansen, R., Tenhaef, N., Moch, M., Wiechert, W., Noack, S., and Oldiges, M. (2019) FeedER: a feedback-regulated enzyme-based slow-release system for fed-batch cultivation in microtiter plates. *Bioprocess Biosyst. Eng. 42*, 1843−1852.
(25) Lange, C., Mustafi, N., Frunzke, J., Kennerknecht, N., Wessel, M., Bott, M., and Wendisch, V. F. (2012) Lrp of *Corynebacterium glutamicum* controls expression of the *brnFE* operon encoding the export system for L-methionine and branched-chain amino acids. *J. Biotechnol. 158*, 231−241.
(26) Pfeifer-Sancar, K., Mentz, A., Rückert, C., and Kalinowski, J. (2013) Comprehensive analysis of the *Corynebacterium glutamicum* transcriptome using an improved RNAseq technique. *BMC Genomics 14*, 888.
(27) Kirchner, O., and Tauch, A. (2003) Tools for genetic engineering in the amino acid-producing bacterium *Corynebacterium glutamicum*. *J. Biotechnol. 104*, 287−299.
(28) Tauch, A., Kirchner, O., Löffler, B., Götker, S., Pühler, A., and Kalinowski, J. (2002) Efficient Electrotransformation of *Corynebacterium diphtheriae* with a Mini-Replicon Derived from the *Corynebacterium glutamicum* Plasmid pGA1. *Curr. Microbiol. 45*, 362−367.
(29) Ogden, S., Haggerty, D., Stoner, C. M., Kolodrubetz, D., and Schleif, R. (1980) The *Escherichia coli* L-arabinose operon: binding sites of the regulatory proteins and a mechanism of positive and negative regulation. *Proc. Natl. Acad. Sci. U. S. A. 77*, 3346−3350.
(30) Kennerknecht, N., Sahm, H., Yen, M.-R., Pátek, M., Saier, M. H., Jr, and Eggeling, L. (2002) Export of L-isoleucine from *Corynebacterium glutamicum*: a two-gene-encoded member of a new translocator family. *J. Bacteriol. 184*, 3947−3956.
(31) Hans, S., Gimpel, M., Glauche, F., Neubauer, P., and Cruz-Bournazou, M. N. (2018) Automated Cell Treatment for Competence and Transformation of *Escherichia coli* in a High-Throughput Quasi-Turbidostat Using Microtiter Plates. *Microorganisms 6*, 60.
(32) Sarnaik, A., Liu, A., Nielsen, D., and Varman, A. M. (2020) High-throughput screening for efficient microbial biotechnology. *Curr. Opin. Biotechnol. 64*, 141−150.
(33) Weinstock, M. T., Hesek, E. D., Wilson, C. M., and Gibson, D. G. (2016) *Vibrio natriegens* as a fast-growing host for molecular biology. *Nat. Methods 13*, 849−851.
(34) Brophy, J. A., Triassi, A. J., Adams, B. L., Renberg, R. L., Stratis-Cullum, D. N., Grossman, A. D., and Voigt, C. A. (2018) Engineered integrative and conjugative elements for efficient and inducible DNA transfer to undomesticated bacteria. *Nature Microbiology 3*, 1043−1053.
(35) Simon, R., Priefer, U., and Pühler, A. (1983) A Broad Host Range Mobilization System for In Vivo Genetic Engineering: Transposon Mutagenesis in Gram Negative Bacteria. *Bio/Technology 1*, 784−791.
(36) Abe, S., Takayama, K.-I., and Kinoshita, S. (1967) Taxonomical Studies on Glutamic Acid-Producing Bacteria. *J. Gen. Appl. Microbiol. 13*, 279−301.
(37) Keilhauer, C., Eggeling, L., and Sahm, H. (1993) Isoleucine synthesis in *Corynebacterium glutamicum*: molecular analysis of the *ilvB-ilvN-ilvC* operon. *J. Bacteriol. 175*, 5595−5603.
(38) Mülhardt, C. (2007) *Molecular Biology and Genomics*, pp 105−129, Elsevier.
(39) Schäfer, A., Schwarzer, A., Kalinowski, J., and Pühler, A. (1994) Cloning and characterization of a DNA region encoding a stress-sensitive restriction system from *Corynebacterium glutamicum* ATCC 13032 and analysis of its role in intergeneric conjugation with *Escherichia coli*. *J. Bacteriol. 176*, 7309−7319.
(40) McKinney, W. (2010) Data Structures for Statistical Computing in Python. *Proceedings of the 9th Python in Science Conference.*, 56−61.
(41) Harris, C. R., Millman, K. J., van der Walt, S. J., Gommers, R., Virtanen, P., Cournapeau, D., Wieser, E., Taylor, J., Berg, S., Smith, N. J., et al. (2020) Array programming with NumPy. *Nature 585*, 357−362.
(42) Ellson, J., Gansner, E., Koutsofios, L., North, S. C., and Woodhull, G. (2002) Graphviz-Open source graph drawing tools. *International Symposium on Graph Drawing. 2265*, 483−484.
(43) Barrett, P., Hunter, J., Miller, J. T., Hsu, J.-C., and Greenfield, P. (2005) matplotlib-A Portable Python Plotting Package. In *Astronomical data analysis software and systems XIV, ASP Conference Series*, Vol. *347*, p 91.
(44) Waskom, M., Botvinnik, O., Gelbart, M., Ostblom, J., Hobson, P., and Lukauskas, S. (2020) *mwaskom/seaborn v0.11.0.rc0*, https://newreleases.io/project/github/mwaskom/seaborn/release/v0.11.0.

https://dx.doi.org/10.1021/acssynbio.0c00599
ACS Synth. Biol. 2021, 10, 589−599

4. Affidavit

I declare under oath that I have produced my thesis independently and without any undue assistance by third parties under consideration of the 'Principles for the Safeguarding of Good Scientific Practice at Heinrich Heine University Düsseldorf'. This thesis has not been presented at any other university or faculty, and I have undertaken no prior attempts to attain a doctoral degree.

Robert Stella

5. Appendix

5.1. Supplementary Information "Biosensor-based growth-coupling and spatial separation as a novel evolution strategy to improve microbial small molecule production"

Table S1

Overview of mutations in 15 L-valine producer mutants. Only high frequency mutations (>35%) are shown, unless no high frequency mutations were found (ND); *fs*: frameshift mutation, *sv*: structural variant, *ins*: insertion.

#	Strain	Experiment	Phenotype	Mutation	Occurence (%)
C1	P_{brnF}-*pfkA*	rbALE in liquid media	cheater	Lrp (M1I)	100
C2	P_{brnF}-*pfkA*	rbALE in liquid media	cheater	sv, duplication *pfkA*	18
C3	P_{brnF}-*pfkA*	rbALE in liquid media	cheater	Lrp (F139L)	100
C4	P_{brnF}-*hisD*	rbALE in liquid media	cheater	sv *lrp*-P_{brnF}	ND
C5	P_{brnF}-*hisD*	rbALE in liquid media	cheater	C to A *lrp*-P_{brnF}	100
C6	P_{brnF}-*hisD*	rbALE in liquid media	cheater	sv *lrp*-P_{brnF}	ND
V1	P_{brnF}-*pfkA*	FACS-based ALE	L-valine producer; 2.5 mM	*ilvN* sv	46
V2	P_{brnF}-*pfkA*	1st plate-based ALE, BHI plate	L-valine producer; 4.8 mM	IlvN (F29L) #4	50,9
V3	P_{brnF}-*pfkA*	1st plate-based ALE, CGXII plate large colony	L-valine producer; 10.0 mM	IlvN (F29L) #2	100
V4	P_{brnF}-*pfkA*	1st plate-based ALE, CGXII plate large colony	L-valine producer; 10.8 mM	IlvN (F29I)	100
V5	P_{brnF}-*hisD*	1st plate-based ALE, CGXII plate large colony	L-valine producer; 1.5 mM	IlvN fs (ins 442G)	96,4
				A391A in NCgl0375(-), NCgl0375, cation transport ATPase	100
V6	P_{brnF}-*hisD*	1st plate-based ALE, CGXII plate large colony	L-valine producer; 10.5 mM	IlvN (D17E)	34,2
V7	P_{brnF}-*hisD*	1st plate-based ALE, CGXII plate large colony	L-valine producer; 9.9 mM	IlvN (F29L) #3	100
V8	P_{brnF}-*hisD*	1st plate-based ALE, CGXII plate small colony	L-valine producer; 3.5 mM	*ilvN* ins (105CCTCGTGTC)	40
				A to T intergenic region of NCgl1020 (major facilitator superfamily permease) and NCgl1021 (transposase)	52,4
V9	P_{brnF}-*hisD*	1st plate-based ALE, CGXII plate small colony	L-valine producer; 7.0 mM	IlvN (I158M)	63,6
V10	P_{brnF}-*pfkA*	2nd HT plate-based ALE	L-valine producer; 5.8 mM	IlvB (D133G)	100

V11	P_{brnF}-*pfkA*	2nd HT plate-based ALE	L-valine mM	producer;	12.0	IlvB (R141G)	87,7
V12	P_{brnF}-*pfkA*	2nd HT plate-based ALE	L-valine mM	producer;	15.0	IlvN (S155F)	100
V13	P_{brnF}-*hisD*	2nd HT plate-based ALE	L-valine mM	producer;	11.2	IlvN (A42E)	100
V14	P_{brnF}-*hisD*	2nd HT plate-based ALE	L-valine mM	producer;	13.1	IlvN (I22M)	100
V15	P_{brnF}-*hisD*	2nd HT plate-based ALE	L-valine mM	producer;	10.7	IlvN (F29L) #1	100

Table S2
Amount of colonies, and size of colony, on agar plates CGXII 2% glucose or BHI media. ND, not determined.

strain	*plate media*	*dilution*	*normal colonies*	*large colonies*
P_{brnF}-*pfkA*	CGXII	10^6	87	0
P_{brnF}-*pfkA*	CGXII	10^5	1004	0
P_{brnF}-*pfkA*	CGXII	10^4	ND	2
P_{brnF}-*pfkA*	CGXII	10^3	ND	10
P_{brnF}-*pfkA*	BHI	10^6	151	ND
P_{brnF}-*pfkA*	BHI	10^5	924	ND
WT	CGXII	10^6	104	ND
WT	CGXII	10^5	828	ND
P_{brnF}-*hisD*	CGXII	10^6	267	0
P_{brnF}-*hisD*	CGXII	10^5	1376	1
P_{brnF}-*hisD*	CGXII	10^4	ND	10
P_{brnF}-*hisD*	CGXII	10^3	ND	>30
P_{brnF}-*hisD*	BHI	10^6	219	ND
P_{brnF}-*hisD*	BHI	10^5	2308	ND
WT	CGXII	10^6	210	ND
WT	CGXII	10^5	1296	ND

Table S3
Bacterial strains and plasmids used in this study.

Strain/plasmid	Genotype and relevant characteristic	Reference
E. coli DH5a	*supE44 ΔlacU169* (ϕ80*lacZ*DM15) *hsdR17 recA1 endA1 gyrA96 thi-1 relA1*	Invitrogen (Karlsruhe, Germany)
C. glutamicum ATCC13032	Biotin-auxotrophic wild type	(Kalinowski et al., 2003)
C. glutamicum:: *PbrnF-pfkA*	Integrated lrp sensor construct (terminator, *lrp*, *lrp-brnF* intergenic region and first 30 bp of *brnF* followed by a stopcodon, RBS and linker) upstream of *pfkA*	This study
C. glutamicum:: *PbrnF-hisD*	Integrated lrp sensor construct (terminator, *lrp*, *lrp-brnF* intergenic region and first 30 bp of *brnF* followed by a stopcodon, RBS and linker) upstream of *hisD*	This study
C. glutamicum:: *PbrnF-pfkA* **/** *pJC1-lrp-brnF'-eyfp*	*C. glutamicum PbrnF-pfkA* harboring pJC1-lrp-brnF'-eyfp	This study
C. glutamicum:: *PbrnF-hisD* **/** *pJC1-lrp-brnF'-eyfp*	*C. glutamicum PbrnF-hisD* harboring pJC1-lrp-brnF'-eyfp	This study
pJC1-*lrp-brnF'-eyfp*	Kan^R, Lrp sensor plasmids containing a terminator (term part), *lrp,* the *lrp-brnF* intergenic region, the first 30 bp of *brnF* followed by a stopcodon, RBS and linker and *eyfp*	(Mustafi et al., 2012)
pK19-*mobsacB*	Used for allelic exchange in *C. glutamicum*; $oriV_{E.c.}$, *sacB lacZα KanR*	(Schäfer et al., 1994)
pJC1-*venus*-term	Used to obtain term part, Kan^R	(Baumgart et al., 2013)
pK19-*mobsacB-pfkA-lrp-brnF'*	Vector for integration of the Lrp sensor construct upstream of *pfkA*	This Study
pK19-*mobsacB-hisD-lrp-brnF'*	Vector for integration of the Lrp sensor construct upstream of *hisD*	This Study

Table S4
Oligonucleotides used in this study

name	*sequence*
term_fw	TTTTGGCGGATGAGAGAAGA
term_rv	CAAAAGAGTTTGTAGAAACGCA
lrp_fw	GTTTCTACAAACTCTTTTGTCACACCTGGGGGCGAGC
lrp_rv	ATGATATCTCCTTCTTAAAGTTCAGCT
hisD_up_fw	CCTGCAGGTCGACTCTAGAGTCCGGTGTCGCTGAAGTTAA
hisD_up_fw	TCTTCTCTCATCCGCCAAAAACCTATTGTATTCCCCACGTAAC
hisD_down_fw	CTTTAAGAAGGAGATATCATATGTTGAATGTCACTGACCTGC
hisD_down_fw	TTGTAAAACGACGGCCAGTGGACAGCCCACACCTCATCAA
pfkA_up_fw	CCTGCAGGTCGACTCTAGAGAGAGTCGCCCCGATAAGTTT
pfkA_up_fw	TCTTCTCTCATCCGCCAAAATCTGACCATCTTATTTAATCGCCA
pfkA_down_fw	CTTTAAGAAGGAGATATCATATGCGAATTGCTACTCTCACG
pfkA_down_fw	TTGTAAAACGACGGCCAGTGATACCTGCGTGCAGAGCAAT

Supplementary data 1

Sequence of *lrp*-P_{brnF} integration upstream from *pfkA*, intergenic region upstream of *pfkA* is given, showing the first codon of *pfkA* (underlined), the terminator sequence (red), *lrp* (green), the first 30 bp of *brnF* (yellow) and the linker sequence (blue)

GGTGAGCCAGTCTAGAGACAAAATTTTTCCGCGGGGGTTTTCTTGATCTGATCCGACAACCCAATGGG
GGCAAAAATGTGTCCGACCAAAAATTGTGCAGCACACCACATGCCCGCTCGGACAATGTCGATTTGTT
AATGAAACTGCAGCTCTGGCGATTAAATAAGATGGTCAGATTTTGGCGGATGAGAGAAGATTTTCAGC
CTGATACAGATTAAATCAGAACGCAGAAGCGGTCTGATAAAACAGAATTTGCCTGGCGGCAGTAGCGC
GGTGGTCCCACCTGACCCCATGCCGAACTCAGAAGTGAAACGCCGTAGCGCCGATGGTAGTGTGGGGT
CTCCCCATGCGAGAGTAGGGAACTGCCAGGCATCAAATAAAACGAAAGGCTCAGTCGAAAGACTGGGC
CTTTCGTTTTATCTGTTGTTTGTCGGTGAACGCTCTCCTGAGTAGGACAAATCCGCCGGGAGCGGATT
TGAACGTTGCGAAGCAACGGCCCGGAGGGTGGCGGGCAGGACGCCCGCCATAAACTGCCAGGCATCAA
ATTAAGCAGAAGGCCATCCTGACGGATGGCCTTTTTGCGTTTCTACAAACTCTTTTGTCACACCTGGG
GGCGAGCTGGTTTCACCACTTTCATAGCAAAACGTGATGAGATCTTTGCAATTCCTGGCACGGTTTGA
ATGTGACTGGATAAAAATTGCTCATACGCCTCCAAATCAGCAACGCCGATGCGGACAAAATAATCTGG
CGAACCAAAAAGCCTGTGCAACTCCAGTACTTCATCATGCTGCGCAACGGAGCTTTCAAAATTGTCTA
CAGTGGAGCGGTCGAAGTTGCTGAGAGTGACATCCACGGTCACCTCAAATCCACGATTCATCACCGCA
GGGTGAATGTCCGCGCTGTAGCCCAAAATGATTCCTTCGGCTTCCAAACGCTGCACCCTCCTCAAGCA
AGGTCCCGGAGTGAGATGCACCTTGTCAGCCAGTGCGAGATTTGAGATGCGCGCATTCGCGCTAAGCT
CCGCAATAATTGCGCGATCAATGGAATCTAGCTTCATATATTGCACAATAGCCTAGTTGAGGTGCGCA
AACTGGCAACAAAACTACCCGGCAATTGTGTGATGATTGTAGTGTGCAAAAAACGCAAGAGATTCATT
CAAGCTGAACTTTAAGAAGGAGATATCATATG

Supplementary data 2

Sequence of *lrp*-P_{brnF} integration upstream from *hisD*, intergenic region upstream of *hisD* is given, showing the first codon of *hisD*. (underlined), the terminator sequence (red), *lrp* (green), the first 30 bp of *brnF* (yellow) and the linker sequence (blue)

CATATGATATCTCCTTCTTAAAGTTCAGCTTGAATGAATCTCTTGCGTTTTTTGCACACTACAATCAT
CACACAATTGCCGGGTAGTTTTGTTGCCAGTTTGCGCACCTCAACTAGGCTATTGTGCAATATATGAA
GCTAGATTCCATTGATCGCGCAATTATTGCGGAGCTTAGCGCGAATGCGCGCATCTCAAATCTCGCAC
TGGCTGACAAGGTGCATCTCACTCCGGGACCTTGCTTGAGGAGGGTGCAGCGTTTGGAAGCCGAAGGA
ATCATTTTGGGCTACAGCGCGGACATTCACCCTGCGGTGATGAATCGTGGATTTGAGGTGACCGTGGA
TGTCACTCTCAGCAACTTCGACCGCTCCACTGTAGACAATTTTGAAAGCTCCGTTGCGCAGCATGATG
AAGTACTGGAGTTGCACAGGCTTTTTGGTTCGCCAGATTATTTTGTCCGCATCGGCGTTGCTGATTTG
GAGGCGTATGAGCAATTTTTATCCAGTCACATTCAAACCGTGCCAGGAATTGCAAAGATCTCATCACG
TTTTGCTATGAAAGTGGTGAAACCAGCTCGCCCCCAGGTGTGACAAAAGAGTTTGTAGAAACGCAAAA
AGGCCATCCGTCAGGATGGCCTTCTGCTTAATTTGATGCCTGGCAGTTTATGGCGGGCGTCCTGCCCG
CCACCCTCCGGGCCGTTGCTTCGCAACGTTCAAATCCGCTCCCGGCGGATTTGTCCTACTCAGGAGAG
CGTTCACCGACAAACAACAGATAAAACGAAAGGCCCAGTCTTTCGACTGAGCCTTTCGTTTTATTTGA
TGCCTGGCAGTTCCCTACTCTCGCATGGGGAGACCCCACACTACCATCGGCGCTACGGCGTTTCACTT
CTGAGTTCGGCATGGGGTCAGGTGGGACCACCGCGCTACTGCCGCCAGGCAAATTCTGTTTTATCAGA
CCGCTTCTGCGTTCTGATTTAATCTGTATCAGGCTGAAAATCTTCTCTCATCCGCCAAAAACCTATTG
TATTCCCCACGTAACAAGTTTCTGATTTGGGTACATCAGAGTTCATTTGAATTAGACTTAAAACTTAA
AATGACCACCCCAGATTTACCTGAATTAAACCCGCTTTCACCTTTGAGATACTGGAAGGA

Supplementary data 3

PDF export of the jupyter notebook containing the information on the rbALE simulation model.

In [ ]:

```
# Imports from the pyfoomb package.
import pyfoomb
print(f'Current package version of {pyfoomb.__name__}: {pyfoomb.__version__}')

from pyfoomb import BioprocessModel
from pyfoomb import Caretaker
from pyfoomb import Visualization
from pyfoomb import TimeSeries
from pyfoomb import Helpers
from pyfoomb import Measurement
from pyfoomb import ObservationFunction
from pyfoomb import ParameterMapper
import joblib
import glob
import re

from matplotlib import pyplot
import numpy as np
import pandas as pd
import seaborn as sns
```

In [2]:

```
# Simplified process model to analyze batch experiments of growth-coupled strains
class BatchModel(BioprocessModel):


    def specific_growth_rate_mu(self, S):
        mu_max = self.model_parameters['mu_max']
        K_S = self.model_parameters['K_S']
        K_A = self.model_parameters['K_A']
        Act = self.model_parameters['Act']
        mu = mu_max * S / (K_S + S) * Act /(K_A + Act)
        return mu

    def specific_substrate_consumption_rate_qS(self, mu):
        Y_XS = self.model_parameters['Y_XS']
        qS = -mu/Y_XS
        return qS

    def rhs(self, t, y, sw):

        # Unpack the state vector. The states are alphabetically ordered.
        S, X = y

        # Calculate specific rates.
        mu = self.specific_growth_rate_mu(S)
        qS = self.specific_substrate_consumption_rate_qS(mu)

        # Calculate state derivatives.
        dXdt = mu * X
        dSdt = qS * X

        # Return list of state derivatives in the same order as the state vector was unpacked.
        return [dSdt, dXdt]

    def state_events(self, t, y, sw):
        S, X = y
        return [S]

    def change_states(self, t, y, sw):

        S, X = y

        if sw[0]:
            S = 0
        return [S, X]

    def get_specific_rates_time_series(self, model_states:list):

        # Get a specific "TimeSeries" object, specified by its "name" and "replicate_id".
        state_S = Helpers.extract_time_series(model_states, name='S', replicate_id=self.replicate_id)

        # Get the timepoints and values needed for specific rate calculation.
        _t = state_S.timepoints
        _S = state_S.values

        # Calculate specific rates vectors.
        _mu = self.specific_growth_rate_mu(_S)
        _qS = self.specific_substrate_consumption_rate_qS(_mu)

        # Create new corresponding TimeSeries objects.
        mu = TimeSeries(name='mu', replicate_id=self.replicate_id, timepoints=_t, values=_mu)
        qS = TimeSeries(name='qS', replicate_id=self.replicate_id, timepoints=_t, values=_qS)

        return [mu, qS]

model_parameters = {
    'mu_max' : 0.5,
    'K_S' : 0.7,
    'K_A' : 0.0,
    'Act' : 0.01,
    'Y_XS' : 0.55, #Hemmerich et al (2018) BTJ
}

initial_values = {
    'X0' : 0.75,
    'S0' : 20,
}
```

In [3]:
```python
# Defines an observation function class, that inherits from "ObservationFunction".
# For backscatter measurements (BS), a linear calibration model is used.
class BS(ObservationFunction):

    def observe(self, model_values):
        # parameter unpacking
        a = self.observation_parameters['a']
        b = self.observation_parameters['b']
        return (model_values + b) / a

# Defines the observed model state and parameters for the observation function.
observation_parameters_bs = {
    'observed_state' : 'X',
    'a' : 0.06,
    'b' : 0.7,
}

observations_functions = [
    (BS, observation_parameters_bs),
]
```

In [4]:
```python
# Instantiate a Caretaker, which manages the model and its parametrization.
caretaker = Caretaker(
    bioprocess_model_class=BatchModel,
    model_parameters=model_parameters,
    initial_values=initial_values,
    observation_functions_parameters=observations_functions,
    replicate_ids=['1st', '2nd', '3rd', '4th', '5th', '6th', '7th', '8th', '9th']
)
```

In [24]:
```python
# Create parameter mappings for the replicate_ids.
mappings = [
    ParameterMapper(replicate_id='1st', global_name='X0', local_name='X0_R1', value=0.7),
    ParameterMapper(replicate_id='2nd', global_name='X0', local_name='X0_R2', value=0.7),
    ParameterMapper(replicate_id='3rd', global_name='X0', local_name='X0_R3', value=0.7),
    ParameterMapper(replicate_id='4th', global_name='X0', local_name='X0_R4', value=0.7),
    ParameterMapper(replicate_id='5th', global_name='X0', local_name='X0_R5', value=0.7),
    ParameterMapper(replicate_id='6th', global_name='X0', local_name='X0_R6', value=0.7),
    ParameterMapper(replicate_id='7th', global_name='X0', local_name='X0_R7', value=0.02),
    ParameterMapper(replicate_id='8th', global_name='X0', local_name='X0_R8', value=0.02),
    ParameterMapper(replicate_id='9th', global_name='X0', local_name='X0_R9', value=0.02),
    ParameterMapper(replicate_id='1st', global_name='K_A', local_name='K_A_R1', value=0.0),
    ParameterMapper(replicate_id='2nd', global_name='K_A', local_name='K_A_R2', value=0.0),
    ParameterMapper(replicate_id='3rd', global_name='K_A', local_name='K_A_R3', value=0.0),
    ParameterMapper(replicate_id='4th', global_name='K_A', local_name='K_A_R4', value=0.05),
    ParameterMapper(replicate_id='5th', global_name='K_A', local_name='K_A_R5', value=0.05),
    ParameterMapper(replicate_id='6th', global_name='K_A', local_name='K_A_R6', value=0.05),
    ParameterMapper(replicate_id='7th', global_name='K_A', local_name='K_A_R7', value=0.05),
    ParameterMapper(replicate_id='8th', global_name='K_A', local_name='K_A_R8', value=0.05),
    ParameterMapper(replicate_id='9th', global_name='K_A', local_name='K_A_R9', value=0.05),
]

# Apply the mappings.
caretaker.apply_mappings(mappings)
#caretaker.parameter_mapping
```

In [25]:
```python
df_dict = pd.read_excel('Cglut_BioSensor_data.xlsx', header=[0, 1], index_col=0, sheet_name=None)
#for _df in df_dict:
#    display(df_dict[_df])
```

In [7]:
```python
# Define linear error model
def linear_error_model(values, error_parameters:dict):
    slope = error_parameters['slope']
    offset = error_parameters['offset']
    return values*slope + offset

error_parameters = {
    'slope' : 0.05,
    'offset' : 0.01,
}
```

In [8]:
```python
# Create an empty list, which will collect all Measurement objects
data = []

# Iterate over replicates
for _replicate_id in df_dict.keys():
    _df = df_dict[_replicate_id]
    names = np.unique([mi[0] for mi in _df.columns])
    for name in names:
        # Create corresponding Measurement object
        _measurement = Measurement(
            name=name,
            replicate_id = _replicate_id,
            timepoints=_df.index,
            values=_df[(name, 'values')].to_numpy(),
            error_model=linear_error_model,
            error_model_parameters=error_parameters
        )
        # Append to list
        data.append(_measurement)
```

In [9]:
```python
# Define parameter bounds for model fitting
unknowns_and_bounds = {'X0_R1': (0.6, 0.8),
 'X0_R2': (0.6, 0.8),
```

```
 'X0_R3': (0.6, 0.8),
 'X0_R4': (0.6, 0.8),
 'X0_R5': (0.6, 0.8),
 'X0_R6': (0.6, 0.8),
 'X0_R7': (0.01, 0.03),
 'X0_R8': (0.01, 0.03),
 'X0_R9': (0.01, 0.03),
 'mu_max': (0.4, 0.6),
 'K_S': (0.6, 0.8),
 'a': (0.05, 0.07),
 'b': (0.6, 0.8),
 'Act': (0.01, 0.02),
 'K_A_R4': (0.03, 0.05),
 'K_A_R5': (0.03, 0.05),
 'K_A_R6': (0.03, 0.05),
 'K_A_R7': (0.03, 0.05),
 'K_A_R8': (0.03, 0.05),
 'K_A_R9': (0.03, 0.05)}
```

In [10]:
```
# Setup optimization routine
optimizers = ['de1220', 'ihs', 'simulated_annealing', 'pso']
mult = int(joblib.cpu_count()/len(optimizers))

rtol = 1e-3
metric = 'WSS'
evolutions = 5
max_evotime = 5
```

In [11]:
```
# Run parameter estimation
estimates, est_info = caretaker.estimate_parallel(
    unknowns=list(unknowns_and_bounds.keys()),
    bounds=list(unknowns_and_bounds.values()),
    measurements=data,
    report_level=0,
    optimizers=optimizers*mult,
    metric=metric,
    rtol_islands=rtol,
    evolutions=evolutions,
    max_evotime_min=max_evotime
)
```

In [23]:
```
# estimated parameters
estimates
```

Out[23]:
```
{'a': 0.056660737496040135,
 'Act': 0.010637860189401136,
 'b': 0.6606944515624659,
 'K_A_R4': 0.03021388367695973,
 'K_A_R5': 0.03272040518629986,
 'K_A_R6': 0.031908694124411153,
 'K_A_R7': 0.03677658438824084,
 'K_A_R8': 0.034878777033044452,
 'K_A_R9': 0.03440687067569643,
 'K_S': 0.6001858536472509,
 'mu_max': 0.5109246553724861,
 'X0_R1': 0.7975373209010698,
 'X0_R2': 0.7384357901019495,
 'X0_R3': 0.7582043323049971,
 'X0_R4': 0.7431273125775794,
 'X0_R5': 0.7495193307373414,
 'X0_R6': 0.713027384973678,
 'X0_R7': 0.025831902421433295,
 'X0_R8': 0.021968294967313336,
 'X0_R9': 0.0191507286749914}
```

In [12]:
```
# Plot fitting results
_fig1 = Visualization.compare_estimates(parameters=estimates, measurements=data, caretaker=caretaker)
```

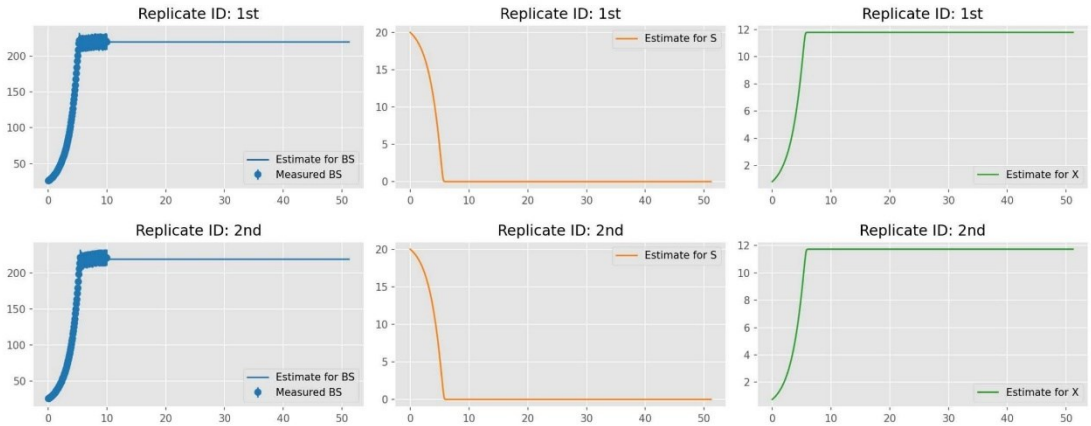

Appendix

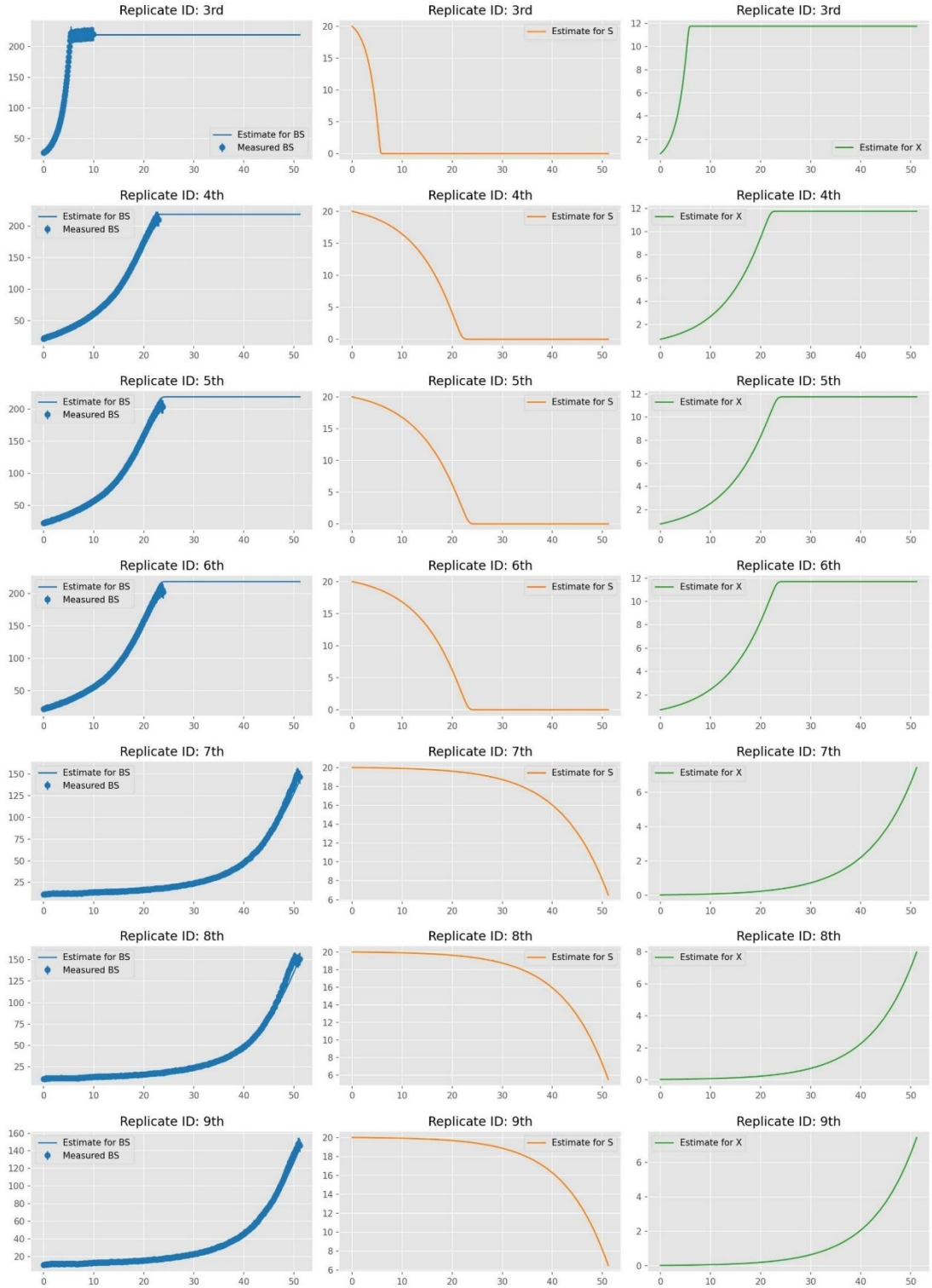

In [26]:

```
# Process model to study ALE experiments based on repetitive batches
class rbBatchModel(BioprocessModel):


    def specific_growth_rate_mu(self, S, Act, K_A):
        mu_max = self.model_parameters['mu_max']
        K_S = self.model_parameters['K_S']
        mu = mu_max * S / (K_S + S) * Act /(K_A + Act)
        return mu
```

```
    def specific_substrate_consumption_rate_qS(self, mu):
        Y_XS = self.model_parameters['Y_XS']
        qS = -mu / Y_XS
        return qS

    def rhs(self, t, y, sw):

        # Unpack the state vector. The states are alphabetically ordered.
        S, X_neg, X_ori, X_pos, X_tot = y

        # Activator concentration.
        Act_ori = self.model_parameters['Act_ori']
        Act_pos = self.model_parameters['Act_pos']

        # Affinity constants of regulator binding.
        K_A_ori = self.model_parameters['K_A_ori']
        K_A_neg = self.model_parameters['K_A_neg']


        # Calculate specific rates.
        mu_ori = self.specific_growth_rate_mu(S, Act_ori, K_A_ori)
        mu_pos = self.specific_growth_rate_mu(S, Act_pos, K_A_ori)
        mu_neg = self.specific_growth_rate_mu(S, Act_ori, K_A_neg)
        qS_ori = self.specific_substrate_consumption_rate_qS(mu_ori)
        qS_pos = self.specific_substrate_consumption_rate_qS(mu_pos)
        qS_neg = self.specific_substrate_consumption_rate_qS(mu_neg)

        # Calculate state derivatives
        dX_oridt = mu_ori * X_ori
        dX_posdt = mu_pos * X_pos
        dX_negdt = mu_neg * X_neg
        dX_totdt = dX_oridt + dX_posdt + dX_negdt
        dSdt = qS_ori * X_ori + qS_pos * X_pos + qS_neg * X_neg

        # Return list of state derivatives in the same order as the state vector was unpacked.
        return [dSdt, dX_negdt, dX_oridt, dX_posdt, dX_totdt]

    def state_events(self, t, y, sw):

        # Unpack the state vector. The states are alphabetically ordered.
        # S is used as event to prevent mutation when there is not growth.
        S, X_neg, X_ori, X_pos, X_tot = y

        transfer_1 = self.model_parameters['transfer_1']
        transfer_2 = self.model_parameters['transfer_2']
        transfer_3 = self.model_parameters['transfer_3']
        transfer_4 = self.model_parameters['transfer_4']

        # These events are hit when the expressions evaluate to zero.
        event_transfer_1 = transfer_1 - t
        event_transfer_2 = transfer_2 - t
        event_transfer_3 = transfer_3 - t
        event_transfer_4 = transfer_4 - t

        return [S, event_transfer_1, event_transfer_2, event_transfer_3, event_transfer_4]


    def change_states(self, t, y, sw):

        S, X_neg, X_ori, X_pos, X_tot = y

        dilution = self.model_parameters['dilution']
        S_transfer = self.model_parameters['S_transfer']

        transfer_1 = self.model_parameters['transfer_1']
        transfer_2 = self.model_parameters['transfer_2']
        transfer_3 = self.model_parameters['transfer_3']
        transfer_4 = self.model_parameters['transfer_4']

        if sw[1] and t==transfer_1:
            X_neg, X_ori, X_pos, X_tot = dilution * np.array([X_neg, X_ori, X_pos, X_tot])
            S = (S*dilution) + S_transfer

        if sw[2] and t==transfer_2:
            X_neg, X_ori, X_pos, X_tot = dilution * np.array([X_neg, X_ori, X_pos, X_tot])
            S = (S*dilution) + S_transfer

        if sw[3] and t==transfer_3:
            X_neg, X_ori, X_pos, X_tot = dilution * np.array([X_neg, X_ori, X_pos, X_tot])
            S = (S*dilution) + S_transfer

        if sw[4] and t==transfer_4:
            X_neg, X_ori, X_pos, X_tot = dilution * np.array([X_neg, X_ori, X_pos, X_tot])
            S = (S*dilution) + S_transfer

        return [S, X_neg, X_ori, X_pos, X_tot]

initial_values = {
    'X_ori0' : 0.2,
    'X_neg0' : 0,
    'X_pos0' : 0,
    'X_tot0' : 0.2,
    'S0' : 20,
}
```

In [32]:

```
# # Define model parameters for pfkA strain
model_parameters_pfkA = {
    'mu_max' : 0.5109246553724861,
    'K_S' : 0.6001858536472509,
    'Act_ori' : 0.010637860189401136,
```

```
    'Act_pos' : 0.010637860189401136,
    'K_A_ori' : 0.031614328, #Mean from three replicate estimates
    'K_A_neg' : 0.0,
    'Y_XS' : 0.55, #Hemmerich et al (2018) BTJ
    'transfer_1': 40,
    'transfer_2': 80,
    'transfer_3': 120,
    'transfer_4': 160,
    'dilution' : 0.02,
    'S_transfer' : 20
}

## Replicate values

# Ratio of positive to negative mutants at start of simulation
x_pos_number = np.array([1, 3, 5, 7, 9]) #starting number of X_pos strain --> converted to mass below
x_neg_number = np.array([9, 7, 5, 3, 1]) #starting number of X_neg strain --> converted to mass below

cell_weight = 10**-12 # Assumed weight of one cell, to convert cell counts to biomass
x_pos_list = x_pos_number * cell_weight #starting mass of X_pos strain
x_neg_list = x_neg_number * cell_weight #starting mass of X_pos strain

# Act_pos values for replicates
Act_modifier_list = [10, 25, 50, 100, 1000] # multitudes of Act_pos
Act_modifier_values = model_parameters_pfkA['Act_pos'] * np.array(Act_modifier_list) #calculate actual values

# Names based on set values for the replicates, for identification
rep_names = ['Act: ' + str(act) + 'x, P/N: ' + str(p) + ':' + str(n) for p, n in zip(x_pos_number, x_neg_number) for act in Act_modifier_list]
```

In [33]:

```
# Instantiate a Caretaker, which manages the model and its parametrization.

caretaker_pfkA = Caretaker(
    bioprocess_model_class=rbBatchModel,
    model_parameters=model_parameters_pfkA,
    initial_values=initial_values,
    replicate_ids=rep_names
)

# Add the replicates, all combinations of pos:neg ratio at start and Act_pos values
for i, _ in enumerate(x_pos_list):
    for j, val in enumerate(Act_modifier_values):

        mappings = [
            ParameterMapper(replicate_id = rep_names[i*len(Act_modifier_list) + j], global_name='X_neg0', value=x_neg_list[i]),
            ParameterMapper(replicate_id = rep_names[i*len(Act_modifier_list) + j], global_name='X_pos0', value=x_pos_list[i]),
            ParameterMapper(replicate_id = rep_names[i*len(Act_modifier_list) + j], global_name='Act_pos', value=val)
        ]
        caretaker_pfkA.apply_mappings(mappings)
```

In [36]:

```
# Simulate repetitive batch cultivations
max_time = 210

simulation_pfkA = caretaker_pfkA.simulate(t=max_time)
```

In [38]:

```
# Collect all relevant parameters and data from the simulation objects and store in pandas df

list_of_dicts = [] #initiate empty dict for data storage
sim_dict = {'pfkA':simulation_pfkA} #collect simulation object in a dict, facilitates easy expansions with other simulations

for sim in sim_dict: # loop over simulation objects
    for sample in sim_dict[sim]: # extract data per replicate per simuation object
        _ = {}
        _['strain'] = sim
        _['time'] = Helpers.extract_time_series(sim_dict[sim], name=sample.name, replicate_id = sample.replicate_id).timepoints
        _['measurement'] = [sample.name]
        _['replicate'] = [sample.replicate_id]
        _['value'] = Helpers.extract_time_series(sim_dict[sim], name=sample.name, replicate_id = sample.replicate_id).values
        list_of_dicts.append(_)

df = pd.DataFrame.from_dict(list_of_dicts)
df = df.apply(pd.Series.explode).reset_index() #Convert to long format
df = df.astype({'time': 'float', 'value':'float'})

df.to_excel('simulation_df_for_manuscript_plot.xlsx')

pyplot.figure(figsize=(32, 16))
sns.set_theme(style="ticks", font_scale=2)

sns.relplot(data = df, x = 'time', y = 'value', hue = 'measurement', col='replicate', style="strain", linewidth = 3, kind="line", col_wrap=4)
```

Out[38]:

```
<seaborn.axisgrid.FacetGrid at 0x1c5822a7af0>
<Figure size 2304x1152 with 0 Axes>
```

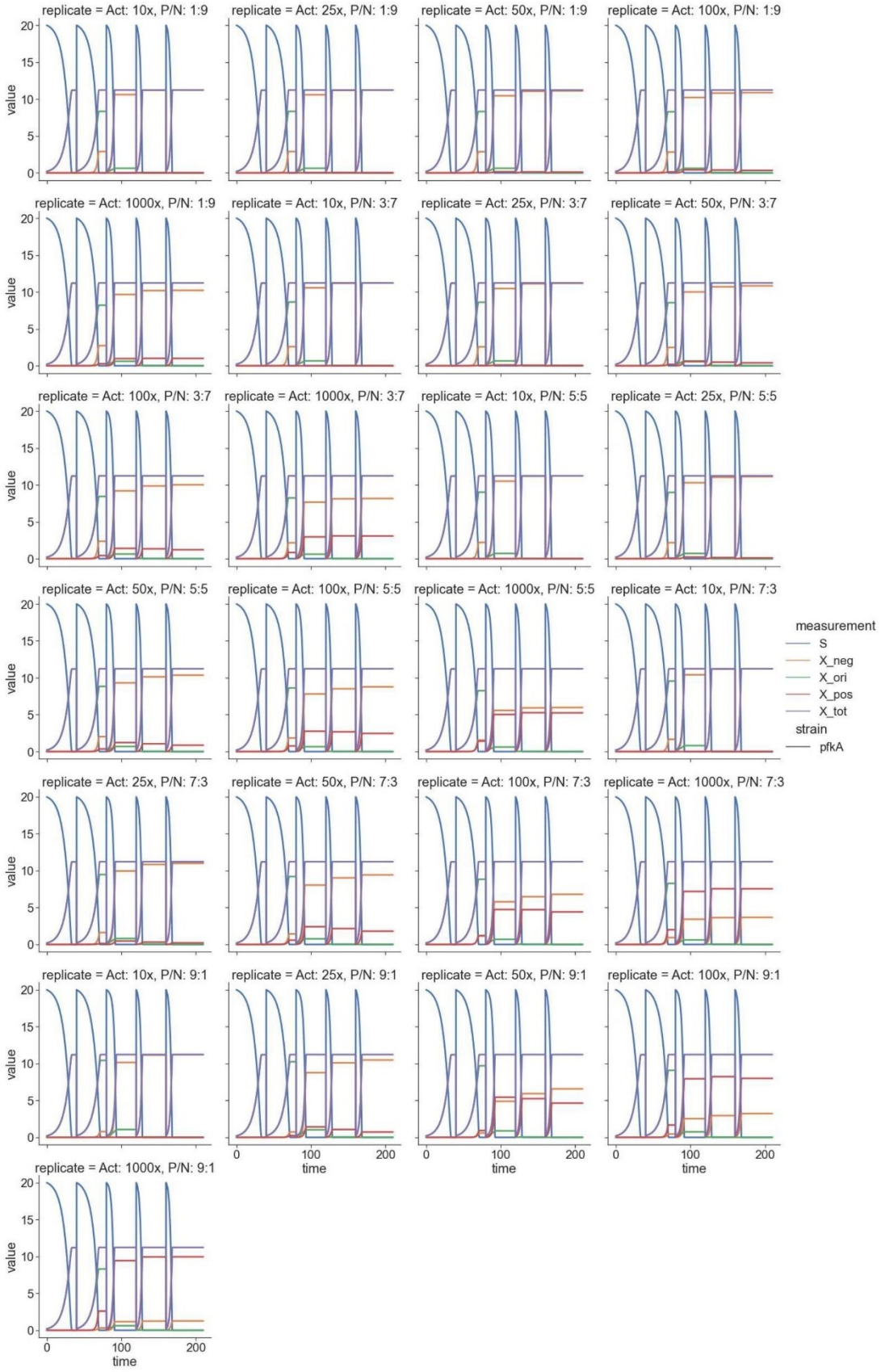
replicate = Act: 10x, P/N: 1:9
replicate = Act: 25x, P/N: 1:9
replicate = Act: 50x, P/N: 1:9
replicate = Act: 100x, P/N: 1:9
replicate = Act: 1000x, P/N: 1:9
replicate = Act: 10x, P/N: 3:7
replicate = Act: 25x, P/N: 3:7
replicate = Act: 50x, P/N: 3:7
replicate = Act: 100x, P/N: 3:7
replicate = Act: 1000x, P/N: 3:7
replicate = Act: 10x, P/N: 5:5
replicate = Act: 25x, P/N: 5:5
replicate = Act: 50x, P/N: 5:5
replicate = Act: 100x, P/N: 5:5
replicate = Act: 1000x, P/N: 5:5
replicate = Act: 10x, P/N: 7:3
replicate = Act: 25x, P/N: 7:3
replicate = Act: 50x, P/N: 7:3
replicate = Act: 100x, P/N: 7:3
replicate = Act: 1000x, P/N: 7:3
replicate = Act: 10x, P/N: 9:1
replicate = Act: 25x, P/N: 9:1
replicate = Act: 50x, P/N: 9:1
replicate = Act: 100x, P/N: 9:1
replicate = Act: 1000x, P/N: 9:1
value
time
measurement
S
X_neg
X_ori
X_pos
X_tot
strain
pfkA

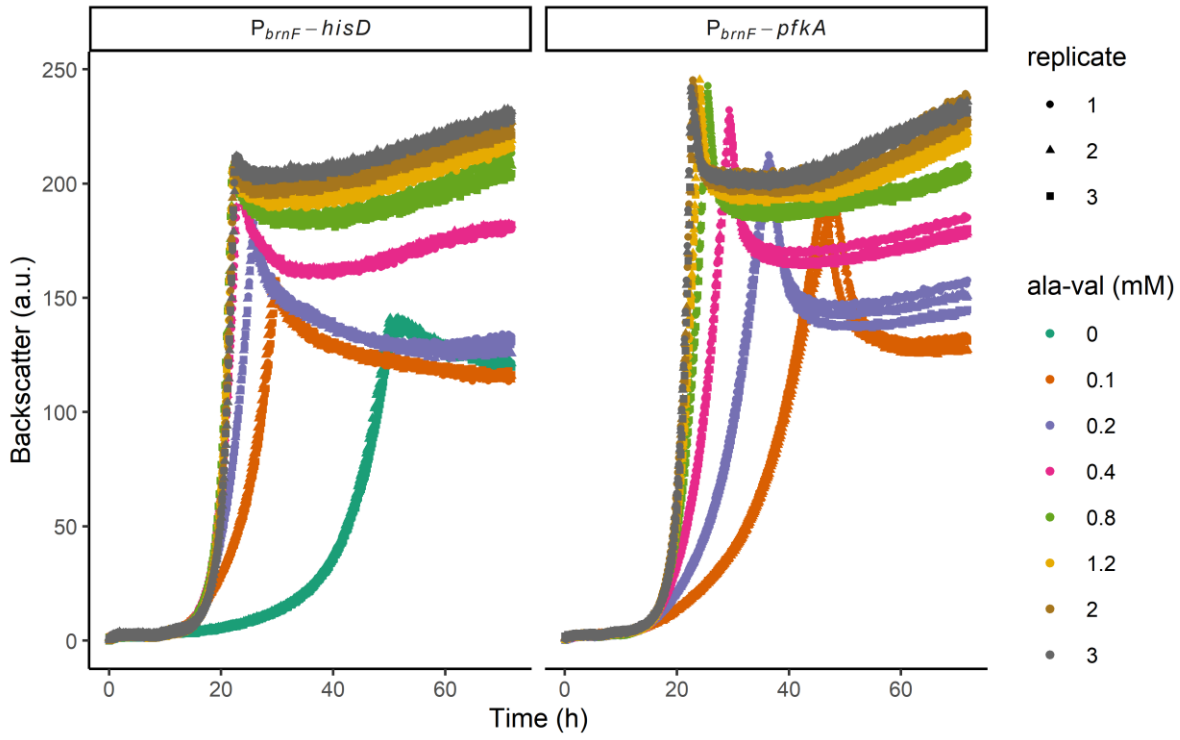

Figure S1

Microtiter growth of *C. glutamicum* growth-coupled strains P_{brnF}-*hisD* and P_{brnF}-*pfkA* supplemented with different amounts of ala-val dipeptide (0-3 mM), grown in CGXII 2% glucose. Supplementary information to the results shown in Figure 1C.

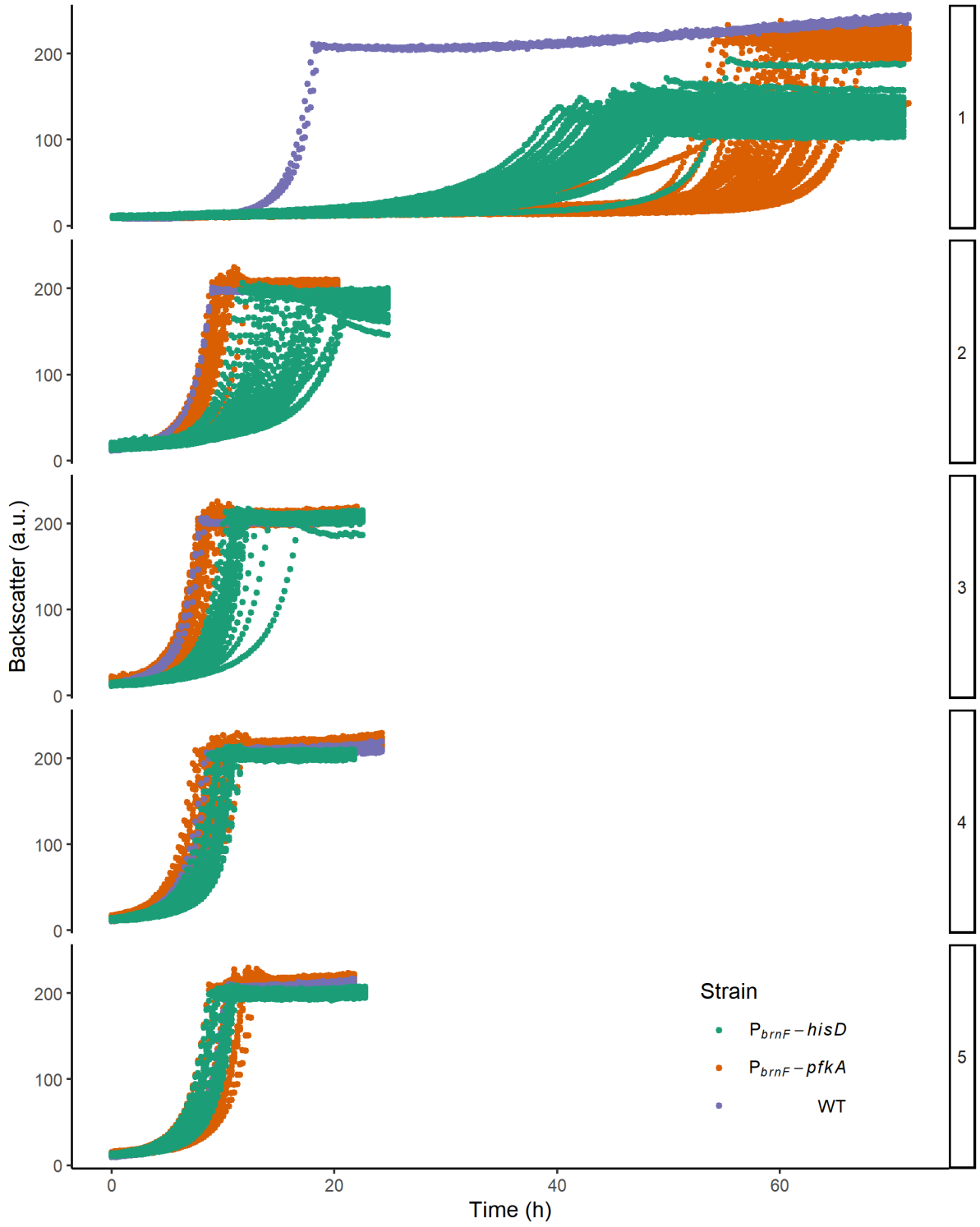

Figure S2

Growth of cultures after FACS-based selection. Backscatter values of five *C. glutamicum* repetitive batch cultivations in CGXII 2% glucose media after FACS sorting, covering 44 P_{brnF}-*pfkA* P_{brnF}-*pfkA* pJC1-*lrp-brnF'-eyfp* and P_{brnF}-*hisD* P_{brnF}-*pfkA* pJC1-*lrp-brnF'-eyfp* cultures and three *C. glutamicum* WT controls. Supplementary information to the results shown in Figure 4B.

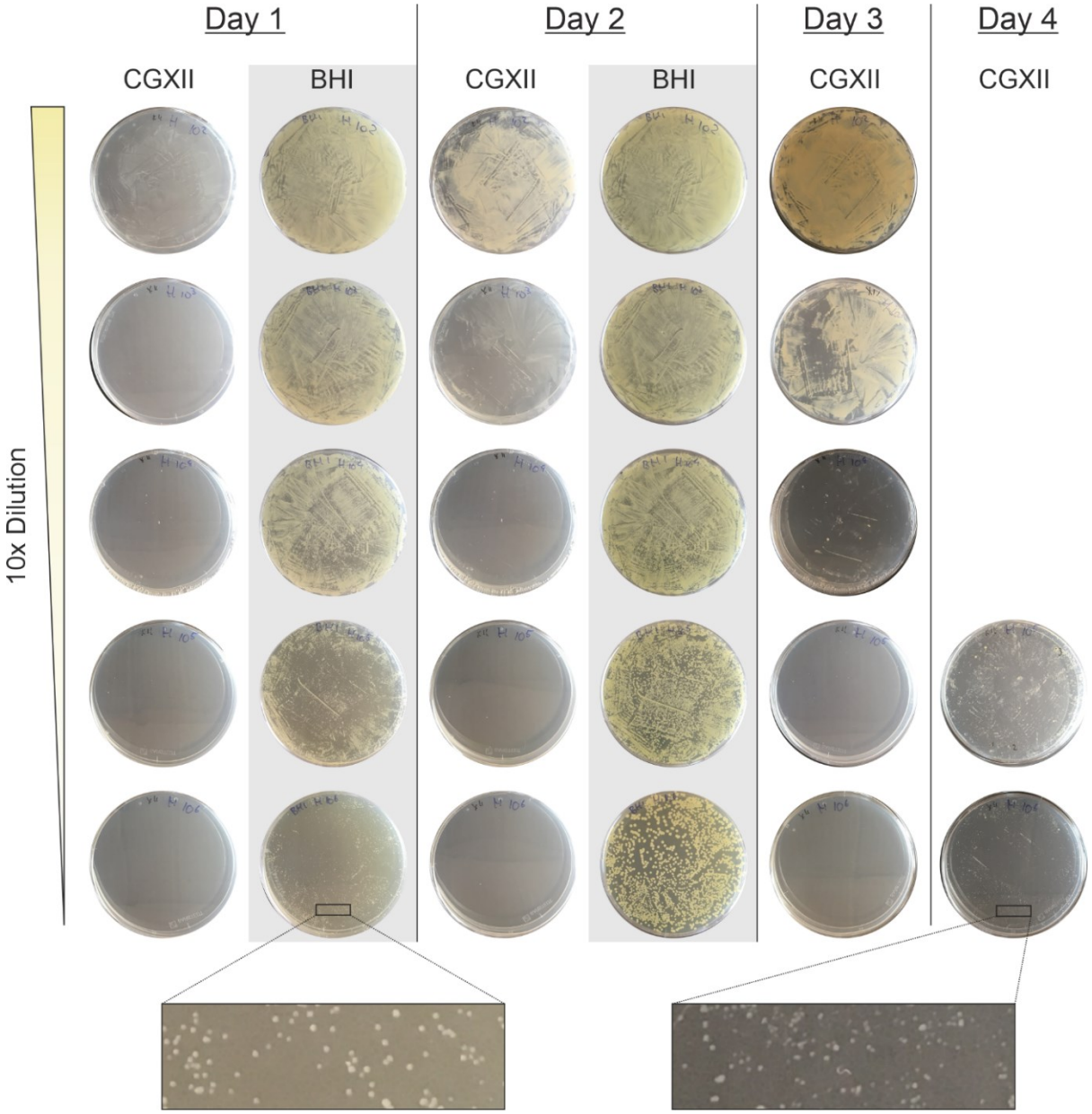

Figure S3
Growth of *C. glutamicum*::P_{brnF}-*hisD* on agar plates containing CGXII 2% glucose or BHI media. Different amounts of culture solutions were plated and photographs were taken after multiple days of incubation.

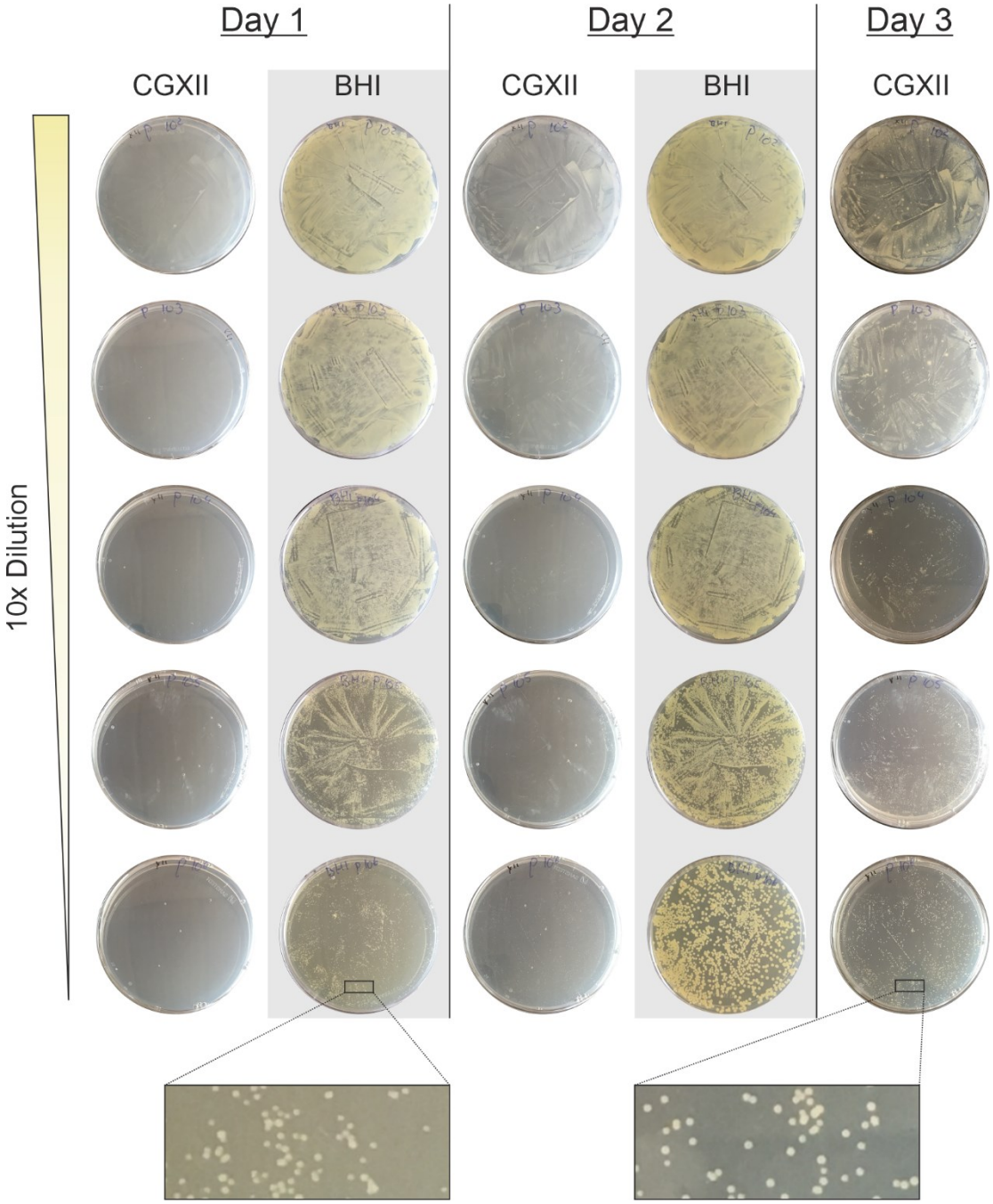

Figure S4
Growth of *C. glutamicum*::P$_{brnF}$-*pfkA* on agar plates containing CGXII 2% glucose or BHI media. Different amounts of culture solutions were plated and photographs were taken after multiple days of incubation.

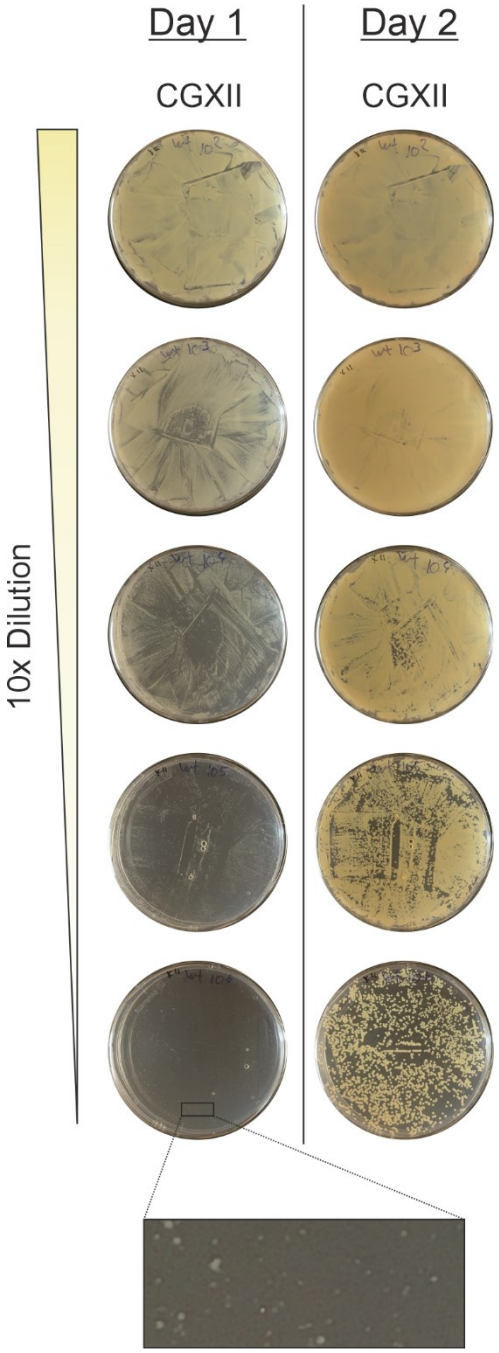

Figure S5
Growth of *C. glutamicum* WT on agar plates containing CGXII 2% glucose media. Different amounts of culture solutions were plated and photographs were taken after multiple days of incubation.

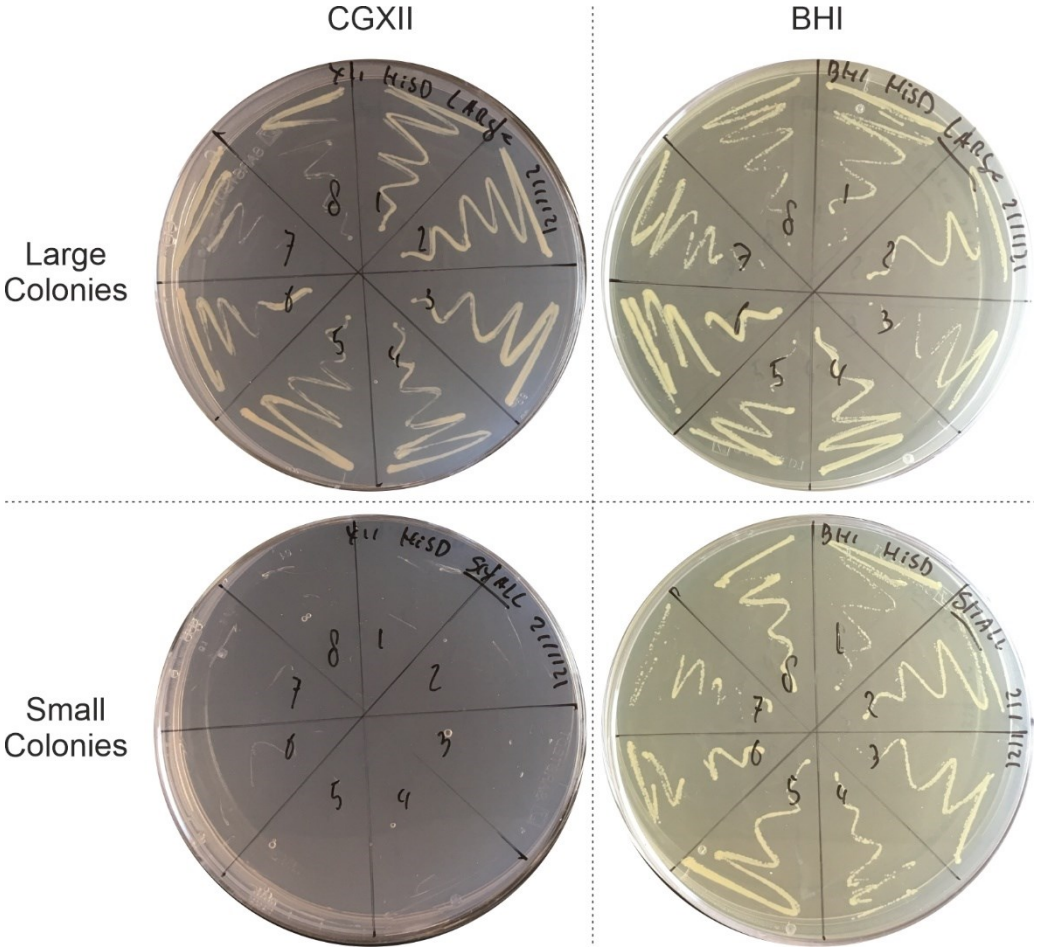

Figure S6

Growth of restreaked *C. glutamicum*::P_{brnF}-*hisD* colonies on agar plates containing CGXII 2% glucose or BHI media, after one day. Restreaking was done for 8 colonies, either large colonies or small colonies grown on CGXII 2% glucose media.

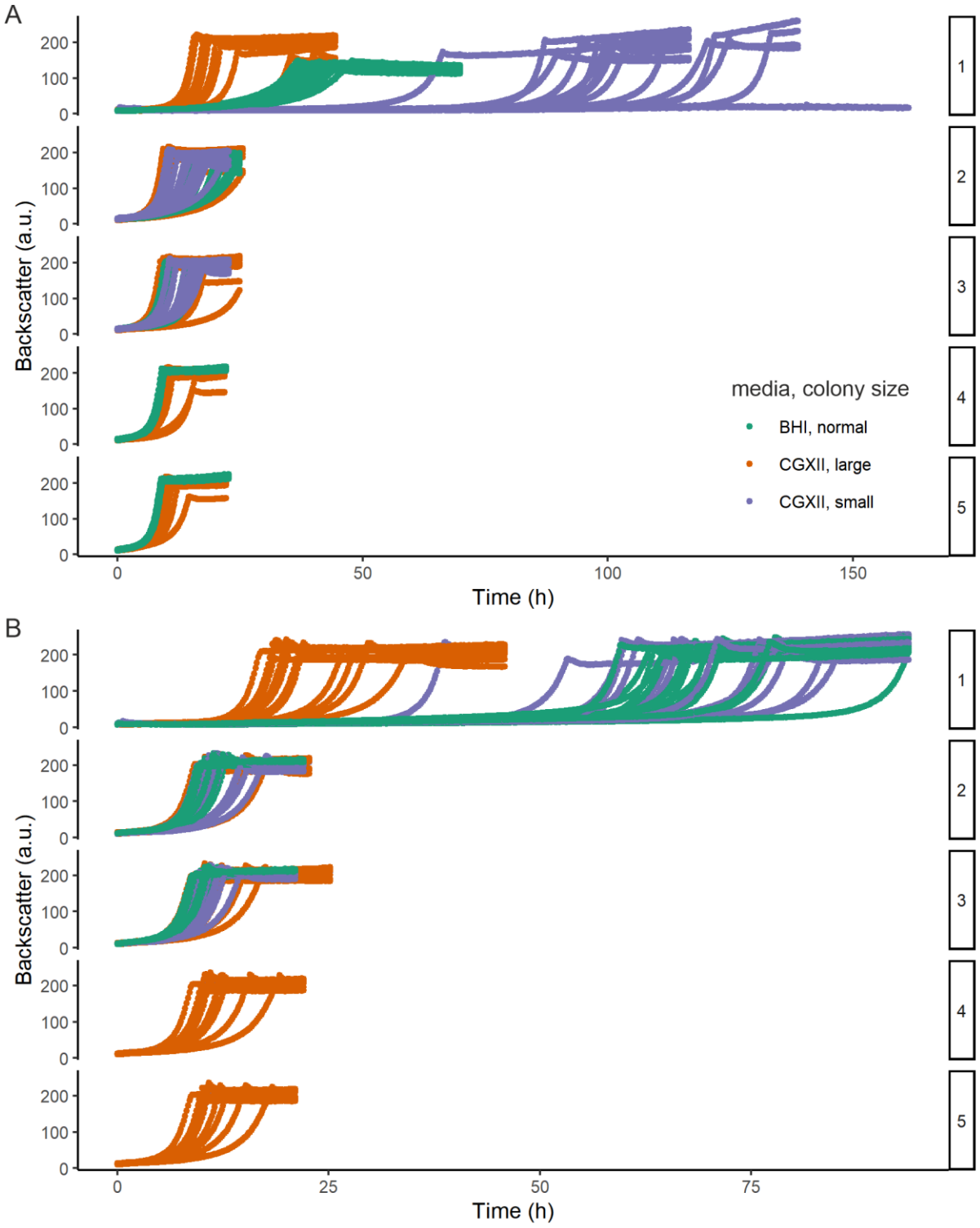

Figure S7

Backscatter values of *C. glutamicum*::P_{brnF}-*pfkA* and P_{brnF}-*hisD* cultures from plate-based evolutions, covering 15 cultures started from large colonies on CGXII plates, 15 cultures from small colonies on CGXII plates, and 15 cultures from normal colonies on BHI plates, for P_{brnF}-*hisD* (A) and P_{brnF}-*pfkA* (B). Supplementary information to the results shown in Figure 5B.

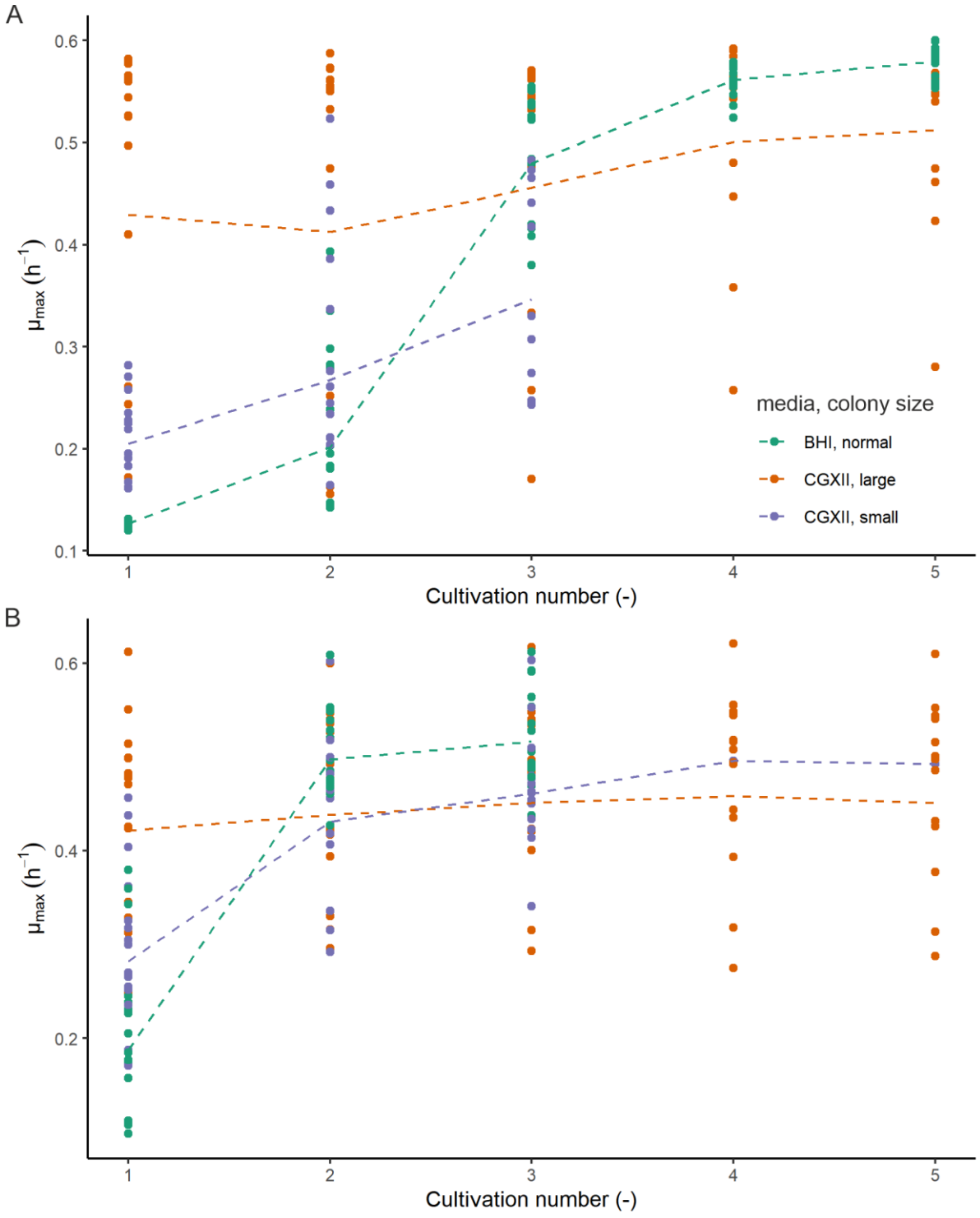

Figure S8

Growth rates of *C. glutamicum*::P*brnF*-*pfkA* and P*brnF*-*hisD* cultures from plate-based evolutions, covering 15 cultures started from large colonies on CGXII plates, 15 cultures from small colonies on CGXII plates, and 15 cultures from normal colonies on BHI plates, for P*brnF*-*hisD* (A) and P*brnF*-*pfkA* (B). Dots denote specific growth rates (μ_{max}) of each independent culture per repetitive batch, the line represents average per culture per strain. Supplementary information to the results shown in Figure 5B.

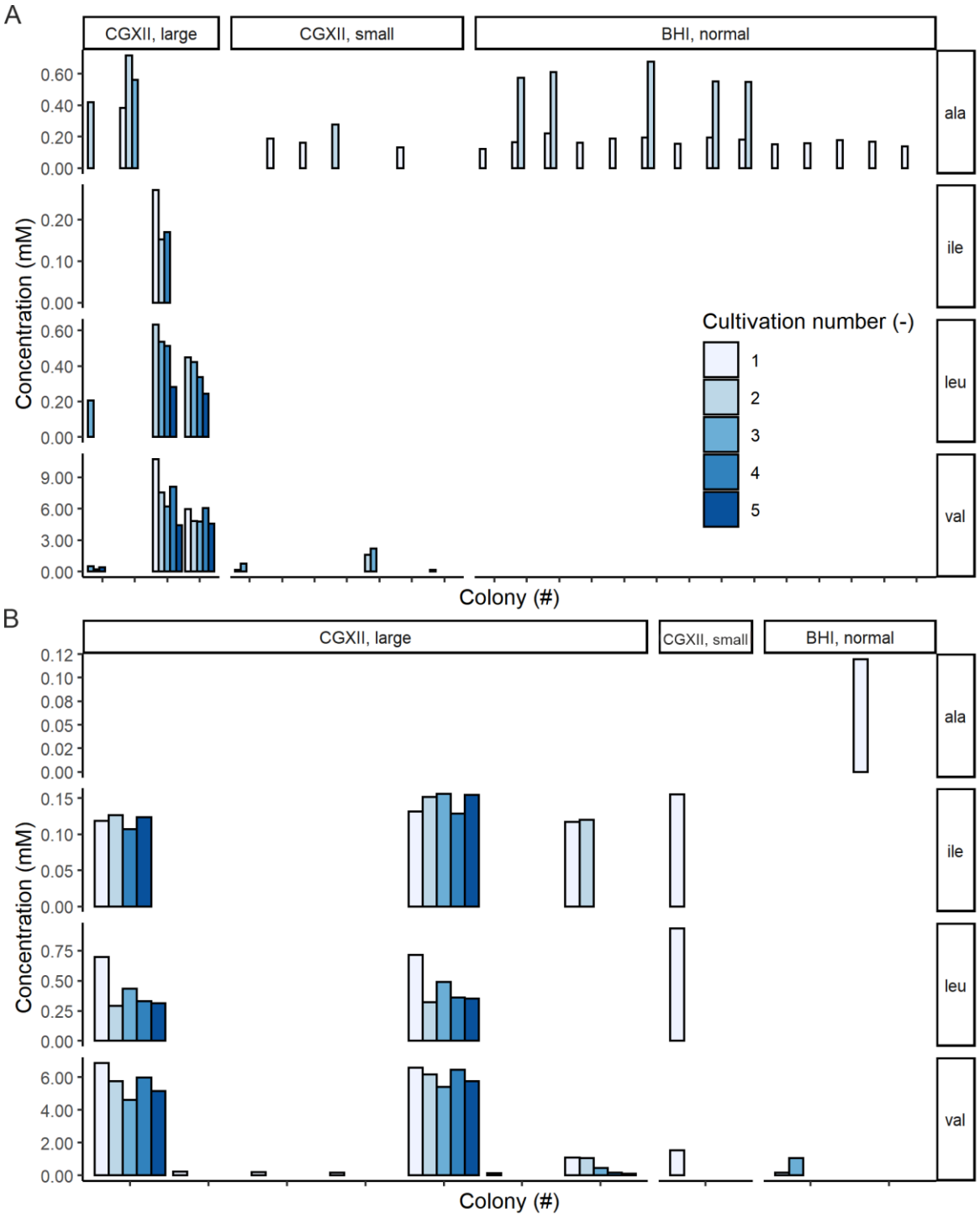

Figure S9

Amico acid production of *C. glutamicum*::P$_{brnF}$-*pfkA* and P$_{brnF}$-*hisD* cultures from plate-based evolutions, started from large colonies on CGXII plates, from small colonies on CGXII plates, and from normal colonies on BHI plates, for P$_{brnF}$-*hisD* (A) and P$_{brnF}$-*pfkA* (B). Fifteen colonies were picked for each plate-strain combination. Results are shown for clones that produced detectable amounts of amino acid (>0.1mM) in at least one repetitive culture. Color scales indicate results for a maximum of five repetitive cultures. Supplementary information to the results shown in Figure 5B.

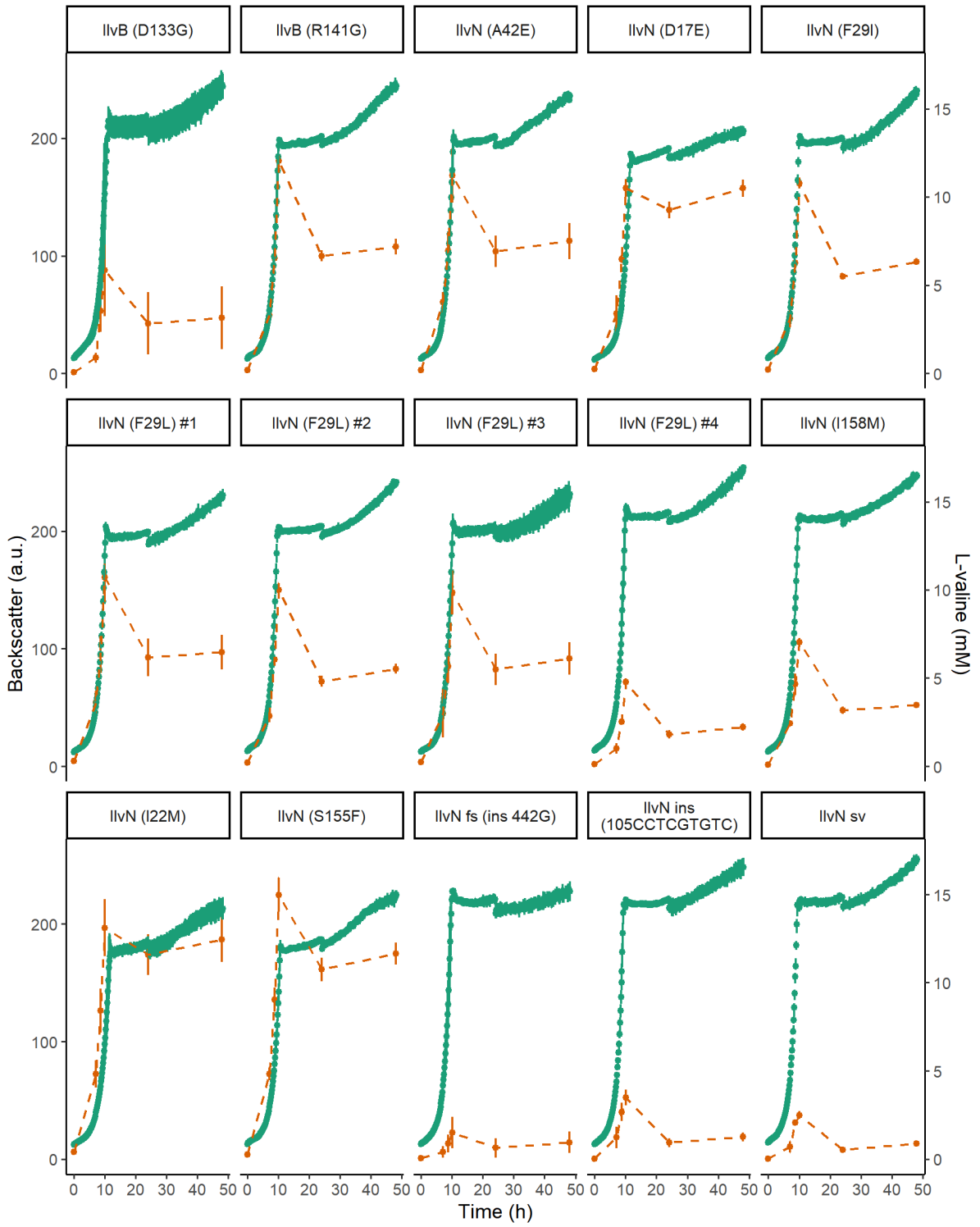

Figure S10

Growth and L-valine production of 15 L-valine producer mutants. Mean values and standard deviations of three biological replicates are shown; *fs*: frameshift mutation, *sv*: structural variant, *ins*: insertion. Supplementary information to the results shown in Figure 6C.

Literature

Baumgart, M., Luder, K., Grover, S., Gätgens, C., Besra, G.S., Frunzke, J., 2013. IpsA, a novel LacI-type regulator, is required for inositol-derived lipid formation in *Corynebacteria* and *Mycobacteria*. BMC Biol. 11, 1–14. https://doi.org/10.1186/1741-7007-11-122

Kalinowski, J., Bathe, B., Bartels, D., Bischoff, N., Bott, M., Burkovski, A., Dusch, N., Eggeling, L., Eikmanns, B.J., Gaigalat, L., Goesmann, A., Hartmann, M., Huthmacher, K., Krämer, R., Linke, B., McHardy, A.C., Meyer, F., Möckel, B., Pfefferle, W., Pühler, A., Rey, D.A., Rückert, C., Rupp, O., Sahm, H., Wendisch, V.F., Wiegräbe, I., Tauch, A., 2003. The complete *Corynebacterium glutamicum* ATCC 13032 genome sequence and its impact on the production of L-aspartate-derived amino acids and vitamins. J. Biotechnol. 104, 5–25. https://doi.org/10.1016/S0168-1656(03)00154-8

Mustafi, N., Grünberger, A., Kohlheyer, D., Bott, M., Frunzke, J., 2012. The development and application of a single-cell biosensor for the detection of l-methionine and branched-chain amino acids. Metab. Eng. 14, 449–457. https://doi.org/10.1016/j.ymben.2012.02.002

Schäfer, A., Tauch, A., Jäger, W., Kalinowski, J., Thierbach, G., Pühler, A., 1994. Small mobilizable multi-purpose cloning vectors derived from the *Escherichia coli* plasmids pK18 and pK19: selection of defined deletions in the chromosome of *Corynebacterium glutamicum*. Gene 145, 69–73. https://doi.org/10.1016/0378-1119(94)90324-7

5.2. Supplementary Information "Biosensor-based isolation of amino acid-producing *Vibrio natriegens* strains"

Table S1
Oligonucleotides used in this study

name	***sequence***
lrp_fw	tgccgggcctcttgcgggattcacacctgggggcgagc
lrp_rv	atgaagctagattccattgatcgcgc
lrp_eYFP_fw	tgaaaagaggagaaataatctatggtgagcaagggcgag
lrp_eYFP_rv	ttgcatcaacgcatatagcgttacttgtacagctcgtccatg
PbrnFE_rv	agattatttctcctcttttcagcttgaatgaatctcttgc
P100_PbrnFE_fw	tcaatggaatctagcttcatagattatttctcctcttttcattgacggctagctcagtcctaggtacagtgctagcatattgcacaatagcctag
P101_PbrnFE_fw	tcaatggaatctagcttcatagattatttctcctcttttcatttacagctagctcagtcctaggtattatgctagcatattgcacaatagcctag
P104_PbrnFE_fw	tcaatggaatctagcttcatagattatttctcctcttttcattgacagctagctcagtcctaggtattgtgctagcatattgcacaatagcctag
P106_PbrnFE_fw	tcaatggaatctagcttcatagattatttctcctcttttcatttacggctagctcagtcctaggtatagtgctagcatattgcacaatagcctag
P108_PbrnFE_fw	tcaatggaatctagcttcatagattatttctcctcttttcactgacagctagctcagtcctaggtataatgctagcatattgcacaatagcctag
P110_PbrnFE_fw	tcaatggaatctagcttcatagattatttctcctcttttcatttacggctagctcagtcctaggtacaatgctagcatattgcacaatagcctag
lysG_eYFP_fw	cactatggcgtgctgcccgggttaattaaggcgcgccactagtatggtgagcaagggcgag
lysG_eYFP_rv	gagtgaaacgttatctagacttgtacagctcgtcc
lysG_araC_fw	gtctagataacgtttcactccatccaaaaaaac
lysG_araC_rv	gcgtccggcgtagagttatgacaacttgacggc
lysG_fw	gtcactatggcgtgctgcccctaaggccgcaatccctc
lysG_rv	tgaaaagaggagaaataatctatgaaccccattcaactgg
PlysE_100_fw	tagccgtcaatgaagctatattaaaccatgttaag
PlysE_108_fw	tagctgtcagtgaagctatattaaaccatgttaag
PlysE_101_fw	tagctgtaaatgaagctatattaaaccatgttaag
PlysE_106_fw	tagccgtaaatgaagctatattaaaccatgttaag
PlysE_110_fw	tagccgtaaatgaagctatattaaaccatgttaag
PlysE_104_fw	tagctgtcaatgaagctatattaaaccatgttaag
PlysE_rv	cctcgcccttgctcaccatagattatttctcctcttttcatctaggtccgatggacag
P100_lysG_fw	agattatttctcctcttttcagctagcactgtacctaggactgagctagccgtcaatgaagcta
P100_lysG_rv	tagcttcattgacggctagctcagtcctaggtacagtgctagctgaaaagaggagaaataatct
P108_lysG_fw	agattatttctcctcttttcagctagcattatacctaggactgagctagctgtcagtgaagcta
P108_lysG_rv	tagcttcactgacagctagctcagtcctaggtataatgctagctgaaaagaggagaaataatct
P101_lysG_fw	agattatttctcctcttttcagctagcataatacctaggactgagctagctgtaaatgaagcta
P101_lysG_rv	tagcttcatttacagctagctcagtcctaggtattatgctagctgaaaagaggagaaataatct
P106_lysG_fw	agattatttctcctcttttcagctagcactatacctaggactgagctagccgtaaatgaagcta
P106_lysG_rv	tagcttcatttacggctagctcagtcctaggtatagtgctagctgaaaagaggagaaataatct
P110_lysG_fw	agattatttctcctcttttcagctagcattgtacctaggactgagctagccgtaaatgaagcta
P110_lysG_rv	tagcttcatttacggctagctcagtcctaggtacaatgctagctgaaaagaggagaaataatct
P104_lysG_fw	agattatttctcctcttttcagctagcacaatacctaggactgagctagctgtcaatgaagcta
P104_lysG_rv	tagcttcattgacagctagctcagtcctaggtattgtgctagctgaaaagaggagaaataatct

Supplementary data 1

Excel table containing the mutations identified in isolated producer mutants, with a frequency more than 50%.

phenotype	Chromo-some	Location	Mutation	description
L-Histidine producer	1	115403	G to A	G256G in PN96_RS00520(-), sodium:calcium antiporter
	1	131112	C to T	exchange V516I in PN96_RS00615(-), valine--tRNA ligase
	1	812084	G to A	exchange L433F in PN96_RS03785(-), IMP dehydrogenase
	1	823713	G to A	exchange P149S in PN96_RS03830(-), hypothetical protein
	1	834364	G to A	exchange G78S in PN96_RS03875(+), ggdef family protein
	1	1593933	C to T	exchange V395I in PN96_RS07440(-), D-serine ammonia-lyase
	1	1807938	C to T	LEFT: PN96_RS08370 (two-component system response regulator TorR) RIGHT: PN96_RS08375 (molecular chaperone TorD)
	1	1811558	C to T	LEFT: PN96_RS08385 (DNA transformation protein) RIGHT: PN96_RS08390 (TVP38/TMEM64 family protein)
	1	1814095	C to T	exchange G339D in PN96_RS08405(-), starch synthase
	1	1827130	C to T	LEFT: PN96_RS08455 (ATP-dependent Clp protease adaptor ClpS) RIGHT: PN96_RS08460 (cold shock domain protein CspD)
	1	1838467	C to T	exchange R126Q in PN96_RS08510(-), hypothetical protein
	1	1876168	C to T	exchange A17T in PN96_RS08665(-), NADH dehydrogenase
	1	2233378	G to A	E259E in PN96_RS10395(+), ppnK, NAD(+) kinase
	1	2437594	G to A	exchange A74T in PN96_RS11265(+), hypothetical protein
	1	2438953	G to A	exchange D120N in PN96_RS11275(+), adenosylcobinamide-phosphate synthase
	1	2446295	G to A	exchange P358L in PN96_RS11305(-), carbamoyl-phosphate synthase small subunit
	1	2713798	G to A	exchange V277I in PN96_RS12575(+), glycosyl transferase
	2	837562	G to A	exchange V303I in PN96_RS23680(+), hypothetical protein
	2	1725147	C to T	LEFT: PN96_RS22740 (RNA helicase) RIGHT: PN96_RS22745 (GTPase)
	2	1741863	C to T	exchange T13I in PN96_RS22830(+), dehydrogenase
	2	1808658	C to T	exchange S137F in PN96_RS23135(+), copper-binding protein
	2	1810687	C to T	exchange A85V in PN96_RS23145(+), CARB/PSE/RTG family carbenicillin-hydrolyzing class A beta-lactamase
	2	1809346	C to T	exchange D293N in PN96_RS23140(-), ferric reductase
L-arginine producer	1	49410	C_T	D8D in PN96_RS00240(+), rrf, 5S ribosomal RNA
	1	73517	C_T	exchange P77S in PN96_RS00335(+), MSHA biogenesis protein MshM
	1	865314	G_A	L155L in PN96_RS04020(-), DNA polymerase II

	1	869721	C_T	LEFT: PN96_RS04035 (CDP-diacylglycerol--glycerol-3-phosphate 3-phosphatidyltransferase) RIGHT: PN96_RS04040 (tRNA-Cys)
	1	903971	C_T	exchange S91F in PN96_RS04195(+), C4-dicarboxylate ABC transporter
	1	976169	C_T	exchange P77L in PN96_RS04620(+), hypothetical protein
	1	986013	C_T	exchange D349N in PN96_RS04685(-), glycosyl transferase
	1	989537	C_T	Q67Q in PN96_RS04695(-), glycosyl transferase
	1	1010834	C_T	exchange V594I in PN96_RS04790(-), 5-dehydro-2-deoxygluconokinase
	1	1012576	C_T	exchange G13D in PN96_RS04790(-), 5-dehydro-2-deoxygluconokinase
	1	1073047	C_T	exchange P77L in PN96_RS05090(+), agmatine deiminase
	1	1522991	G_A	exchange S140F in PN96_RS07100(-), hypothetical protein
	1	1534883	G_A	R243R in PN96_RS07185(-), integrase
	1	1617073	G_A	exchange P313S in PN96_RS07530(-), Na+/H+ antiporter NhaA
	1	1667869	G_A	I15I in PN96_RS07740(-), envelope stress response membrane protein PspB
	1	1711044	G_A	exchange D44N in PN96_RS07940(+), tRNA 2-thiouridine(34) synthase MnmA
	1	2298044	C_T	LEFT: PN96_RS10675 (Fe-S cluster assembly transcriptional regulator IscR) RIGHT: PN96_RS10680 (tRNA (cytosine(32)/uridine(32)-2'-O)-methyltransferase TrmJ)
	1	2362338	G_A	L29L in PN96_RS10965(-), phospho-2-dehydro-3-deoxyheptonate aldolase
	1	2395134	G_A	L345L in PN96_RS11115(-), lysine--tRNA ligase
	1	2413061	G_A	exchange A186V in PN96_RS11195(-), threonine synthase
	1	2424548	G_A	LEFT: PN96_RS11240 (TIGR01212 family radical SAM protein) RIGHT: PN96_RS11245 (glutamate synthase subunit alpha)
	1	2424713	G_A	LEFT: PN96_RS11240 (TIGR01212 family radical SAM protein) RIGHT: PN96_RS11245 (glutamate synthase subunit alpha)
	1	2507356	G_A	LEFT: PN96_RS11565 (general secretion pathway protein GspA) RIGHT: PN96_RS11570 (multifunctional CCA tRNA nucleotidyl transferase/2'3'-cyclic phosphodiesterase/2'nucleotidase/phosphatase)
	1	2531276	G_A	exchange V52M in PN96_RS11675(+), mannitol-1-phosphate 5-dehydrogenase
	1	2541977	C_T	Stop W486* in PN96_RS11720(-), acetolactate synthase 3 large subunit
	1	2542548	T_C	exchange Y296C in PN96_RS11720(-), acetolactate synthase 3 large subunit
	1	2944784	C_T	exchange P349S in PN96_RS13655(+), ATP-dependent protease
	2	1389	G_A	exchange R278Q in PN96_RS15190(+), undecaprenyl-phosphate glucose phosphotransferase
	2	424370	C_T	exchange A41V in PN96_RS17005(+), hypothetical protein

	2	570984	C_T	exchange L15F in PN96_RS17675(+), potD, ABC transporter substrate-binding protein
	2	573727	G_A	L163L in PN96_RS17685(-), helix-turn-helix transcriptional regulator
	2	1429517	C_T	C151C in PN96_RS21465(+), NAD-dependent epimerase
	2	1481365	C_T	exchange S199N in PN96_RS21670(-), hypothetical protein
	2	1571536	C_T	E183E in PN96_RS22060(-), TetR family transcriptional regulator
	2	1591939	G_A	exchange V47I in PN96_RS22155(+), DNA-binding response regulator
L-Lysine producer	1	311032	C_T	exchange S91N in PN96_RS01540(-), ABC transporter ATP-binding protein
	1	383058	G_A	exchange G62R in PN96_RS01835(+), prepilin peptidase
	1	527108	C_T	E93E in PN96_RS02495(-), arsenate reductase (glutaredoxin)
	1	532174	C_T	exchange H56Y in PN96_RS02525(+), 4-hydroxy-tetrahydrodipicolinate synthase
	1	2275172	G_A	exchange G283D in PN96_RS10565(+), hypothetical protein
	2	128078	C_T	LEFT: PN96_RS15770 (hypothetical protein) RIGHT: PN96_RS15775 (proton/glutamate symporter)
	2	222295	C_T	LEFT: PN96_RS16130 (peptidase M16) RIGHT: PN96_RS16135 (chondroitinase)
	2	315182	C_T	LEFT: PN96_RS16460 (peptide ABC transporter substrate-binding protein) RIGHT: PN96_RS16465 (murein peptide amidase A)
	2	404227	C_T	A114A in PN96_RS16890(-), thiamine phosphate synthase
	2	434751	C_T	exchange P121S in PN96_RS17055(+), cell envelope biogenesis protein TonB
	2	476637	C_T	exchange T809I in PN96_RS17235(+), ABC transporter
	2	497820	C_T	exchange S201L in PN96_RS17330(+), phosphonate ABC transporter permease
	2	518361	C_T	exchange S52F in PN96_RS17415(+), LruC domain-containing protein
	2	559540	C_T	exchange G64D in PN96_RS17630(-), hypothetical protein
	2	610383	C_T	exchange G99R in PN96_RS17840(-), NAD(P)H-dependent oxidoreductase
	2	698150	C_T	R65R in PN96_RS18265(+), hypothetical protein
	2	1046405	G_A	LEFT: PN96_RS19765 (hypothetical protein) RIGHT: PN96_RS19770 (hypothetical protein)
	2	1051005	G_A	exchange V92I in PN96_RS19785(+), DUF1338 domain-containing protein
	2	1094072	C_T	exchange E125K in PN96_RS19985(-), Cu(I)-responsive transcriptional regulator
	2	1107582	G_A	N243N in PN96_RS20030(-), 9-hexadecenoic acid cis-trans isomerase
	2	1110924	G_A	exchange G432R in PN96_RS20040(+), arylsulfatase
	2	1313905	C_T	exchange M75I in PN96_RS20985(-), hypothetical protein
	2	1321926	C_T	G532G in PN96_RS21020(+), lipase

L-lysine improved producer	1	1818351	A_G	exchange S500P in PN96_RS08415(-), DNA topoisomerase I
	2	1533754	C_G	LEFT: PN96_RS21890 (hypothetical protein) RIGHT: PN96_RS21895 (phosphate ABC transporter substrate-binding protein)

5.3. Supplementary Information “Automated Rational Strain Construction Based on High-Throughput Conjugation”

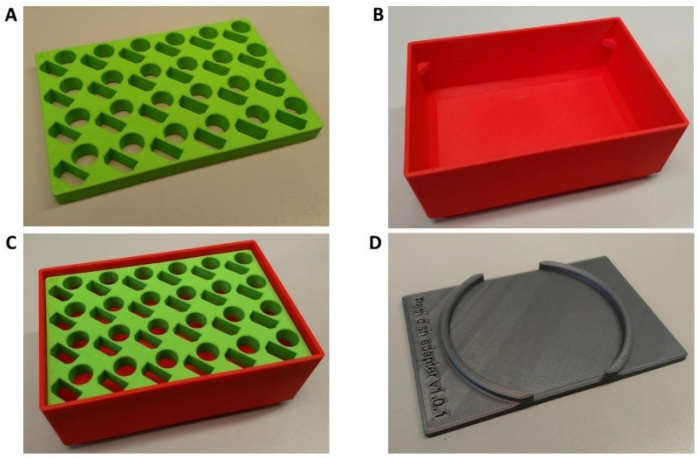

Figure S1: Images of 3D printed parts used in this study. All files are freely available at `https://github.com/MicroPhen/taco`. (A) Plate for placement of 1.5 mL or 2 mL reaction tubes. Filename: "reaction-tube-adapter-for-ot-cc.stl". (B) Trough for crushed ice with SBS format base and SBS format opening. Filename: "ot-cooling-carrier.stl". (C) Assembly of reaction tube holder A in crushed ice trough B. (D) Petri dish adapter for 100 mm Petri dishes. Filename: "petri_dish_adapter.stl".

Table S1: Primers used in this study.

Name	Sequence	Template	Description
1_*lrp*_pEC-T_fw	cagctatgacatgattacgtcacacctgggggcgagc	*C. g.* genomic DNA	To obtain *lrp* part for pEC-Tmob18-*lrp-eyfp* backbone construction
2_*lrp*_pEC-T_rv	catggatccccgggtaccccatggaagctagattccattgatcgcgcaattattg	*C. g.* genomic DNA	To obtain *lrp* part for pEC-Tmob18-*lrp-eyfp* backbone construction
3_*eyfp*_pEC-T_fw	ctagcttccatggggtacccggggatccatgggtgagcaagggcgagga	pJC1-*lrp-brnF'-eyfp**	To obtain *eyfp* part for pEC-Tmob18-*lrp-eyfp* backbone construction
4_*eyfp*_pEC-T_rv	caggtcgactctagagttacttgtacagctcgtccatgc	pJC1-*lrp-brnF'-eyfp**	To obtain *eyfp* part for pEC-Tmob18-*lrp-eyfp* backbone construction
5_*lrp*_AT_R1_fw	tcaatggaatctagcttcATatattGCACAATAGCCTAGTTGAGGTGC GCAAACTG	*C. g.* genomic DNA	Forward primer to create *lrp* start codon and RBS variant
6_*lrp*_AT_R2_fw	tcaatggaatctagcttcATatattCCATTTTAGCCTAGTTGAGGTGC GCAAACTG	*C. g.* genomic DNA	Forward primer to create *lrp* start codon and RBS variant
7_*lrp*_AT_R3_fw	tcaatggaatctagcttcATatattGGTAGGATTGCTAGTTGAGGTG CGCAAACTG	*C. g.* genomic DNA	Forward primer to create *lrp* start codon and RBS variant
8_*lrp*_AC_R1_fw	tcaatggaatctagcttcACatattGCACAATAGCCTAGTTGAGGTGC GCAAACTG	*C. g.* genomic DNA	Forward primer to create *lrp* start codon and RBS variant
9_*lrp*_AC_R2_fw	tcaatggaatctagcttcACatattCCATTTTAGCCTAGTTGAGGTGC GCAAACTG	*C. g.* genomic DNA	Forward primer to create *lrp* start codon and RBS variant
10_*lrp*_AC_R3_fw	tcaatggaatctagcttcACatattGGTAGGATTGCTAGTTGAGGTG CGCAAACTG	*C. g.* genomic DNA	Forward primer to create *lrp* start codon and RBS variant
11_*lrp*_AA_R1_fw	tcaatggaatctagcttcAAatattGCACAATAGCCTAGTTGAGGTGC GCAAACTG	*C. g.* genomic DNA	Forward primer to create *lrp* start codon and RBS variant
12_*lrp*_AA_R2_fw	tcaatggaatctagcttcAAatattCCATTTTAGCCTAGTTGAGGTGC GCAAACTG	*C. g.* genomic DNA	Forward primer to create *lrp* start codon and RBS variant
13_*lrp*_AA_R3_fw	tcaatggaatctagcttcAAatattGGTAGGATTGCTAGTTGAGGTG CGCAAACTG	*C. g.* genomic DNA	Forward primer to create *lrp* start codon and RBS variant
14_*lrp*_R1_plus30	tcgcccttgctcaccATATGATATCTCCTTCTTAAAGTTCAGCTT GAATGAATCTCTTGCGT	*C. g.* genomic DNA	Reverse primer to create *brnF* promoter and *eyfp* RBS variant
15_*lrp*_R1_plus15	tcgcccttgctcaccATATGATATCTCCTTCTTAAAGTTCATTGC GTTTTTTGCACACTACA	*C. g.* genomic DNA	Reverse primer to create *brnF* promoter and *eyfp* RBS variant
16_*lrp*_R1_plus0	tcgcccttgctcaccATATGATATCTCCTTCTTAAAGTTCAACTA CAATCATCACACAATTGCCG	*C. g.* genomic DNA	Reverse primer to create *brnF* promoter and *eyfp* RBS variant
17_*lrp*_R1_min15	tcgcccttgctcaccATATGATATCTCCTTCTTAAAGTTCACAAT TGCCGGGTAGTTTTGTTG	*C. g.* genomic DNA	Reverse primer to create *brnF* promoter and *eyfp* RBS variant
18_*lrp*_R2_plus30	tcgcccttgctcaccATATGATATGGTCGGATTAAAGTTCAGCTT GAATGAATCTCTTGCGT	*C. g.* genomic DNA	Reverse primer to create *brnF* promoter and *eyfp* RBS variant
19_*lrp*_R2_plus15	tcgcccttgctcaccATATGATATGGTCGGATTAAAGTTCATTGC GTTTTTTGCACACTACA	*C. g.* genomic DNA	Reverse primer to create *brnF* promoter and *eyfp* RBS variant
20_*lrp*_R2_plus0	tcgcccttgctcaccATATGATATGGTCGGATTAAAGTTCAACTA CAATCATCACACAATTGCCG	*C. g.* genomic DNA	Reverse primer to create *brnF* promoter and *eyfp* RBS variant
21_*lrp*_R2_min15	tcgcccttgctcaccATATGATATGGTCGGATTAAAGTTCACAAT TGCCGGGTAGTTTTGTTG	*C. g.* genomic DNA	Reverse primer to create *brnF* promoter and *eyfp* RBS variant
22_*lrp*_R3_plus30	tcgcccttgctcaccATATGATATCTCCTTTTTAAAGTTCAGCTT GAATGAATCTCTTGCGT	*C. g.* genomic DNA	Reverse primer to create *brnF* promoter and *eyfp* RBS variant
23_*lrp*_R3_plus15	tcgcccttgctcaccATATGATATCTCCTTTTTAAAGTTCATTGC GTTTTTTGCACACTACA	*C. g.* genomic DNA	Reverse primer to create *brnF* promoter and *eyfp* RBS variant
24_*lrp*_R3_plus0	tcgcccttgctcaccATATGATATCTCCTTTTTAAAGTTCAACTA CAATCATCACACAATTGCCG	*C. g.* genomic DNA	Reverse primer to create *brnF* promoter and *eyfp* RBS variant
25_*lrp*_R3_min15	tcgcccttgctcaccATATGATATCTCCTTTTTAAAGTTCACAAT TGCCGGGTAGTTTTGTTG	*C. g.* genomic DNA	Reverse primer to create *brnF* promoter and *eyfp* RBS variant